Development of Thaw-induced Gelation (TIG) of Alginate Hydrogels for the Encapsulation of Post-cryopreserved Cells and Therapeutic Cargos

BY

DUSTIN JOSEPH HADLEY

DISSERTATION

Submitted in partial satisfaction of the requirements for the degree of

DOCTOR OF PHILOSOPHY

in

Biomedical Engineering

In the

OFFICE OF GRADUATE STUDIES

of the

UNIVERSITY OF CALIFORNIA, DAVIS

Approved:

_____

Eduardo A. Silva, Chair

_____

J. Kent Leach

_____

Randy P. Carney

2021

ACKNOWLEDGEMENTS

While the thesis marks the completion of the trials of graduate school, the journey was always my objective. The path to this moment was rewarding, with many to acknowledge and thank their mentorship and support. I have grown immeasurably from these people in intellect, wisdom, and emotional maturity over these last couple of years while working on this thesis.

First, I would like to extend my thanks to Dr. Eduardo Silva, my thesis advisor. His mentorship and guidance were invaluable towards my development as an independent scientist and my growth as a leader. I became Eduardo's student after transferring from Dr. Revzin's lab. Although it took a while to be recognized as a member of his lab, perseverance and a willingness to adapt led to the conceptualization of novel gelation schemes presented in this thesis. I recall when I first presented the results that cryopreserved cells could be encapsulated in a hydrogel while thawing on my birthday in 2017. Eduardo, a grounding pillar, was hesitant towards the idea. A year later, it became a central focus of my project, supported by Eduardo, although it deviated from the common themes of the lab. In this way, I am grateful for the balanced responsiveness he maintains in scientific pursuits and mentorship. Through reflection and time, he has inspired aspects of mentorship, leadership, and the scientific process that will forever be held in the highest regard. Through my interactions with Eduardo, I have built my confidence as a scientist.

I would also like to thank additional mentors who have led me to graduate school and develop the work presented in this thesis. I appreciate the members of my dissertation committee, Dr. Kent Leach and Randy Carney, for their support and

guidance. I also extend my appreciation to Alexander Revzin and previous members of his lab, Dr. Timothy Kwa and Dr. Zimple Matharu, for motivating me to attend graduate school and kindling my enthusiasm for research. Similarly, I am grateful for the many mentorship and teaching opportunities through the teaching assistant program. Specifically, I'd like to acknowledge Dr. Rucha Joshi and Dr. Jamal Lewis for their support not only in becoming a better educator. Moreover, the seeds of my development as a scientist were planted by the science and math teachers at Steele Canyon High School. Specifically, I would like to acknowledge and thank Betty Jensen.

I am further grateful for my colleagues and friends I had the pleasure of knowing and working with. Priscilla Williams, Justin Madrigal, Roberta Stilhano, Kevin Campbell, Shahin Shams, Jonathan Ho, Lauren Uyesaka, and many others have been tremendous scientific and personal support. Throughout the UC Davis Biomedical engineering program, a collaborative atmosphere enables a level of friendship I hope to cultivate in future work environments.

Lastly, I would like to thank my family and friends. Ten plus years of support through this upper education path has been invaluable to me. Although often teasing about when it will end, their understanding of how important the journey was for me has made the process immeasurable more manageable.

ABSTRACT

Cell-based therapies have been a growing topic of interest within biomedical research. Despite many advances, the challenges with clinical translation twenty years ago persist today: problems associated with scaling up production and cell death associated with implantation. For clinical success, a holistic approach incorporating the current challenges in cell-based therapies would increase the probability of success. Two prospective methods to improve cell delivery outcomes include biomaterials and spheroids. Nevertheless, it is unclear how innovations with these methods will integrate with the need to preserve cell-based therapies via cryopreservation, the storage of cells in frozen stasis. Notably, the freezing and thawing process has negative consequences for cell replication, unintended differentiation, poor recovery, and morphological and functional changes. These issues are worsened when freezing larger tissues or constructs, such as spheroids and cells encapsulated in hydrogels. To address this challenge, we developed a novel gelation procedure for alginate hydrogels capable of encapsulating cells as they thaw from a cryopreserved state, which we call thaw-induced gelation. This method is a distinct alternative to cryopreserving cell-based therapies whole.

We developed three new alginate hydrogels compatible with cryopreservation: homo-IPN, alginate cryogels, and hydrogel capsules. Using each method with cryopreserved cells could instruct cell aggregation to form spheroids. Additionally, these hydrogels showed promise for protecting cargo from freeze/thaw damage and could enhance electrostatic-based release from the hydrogels. Lastly, we interrogated the optimal procedure to cryopreserve cells to obtain spheroids

using HUVECs, MSCs, and a combination of both cell types. Our results suggested that best practices are likely cell-dependent, indicating cryopreservation will not have a one-size-fits-all approach for potential cell therapies. Overall, thaw-induced gelation represents one of the first efforts to design hydrogel-based systems around the mechanisms of cryopreservation, minimizing the conflicts with cryopreserving tissue-engineered constructs whole. Together, the system represents an alternative approach to incorporating cryopreservation with prospective additional uses in tissue or disease modeling, scale-up production of 3D cultures, and studying the effects of cryopreservation.

TABLE OF CONTENTS

LIST OF FIGURES

CHAPTER 1

CHAPTER 3

CHAPTER 4

CHAPTER 5

CHAPTER 6

CHAPTER 7

CHAPTER 8

LIST OF APPENDICES

CHAPTER 1

Introduction

1.1 Problem statement

Increasing motivation to develop novel cell therapy strategies

Cell-based therapies, tissue engineering, and 3D organoid tissue models have been a growing topic of interest within biomedical research, transforming what was deemed science fiction into a possibility on the horizon. While some researchers see obstacles that will take tremendous effort to overcome with specific tissues, treatments like chimeric antigen receptor (CAR) T-cell therapies have dramatically altered the capacity to treat lymphoid malignancies [1]. In the early years of tissue engineering, the term was applied for prosthetic devices and surgical manipulation of tissues. These treatments do not include the generation of new tissue utilizing biological tissue or cells, materials, and signals described as tissue engineering today [2]. Despite many advances, the future challenges of the early 2000s persist: problems associated with scaling up production and cell death associated with implantation. Coinciding with these challenges, organ transplants remain the primary method for obtaining replacement tissues, resulting in an increasing number of patients on the organ transplant waitlist [3]. To meet the large-scale demand for tissues and organs is an ever-present challenge being addressed by many biomedical engineers.

One topic of interest to many biomedical engineers is developing vascularized tissue-engineered constructs or improving the vasculature of diseased tissue. Ischemic vascular diseases are a significant cause of mortality in the United States. In particular,

peripheral artery disease (PAD) can result in loss of limb function or death and currently affects over 25 million Americans [4]. Many who suffer from critical limb ischemia, an advanced form of PAD, succumb to their condition even after treatments because their cells are dysfunctional and unresponsive to drug treatments [5]. The dysfunction of native cells has led to a growing interest in cell-based therapies, but revascularization rates with these strategies still present a challenge [6, 7]. Given the more recent events with COVID-19, the need to address endothelial diseases is more pertinent than ever [8].

Trends in tissue engineering: spheroids and hydrogels

Traditionally, clinical cell therapy involves the systemic infusion or local bolus injection of cells to the body [9]. Typically, these strategies will result in low local viability [10], and *ex vivo* manipulation of cells is expensive and time-consuming. Researchers have been exploring and advocating for two prospective methods to improve cell delivery outcomes: the use of biomaterials and 3D aggregates of cells, commonly referred to as spheroids [11-15]. While many prospective cell-based therapies face challenges because more than 90% of cells transplanted rapidly die [16], spheroids and cells encapsulated in biomaterial-derived hydrogels can act as functional units to develop more functional tissue constructs. For example, the concept of developing endothelial spheroids or encapsulated spheroids in a hydrogel as a vascularization unit is one application for cell therapy or tissue model. Notably, the ineffective oxygen diffusion to the core of the spheroid or hydrogel could trigger the upregulation of hypoxia-inducible factor (HIF-1α) [17]. Spheroids greater than 100 μm have exhibited a greater upregulation of HIF-1α and vascular endothelial growth factor (VEGF) compared to smaller spheroids [17, 18],

suggesting a potential benefit of encapsulation of these into larger hydrogels to induce similar outcomes. Nevertheless, some cell types, such as mesenchymal stromal cells (MSCs), appear to distribute their cell density within the aggregate to prevent hypoxia [19]. Unsurprisingly, many studies into potential cell therapies have increasingly incorporated these perspectives of hydrogels and spheroids (Figure 1.1). Although the amount of published work into cell therapies increases each year, other terms, like alginate, remain relatively constant relative to this overall growth. The accelerating adoption of hydrogels and spheroids into research of potential cell therapies emphasizes the excitement that these approaches to tissue engineering aspire in researchers. Nevertheless, for clinical success, a holistic approach, incorporating processes and research required to scale up production under good manufacturing practices to develop a product with an established quality, shelf life, and standard operating procedure for clinicians, would increase the probability of success.

Cryopreservation and the incorporation of manufacturing perspectives

From organ and tissue transplantation to tissue-engineering strategies, novel technologies should tolerate cryopreservation to enable outsourced manufacturing, transportation, and the inevitable delays due to logistical hurdles [20]. Cryopreservation, the storage of cells in frozen stasis, is likely necessary for cell therapies to reach actuation in clinics. However, the freezing and thawing process has demonstrated negative consequences to MSC replication [21, 22], unintended differentiation and poor recovery of embryonic stem cells [23], and morphological and functional changes in hepatocytes [24]. Given that these consequences directly contrast the intended use of these cells as

therapies, there is motivation to study ways to improve cryopreservation with developing treatments. Nevertheless, the incorporation of cryopreservation within cell therapy research has steadily declined since the late 1990s (Figure 1.2). Notably, this is not to say studies have been declining, but the number of publications on cell therapies is outstripping efforts to incorporate cryopreservation. These trends in publications are also occurring in clinical trials; of the over 35,000 clinical trials into cell therapies ongoing or otherwise, about 0.54% of those incorporated cryopreservation (Figure 1.3). This trend is worse with active trials, with only 0.49%. To create better outcomes from clinical trials, it will be necessary to understand best practices for cryopreserved cells and how cells are damaged. The primary stage influencing cell survival during cryopreservation is not the storage at the ultralow temperatures but the dynamic stages of freezing and thawing [22]. During these periods, the cells are exposed to conditions that can destroy cell membranes and organelles by intracellular and extracellular ice formation [25-28]. While those conditions are actively avoided by placing cells in a hypertonic solution, osmotic effects may also cause damage in the form of denatured proteins and osmotic shock [29, 30]. Critically, this transition would occur during vital stages of manufacturing and delivery. For example, a cryopreservation stage could be involved after cells are seeded onto a scaffold during manufacturing and thawed before being applied to a patient. With the many potential opportunities for cell therapy to fail, biomedical advancements which incorporate cryopreservation perspectives may be a beneficial holistic approach to developing model tissues, tissue engineering constructs, or cell therapies.

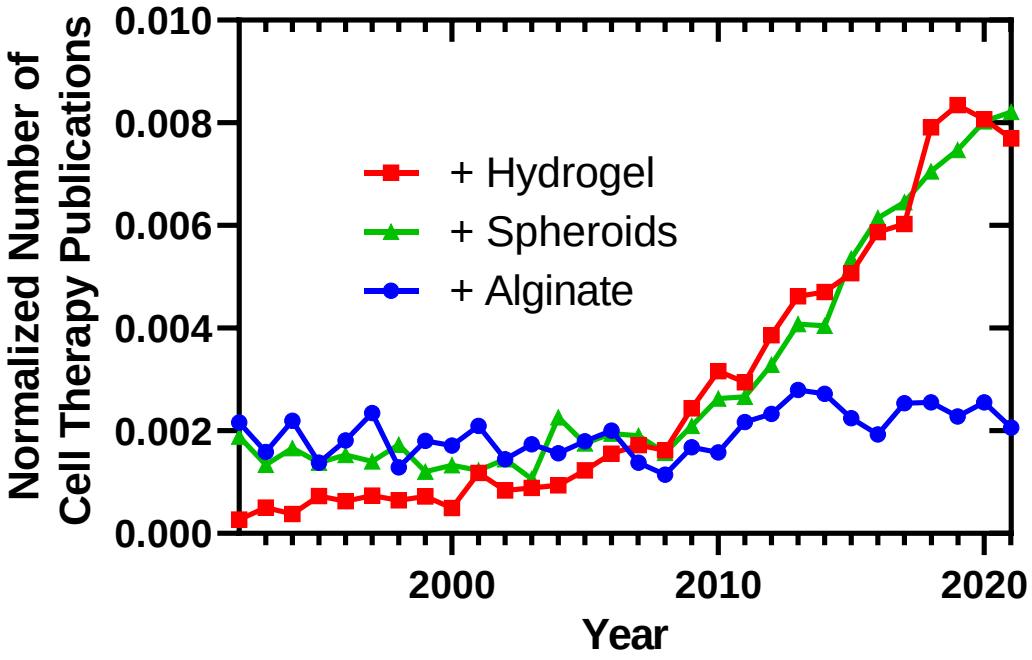

Figure 1.1 The number of published research of cell therapies increasingly incorporate hydrogels and spheroids. The number of published research since 1992 was collected on pubmed.gov. These amounts were found by searching the terms “cell therapy,” “cell therapy + hydrogels,” “cell therapy + spheroids,” and “cell therapy + alginate.” To better understand how the secondary terms have changed with respect to cell therapy research, we normalized the two term search results by the search results for “cell therapy” alone.

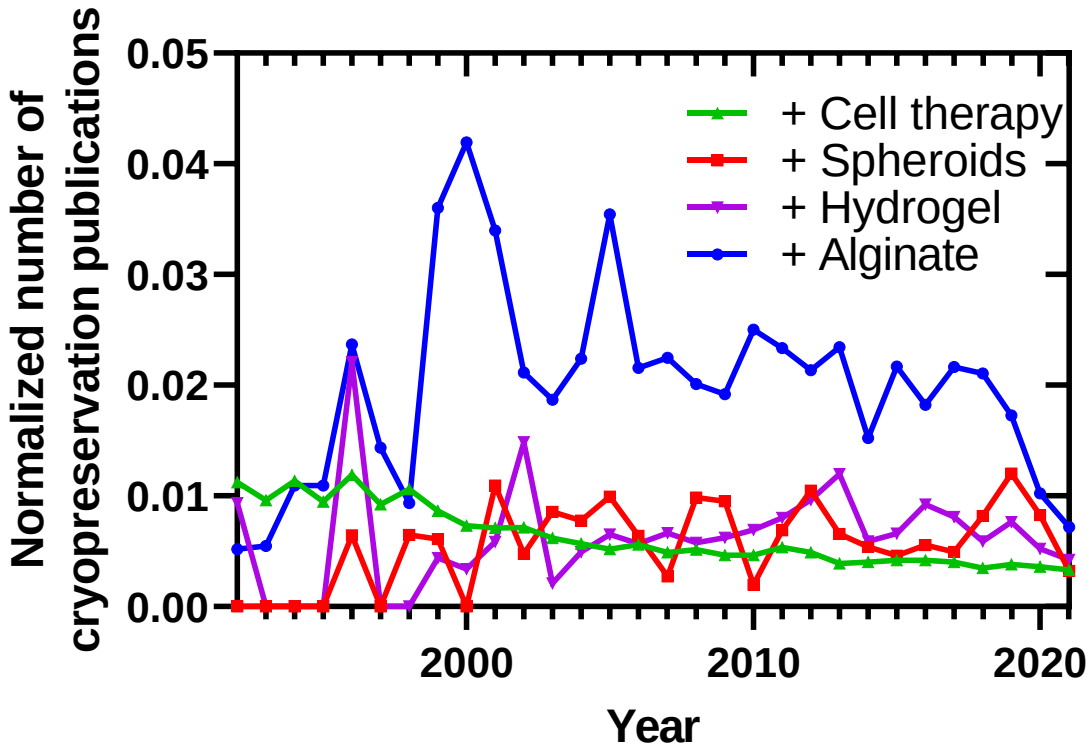

Figure 1.2 The number of published research into popular trends of cell therapies has had steady or decreasing incorporation of cryopreservation. The number of published research since 1992 was collected on pubmed.gov. These amounts were found by searching the terms “cell therapy,” “hydrogels,” “spheroids,” and “alginate” with and without the additional term “cryopreservation.” To better understand how research had changed their incorporation of cryopreservation, we normalized the values obtained from the two-term search results by the search results for each term alone (i.e., [“Alginate + Cryopreservation”] / [“Alginate”]).

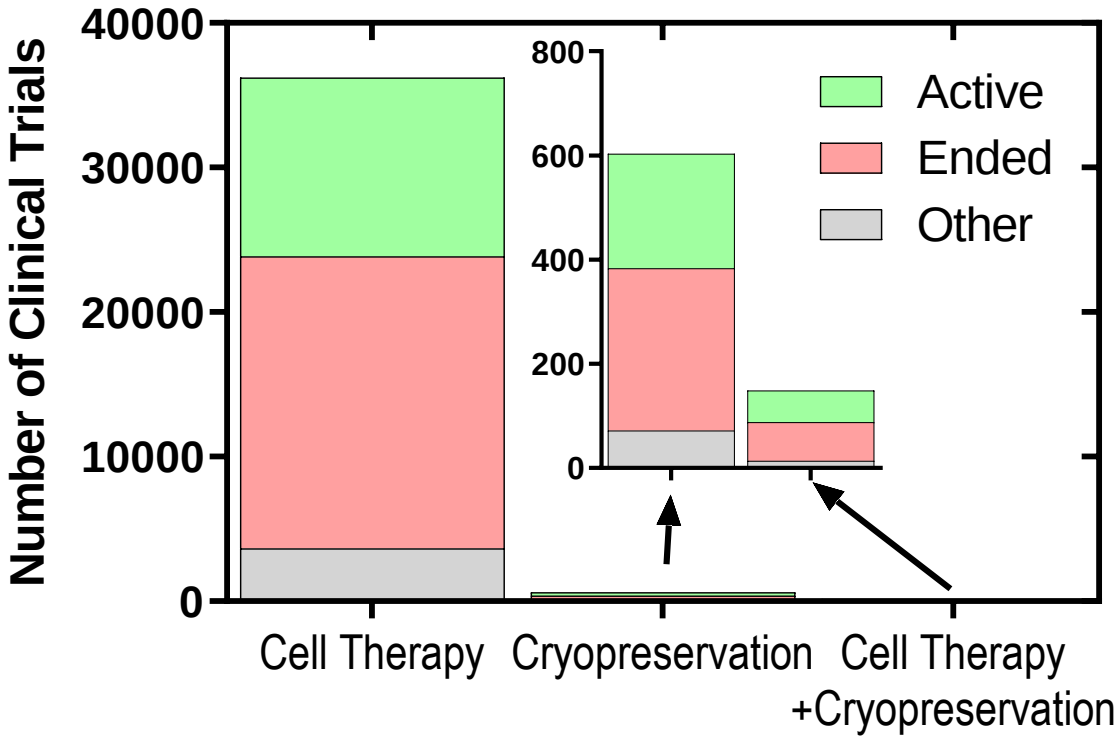

Figure 1.3 A marginal number of clinical trials incorporate cryopreservation compared to the overall number of cell therapy clinical trials. Data gathered from clinicaltrials.gov indicate several ongoing and ended clinical trials for cell therapies as of early 2021. The number of clinical trials referencing cryopreservation is less than 2% compared to cell therapies. Less than one-third of those are clinical trials referencing both terms.

1.2 Hypothesis and specific aims

The global hypothesis guiding this dissertation is that alginate hydrogels created by thaw-induced gelation can instruct cell recovery post-cryopreservation and be cryoprotective for encapsulated cargo, leading to improved cell viability, metabolic recovery, and function of cryopreserved cells. This hypothesis has been addressed with the following specific aims:

Aim 1: Develop and characterize the strategy of thaw-induced gelation as a method for creating alginate hydrogels from previously frozen samples.

Aim 2: Characterize and optimize critical properties of these hydrogels for encapsulating previously frozen proteins and cryopreserved cells.

Aim 3: Using thaw-induced gelation as a potential strategy, determine an optimal procedure for developing endothelial spheroids from HUVECs, post-cryopreservation.

1.3 Significance

The strategies developed and many outcomes in this thesis may considerably influence a new trend in cryopreservation research of potential tissue models and cell therapies. Current practices are to apply cryopreservation directly to preestablished tissue engineering strategies. However, this trend in research does not prioritize the necessary processes required to create cell therapies or models as a product. While it is well understood that clinical success or cell models for industrial research will require scalable techniques, these products will also require long-term storage and transport. To date,

clinical trials incorporating cryopreservation within their protocols have been severely lacking and are even cited as a cause for clinical trial failure [31-33]. Nevertheless, new and exciting tissue-engineered constructs are being developed without the cryopreservation perspective. Therefore, this work represents one of the first attempts to design biomaterial strategies to encapsulate and instruct previously cryopreserved cells. This process is intertwined with cryopreservation, synergizing the effects of freezing and thawing into functional outcomes. The developments discussed in this thesis provide many platforms for incorporating hydrogels with post-cryopreserved cells that may provide broad utility for previously considered applications of these materials in tissue engineering applications of cell therapies or tissue models.

1.4 Thesis overview

The following chapters will look at the background and motivation of the problem, the current state of the field in addressing these issues, and how the work presented in this dissertation contributes towards enabling tissue-engineered cell constructs to be created post-cryopreservation with instructive hydrogels. Chapter 2 introduces biological and engineering concepts that serve as the foundation of the work in this thesis. Chapter 3 addresses the first aim by describing the development of the thaw-induced gelation (TIG) technique and its potential use in controlled-release systems. Chapters 4 and 5 describe the formation of alginate hydrogels from a frozen alginate solution crosslinked via TIG, expanding on aim 1 by describing their unique mechanical properties. This work extended into aims 2 and 3 with the cryopreservation of cells, potentially resulting in an alginate cryogel described in chapter 5 and potential cryoprotective benefits for growth

factors expected to influence growth factors vasculogenic potential of endothelial cells in chapter 4. Chapters 6, 7, and 8 use the alternative TIG outcome of hydrogel capsules. While chapters 6 and 7 were done in parallel to work presented in chapters 4 and 5, the alginate capsules were the foundation for our studies addressing aim 3 in chapter 8, establishing whether it is better to form a spheroid from post-cryopreserved cells in a dispersed solution or to cryopreserve whole spheroids. Chapter 9 closes with the conclusions on the significance of this work, suggestions for future work, and the potential outcomes of these next steps.

1.5 References

[1] D. Sermer and R. Brentjens, "CAR T-cell therapy: Full speed ahead," (in eng), *Hematol Oncol,* vol. 37 Suppl 1, pp. 95-100, Jun 2019, doi: 10.1002/hon.2591.

[2] C. A. Vacanti, "The history of tissue engineering," (in eng), *Journal of cellular and molecular medicine,* vol. 10, no. 3, pp. 569-576, Jul-Sep 2006, doi: 10.1111/j.1582-4934.2006.tb00421.x.

[3] "National Waitlist Additions through November 19, 2021." http://optn.transplant.hrsa.gov (accessed.

[4] D. Lloyd-Jones *et al.*, "Heart disease and stroke statistics--2010 update: a report from the American Heart Association," (in eng), *Circulation,* vol. 121, no. 7, pp. e46-e215, Feb 23 2010, doi: 10.1161/circulationaha.109.192667.

[5] G. O. Ouma, M. H. U. Jonas Ra Fau - Usman, E. R. Usman Mh Fau - Mohler, 3rd, and E. R. Mohler, 3rd, "Targets and delivery methods for therapeutic angiogenesis in peripheral artery disease," (in eng), no. 1477-0377 (Electronic).

[6] L. L. Y. Chiu, M. Montgomery, Y. Liang, H. Liu, and M. Radisic, "Perfusable branching microvessel bed for vascularization of engineered tissues," *Proceedings of the National Academy of Sciences,* 10.1073/pnas.1210580109 vol. 109, no. 50, p. E3414, 2012.

[7] W. Suh *et al.*, "Transplantation of endothelial progenitor cells accelerates dermal wound healing with increased recruitment of monocytes/macrophages and neovascularization," (in eng), *Stem cells (Dayton, Ohio),* vol. 23, no. 10, pp. 1571-8, Nov-Dec 2005, doi: 10.1634/stemcells.2004-0340.

[8] P. Libby and T. Lüscher, "COVID-19 is, in the end, an endothelial disease," (in eng), *Eur Heart J,* vol. 41, no. 32, pp. 3038-3044, Sep 1 2020.

[9] P. A. Williams and E. A. Silva, "The Role of Synthetic Extracellular Matrices in Endothelial Progenitor Cell Homing for Treatment of Vascular Disease," (in eng), *Ann Biomed Eng,* vol. 43, no. 10, pp. 2301-13, Oct 2015, doi: 10.1007/s10439-015-1400-x.

[10] E. A. Silva, E. S. Kim, H. J. Kong, and D. J. Mooney, "Material-based deployment enhances efficacy of endothelial progenitor cells," (in eng), *Proc Natl Acad Sci U S A,* vol. 105, no. 38, pp. 14347-52, Sep 23 2008, doi: 10.1073/pnas.0803873105.

[11] H. Gurruchaga *et al.*

[12] E. M. Anderson, B. J. Kwee, S. A. Lewin, T. Raimondo, M. Mehta, and D. J. Mooney, "Local delivery of VEGF and SDF enhances endothelial progenitor cell recruitment and resultant recovery from ischemia," (in eng), *Tissue engineering. Part A,* vol. 21, no. 7-8, pp. 1217-1227, 2015, doi: 10.1089/ten.TEA.2014.0508.

[13] S. S. Ho, K. C. Murphy, B. Y. Binder, C. B. Vissers, and J. K. Leach, "Increased Survival and Function of Mesenchymal Stem Cell Spheroids Entrapped in Instructive Alginate Hydrogels," (in eng), *Stem Cells Transl Med,* vol. 5, no. 6, pp. 773-81, Jun 2016.

[14] N. Gjorevski *et al.*, "Designer matrices for intestinal stem cell and organoid culture," in *Nature*, vol. 539, no. 7630). England, 2016, pp. 560-564.

[15] A. L. Torres, S. J. Bidarra, M. T. Pinto, P. C. Aguiar, E. A. Silva, and C. C. Barrias, "Guiding morphogenesis in cell-instructive microgels for therapeutic

angiogenesis," *Biomaterials,* vol. 154, pp. 34-47, 2018/02/01/ 2018, doi: https://doi.org/10.1016/j.biomaterials.2017.10.051.

[16] M. Hofmann *et al.*, "Monitoring of bone marrow cell homing into the infarcted human myocardium," (in eng), *Circulation,* vol. 111, no. 17, pp. 2198-202, May 3 2005, doi: 10.1161/01.Cir.0000163546.27639.Aa.

[17] S. H. Bhang *et al.*, "Angiogenesis in ischemic tissue produced by spheroid grafting of human adipose-derived stromal cells," *Biomaterials,* vol. 32, no. 11, pp. 2734-2747, 2011/04/01/ 2011, doi: https://doi.org/10.1016/j.biomaterials.2010.12.035.

[18] M. L. Skiles, S. Sahai, L. Rucker, and J. O. Blanchette, "Use of Culture Geometry to Control Hypoxia-Induced Vascular Endothelial Growth Factor Secretion from Adipose-Derived Stem Cells: Optimizing a Cell-Based Approach to Drive Vascular Growth," *Tissue Engineering Part A,* vol. 19, no. 21-22, pp. 2330-2338, 2013/11/01 2013, doi: 10.1089/ten.tea.2012.0750.

[19] K. C. Murphy *et al.*, "Measurement of oxygen tension within mesenchymal stem cell spheroids," (in eng), *J R Soc Interface,* vol. 14, no. 127, Feb 2017.

[20] B. Hampson. "5 Considerations in the Preparation for Commercializing Cell Therapy." https://www.pctcelltherapy.com/pct-pulse/5-considerations-in-the-preparation-for-commercializing-cell-therapy (accessed 2018).

[21] S. Renzi, T. Lombardo, S. Dotti, S. S. Dessì, P. De Blasio, and M. Ferrari, "Mesenchymal stromal cell cryopreservation," (in eng), *Biopreserv Biobank,* vol. 10, no. 3, pp. 276-81, Jun 2012, doi: 10.1089/bio.2012.0005.

[22] D. Freimark *et al.*, "Systematic parameter optimization of a Me(2)SO- and serum-free cryopreservation protocol for human mesenchymal stem cells," in *Cryobiology*, vol. 63, no. 2). Netherlands: © 2011 Elsevier Inc, 2011, pp. 67-75.

[23] V. Wagh *et al.*, "Effects of cryopreservation on the transcriptome of human embryonic stem cells after thawing and culturing," (in eng), *Stem Cell Rev Rep,* vol. 7, no. 3, pp. 506-17, Sep 2011, doi: 10.1007/s12015-011-9230-1.

[24] X. Stéphenne, M. Najimi, and E. M. Sokal, "Hepatocyte cryopreservation: is it time to change the strategy?," (in eng), *World J Gastroenterol,* vol. 16, no. 1, pp. 1-14, Jan 7 2010.

[25] D. Gao and J. K. Critser, "Mechanisms of Cryoinjury in Living Cells," *ILAR Journal,* vol. 41, no. 4, pp. 187-196, 2000, doi: 10.1093/ilar.41.4.187.

[26] E. Müller-Schweinitzer, W. Brett, H.-R. Zerkowski, and W. E. Haefeli, "The mechanism of cryoinjury: In vitro studies on human internal mammary arteries," *British Journal of Pharmacology,* https://doi.org/10.1038/sj.bjp.0703326 vol. 130, no. 3, pp. 636-640, 2000/06/01 2000, doi: https://doi.org/10.1038/sj.bjp.0703326.

[27] S. L. Ebertz and L. E. McGann, "Cryoinjury in endothelial cell monolayers," (in eng), *Cryobiology,* vol. 49, no. 1, pp. 37-44, Aug 2004, doi: 10.1016/j.cryobiol.2004.04.003.

[28] A. B. Sultani, L. A. Marquez-Curtis, J. A. Elliott, and L. E. McGann, "Improved Cryopreservation of Human Umbilical Vein Endothelial Cells: A Systematic Approach," (in eng), *Sci Rep,* vol. 6, p. 34393, Oct 6 2016.

[29] J. O. M. Karlsson and M. Toner, "Long-term storage of tissues by cryopreservation: critical issues," *Biomaterials,* vol. 17, no. 3, pp. 243-256, 1996/01/01/ 1996, doi: https://doi.org/10.1016/0142-9612(96)85562-1.

[30] X. Xu, Y. Liu, Z. Cui, Y. Wei, and L. Zhang, "Effects of osmotic and cold shock on adherent human mesenchymal stem cells during cryopreservation," in *J Biotechnol*, vol. 162, no. 2-3). Netherlands: © 2012 Elsevier B.V, 2012, pp. 224-31.

[31] M. Benekli, B. Anderson, D. Wentling, S. Bernstein, M. Czuczman, and P. McCarthy, "Severe respiratory depression after dimethylsulphoxide-containing autologous stem cell infusion in a patient with AL amyloidosis," *Bone Marrow Transplantation,* vol. 25, no. 12, pp. 1299-1301, 2000/06/01 2000, doi: 10.1038/sj.bmt.1702452.

[32] M. A. Higman, J. D. Port, N. J. Beauchamp, and A. R. Chen, "Reversible leukoencephalopathy associated with re-infusion of DMSO preserved stem cells," *Bone Marrow Transplantation,* vol. 26, no. 7, pp. 797-800, 2000/10/01 2000, doi: 10.1038/sj.bmt.1702589.

[33] G. Moll *et al.*, "Cryopreserved or Fresh Mesenchymal Stromal Cells: Only a Matter of Taste or Key to Unleash the Full Clinical Potential of MSC Therapy?," in *Biobanking and Cryopreservation of Stem Cells*, F. Karimi-Busheri and M. Weinfeld Eds. Cham: Springer International Publishing, 2016, pp. 77-98.

CHAPTER 2

Review of biomaterials and spheroids use in therapeutic angiogenic applications and consequential influences from cryopreservation and frozen storage

2.1 Introduction

This chapter provides the contextual and conceptual framework, background knowledge, and interactions between concepts that set up and motivate the central hypothesis of this thesis. We first provide a background of therapeutic angiogenesis strategies to address the motivations for using hydrogels and spheroids. Next, a background in cryopreservation, including the history and critical insights, will be discussed. This discussion will introduce important engineering design parameters for therapeutic angiogenesis, spheroids, hydrogels, and cryopreservation. Together, the interactions between techniques will highlight the interconnected parameters that influence the therapeutic efficacy of cell therapy strategies, indicating the need for further research to improve the clinical success of tissue engineering strategies.

2.2 Motivation for cell-based therapies

The continual interest in cell therapies for treating disease and regenerating tissue has resulted in a growing industry motivated to develop equally diverse and robust systems. In 2014, the stem cell market was projected to reach $330 million by 2020, despite the current $187 million market [1]. The cell therapy market is currently projected

to grow to $401 million by 2026 [2]. While this disconnect between expectations and outcomes could be due to the excitement around the potential benefits of this technology, factors not considered within the research stages could be placing restraints on the growth of this field. At present, the field is dominated by research and research support activities.

Consequently, to successfully translate cell therapies to the clinic, aspects required for the industry need to be considered at the research level. For example, cell source, storage, and expansion are clinical concerns to be addressed. Cell storage and expansion can be addressed by utilizing cryopreservation techniques and supporting biomaterials to enable three-dimensional cell cultures that facilitate "on-demand" access to these treatments to patients [3]. Other challenges can be addressed partially through cryopreservation, but still need to be considered. These can include transportation of the cell-based product to the patient-treatment site and, more importantly, expanding the cells to a therapeutic dose. Despite this understanding, research efforts are primarily addressing a specific disease using approaches that incorporate the tissue engineering triad: cell, biomaterial scaffold, and signals [4]. Although these attempts are holistic in addressing different aspects of tissue, additional product development perspectives will be necessary to translate these to regenerative medicines. To further build an appreciation for tissue-engineered constructs as products, technologies, and processes being developed by biomedical researchers on the topic of cardiovascular diseases.

2.3 Examples of tissue engineering for cardiovascular diseases

We believe the work presented in this thesis could apply to many future tissue engineering applications. Nonetheless, we will address the topic of therapeutic neovascularization and angiogenesis as foundational motivations for our work. Cardiovascular diseases have been estimated to affect 49.2% of adults over 20 years old [5]. There is a need for new therapeutic strategies to reduce the loss of function or death because of these diseases. Vascular complications are commonly associated with problematic healing, potentially leading to wound ischemia. One possible direct treatment of ischemia is to promote vascularization of the tissue. However, vascularization of the wound site can take several days. In one study, it took 14 days for the capillaries of a vascular model developed *in vitro* to integrate with the native vasculature [6]. In a wound, the first five days usually involve activity from macrophages and monocytes for remodeling and infection control [7]. Generally, healing and repair take time, and this time is extended in diseased tissue.

Consequently, there are ever-growing economic motivations to treat these diseases: the estimated direct cost of cardiovascular diseases per year doubled between 1996 and 2016 [5]. There have been over 80 clinical trials using patients' cells reinfused *in vitro* with cell-based therapies for revascularization using endothelial progenitor transplants having modest success [8-10]. Nevertheless, bolus delivery of endothelial progenitor cells can be ineffective in preventing necrosis in ischemic murine limbs [8]. While there are numerous approaches to combat these issues, in particular, the use of spheroids and hydrogels suggests a simple approach in which forming cells into a 3D conformation viability and function. Generally, the incorporation of cells, a scaffolding material, and appropriate signals can improve outcomes for cell-based therapies by

improving cell viability, keeping cells on task, and keeping cells localized in the region of interest.

The design of a hydrogel for therapeutic angiogenesis typically needs to be biocompatible, non-toxic, and provide topographical and chemical cues. These requirements are derived from the cellular invasion, directionality, and correct polarity required for lumen formation [11, 12]. For example, material-based methods to deliver recruiting and homing factors have been used to control release for neovascularization and revascularization applications [12]. In this context, the objective with materials is to create gradients of the factors which will promote local healing, such as through the recruitment of endogenous endothelial progenitor cells [12]. The limiting factor with this approach is the potential exhaustion of deliverable factors before endothelial cells arrive. Another instructive outcome provided by some hydrogels is controlling nutrient and oxygen diffusion to the cells [13-16]. The conditions created from hydrogels can prime cells for the, often, nutrient deficit and hypoxia environment of ischemic tissue [17-20]. Grossly, hydrogels can direct the conditions in which loaded elements like cells and growth factors interact with the target tissues.

Spheroids are another system being considered as an improvement over the delivery of individual cells. Spheroids create and impose physical interactions that more closely reflect the behavior of native tissue compared to individual cells [21]. This is because spheroids retain endogenous ECM to promote connections with each other and their environment, resulting in prolonged cell survival [27-29]. The transplantation of mesenchymal stem cells (MSCs), also called mesenchymal stromal cells, as spheroids have been shown to prevent apoptosis and increase cell function [22]. Moreover, the use

of endothelial cells as spheroids has been shown to improve their vasculogenic potential compared to dispersed cells [23]. Mechanistically, cell-cell adhesion in endothelial cells is performed mainly by VE-cadherins [24]. Vascular endothelial growth factor receptor 2 (VEGFR2) forms a complex with VE-cadherin for survival and angiogenesis [25]. Spheroids also improve post-implantation cell viability and keep cells more localized at the delivery site compared to individual cells [26]. Therefore, spheroids are an appealing approach for addressing the functional repair mechanism of cells.

Lastly, cell signals are another vital aspect for ensuring the efficacy of revascularization strategies. Generally, random spatial distribution is undesirable in creating vasculature due to effects on perfusion [6, 27, 28]. The outcome of irregularly organized networks leads to the pruning of vessels [11]. Therefore, there is a need to provide a spatial cue for the directional growth of vessels. The use of spheroids provides a point source of cells that can then interact with any environmental cues to form sprouts. Furthermore, hydrogels can provide mechanical cues to direct sprouting and migration behavior [15, 29]. Additionally, hydrogels and spheroids can provide mechanical cues to direct cellular phenotype for vascularization [15, 30-32]. Among the signaling mechanisms briefly described, this aspect of tissue engineering provides directions for regenerative strategies.

At this time, methods for creating vessels are focused on *in vitro* models [33-36]. While these models are excellent for drug discovery and organ-on-chip applications, their potential for clinical translation currently presents significant challenges. These models are difficult to translate into a transplantable scaffold due to the tight geometries of the microfluidic device, resulting in a small construct that is difficult to remove. Furthermore,

the isolation of capillaries developed *ex vivo* takes time and would likely require cryopreservation for transport or storage. To overcome current challenges in cell-therapy translations to clinical settings, steps need to be simplified, synchronized, and scalable.

2.4 Advances in spheroid culture

The use of spheroids offers many advantages for instructing cells' function that can better recapitulate the desired healing response *in vivo*. While the 3D structure could lead to heterogeneous responses dependent on aggregate size and composition, the response is typically seen as a magnitude desired by tissue engineering. As previously described, there is an inherent need to enhance cell viability and post-implantation performance in cell therapies. Spheroids overcome some of these limitations compared to single cells but face further challenges with insufficient cells and damage from cryopreservation [26, 37-40]. Despite this, spheroids are becoming increasingly popular in cell therapy research. For example, MSCs have the potential to differentiate into chondrocytes, osteocytes, adipocytes, and hepatocytes. Fittingly, the capability of these differentiated outcomes can be improved in spheroid cultures [41-43]. Furthermore, spheroids can act as vascularization units: the inefficient oxygen diffusion to cells in the core of spheroids has been shown to trigger the upregulation of hypoxia-inducible factor (HIF-1α) [18]. Notably, spheroids greater than 100 μm have exhibited a more significant upregulation of HIF-1α and vascular endothelial growth factor (VEGF) than smaller spheroids [18, 44]. Additionally, spheroids have been shown to have a higher expression of stromal cell-derived factor (SDF)-1 [18], a hypoxia-regulated chemokine important for the homing of endothelial progenitor cells to develop microvasculature [14]. Therefore,

implanted cell aggregates are generally considered to remain more localized at the implantation site and perform their desired function better than dispersed cells.

Spheroids can be developed with a variety of methods. Essentially, spheroids are cells formed into 3D architectures supported by intensive cell-cell contacts and endogenous ECM [21], which prolong cell survival and direct differentiation [45-47]. Therefore, researchers employ many methods to form spheroids that encourage these cell-cell interactions: hanging drop [46, 48], spinner flasks [41], microfluidic devices [49], and low-adhesion substrates [23]. Static methods are typically gravity-driven, gentle, and can vary in labor and output. However, the static environments in microwells or hanging drop have been noted to result in depletion of nutrients and concentrate cell waste [50]. In contrast, spinner flasks involve shear forces that produce multiple spheroids of various sizes but expose cells to potentially destructive shear forces. Generally, unless convective fluid flow is involved, such as with the spinner flask method, diffusion limitations affect nutrients' availability and exposure to cellular waste. In order to meet the number of spheroids necessary for generating tissue, efficient spheroid fabrication methods must be compatible with scaling-up and automatization [21]. The importance of this manner has been a focus in new research, such as developing wrinkle patterns formed by swelling a non-adhesive hydrogel to generate thousands of MSC spheroids in a single well [51]. As an alternative to this method which results in varying spheroid sizes, microwells stamped into agarose can create hundreds of spheroids that are more monodispersed [52-54]. Generally, the formation of spheroids can be as simple as bringing cells together, but geometry, cell density, and substrate can direct the efficacy of spheroid formation.

The appropriate cell density is vital for controlling the efficiency in which aggregation occurs and the size of the spheroid [55, 56]. Moreover, local cell density is a crucial component preventing dissociated cells from undergoing apoptosis without a substrate [57-59]. At a minimum, anchorage-dependent cells will often slow down proliferation without cell-cell interactions [60]. Consequentially, seeding density can impact the functional outcomes of therapeutic cells. In one study, MSC spheroids formed from an initial 40,000 cells appear to produce more VEGF, normalized to DNA content, than smaller spheroids formed from 10,000 cells [56]. Nevertheless, some cell types, like MSCs, can self-regulate their density as spheroids [55], resulting in spheroids that did not develop necrotic cores at sizes other cell types would. Notably, while too few cells result in a dissociated cell environment ending in apoptosis [58, 61], once formed, spheroids can exhibit enhanced resistance to apoptosis [31, 56, 62]. Together, these studies indicate how functional outcomes from spheroids can depend on cell type and number.

Moreover, 3D dimensional cell cultures are not limited to spheroids; rods, tori, and honeycombs can also be generated by specific microscale geometries [52]. These geometries affect the diffusible gradient of nutrients and cell signaling [61; 62] and mechanical forces [63]. Specifically, circular wells were better than rectangular in microwell-based systems due to better diffusion of nutrients and oxygen [64]. These geometries can be quickly produced with non-adherent materials, such as agarose, by making stamps or molds [53, 54]. Not all materials need to be non-adherent as well. Fibrinogen-modified PEG-DA hydrogels were previously used to study the influence of mechanical stiffness on the spheroid formation of Huh7.5 cells [65]. Their results suggested that softer matrices, which mimicked normal liver tissue, led to more

proliferation and albumin secretion. Moreover, some additives to spheroid culture can prevent cells from interacting with surfaces. Methylcellulose is a material often added to techniques employed for spheroid formation, limiting cell-environment interactions, resulting in preferential cell-cell aggregation [66]. Therefore, additional important parameters in spheroid formation are the vessel's geometry and how cells interact with the vessel.

Even with their appeal, spheroids are often more challenging to characterize thoroughly than individual cells. Techniques that require individual cells become complicated to perform with spheroids as the cell aggregates must be digested. Broadly, high-throughput screening analytical protocols well established for 2D cell cultures can be rendered useless in 3D [67]. For example, lactate dehydrogenase (LDH) cell viability assays can show fluorescence even after chemically stopping the reaction [68]. Moreover, confocal imaging has a limited penetration depth, making it difficult to characterize the behavior difference from different spheroid sizes [69]. Notably, for assays requiring the digestion of larger spheroids, the necrotic cores of cells appeared more resistant to degradation. Similarly, we suspect diffusion limitations of analytes prevent an adequate assessment of the whole spheroids. These concerns were also recognized in the context of spheroid staining with larger molecules, such as antibodies [70]. Therefore, although spheroids improve the relevance of *in vitro* results, they present analytical challenges.

2.5 Application of hydrogels for cell delivery

Successful cell transplantation can be summarized in three outcomes for cells: survival, migration, and integration [71]. Spheroids have been shown to improve cell survival and migration, highlighting a recurring theme where anchorage-dependent cells benefit from cell-cell contacts. Therefore, while cell-material contacts can promote cell survival, cell-cell contacts should also be considered in biomaterial approaches, such as promoting the formation of spheroids or encapsulation of spheroids. Hydrogels are an appealing class of biomaterials as they can maintain phenotype by reducing exposure of the encapsulated cells to their environment [72]. Hydrogels are non-soluble networks of polymer whose volume is primarily composed of water. The resulting mesh holds some structural similarities to the extracellular matrix, and, consequently, hydrogels are often designed to mimic the extracellular matrix for their targeted cell. For example, an increased mesh size has been shown to increase cellular proliferation for MCF-7 breast cancer cells and MC3T3-E1 osteoprogenitor cells [73, 74]. Alternatively, the encapsulation of cells within hydrogel capsules can improve the function of cells. For example, hepatocytes within a poly(ethylene glycol) (PEG) capsule showed greater albumin expression within the capsules than the AggreWell system [75]. Even with a 17% loss in viability [75], the capsule's mechanical and diffusive properties can be tuned, enabling large-scale suspension cultures of anchorage-dependent cells or tissues protected from the shear forces of the convective media [76]. Together, hydrogels show advantages as instructive material and as an engineered extracellular matrix.

Alginate is an appealing material for making hydrogels as it is considered to undergo a mild gelation process and will not produce some harmful immunogenic responses that could occur in some synthetic polymers [77]. Alginate is a naturally

occurring block copolymer composed of (1-4)-linked β-D-mannuronate (M) and α-L-guluronate (G) residues. It is organized in blocks of repeating M, G, or alternating M and G residues [78, 79]. These polymers have a high degree of coordination with divalent cations to blocks of G residues [80]. Essentially, alginate polymers undergo a gentle ionic cross-linking between different polymer chains facilitated by a divalent cation. The interaction of these two components leads to ionic cross-linking of hydrogels under conditions that are considered relatively mild [80], occurring in isotonic solutions at room temperatures. Beneficially, alginate does not readily degrade *in vivo* [81], lacks cellular recognition [82], and can be used as a framework where desired attributes can be developed by chemical or structural modification [29, 83-86].

Of the many methods for forming an alginate hydrogel, ionic cross-linking with calcium ions is one of the most prevalent. The divalent cation can be introduced internally, where it readily cross-links with surrounding polymer, or externally, requiring diffusion into the polymer. Consequentially for alginate hydrogels cross-linked by an external source of calcium, this approach generates heterogeneous hydrogels from the radial concentration gradient of calcium around the alginate [87]. However, the use of external gelation enables more rapid gelation than internal gelation methods using $CaCO_3$ [88, 89], chelated forms of calcium [90], and slow dissolving salts, such as $CaSO_4$ [16, 91-94]. Notably, the osmotic pressure created by adding the divalent cations to a solution should be considered to prevent osmotic stresses to cells. Notably, a 100 mM concentration of $CaCl_2$ commonly used to form alginate hydrogels is already very close to being an isotonic solution for cells (300 mOsmol/L). The addition of these salts to a solution will create a hypertonic solution. Therefore, although the gelation of alginate with the divalent cations

is considered to be mild, consideration of exposure time and magnitude are important engineering parameters for encapsulating cells.

As an instructional material to form spheroids or promote cell aggregation, cells do not actively bind to alginate [95]. While this property can be beneficial for promoting cell-cell interactions, another function of biomaterials is enabling cell spreading and adhesion to improve the survival and proliferation of anchorage-dependent cells [96, 97]. For example, RGD-modified alginate has been used to deliver stem cells for myocardial repair [98], resulting in increased angiogenesis and improved cell survival of human mesenchymal stem cells. Commonly, fibrin can be added to provide cell adhesion sites, permit scaffold remodeling, and promote the migration of cells out of the hydrogel [77, 99]. Fibrin is a naturally occurring scaffold material for leukocytes and endothelial cells utilized during wound healing that can be obtained from plasma [100-102]. The viscosity of fibrin can be controlled by altering NaCl concentrations [103]. Furthermore, the strength of the fibrin gels might be enhanced by calcium ions [15], suggesting potential interactions with alginate gelation. Specifically, MSC spheroids in stiffer fibrin hydrogel secreted the most VEGF, but PGE_2 expression was higher in more compliant hydrogels [15]. While we only briefly discuss the use of fibrin in Appendix B, these gels are particularly interested as they have been shown to promote wound healing of MSCs by the production of VEGF and PGE2 [15, 62]. Unlike alginate, fibrin allows for cell binding and has multiple approaches to control degradation, including native cellular pathways for remodeling [104, 105]. The application of both could provide each material with distinct advantages for cells.

2.6 Cryopreservation: background, benefits, and challenges

Cryopreservation is currently the only process capable of preserving cells, tissues, and cell-based products for extended periods. This technology enables access and transport of these cells and their derivatives, such as what is done with biobanks [3, 106]. Successful cryopreservation should maintain the characteristics and functions of the cells. To accomplish this task, cells are suspended in a solution containing one or more cryoprotectants (CPAs) that aid in maintaining the viability during the transition to and from the low temperatures that effectively place the biological clock in a stasis [104]. While low temperatures are not inherently harmful to cells, inevitable damage occurs during the cooling and thawing from intracellular ice formation, extracellular ice formation, and osmotic forces [107-110]. Consequently, cryopreservation faces challenges of batch variability, lower cell function, and reduced cell viability.

The primary methods used to cryopreserve cells are vitrification and slow cooling. Both methods utilize a CPA to improve the survival rates, albeit at different concentrations [107, 111]. Vitrification involves the rapid freezing of samples using a high concentration of cryoprotectants, e.g., up to 40% (v/v) dimethyl sulfoxide (Me_2SO), such that the glass transition temperature is surpassed before ice formation occurs. Alternatively, slow cooling involves a controlled cooling rate, often -1 °C/min, with a lower CPA concentration, often less than 12% (v/v) Me_2SO. The slow cooling process dehydrates the cells to prevent intracellular ice formation when freezing. The method utilized for cryopreservation depends on the samples' size [112]. Specifically, vitrification is commonly used for smaller volumes of dispersed samples, such as the cryopreservation of oocytes at fertility clinics [108, 113]. These dispersed cells are placed in long tubes to

maximize the cooling rate to the cells, increasing the surface area to volume ratio compared to slow cooling cryopreservation vessels. Mechanistically, thermal energy crosses an area, referred to as thermal flux, to change the quality of the mass, specifically its thermal energy. The greater surface area to volume ratio of vitrification indicates more heat transfer per volume, either due to an increased volume or decreased volume. Therefore, tissue samples will inherently limit the rate of diffusion of the CPA and slow the cooling rate due to their larger three-dimensional structure compared to dispersed cells [114]. Therefore, vitrification becomes more challenging to accomplish in samples with a required volume to be cryopreserved. Consequently, larger cell constructs are typically cryopreserved through the slow cooling method. Similarly, cells encapsulated within hydrogels are also more likely to be cryopreserved with the slow cooling method [109]. Broadly, there are advocates of both cryopreservation methods, even when engineering barriers suggest the method would be disadvantageous.

Essential parameters for successful cryopreservation include the permeability of CPAs, the cooling rate, long-term storage temperatures, thawing rate, and the rate at which the CPA can be diluted. Consequently, applying the additional context of cryopreservation to studies comes with its own set of experiments. Expressly, it is widely accepted that the four-tiered approach argued by Baust et al. encompasses the regulatory requirement to demonstrate identity, purity, and stability of cell therapy products undergoing cryopreservation [115, 116]. This assessment includes membrane integrity, apoptotic and necrotic molecular mechanisms, functionality, and biochemical mechanisms encompassing genomic, epigenetic, and proteomic assays. Notably, assessment immediately after thawing could overestimate cell recovery as a substantial

amount of cell death from cryopreservation is apoptotic, occurring within 24 to 48 hours post-thawing [110, 117, 118]. Therefore, cells stressed by suboptimal culture conditions prior to cryopreservation may have impaired viability and function post-cryopreservation [115]; these outcomes might not be completely encapsulated with a membrane integrity assay or a metabolic activity assay, such as Alamar Blue.

Slow cooling cryopreservation involves a balance between dehydration and ice formation. Succinctly described, Peter Mazur's two-factor hypothesis of freezing injury suggested that rapidly cooled cells are killed by intracellular ice formation, while too slow of cooling results in cell death by prolonged exposure to dehydration effects, pH changes, and precipitations of solutes [119]. Important implications of these processes include the ice formation while thawing and the high molar concentration of CPAs required to permeate the cell. However, not all cells and tissues respond to cryopreservation equally. Therefore, it is considered necessary to optimize the cryopreservation protocol for the cell types of interest. Off-the-shelf protocol use can then result in unintended selection pressures, resulting in epigenetic changes [120]. Furthermore, the presence of apoptotic and necrotic cells might differ between cell types using the same cryopreservation protocol, leading to uncertainty in the development of an inflammatory response or immunological reactions between cell products [121]. Therefore, more methodological or quality by design approaches might be more appropriate than off-the-shelf cryopreservation protocols or those empirically derived through optimizing a specific cellular product [122, 123]. To address this approach, cryopreservation techniques should address the following interrelated elements, which post their own challenges: container system, CPA, protocol for adding and removing the CPA, mode of cooling and thawing,

and storage conditions. The incorporation of these considerations with tissue engineering indicates additional challenges towards developing viable protocols.

2.7 Advances in cryopreservation techniques using biomaterials and spheroids

Despite engineering challenges associated with cryopreservation, there have been some successful studies with the cold storage of spheroids and cells encapsulated in hydrogels. One example technique that incorporates cryopreservation, hydrogel formation, and cell encapsulation is the cryogelation of polyvinyl alcohol (PVA) gels. Cryogelation is a hydrogel formation technique in which freezing stabilizes polymer entanglements, resulting in a hydrogel after thawing. This method for creating cryogels has been repeatedly explored with polyvinyl alcohol [124-128], sometimes adding additional polymers to influence cell-matrix interactions or mechanical properties. Given the gelation method's freeze-thaw context, the technique has also been applied to encapsulating cryopreserved cells [129]. PVA alone was not sufficient for cryopreservation, as viability was improved with increased DMSO concentrations. Regardless, this perspective of encapsulation to avoid multiple cell culture stages can be justified where seeding a prefabricated scaffold avoids further manipulation within the clinics. While PVA hydrogels have gelation mechanics that match processes for cryopreservation, the material does not lend itself to cell adhesion or specific geometries to influence cell-cell interactions. Consequently, to promote cell migration, additional materials can be added. Specifically, chitosan, gelatin, fibrin, and matrigel have been added to PVA hydrogels to promote the migration of cells seeded onto the material [130, 131]. In PVA cryogels, cells and additives clearly impact the final hydrogel structure [129].

This outcome is suggested to be a response to changes in freezing rate and change in osmolality. Consequently, the accounting for changes in osmolality of the freezing solution and the consequential impact on the cells and hydrogel represents the disconnect between studies that focus more on tissue engineering and those that focus on cryopreservation.

A major challenge with spheroids with respect to cryopreservation is how the freezing and thawing process could affect the cellular organization. While previous work has shown a reduced capacity for cell-cell interactions following cryopreservation [132], the utility of spheroids is derived by an organization that better recapitulated the native *in vivo* environment. In the context of the differential adhesion hypothesis or differential interfacial tension hypothesis, these influences on cell adhesion and actin formation from cryopreservation could impact the structuring of spheroids [133-135]. Nevertheless, although the cryopreservation of spheroids is often described as being comparable to individual cells with cryopreservation [136, 137], the formation of spheroids from post-cryopreserved cells has been shown to be beneficial for stem cells derived from adipose and dental follicle tissue [138, 139]. Together, there is potential to incorporate cryopreservation with spheroids and hydrogels, yet there are distinct engineering barriers that need to be recognized to be successful.

2.8 Engineering barriers towards cryopreservation of spheroids and hydrogels

Cryopreservation cannot perfectly preserve cells in a glassy state. Inherently with the balance between ice formation and dehydration controlled by the cooling rate, not all

cells will inevitably survive. This outcome has detrimental outcomes and interactions for cell products incorporating the three-dimensional geometry of spheroid and hydrogels. Most apparent is how the loss of viable cells impacts the expected concentrations of functional cells. Although there is a known benefit of cell aggregation and cells encapsulated within biomaterials, there is no consensus on the ideal density of cells per aggregate nor within a scaffold. Optimal conditions are likely to depend on cell type and phenotype [23, 31, 56]. However, the loss of viable cells and reduced functionality could alter these cellular products' desired outcomes. Moreover, the cryopreservation of larger structures, such as spheroids or hydrogel-encapsulated cells, can decrease the efficacy of cryopreservation protocols. Overall, the combination of techniques might prove to be more disadvantageous than doing each independently. Nevertheless, the cells are diverse in composition and function, so it might be more productive, from a development perspective, to adequately know the various parameters that interact with each other than to attempt establishing a universal protocol or recommendation.

Diffusion is a fundamental process that enables cryopreservation, aggregation of cells, and hydrogel formation. It is the random motion of molecules due to collision with other molecules in space. As more concentrated regions of particles have more collisions than in areas with less of those particles, the movement of particles is typically from areas of high concentrations to low concentrations. Fick's 1st law of diffusion succinctly describes this process:

$$J = -D_{ij} \nabla C.$$

J is the flux of particles, the movement of a quantity through an area, D is the diffusion coefficient relating to the diffusion of a solute in a solvent, and ∇C is the concentration

gradient. The equation essentially says that there is a positive movement of particles in a direction away from the high concentration area and towards the lower concentration area. This phenomenon is critical to biological processes in general. The timescales in which particle moves are a crucial parameter affecting homeostasis *in vivo* and many of the topics mentioned in this chapter. The diffusion of CPA needs to occur before freezing to act on all cells adequately. Furthermore, the CPA must diffuse out of the cell solution to prevent cytotoxicity or osmotic shock [108, 115, 140, 141]. For spheroids, the aggregation of cells limits the diffusion of dissolved gases, such as oxygen. Because spheroids are very metabolically active, oxygen depletion in the core leads to a hypoxia environment. Hydrogels can also limit the diffusion of dissolved gases, indicating how spheroids and hydrogels could also limit the diffusion of the CPAs.

However, cryopreservation is a process involving dynamic temperature shifts. Temperature changes alter the solubility, diffusion, and potential cytotoxicity of several elements involved with cryopreservation and hydrogel formation [107, 140, 142]. The movement of thermal energy also acts similar to particles because the thermal energy is carried by particles, and therefore has a similar equation as Fick's 1st law of diffusion, the Fourier equation:

$$q = -k\,\nabla T,$$

where q is the thermal flux, which moves down the temperature gradient (∇T), dependent on the thermal conductivity of the material (k). Notably, there are interactions between thermal flux and diffusion. One interaction is that the diffusion coefficient is proportional to the temperature of the solution. Additionally, the diffusion coefficient is inversely proportional to the size of the solute diffusing in solution. Therefore, the movement of

particles via diffusion occurs more rapidly with smaller particles and in warmer mediums. Moreover, thermal conductivity is proportional to the viscosity of the solution, and the diffusion coefficient is inversely proportional to the viscosity of the solution. In the dynamic context of cryopreservation, the diffusion of particles is not possible in the frozen state. However, once in a liquid solution, elements will dynamically alter their diffusion rate and temperature change due to the change in thermal energy involved with cryopreservation. Cryopreservation can occur without knowing exactly how all these interactions occur because the objective is saturation during freezing and dilution during thawing. Prior to freezing, cells, encapsulated cells in hydrogels, and spheroid represent areas of no CPA concentration surrounded by a high concentration of CPA. In the context of flux, the area CPA moves into its surrounding cells, making this process relatively fast. In contrast, thawing involves the dilution of CPA, as cryopreserved cells are moved into solutions without CPA. To aid in this process, warm temperatures are used. Importantly for spheroids or cryopreserved hydrogels containing cells, the 3D structure limits the diffusion of CPA and thermal energy, potentially leading to more osmotic and heat shock [143-147].

In these ways, cryopreservation faces additional challenges with larger samples. In addition to a balance between dehydration and ice formation with the cooling rate, these factors will also be influenced by the size of the cell constructs. Specifically, the size of these constructs might not be addressed by altering the cooling rate alone.

Cryopreservation is also expected to influence hydrogel integrity. While the hydrogel can provide nucleation sites to prevent the formation of large damaging ice crystals, it also hinders the diffusion of CPAs. Nevertheless, the 3D structure will provide

barriers towards uniform cooling, leading to heterogeneous ice structures. Consequently, freezing encapsulated cells has been previously shown to break down microbead hydrogels [148]. There are potential negative impacts of polymer fragments, which can result from extracellular ice formation, for the designed mechanical properties of the biomaterials [149]. Alternatively, hydrogels could be formed post-cryopreservation. Under this protocol, there would be no structure hindering the diffusion of particles. Moreover, the solution can be mixed, using convective forces to improve CPA exposure to cells. Notably, the binding kinetics of calcium ions to the G residue blocks of alginate is also dependent on the system's thermal energy. Nevertheless, the incorporation of cryopreservation and hydrogels will result in changes to each regardless of when the hydrogel is formed in relation to cryopreservation.

Similarly, the cryopreservation of cells with cell-cell or cell-ECM contacts also enhances the risk of freeze-thaw injury compared to single cells suspensions. These conditions have been shown to make the cells more susceptible to mechanical ruptures, cell detachments, and necrosis [146, 150-153]. While this could result from ice formation, intracellular ice formation has been previously suggested to be the result of damage rather than the cause [154]. Specifically, using a hypertonic solution for dehydration is standard practice [155, 156], with incomplete dehydration resulting in intracellular water capable of freezing. Furthermore, the transition from this hypertonic solution to an isotonic one is known to cause swelling, leading to osmotic shock and possibly lysis [145, 155, 157]. Spheroids are likely to be more susceptible to osmotic shock because of the distribution of viable cells in the aggregate typically results in a heterogenous structure with varying cell density [146]. Therefore, the use of spheroids would result in an

increased risk in intracellular ice formation during freezing, osmotic shock, and lysis during thawing. Furthermore, spheroids could be structurally damaged by extracellular ice formation between cells in the aggregate. The alternative would be to form spheroids from dispersed cells post-cryopreservation. However, this protocol faces its challenges with post-cryopreserved cells having reduced capacity to form cell-cell interactions [132]. Therefore, to design procedures for spheroids from cryopreserved cells, optimization should be performed for the desired cell type to determine the most favorable outcome for post-cryopreservation recovery and function.

2.9 Summary

There is a need for improving the way cryopreservation is addressed in applications where cells are going to be delivered to a patient or used as models to study diseases. The field of cell therapies is primed for innovation, specifically for therapeutic angiogenesis. While hydrogels and spheroids are methods under consideration for improving the efficacy of potential cell therapies, the utilization of these techniques contrasts the mechanisms for successful cryopreservation. Cryopreservation provides a defined avenue for improving the accessibility of cell-based products that, as of date, limits the preclinical success in trials. Therefore, we believe the development of spheroid and hydrogel strategies for cell products should align with an assessment for their efficacy after or along with cryopreservation. In the following chapters, we will discuss how alginate hydrogels can be used for post-cryopreservation encapsulation of therapeutic cargo and cells with a method we designed to accommodate the cryostorage of these products. This work attempts to address engineering parameters in hydrogel formation,

spheroid formation, and cryopreservation. Given the discussion in this chapter, we were motivated to develop a technique that bypasses the challenges with cryopreserving spheroids or cells encapsulated in hydrogels by designing a strategy that performs these actions when breaking cells out from their frozen stasis.

2.10 References

[1] "Stem Cell Therapy Market by Treatment Mode (Autologous & Allogeneic). (Therapeutic Applications (CNS, CVS, GIT, Wound Healing, Musculoskeletal, Eye, & Immune System)—Regulatory Landscape, Pipeline Analysis & Global Forecasts to 2020." http://www.marketsandmarkets.com/Market-Reports/stem-cell-technologies-and-global-market-48.html (accessed 10/10/2018).

[2] "Stem Cell Therapy Market by Type (Allogeneic, Autologous), Therapeutic Application (Musculoskeletal, Wound & Injury, CVD, Autoimmune & Inflammatory), Cell Source (Adipose tissue, Bone Marrow, Placenta/Umbilical Cord) - Global Forecasts to 2026." https://www.marketsandmarkets.com/Market-Reports/stem-cell-technologies-and-global-market-48.html (accessed 09/06/2021).

[3] J. M. Baust, W. L. Corwin, R. VanBuskirk, and J. G. Baust, "Biobanking: The Future of Cell Preservation Strategies," in *Biobanking in the 21st Century*, F. Karimi-Busheri Ed. Cham: Springer International Publishing, 2015, pp. 37-53.

[4] F. J. O'Brien, "Biomaterials & scaffolds for tissue engineering," *Materials Today,* vol. 14, no. 3, pp. 88-95, 2011/03/01/ 2011, doi: https://doi.org/10.1016/S1369-7021(11)70058-X.

[5] S. S. Virani *et al.*, "Heart Disease and Stroke Statistics—2021 Update," *Circulation,* vol. 143, no. 8, pp. e254-e743, 2021/02/23 2021, doi: 10.1161/CIR.0000000000000950.

[6] L. L. Chiu, M. Montgomery, Y. Liang, H. Liu, and M. Radisic, "Perfusable branching microvessel bed for vascularization of engineered tissues," (in eng), *Proc Natl Acad Sci U S A,* vol. 109, no. 50, pp. E3414-23, Dec 11 2012.

[7] W. Suh *et al.*, "Transplantation of endothelial progenitor cells accelerates dermal wound healing with increased recruitment of monocytes/macrophages and neovascularization," in *Stem Cells*, vol. 23, no. 10). United States, 2005, pp. 1571-8.

[8] E. A. Silva, E.-S. Kim, H. J. Kong, and D. J. Mooney, "Material-based deployment enhances efficacy of endothelial progenitor cells," *Proceedings of the National Academy of Sciences,* vol. 105, no. 38, p. 14347, 2008, doi: 10.1073/pnas.0803873105.

[9] J. Yamaguchi *et al.*, "Stromal cell-derived factor-1 effects on ex vivo expanded endothelial progenitor cell recruitment for ischemic neovascularization," (in eng), *Circulation,* vol. 107, no. 9, pp. 1322-8, Mar 11 2003, doi: 10.1161/01.cir.0000055313.77510.22.

[10] M. B. Britten *et al.*, "Infarct remodeling after intracoronary progenitor cell treatment in patients with acute myocardial infarction (TOPCARE-AMI): mechanistic insights from serial contrast-enhanced magnetic resonance imaging," in *Circulation*, vol. 108, no. 18). United States, 2003, pp. 2212-8.

[11] P. Carmeliet, "Mechanisms of angiogenesis and arteriogenesis," *Nature Medicine,* vol. 6, no. 4, pp. 389-395, 2000/04/01 2000, doi: 10.1038/74651.

[12] P. A. Williams and E. A. Silva, "The Role of Synthetic Extracellular Matrices in Endothelial Progenitor Cell Homing for Treatment of Vascular Disease," (in eng), *Ann Biomed Eng,* vol. 43, no. 10, pp. 2301-13, Oct 2015, doi: 10.1007/s10439-015-1400-x.

[13] M. C. Peters, P. J. Polverini, and D. J. Mooney, "Engineering vascular networks in porous polymer matrices," in *J Biomed Mater Res*, vol. 60, no. 4). United States: 2002 Wiley Periodicals, Inc. J Biomed Mater Res 60: 668-678, 2002, 2002, pp. 668-78.

[14] E. M. Anderson, B. J. Kwee, S. A. Lewin, T. Raimondo, M. Mehta, and D. J. Mooney, "Local delivery of VEGF and SDF enhances endothelial progenitor cell recruitment and resultant recovery from ischemia," (in eng), *Tissue engineering. Part A,* vol. 21, no. 7-8, pp. 1217-1227, 2015, doi: 10.1089/ten.TEA.2014.0508.

[15] K. C. Murphy, J. Whitehead, D. Zhou, S. S. Ho, and J. K. Leach, "Engineering fibrin hydrogels to promote the wound healing potential of mesenchymal stem cell spheroids," (in eng), *Acta biomaterialia,* vol. 64, pp. 176-186, 2017, doi: 10.1016/j.actbio.2017.10.007.

[16] P. A. Williams, K. T. Campbell, H. Gharaviram, J. L. Madrigal, and E. A. Silva, "Alginate-Chitosan Hydrogels Provide a Sustained Gradient of Sphingosine-1-Phosphate for Therapeutic Angiogenesis," *Annals of Biomedical Engineering,* vol. 45, no. 4, pp. 1003-1014, 2017/04/01 2017, doi: 10.1007/s10439-016-1768-2.

[17] C. K. Sen, "Wound healing essentials: let there be oxygen," (in eng), *Wound repair and regeneration : official publication of the Wound Healing Society [and] the*

European Tissue Repair Society, vol. 17, no. 1, pp. 1-18, Jan-Feb 2009, doi: 10.1111/j.1524-475X.2008.00436.x.

[18] S. H. Bhang *et al.*, "Angiogenesis in ischemic tissue produced by spheroid grafting of human adipose-derived stromal cells," *Biomaterials,* vol. 32, no. 11, pp. 2734-2747, 2011/04/01/ 2011, doi: https://doi.org/10.1016/j.biomaterials.2010.12.035.

[19] L. Hou, J. J. Kim, Y. J. Woo, and N. F. Huang, "Stem cell-based therapies to promote angiogenesis in ischemic cardiovascular disease," (in eng), *Am J Physiol Heart Circ Physiol,* vol. 310, no. 4, pp. H455-65, Feb 15 2016, doi: 10.1152/ajpheart.00726.2015.

[20] K. H. Han, A. K. Kim, M. H. Kim, D. H. Kim, H. N. Go, and D. I. Kim, "Enhancement of angiogenic effects by hypoxia-preconditioned human umbilical cord-derived mesenchymal stem cells in a mouse model of hindlimb ischemia," (in eng), *Cell Biol Int,* vol. 40, no. 1, pp. 27-35, Jan 2016, doi: 10.1002/cbin.10519.

[21] M. W. Laschke and M. D. Menger, "Life is 3D: Boosting Spheroid Function for Tissue Engineering," *Trends in Biotechnology,* vol. 35, no. 2, pp. 133-144, 2017/02/01/ 2017, doi: https://doi.org/10.1016/j.tibtech.2016.08.004.

[22] S. H. Bhang, S. Lee, J.-Y. Shin, T.-J. Lee, and B.-S. Kim, "Transplantation of Cord Blood Mesenchymal Stem Cells as Spheroids Enhances Vascularization," *Tissue Engineering Part A,* vol. 18, no. 19-20, pp. 2138-2147, 2012/10/01 2012, doi: 10.1089/ten.tea.2011.0640.

[23] C. E. Vorwald, K. C. Murphy, and J. K. Leach, "Restoring vasculogenic potential of endothelial cells from diabetic patients through spheroid formation," (in eng), *Cell Mol Bioeng,* vol. 11, no. 4, pp. 267-278, Aug 2018.

[24] P. Carmeliet *et al.*, "Targeted deficiency or cytosolic truncation of the VE-cadherin gene in mice impairs VEGF-mediated endothelial survival and angiogenesis," in *Cell*, vol. 98, no. 2). United States, 1999, pp. 147-57.

[25] B. G. Coon *et al.*, "Intramembrane binding of VE-cadherin to VEGFR2 and VEGFR3 assembles the endothelial mechanosensory complex," (in eng), *J Cell Biol,* vol. 208, no. 7, pp. 975-86, Mar 30 2015, doi: 10.1083/jcb.201408103.

[26] M. A. Gionet-Gonzales and J. K. Leach, "Engineering principles for guiding spheroid function in the regeneration of bone, cartilage, and skin," *Biomedical Materials,* vol. 13, no. 3, p. 034109, 2018/03/21 2018, doi: 10.1088/1748-605x/aab0b3.

[27] T. Dvir *et al.*, "Prevascularization of cardiac patch on the omentum improves its therapeutic outcome," (in eng), *Proceedings of the National Academy of Sciences of the United States of America,* vol. 106, no. 35, pp. 14990-14995, 2009, doi: 10.1073/pnas.0812242106.

[28] Y. Liu, S. Sakai, and M. Taya, "Engineering tissues with a perfusable vessel-like network using endothelialized alginate hydrogel fiber and spheroid-enclosing microcapsules," *Heliyon,* vol. 2, no. 2, p. e00067, 2016/02/01/ 2016, doi: https://doi.org/10.1016/j.heliyon.2016.e00067.

[29] K. T. Campbell, R. S. Stilhano, and E. A. Silva, "Enzymatically degradable alginate hydrogel systems to deliver endothelial progenitor cells for potential revasculature applications," (in eng), *Biomaterials,* vol. 179, pp. 109-121, 2018, doi: 10.1016/j.biomaterials.2018.06.038.

[30] O. Chaudhuri *et al.*, "Hydrogels with tunable stress relaxation regulate stem cell fate and activity," *Nature Materials,* vol. 15, no. 3, pp. 326-334, 2016/03/01 2016, doi: 10.1038/nmat4489.

[31] S. S. Ho, K. C. Murphy, B. Y. Binder, C. B. Vissers, and J. K. Leach, "Increased Survival and Function of Mesenchymal Stem Cell Spheroids Entrapped in Instructive Alginate Hydrogels," (in eng), *Stem Cells Transl Med,* vol. 5, no. 6, pp. 773-81, Jun 2016.

[32] A. L. Torres, S. J. Bidarra, M. T. Pinto, P. C. Aguiar, E. A. Silva, and C. C. Barrias, "Guiding morphogenesis in cell-instructive microgels for therapeutic angiogenesis," *Biomaterials,* vol. 154, pp. 34-47, 2018/02/01/ 2018, doi: https://doi.org/10.1016/j.biomaterials.2017.10.051.

[33] J. M. Chan, I. K. Zervantonakis, T. Rimchala, W. J. Polacheck, J. Whisler, and R. D. Kamm, "Engineering of In Vitro 3D Capillary Beds by Self-Directed Angiogenic Sprouting," *PloS one,* vol. 7, no. 12, p. e50582, 2012, doi: 10.1371/journal.pone.0050582.

[34] L. L. Y. Chiu, M. Montgomery, Y. Liang, H. Liu, and M. Radisic, "Perfusable branching microvessel bed for vascularization of engineered tissues," *Proceedings*

of the National Academy of Sciences, 10.1073/pnas.1210580109 vol. 109, no. 50, p. E3414, 2012.

[35] Y. Liu, S. Sakai, and M. Taya, "Engineering tissues with a perfusable vessel-like network using endothelialized alginate hydrogel fiber and spheroid-enclosing microcapsules," *Heliyon,* vol. 2, no. 2, pp. e00067-e00067, 2016, doi: 10.1016/j.heliyon.2016.e00067.

[36] M. L. Moya, Y. H. Hsu, A. P. Lee, C. C. Hughes, and S. C. George, "In vitro perfused human capillary networks," (in eng), *Tissue engineering. Part C, Methods,* vol. 19, no. 9, pp. 730-7, Sep 2013, doi: 10.1089/ten.TEC.2012.0430.

[37] S. Renzi, T. Lombardo, S. Dotti, S. S. Dessì, P. De Blasio, and M. Ferrari, "Mesenchymal stromal cell cryopreservation," (in eng), *Biopreserv Biobank,* vol. 10, no. 3, pp. 276-81, Jun 2012, doi: 10.1089/bio.2012.0005.

[38] D. Freimark *et al.*, "Systematic parameter optimization of a Me(2)SO- and serum-free cryopreservation protocol for human mesenchymal stem cells," in *Cryobiology*, vol. 63, no. 2). Netherlands: 2011 Elsevier Inc, 2011, pp. 67-75.

[39] X. Stéphenne, M. Najimi, and E. M. Sokal, "Hepatocyte cryopreservation: is it time to change the strategy?," (in eng), *World J Gastroenterol,* vol. 16, no. 1, pp. 1-14, Jan 7 2010.

[40] K. Rajagopal, S. K. Chilbule, and V. Madhuri, "Viability, proliferation and phenotype maintenance in cryopreserved human iliac apophyseal chondrocytes," (in eng), *Cell Tissue Bank,* vol. 15, no. 1, pp. 153-63, Mar 2014, doi: 10.1007/s10561-013-9387-8.

[41] H. H. Yoon, S. H. Bhang, J.-Y. Shin, J. Shin, and B.-S. Kim, "Enhanced Cartilage Formation via Three-Dimensional Cell Engineering of Human Adipose-Derived Stem Cells," *Tissue Engineering Part A,* vol. 18, no. 19-20, pp. 1949-1956, 2012/10/01 2012, doi: 10.1089/ten.tea.2011.0647.

[42] S. K. Kapur *et al.*, "Human adipose stem cells maintain proliferative, synthetic and multipotential properties when suspension cultured as self-assembling spheroids," *Biofabrication,* vol. 4, no. 2, p. 025004, 2012/04/23 2012, doi: 10.1088/1758-5082/4/2/025004.

[43] S. Zhang, P. Liu, L. Chen, Y. Wang, Z. Wang, and B. Zhang, "The effects of spheroid formation of adipose-derived stem cells in a microgravity bioreactor on stemness properties and therapeutic potential," *Biomaterials,* vol. 41, pp. 15-25, 2015/02/01/ 2015, doi: https://doi.org/10.1016/j.biomaterials.2014.11.019.

[44] M. L. Skiles, S. Sahai, L. Rucker, and J. O. Blanchette, "Use of Culture Geometry to Control Hypoxia-Induced Vascular Endothelial Growth Factor Secretion from Adipose-Derived Stem Cells: Optimizing a Cell-Based Approach to Drive Vascular Growth," *Tissue Engineering Part A,* vol. 19, no. 21-22, pp. 2330-2338, 2013/11/01 2013, doi: 10.1089/ten.tea.2012.0750.

[45] J. N. Harvestine, N. L. Vollmer, S. S. Ho, C. A. Zikry, M. A. Lee, and J. K. Leach, "Extracellular Matrix-Coated Composite Scaffolds Promote Mesenchymal Stem Cell Persistence and Osteogenesis," (in eng), *Biomacromolecules,* vol. 17, no. 11, pp. 3524-3531, Nov 14 2016, doi: 10.1021/acs.biomac.6b01005.

[46] K. C. Murphy, A. I. Hoch, J. N. Harvestine, D. Zhou, and J. K. Leach, "Mesenchymal Stem Cell Spheroids Retain Osteogenic Phenotype Through α2β1 Signaling," (in eng), *Stem Cells Transl Med,* vol. 5, no. 9, pp. 1229-37, Sep 2016.

[47] A. I. Hoch, V. Mittal, D. Mitra, N. Vollmer, C. A. Zikry, and J. K. Leach, "Cell-secreted matrices perpetuate the bone-forming phenotype of differentiated mesenchymal stem cells," (in eng), *Biomaterials,* vol. 74, pp. 178-87, Jan 2016.

[48] R. Foty, "A simple hanging drop cell culture protocol for generation of 3D spheroids," (in eng), *J Vis Exp,* no. 51, May 6 2011.

[49] H. Ota, T. Kodama, and N. Miki, "Rapid formation of size-controlled three dimensional hetero-cell aggregates using micro-rotation flow for spheroid study," *Biomicrofluidics,* vol. 5, no. 3, p. 034105, 2011/09/01 2011, doi: 10.1063/1.3609969.

[50] K. Moshksayan *et al.*, "Spheroids-on-a-chip: Recent advances and design considerations in microfluidic platforms for spheroid formation and culture," *Sensors and Actuators B: Chemical,* vol. 263, pp. 151-176, 2018/06/15/ 2018, doi: https://doi.org/10.1016/j.snb.2018.01.223.

[51] Z. Zhao, J. Gu, Y. Zhao, Y. Guan, X. X. Zhu, and Y. Zhang, "Hydrogel Thin Film with Swelling-Induced Wrinkling Patterns for High-Throughput Generation of Multicellular Spheroids," *Biomacromolecules,* vol. 15, no. 9, pp. 3306-3312, 2014/09/08 2014, doi: 10.1021/bm500722g.

[52] D. M. Dean, A. P. Napolitano, J. Youssef, and J. R. Morgan, "Rods, tori, and honeycombs: the directed self-assembly of microtissues with prescribed

microscale geometries," *The FASEB Journal,* vol. 21, no. 14, pp. 4005-4012, 2007/12/01 2007, doi: https://doi.org/10.1096/fj.07-8710com.

[53] J. Dahlmann *et al.*, "The use of agarose microwells for scalable embryoid body formation and cardiac differentiation of human and murine pluripotent stem cells," *Biomaterials,* vol. 34, no. 10, pp. 2463-2471, 2013/03/01/ 2013, doi: https://doi.org/10.1016/j.biomaterials.2012.12.024.

[54] C. E. Vorwald, S. S. Ho, J. Whitehead, and J. K. Leach, "High-Throughput Formation of Mesenchymal Stem Cell Spheroids and Entrapment in Alginate Hydrogels," in *Biomaterials for Tissue Engineering: Methods and Protocols*, K. Chawla Ed. New York, NY: Springer New York, 2018, pp. 139-149.

[55] K. C. Murphy *et al.*, "Measurement of oxygen tension within mesenchymal stem cell spheroids," (in eng), *J R Soc Interface,* vol. 14, no. 127, Feb 2017.

[56] K. C. Murphy, J. Whitehead, P. C. Falahee, D. Zhou, S. I. Simon, and J. K. Leach, "Multifactorial Experimental Design to Optimize the Anti-Inflammatory and Proangiogenic Potential of Mesenchymal Stem Cell Spheroids," (in eng), *Stem Cells,* vol. 35, no. 6, pp. 1493-1504, Jun 2017.

[57] M. A. Lancaster *et al.*, "Guided self-organization and cortical plate formation in human brain organoids," *Nature Biotechnology,* vol. 35, no. 7, pp. 659-666, 2017/07/01 2017, doi: 10.1038/nbt.3906.

[58] K. Watanabe *et al.*, "A ROCK inhibitor permits survival of dissociated human embryonic stem cells," in *Nat Biotechnol*, vol. 25, no. 6). United States, 2007, pp. 681-6.

[59] Y. Guo *et al.*, "The effects of ROCK inhibitor Y-27632 on injectable spheroids of bovine corneal endothelial cells," (in eng), *Cellular reprogramming,* vol. 17, no. 1, pp. 77-87, 2015/02// 2015, doi: 10.1089/cell.2014.0070.

[60] G. Mehta, A. Y. Hsiao, M. Ingram, G. D. Luker, and S. Takayama, "Opportunities and challenges for use of tumor spheroids as models to test drug delivery and efficacy," *Journal of Controlled Release,* vol. 164, no. 2, pp. 192-204, 2012/12/10/ 2012, doi: https://doi.org/10.1016/j.jconrel.2012.04.045.

[61] R. Martin-Ibañez, C. Unger, A. Strömberg, D. Baker, J. M. Canals, and O. Hovatta, "Novel cryopreservation method for dissociated human embryonic stem cells in the presence of a ROCK inhibitor," in *Hum Reprod*, vol. 23, no. 12). England, 2008, pp. 2744-54.

[62] K. C. Murphy, S. Y. Fang, and J. K. Leach, "Human mesenchymal stem cell spheroids in fibrin hydrogels exhibit improved cell survival and potential for bone healing," (in eng), *Cell Tissue Res,* vol. 357, no. 1, pp. 91-9, Jul 2014.

[63] S. A. Ruiz and C. S. Chen, "Emergence of Patterned Stem Cell Differentiation Within Multicellular Structures," *STEM CELLS,* vol. 26, no. 11, pp. 2921-2927, 2008/11/01 2008, doi: https://doi.org/10.1634/stemcells.2008-0432.

[64] R. Mori, Y. Sakai, and K. Nakazawa, "Micropatterned organoid culture of rat hepatocytes and HepG2 cells," in *J Biosci Bioeng*, vol. 106, no. 3). Japan, 2008, pp. 237-42.

[65] B. H. Lee, M. H. Kim, J. H. Lee, D. Seliktar, N.-J. Cho, and L. P. Tan, "Modulation of Huh7.5 Spheroid Formation and Functionality Using Modified PEG-Based

Hydrogels of Different Stiffness," *PLOS ONE,* vol. 10, no. 2, p. e0118123, 2015, doi: 10.1371/journal.pone.0118123.

[66] K. Hattermann, J. Held-Feindt, and R. Mentlein, "Spheroid confrontation assay: A simple method to monitor the three-dimensional migration of different cell types in vitro," *Annals of Anatomy - Anatomischer Anzeiger,* vol. 193, no. 3, pp. 181-184, 2011/05/01/ 2011, doi: https://doi.org/10.1016/j.aanat.2010.12.005.

[67] E. Fennema, N. Rivron, J. Rouwkema, C. van Blitterswijk, and J. de Boer, "Spheroid culture as a tool for creating 3D complex tissues," *Trends in Biotechnology,* vol. 31, no. 2, pp. 108-115, 2013/02/01/ 2013, doi: https://doi.org/10.1016/j.tibtech.2012.12.003.

[68] J. Friedrich *et al.*, "A reliable tool to determine cell viability in complex 3-d culture: the acid phosphatase assay," in *J Biomol Screen*, vol. 12, no. 7). United States, 2007, pp. 925-37.

[69] L. Le Roux, A. Volgin, D. Maxwell, K. Ishihara, J. Gelovani, and D. Schellingerhout, "Optimizing imaging of three-dimensional multicellular tumor spheroids with fluorescent reporter proteins using confocal microscopy," *Molecular imaging,* vol. 7, no. 5, pp. 7290-2008, 2008.

[70] T. H. Booij, L. S. Price, and E. H. J. Danen, "3D Cell-Based Assays for Drug Screens: Challenges in Imaging, Image Analysis, and High-Content Analysis," (in eng), *SLAS Discov,* vol. 24, no. 6, pp. 615-627, Jul 2019.

[71] N. Mitrousis, A. Fokina, and M. S. Shoichet, "Biomaterials for cell transplantation," *Nature Reviews Materials,* vol. 3, no. 11, pp. 441-456, 2018/11/01 2018, doi: 10.1038/s41578-018-0057-0.

[72] R. D. Hughes, R. R. Mitry, and A. Dhawan, "Current status of hepatocyte transplantation," (in eng), *Transplantation,* vol. 93, no. 4, pp. 342-7, Feb 27 2012, doi: 10.1097/TP.0b013e31823b72d6.

[73] L. Yu, C. Ni, S. M. Grist, C. Bayly, and K. C. Cheung, "Alginate core-shell beads for simplified three-dimensional tumor spheroid culture and drug screening," *Biomedical Microdevices,* vol. 17, no. 2, p. 33, 2015/02/15 2015, doi: 10.1007/s10544-014-9918-5.

[74] B. H. Lee, B. Li, and S. A. Guelcher, "Gel microstructure regulates proliferation and differentiation of MC3T3-E1 cells encapsulated in alginate beads," (in eng), *Acta Biomater,* vol. 8, no. 5, pp. 1693-702, May 2012.

[75] C. Siltanen *et al.*, "One step fabrication of hydrogel microcapsules with hollow core for assembly and cultivation of hepatocyte spheroids," *Acta Biomaterialia,* vol. 50, pp. 428-436, 2017/03/01/ 2017, doi: https://doi.org/10.1016/j.actbio.2017.01.010.

[76] J. L. Wilson and T. C. McDevitt, "Stem cell microencapsulation for phenotypic control, bioprocessing, and transplantation," *Biotechnology and Bioengineering,* vol. 110, no. 3, pp. 667-682, 2013/03/01 2013, doi: https://doi.org/10.1002/bit.24802.

[77] H. Zhou and H. H. K. Xu, "The fast release of stem cells from alginate-fibrin microbeads in injectable scaffolds for bone tissue engineering," *Biomaterials,* vol. 32, no. 30, pp. 7503-7513, 2011, doi: 10.1016/j.biomaterials.2011.06.045.

[78] K. Y. Lee, J. A. Rowley, P. Eiselt, E. M. Moy, K. H. Bouhadir, and D. J. Mooney, "Controlling Mechanical and Swelling Properties of Alginate Hydrogels Independently by Cross-Linker Type and Cross-Linking Density," *Macromolecules,* vol. 33, no. 11, pp. 4291-4294, 2000/05/01 2000, doi: 10.1021/ma9921347.

[79] K. Y. Lee and D. J. Mooney, "Alginate: properties and biomedical applications," (in eng), *Progress in polymer science,* vol. 37, no. 1, pp. 106-126, 2012, doi: 10.1016/j.progpolymsci.2011.06.003.

[80] G. T. Grant, E. R. Morris, D. A. Rees, P. J. C. Smith, and D. Thom, "Biological interactions between polysaccharides and divalent cations: The egg-box model," *FEBS Letters,* vol. 32, no. 1, pp. 195-198, 1973/05/15 1973, doi: 10.1016/0014-5793(73)80770-7.

[81] K. H. Bouhadir, K. Y. Lee, E. Alsberg, K. L. Damm, K. W. Anderson, and D. J. Mooney, "Degradation of partially oxidized alginate and its potential application for tissue engineering," in *Biotechnol Prog*, vol. 17, no. 5). United States, 2001, pp. 945-50.

[82] J. A. Rowley, G. Madlambayan, and D. J. Mooney, "Alginate hydrogels as synthetic extracellular matrix materials," in *Biomaterials*, vol. 20, no. 1). Netherlands, 1999, pp. 45-53.

[83] J. A. Rowley and D. J. Mooney, "Alginate type and RGD density control myoblast phenotype," in *J Biomed Mater Res*, vol. 60, no. 2). United States: 2002 Wiley Periodicals, Inc. J Biomed Mater Res 60: 217-223, 2002; DOI 10.1002/jbm.1287, 2002, pp. 217-23.

[84] H. J. Kong, M. K. Smith, and D. J. Mooney, "Designing alginate hydrogels to maintain viability of immobilized cells," *Biomaterials,* vol. 24, no. 22, pp. 4023-4029, 2003/10/01/ 2003, doi: https://doi.org/10.1016/S0142-9612(03)00295-3.

[85] A. W. Chan and R. J. Neufeld, "Tuneable semi-synthetic network alginate for absorptive encapsulation and controlled release of protein therapeutics," *Biomaterials,* vol. 31, no. 34, pp. 9040-9047, 2010/12/01/ 2010, doi: https://doi.org/10.1016/j.biomaterials.2010.07.111.

[86] M. M. Capeling *et al.*, "Nonadhesive Alginate Hydrogels Support Growth of Pluripotent Stem Cell-Derived Intestinal Organoids," *Stem Cell Reports,* vol. 12, no. 2, pp. 381-394, 2019/02/12/ 2019, doi: https://doi.org/10.1016/j.stemcr.2018.12.001.

[87] G. Skjåk-Bræk, H. Grasdalen, and O. Smidsrød, "Inhomogeneous polysaccharide ionic gels," *Carbohydrate Polymers,* vol. 10, no. 1, pp. 31-54, 1989/01/01/ 1989, doi: https://doi.org/10.1016/0144-8617(89)90030-1.

[88] C. K. Kuo and P. X. Ma, "Ionically crosslinked alginate hydrogels as scaffolds for tissue engineering: Part 1. Structure, gelation rate and mechanical properties," *Biomaterials,* vol. 22, no. 6, pp. 511-521, 2001/03/15/ 2001, doi: https://doi.org/10.1016/S0142-9612(00)00201-5.

[89] C. K. Kuo and P. X. Ma, "Maintaining dimensions and mechanical properties of ionically crosslinked alginate hydrogel scaffolds in vitro," *Journal of Biomedical Materials Research Part A,* vol. 84A, no. 4, pp. 899-907, 2008/03/15 2008, doi: 10.1002/jbm.a.31375.

[90] S. Utech, R. Prodanovic, A. S. Mao, R. Ostafe, D. J. Mooney, and D. A. Weitz, "Microfluidic Generation of Monodisperse, Structurally Homogeneous Alginate Microgels for Cell Encapsulation and 3D Cell Culture," (in eng), *Adv Healthc Mater,* vol. 4, no. 11, pp. 1628-33, Aug 5 2015.

[91] C. M. Silva, A. J. Ribeiro, I. V. Figueiredo, A. R. Gonçalves, and F. Veiga, "Alginate microspheres prepared by internal gelation: Development and effect on insulin stability," *International Journal of Pharmaceutics,* vol. 311, no. 1, pp. 1-10, 2006/03/27/ 2006, doi: https://doi.org/10.1016/j.ijpharm.2005.10.050.

[92] K. T. Campbell, D. J. Hadley, D. L. Kukis, and E. A. Silva, "Alginate hydrogels allow for bioactive and sustained release of VEGF-C and VEGF-D for lymphangiogenic therapeutic applications," (in eng), *PloS one,* vol. 12, no. 7, pp. e0181484-e0181484, 2017, doi: 10.1371/journal.pone.0181484.

[93] E. A. Silva and D. J. Mooney, "Spatiotemporal control of vascular endothelial growth factor delivery from injectable hydrogels enhances angiogenesis," *Journal of Thrombosis and Haemostasis,* vol. 5, no. 3, pp. 590-598, 2007/03/01 2007, doi: https://doi.org/10.1111/j.1538-7836.2007.02386.x.

[94] E. A. Silva and D. J. Mooney, "Effects of VEGF temporal and spatial presentation on angiogenesis," (in eng), *Biomaterials,* vol. 31, no. 6, pp. 1235-41, Feb 2010.

[95] E. A. Silva, E. S. Kim, H. J. Kong, and D. J. Mooney, "Material-based deployment enhances efficacy of endothelial progenitor cells," (in eng), *Proc Natl Acad Sci U S A,* vol. 105, no. 38, pp. 14347-52, Sep 23 2008, doi: 10.1073/pnas.0803873105.

[96] C. S. Chen, M. Mrksich, S. Huang, G. M. Whitesides, and D. E. Ingber, "Geometric Control of Cell Life and Death," *Science,* vol. 276, no. 5317, p. 1425, 1997, doi: 10.1126/science.276.5317.1425.

[97] F. G. Giancotti, "Complexity and specificity of integrin signalling," *Nature Cell Biology,* vol. 2, no. 1, pp. E13-E14, 2000/01/01 2000, doi: 10.1038/71397.

[98] J. Yu *et al.*, "The use of human mesenchymal stem cells encapsulated in RGD modified alginate microspheres in the repair of myocardial infarction in the rat," *Biomaterials,* vol. 31, no. 27, pp. 7012-7020, 2010/09/01/ 2010, doi: https://doi.org/10.1016/j.biomaterials.2010.05.078.

[99] G. Bhakta *et al.*, "Cryopreservation of alginate-fibrin beads involving bone marrow derived mesenchymal stromal cells by vitrification," in *Biomaterials*, vol. 30, no. 3). Netherlands, 2009, pp. 336-43.

[100] M. C. Barsotti *et al.*, "Fibrin acts as biomimetic niche inducing both differentiation and stem cell marker expression of early human endothelial progenitor cells," *Cell Proliferation,* vol. 44, no. 1, pp. 33-48, 2011/02/01 2011, doi: https://doi.org/10.1111/j.1365-2184.2010.00715.x.

[101] P. de la Puente and D. Ludeña, "Cell culture in autologous fibrin scaffolds for applications in tissue engineering," *Experimental Cell Research,* vol. 322, no. 1, pp. 1-11, 2014/03/10/ 2014, doi: https://doi.org/10.1016/j.yexcr.2013.12.017.

[102] W. D. Spotnitz, P. D. Mintz, N. Avery, T. C. Bithell, S. Kaul, and S. P. Nolan, "Fibrin glue from stored human plasma. An inexpensive and efficient method for local blood bank preparation," (in eng), *The American surgeon,* vol. 53, no. 8, pp. 460-2, Aug 1987.

[103] E. Di Stasio, C. Nagaswami, J. W. Weisel, and E. Di Cera, "Cl- regulates the structure of the fibrin clot," (in eng), *Biophys J,* vol. 75, no. 4, pp. 1973-9, Oct 1998, doi: 10.1016/s0006-3495(98)77638-6.

[104] Y. Li, H. Meng, Y. Liu, and B. P. Lee, "Fibrin Gel as an Injectable Biodegradable Scaffold and Cell Carrier for Tissue Engineering," *The Scientific World Journal,* vol. 2015, p. 10, 2015, Art no. 685690, doi: 10.1155/2015/685690.

[105] D. D. Swartz, J. A. Russell, and S. T. Andreadis, "Engineering of fibrin-based functional and implantable small-diameter blood vessels," (in eng), *American journal of physiology. Heart and circulatory physiology,* vol. 288, no. 3, pp. H1451-60, Mar 2005, doi: 10.1152/ajpheart.00479.2004.

[106] E. J. Woods, S. Thirumala, S. S. Badhe-Buchanan, D. Clarke, and A. J. Mathew, "Off the shelf cellular therapeutics: Factors to consider during cryopreservation and storage of human cells for clinical use," *Cytotherapy,* vol. 18, no. 6, pp. 697-711, 2016/06/01/ 2016, doi: https://doi.org/10.1016/j.jcyt.2016.03.295.

[107] G. D. Elliott, S. Wang, and B. J. Fuller, "Cryoprotectants: A review of the actions and applications of cryoprotective solutes that modulate cell recovery from ultra-low temperatures," *Cryobiology,* vol. 76, pp. 74-91, 2017/06/01/ 2017, doi: https://doi.org/10.1016/j.cryobiol.2017.04.004.

[108] C. J. Hunt, "Cryopreservation: Vitrification and Controlled Rate Cooling," (in eng), *Methods Mol Biol,* vol. 1590, pp. 41-77, 2017, doi: 10.1007/978-1-4939-6921-0_5.

[109] H. Gurruchaga *et al.*, "Advances in the slow freezing cryopreservation of microencapsulated cells," *Journal of Controlled Release,* vol. 281, pp. 119-138, 2018/07/10/ 2018, doi: https://doi.org/10.1016/j.jconrel.2018.05.016.

[110] C. J. Hunt, "Technical Considerations in the Freezing, Low-Temperature Storage and Thawing of Stem Cells for Cellular Therapies," *Transfusion Medicine and Hemotherapy,* vol. 46, no. 3, pp. 134-150, 2019, doi: 10.1159/000497289.

[111] B. J. Fuller, "Cryoprotectants: the essential antifreezes to protect life in the frozen state," *Cryoletters,* vol. 25, no. 6, pp. 375-388, // 2004.

[112] L. L. Kuleshova, S. S. Gouk, and D. W. Hutmacher, "Vitrification as a prospect for cryopreservation of tissue-engineered constructs," *Biomaterials,* vol. 28, no. 9, pp. 1585-1596, 2007/03/01/ 2007, doi: https://doi.org/10.1016/j.biomaterials.2006.11.047.

[113] L. L. Kuleshova, D. R. MacFarlane, A. O. Trounson, and J. M. Shaw, "Sugars Exert a Major Influence on the Vitrification Properties of Ethylene Glycol-Based Solutions and Have Low Toxicity to Embryos and Oocytes," *Cryobiology,* vol. 38, no. 2, pp. 119-130, 1999/03/01/ 1999, doi: https://doi.org/10.1006/cryo.1999.2153.

[114] X. Yu, G. Chen, and S. Zhang, "A model to predict the permeation kinetics of dimethyl sulfoxide in articular cartilage," (in eng), *Biopreserv Biobank,* vol. 11, no. 1, pp. 51-6, Feb 2013, doi: 10.1089/bio.2012.0050.

[115] J. M. Baust, L. H. Campbell, and J. W. Harbell, "Best practices for cryopreserving, thawing, recovering, and assessing cells," in *In Vitro Cell Dev Biol Anim*, vol. 53, no. 10). Germany, 2017, pp. 855-871.

[116] P. W. Andrews *et al.*, "Points to consider in the development of seed stocks of pluripotent stem cells for clinical applications: International Stem Cell Banking Initiative (ISCBI)," (in eng), *Regen Med,* vol. 10, no. 2 Suppl, pp. 1-44, 2015, doi: 10.2217/rme.14.93.

[117] B. C. Heng *et al.*, "Loss of viability during freeze-thaw of intact and adherent human embryonic stem cells with conventional slow-cooling protocols is predominantly due to apoptosis rather than cellular necrosis," (in eng), *J Biomed Sci,* vol. 13, no. 3, pp. 433-45, May 2006, doi: 10.1007/s11373-005-9051-9.

[118] M. A. Savitskaya and G. E. Onishchenko, "Apoptosis in cryopreserved eukaryotic cells," *Biochemistry (Moscow),* vol. 81, no. 5, pp. 445-452, 2016/05/01 2016, doi: 10.1134/S0006297916050023.

[119] P. Mazur, S. P. Leibo, and E. H. Y. Chu, "A two-factor hypothesis of freezing injury: Evidence from Chinese hamster tissue-culture cells," *Experimental Cell Research,* vol. 71, no. 2, pp. 345-355, 1972/04/01/ 1972, doi: https://doi.org/10.1016/0014-4827(72)90303-5.

[120] K. Rajamani, Y. S. Li, D. K. Hsieh, S. Z. Lin, H. J. Harn, and T. W. Chiou, "Genetic and epigenetic instability of stem cells," in *Cell Transplant*, vol. 23, no. 4-5). United States, 2014, pp. 417-33.

[121] R. S. Hotchkiss, A. Strasser, J. E. McDunn, and P. E. Swanson, "Cell death," (in eng), *The New England journal of medicine,* vol. 361, no. 16, pp. 1570-1583, 2009, doi: 10.1056/NEJMra0901217.

[122] C. J. Hunt, D. E. Pegg, and S. E. Armitage, "Optimising cryopreservation protocols for haematopoietic progenitor cells: a methodological approach for umbilical cord blood," (in eng), *Cryo Letters,* vol. 27, no. 2, pp. 73-86, Mar-Apr 2006.

[123] P. D. Mitchell, E. Ratcliffe, P. Hourd, D. J. Williams, and R. J. Thomas, "A quality-by-design approach to risk reduction and optimization for human embryonic stem cell cryopreservation processes," (in eng), *Tissue Eng Part C Methods,* vol. 20, no. 12, pp. 941-50, Dec 2014, doi: 10.1089/ten.TEC.2013.0595.

[124] V. I. Lozinsky *et al.*, "Study of cryostructurization of polymer systems VII. Structure formation under freezing of poly(vinyl alcohol) aqueous solutions," *Colloid and Polymer Science,* vol. 264, no. 1, pp. 19-24, 1986/01/01 1986, doi: 10.1007/BF01410304.

[125] S. J. Kim, S. J. Park, and S. I. Kim, "Swelling behavior of interpenetrating polymer network hydrogels composed of poly(vinyl alcohol) and chitosan," *Reactive and Functional Polymers,* vol. 55, no. 1, pp. 53-59, 2003/02/01/ 2003, doi: https://doi.org/10.1016/S1381-5148(02)00214-6.

[126] Y. Jiang, H. Hussain, and J. Kressler, "Poly(vinyl alcohol) Cryogel Formation Using Biocompatible Ice Nucleating Agents," *Macromolecular Materials and Engineering,* vol. 300, no. 2, pp. 181-190, 2015/02/01 2015, doi: 10.1002/mame.201400229.

[127] S. Rehmani, M. Ahmad, M. U. Minhas, H. Anwar, M. I.-u.-d. Zangi, and M. Sohail, "Development of natural and synthetic polymer-based semi-interpenetrating polymer network for controlled drug delivery: optimization and in vitro evaluation studies," *Polymer Bulletin,* vol. 74, no. 3, pp. 737-761, 2017/03/01 2017, doi: 10.1007/s00289-016-1743-y.

[128] X. Li *et al.*, "Strong, tough and mechanically self-recoverable poly(vinyl alcohol)/alginate dual-physical double-network hydrogels with large cross-link density contrast," *RSC Advances,* 10.1039/C8RA01302K vol. 8, no. 30, pp. 16674-16689, 2018, doi: 10.1039/C8RA01302K.

[129] N. E. Vrana, A. O'Grady, E. Kay, P. A. Cahill, and G. B. McGuinness, "Cell encapsulation within PVA-based hydrogels via freeze-thawing: a one-step scaffold formation and cell storage technique," *Journal of Tissue Engineering and Regenerative Medicine,* vol. 3, no. 7, pp. 567-572, 2009/10/01 2009, doi: https://doi.org/10.1002/term.193.

[130] N. E. Vrana, Y. Liu, G. B. McGuinness, and P. A. Cahill, "Characterization of Poly(vinyl alcohol)/Chitosan Hydrogels as Vascular Tissue Engineering Scaffolds," *Macromolecular Symposia,* vol. 269, no. 1, pp. 106-110, 2008/08/01 2008, doi: https://doi.org/10.1002/masy.200850913.

[131] Y. Liu, N. E. Vrana, P. A. Cahill, and G. B. McGuinness, "Physically crosslinked composite hydrogels of PVA with natural macromolecules: structure, mechanical properties, and endothelial cell compatibility," (in eng), *J Biomed Mater Res B Appl Biomater,* vol. 90, no. 2, pp. 492-502, Aug 2009, doi: 10.1002/jbm.b.31310.

[132] R. Chinnadurai *et al.*, "Actin cytoskeletal disruption following cryopreservation alters the biodistribution of human mesenchymal stromal cells in vivo," (in eng), *Stem Cell Reports,* vol. 3, no. 1, pp. 60-72, Jul 8 2014.

[133] R. A. Foty and M. S. Steinberg, "Cadherin-mediated cell-cell adhesion and tissue segregation in relation to malignancy," in *Int J Dev Biol*, vol. 48, no. 5-6). Spain, 2004, pp. 397-409.

[134] R. A. Foty and M. S. Steinberg, "The differential adhesion hypothesis: a direct evaluation," in *Dev Biol*, vol. 278, no. 1). United States, 2005, pp. 255-63.

[135] M. L. Manning, R. A. Foty, M. S. Steinberg, and E.-M. Schoetz, "Coaction of intercellular adhesion and cortical tension specifies tissue surface tension," (in eng), *Proceedings of the National Academy of Sciences of the United States of America,* vol. 107, no. 28, pp. 12517-12522, 2010, doi: 10.1073/pnas.1003743107.

[136] S. Motoike *et al.*, "Cryopreserved clumps of mesenchymal stem cell/extracellular matrix complexes retain osteogenic capacity and induce bone regeneration," *Stem Cell Research & Therapy,* vol. 9, no. 1, p. 73, 2018/03/21 2018, doi: 10.1186/s13287-018-0826-0.

[137] S. G. Ali and G. A. Bozhok, "Cryopreservation of Multicellular Spheroids Derived from Primary Culture of Newborn Piglet Spinal Ganglion Cells," *Problems of Cryobiology and Cryomedicine,* vol. 29, no. 4, pp. 354-364, 12/17 2019, doi: 10.15407/cryo29.04.354.

[138] X. Guo, S. Li, Q. Ji, R. Lian, and J. Chen, "Enhanced viability and neural differential potential in poor post-thaw hADSCs by agarose multi-well dishes and spheroid culture," in *Hum Cell*, vol. 28, no. 4). Japan, 2015, pp. 175-89.

[139] H. J. Kim *et al.*, "Three-Dimensional Spheroid Formation of Cryopreserved Human Dental Follicle-Derived Stem Cells Enhances Pluripotency and Osteogenic Induction Properties," (in eng), *Tissue Eng Regen Med,* vol. 16, no. 5, pp. 513-523, Oct 2019.

[140] G. M. Fahy, "The relevance of cryoprotectant “toxicity” to cryobiology," *Cryobiology,* vol. 23, no. 1, pp. 1-13, 1986/02/01/ 1986, doi: https://doi.org/10.1016/0011-2240(86)90013-1.

[141] R. Raju, S. J. Bryant, B. L. Wilkinson, and G. Bryant, "The need for novel cryoprotectants and cryopreservation protocols: Insights into the importance of biophysical investigation and cell permeability," in *Biochim Biophys Acta Gen Subj*, vol. 1865, no. 1). Netherlands: © 2020 Elsevier B.V, 2021, p. 129749.

[142] H. Zimmermann, S. G. Shirley, and U. Zimmermann, "Alginate-based encapsulation of cells: Past, present, and future," *Current Diabetes Reports,* vol. 7, no. 4, pp. 314-320, 2007/08/01 2007, doi: 10.1007/s11892-007-0051-1.

[143] K. Liu, Y. Yang, and J. Mansbridge, "Comparison of the stress response to cryopreservation in monolayer and three-dimensional human fibroblast cultures: stress proteins, MAP kinases, and growth factor gene expression," (in eng), *Tissue Eng,* vol. 6, no. 5, pp. 539-54, Oct 2000, doi: 10.1089/107632700750022189.

[144] B. Wowk, "Thermodynamic aspects of vitrification," *Cryobiology,* vol. 60, no. 1, pp. 11-22, 2010/02/01/ 2010, doi: https://doi.org/10.1016/j.cryobiol.2009.05.007.

[145] D. Gao and J. K. Critser, "Mechanisms of Cryoinjury in Living Cells," *ILAR Journal,* vol. 41, no. 4, pp. 187-196, 2000, doi: 10.1093/ilar.41.4.187.

[146] X. Xu, Y. Liu, Z. Cui, Y. Wei, and L. Zhang, "Effects of osmotic and cold shock on adherent human mesenchymal stem cells during cryopreservation," in *J Biotechnol*, vol. 162, no. 2-3). Netherlands: © 2012 Elsevier B.V, 2012, pp. 224-31.

[147] M. Ölander, J. R. Wiśniewski, I. Flörkemeier, N. Handin, J. Urdzik, and P. Artursson, "A simple approach for restoration of differentiation and function in cryopreserved human hepatocytes," in *Arch Toxicol*, vol. 93, no. 3). Germany, 2019, pp. 819-829.

[148] R. Malpique *et al.*, "Alginate Encapsulation as a Novel Strategy for the Cryopreservation of Neurospheres," *Tissue Engineering Part C: Methods,* vol. 16, no. 5, pp. 965-977, 2010/10/01 2009, doi: 10.1089/ten.tec.2009.0660.

[149] S. L. M. Dahl, C. Rhim, Y. C. Song, and L. E. Niklason, "Mechanical Properties and Compositions of Tissue Engineered and Native Arteries," *Annals of Biomedical Engineering,* vol. 35, no. 3, pp. 348-355, 2007/03/01 2007, doi: 10.1007/s10439-006-9226-1.

[150] J. P. Acker, A. Larese, H. Yang, A. Petrenko, and L. E. McGann, "Intracellular ice formation is affected by cell interactions," in *Cryobiology*, vol. 38, no. 4). Netherlands: 1999 Academic Press., 1999, pp. 363-71.

[151] J. P. Acker and L. E. McGann, "Cell–Cell Contact Affects Membrane Integrity after Intracellular Freezing," *Cryobiology,* vol. 40, no. 1, pp. 54-63, 2000/02/01/ 2000, doi: https://doi.org/10.1006/cryo.1999.2221.

[152] S. L. Ebertz and L. E. McGann, "Cryoinjury in endothelial cell monolayers," (in eng), *Cryobiology,* vol. 49, no. 1, pp. 37-44, Aug 2004, doi: 10.1016/j.cryobiol.2004.04.003.

[153] B. L. Liu and J. McGrath, "Response of cytoskeleton of murine osteoblast cultures to two-step freezing," (in eng), *Acta Biochim Biophys Sin (Shanghai),* vol. 37, no. 12, pp. 814-8, Dec 2005, doi: 10.1111/j.1745-7270.2005.00121.x.

[154] K. Muldrew and L. E. McGann, "Mechanisms of intracellular ice formation," (in eng), *Biophys J,* vol. 57, no. 3, pp. 525-32, Mar 1990.

[155] D. E. Pegg and M. P. Diaper, "The effect of initial tonicity on freeze/thaw injury to human red cells suspended in solutions of sodium chloride," *Cryobiology,* vol. 28, no. 1, pp. 18-35, 1991/02/01/ 1991, doi: https://doi.org/10.1016/0011-2240(91)90004-8.

[156] D. E. Pegg, "Principles of Cryopreservation," in *Cryopreservation and Freeze-Drying Protocols*, J. G. Day and G. N. Stacey Eds. Totowa, NJ: Humana Press, 2007, pp. 39-57.

[157] J. O. M. Karlsson and M. Toner, "Long-term storage of tissues by cryopreservation: critical issues," *Biomaterials,* vol. 17, no. 3, pp. 243-256, 1996/01/01/ 1996, doi: https://doi.org/10.1016/0142-9612(96)85562-1.

CHAPTER 3

Development and initial characterization of alginate hydrogels produced via thaw-induced gelation

3.1 Introduction

This chapter describes the initial development of thaw-induced gelation as a scheme for generating alginate hydrogels. For additional context, the project began with attempts to control the release of small sugars and bacteria as it passes through the digestive tract. Initially, work was being performed on methods to formulate an alginate and chitosan hybrid hydrogel for the controlled release of cargo. The intention was to generate a hydrogel that would release cargo at a steady rate within a neutral pH but have little to no release in an acidic environment. Consequently, the material was postulated to remain coherent and not release its cargo after ingestion until it reached the small intestines. We hypothesized that alginate becoming partially insoluble in stomach acid, as the pH was far below its isoelectric point, would improve controlled release only in the more pH-neutral intestines [1, 2]. In contrast, chitosan would become positively charged in the acidic environment of the stomach [3]. Regardless, challenges were observed in making these hydrogels as microbeads due to the rapid clogging of microfluidic channels due to interactions between alginate and chitosan before reaching the end of the flow-focusing channel. To surpass this challenge, we designed an open-source 3D-printable air-jet for the rapid formation of microbeads (APPENDIX A). With this air-jet, rapid bacterial encapsulation was achieved. Within this initial development

phase, we were also considering the necessary storage conditions that would be necessary for clinical success. This research niche became the primary focus, leading to the attempts of hydrogel formation with a frozen starting solution.

The need for controlled delivery of bioactive factors in clinical applications has motivated continuous advancement to develop specialized hydrogel systems [4-6]. While hydrogels have been successfully designed for controlling the release of bioactive cargos, they typically neglect other design considerations fundamental for their implementation in clinical applications. One crucial consideration includes long-term storage conditions. The gold standard for preserving therapeutic agents, and cells, usually involves cold/frozen storage [7]. Therefore, designing hydrogel systems as therapeutic vehicles should ideally address the preservation of cargo and the carrier during storage and application. In this chapter, we set out to design a hydrogel with enhanced electrostatic interactions with specific loaded cargo while involving a step in which the components are frozen for long-term storage. In doing so, we believe the outcome considers potential alterations to the material and cargo from freezing because that cold storage is part of the fabrication process.

Notwithstanding, polymeric carriers can also display protective outcomes for the cold storage of cargo [8]. Alginate and chitosan are two notable examples of naturally occurring polymers being studied for their protective effects for proteins and cells and have been extensively used as drug delivery vehicles due to their low toxicity, widespread availability, and relatively biocompatibility [9-12]. The anionic and cationic properties of alginate and chitosan, respectively, have been exploited to form polyelectrolyte complexes to encapsulate and electrostatically control the release of therapeutic cargos

[11, 13-15]. Generally, electrostatic-controlled release depends on the charge of the target molecule and the polymer at different pH, which is dependent on the isoelectric point of those molecules (Figure 3.1). Despite the potential for charged-based control over the release of molecules from a hydrogel, the main limitation towards the diffusion of molecules is the mesh and pore size. However, cargos smaller than the mesh size of the hydrogel are typically released within 24 hours because the hydrogel does not sufficiently limit diffusion [3, 15, 16]. This limitation to steric-controlled release motivates the need for additional mechanisms that can control the mesh size or entrap cargo, including electrostatics [5, 17].

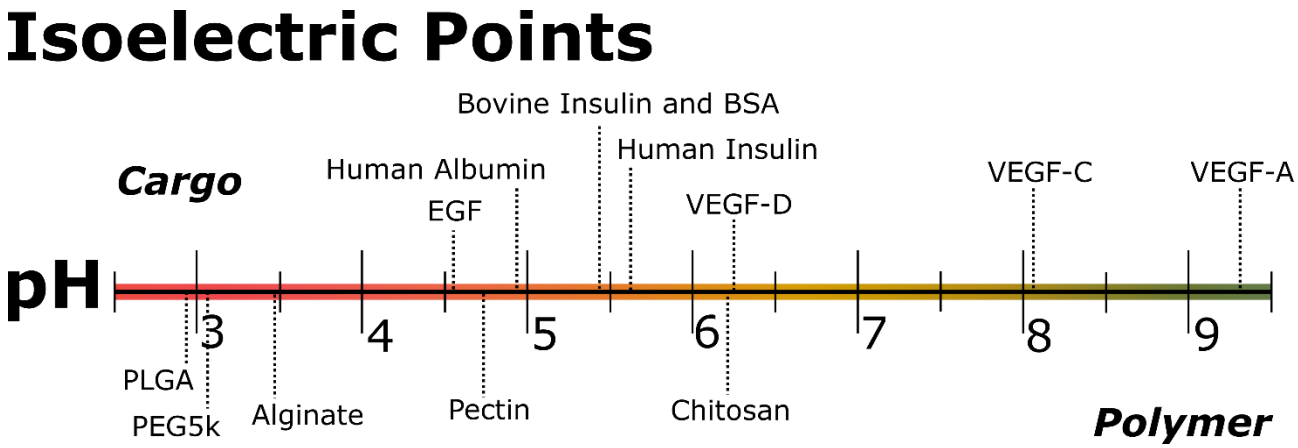

Figure 3.1 Isoelectric points of various polymers and potential cargo. The dotted line from the molecule to the axis labeled "pH" represents the pH in which the molecule has no net charge. Depending on the molecule type, the material may have a positive net charge at a pH less than the isoelectric point (e.g., chitosan) or a negative net charge at a pH greater than its isoelectric point (e.g., alginate). However, some material may become insoluble, as with an acidic solution less than the isoelectric point of alginate.

To generate electrostatic interactions between the polymers that compose a hydrogel and the desired cargo, the two molecules must come in close enough contact with each other for their respective charges to attract. In an electrolyte solution, ions of an opposing charge will surround molecules, potentially shielding larger molecules from electrostatically interacting. The Debye length describes this phenomenon, in which a charge carrier's net electrostatic effect and persistence are altered by electrical screening. Consequently, the potential of a molecule to electrostatically influence another decrease by 1/e for each Debye length. This length is influenced by the salinity of the solution, described as the particle density, charge, and temperature. Effectively, as the temperature decreases, the Debye length increases. Additionally, lower salinity solutions present fewer particles to shield charges. However, lower temperatures can decrease particle charge, and freezing a solution concentrates the salts. Therefore, the method for improving electrostatic interactions becomes an addressable challenge.

Electrostatic interactions can form stable polyelectrolyte complexes by phase-separation events, like those typically used to form a polymeric sponge [18, 19]. Specifically, the growth of ice crystals brings the polymer chains together, aggregating them into dense regions [18]. The phase-separation process can alter the swelling ratio, pore size, and strength of polymeric sponges, presenting a controllable design parameter for dermal applications of sponges [18, 20]. This polymer aggregation is typically preserved through freeze-drying, generating a sponge. However, the freeze-drying process is time-consuming (1-4 days), energy-intensive, and can damage specific cargos, including proteins [20, 21]. Moreover, it is not clear how the sponge will be rehydrated during application. Although the large pores of sponges present less steric control over

cargo release than hydrogels, the polymeric aggregations in sponges are advantageous due to their excellent mechanical toughness (modulus of elasticity 100-400 kPa) [12, 18, 22]. Generating a hydrogel with sponge-like properties presents an opportunity to enhance control over cargo release through possible entrapment in the aggregated polymer. Additionally, there is the potential of this entrapment to improve electrostatic interactions between polymer and cargo. Because the aggregation occurs during the freezing stage, it might be possible to obtain desirable properties from freezing the polymer without lyophilization.

Ionically cross-linked alginate hydrogels can be rapidly formed through submerging an aqueous alginate solution into a divalent cation solution or vice versa [13, 15, 23]. To perform this gelation with the anticipated benefits of freezing, we characterized thaw-induced gelation (TIG). Distinctly, the method involves melting a frozen solution in a complementary solution that permits the gelation of alginate hydrogels. For example, as the frozen polymer solution goes to the liquid phase, calcium ions can then diffuse into what was once a frozen space, cross-linking alginate polymers. Additionally, as a frozen calcium chloride solution thaws, the calcium ions are now accessible in the liquid phase to diffuse down the concentration gradient towards the alginate polymer solution, resulting in hydrogel formation. Succinctly, the thawing phenomenon initiates the diffusion of ions and the availability of cross-linking sites on alginate polymers. We hypothesized that the gelation of alginate hydrogels via TIG is dependent on the thawing rate and diffusion of calcium and alginate. Furthermore, we postulate that freezing alginate leads to phase separation that is partially dissolved and cross-linked when thawing in calcium, dependent on the rate of heat transfer and the rate of calcium diffusion. This latter hypothesis is

expanded upon in chapter 4. Regardless, preserved aggregated polymer was expected to have an enhanced stiffness similar to a sponge. Additionally, the aggregated polymer could entrap smaller cargo, slowing release within the aggregated polymer, and potentially electrostatic interactions. To our knowledge, this was the first attempt to characterize the release of electrostatically active cargos from an alginate hydrogel formed by this method. Generally, thaw-induced gelation and similar methods are underrepresented methods for forming hydrogels.

3.2 Materials and methods

3.2.1 Formation of hydrogels via thaw-induced gelation

LF10/60 alginate polymer (molecular weight ~ 120-150 kDa and >60% G-block; purchased from FMC Biopolymers) and chitosan polymers (medium molecular weight ~ 190-310 kDa and degree of deacetylation of 75-85%; purchased from Sigma) were used in the work presented in this chapter. Alginate and calcium chloride solutions were prepared in 1X phosphate-buffered saline containing calcium and magnesium ions, pH 7 (PBS^{++}; Life Technologies) or diH_2O. These two solutions represent an isotonic and hypotonic solution, respectively. Alginate was diluted to 1 or 2% (w/v), and calcium chloride solutions were prepared at 50, 100, and 200 mM. Chitosan polymers were reconstituted by dissolving at 4% (w/v) in glacial acetic acid (0.066 M; Sigma) and stirred overnight. For mixtures of alginate and chitosan, ratios were prepared by mixing alginate and chitosan stock solutions to desired final weight percentages between two syringes using a syringe connector. Frozen disks used in TIG were prepared by filling cutouts in a rubber sheet with 10, 20, 30, 50, and 100 µL of either the polymer or cross-linker solutions. Rubber mold for the frozen disks was made by cutting holes that were 3, 4, 5, 6, or 8 mm in diameter into a rubber sheet that was 2 mm thick. Unless stated otherwise, 100 µL volumes were used for the frozen component for TIG. After filling with the respective solutions, these molds were placed in -80 ˚C for two hours to become frozen. The frozen disks were submerged into the respective solution for ionic cross-linking between alginate and calcium for gelation. Specifically, a frozen alginate solution was submerged in a bath containing calcium chloride; and a frozen calcium chloride solution was submerged in a bath containing dissolved alginate polymers. Solutions used to thaw the frozen disks were

prepared similarly to the process for the frozen solutions. In most experiments, the frozen or thawing solutions containing the same mixture of polymers and cross-linker were the same. Frozen solutions were dropped into the thawing solution and left to gel for 5 minutes before being taken out and rinsed in 1X PBS^{++} to remove excess thawing solution from the hydrogel surface. A liquid-core capsule was formed from a frozen cross-linker, calcium, thawed in a bath containing alginate. A hydrogel is formed without a liquid core by starting with a frozen alginate solution thawing in a bath containing calcium chloride. With the addition of chitosan, the material becomes a hybrid hydrogel with ionic cross-linking and interactions between the alginate and chitosan polymers. A normal gelation protocol was performed as a control by submerging the molds containing alginate solution into the same calcium chloride solution used in TIG. Alginate sponges were prepared from these alginate hydrogels by freezing in a -80 ˚C freezer for two hours and then lyophilizing. A summary of this fabrication process is presented in Figure 3.2.

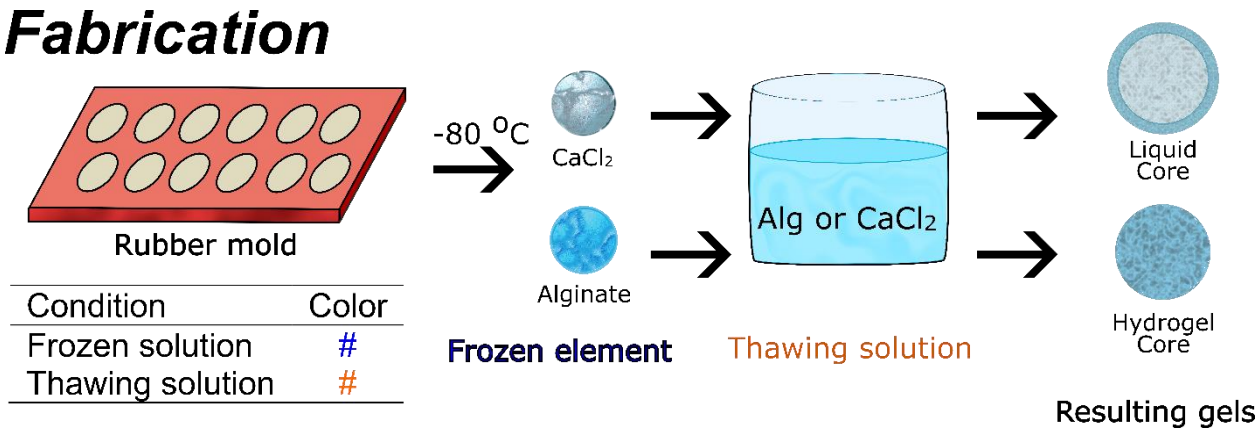

Figure 3.2 Schematic for forming alginate hydrogels via thaw-induced gelation. Polymer or cross-linker solution was frozen in a rubber mold then placed in a -80 °C freezer overnight. Frozen solutions were now removed from the mold and submerged in a thawing solution containing the corresponding cross-linker or polymer to induce hydrogel formation. A hydrogel with a liquid core is formed if a frozen cross-linker is submerged and melted in a polymeric solution. A hydrogel is formed without a liquid core if a frozen polymer solution is submerged and melted in a cross-linker solution.

3.2.2 Alginate hydrogel characterization

Pictures of select alginate hydrogels containing chitosan were hydrated in Orange II dye were taken before and after lyophilization. Orange II was used because it electrostatically interacts with positively charged polymers and can show local distributions of chitosan [24]. Scanning electron microscope (SEM) images were obtained for alginate hydrogel, sponge, and the TIG hybrid hydrogel as previously described with minor modifications [11, 14, 25]. For SEM images, chitosan was not incorporated within the hydrogels. Briefly, hydrogels were immersed in increasing concentrations of ethanol solution until the solvent was 100% ethanol. During this time, exposure to air was limited to prevent drying out. Next, samples underwent critical point drying (CPD). This method is an alternative to solvent replacement and freeze-drying techniques for drying a hydrogel for SEM, resulting in hydrogel collapse from surface tension forces or inducing cryostructuring during ice formation, respectively. Given the hypothesized cryostructuring event from TIG to be interrogated via SEM, CPD was the optimal preparation method for obtaining images without structural collapse or an obfuscating secondary cryostructuring event. Alginate sponges were already dry after being formed by freeze-drying an alginate hydrogel. The samples were then imaged with the Quattro S Scanning Electron Microscope (Thermo Fisher Scientific).

The equilibrium swelling ratio (Q_m) of each gel was determined by first swelling the gels in PBS^{++} for 24 hours. The wet mass was first measured, followed by lyophilizing to obtain a dry sample for measuring the mass without water [11, 26, 27]. This swelling ratio was defined by its mass, as given in the following equation:

$$Q_m = (W_s - W_d)\, W_d^{-1},$$

where W_s is the swollen weight of the hydrogel and W_d is the dry weight. The hydrogels' shear storage modulus (G') was obtained by first swelling in PBS^{++} overnight. Excess fluid was wicked away, and the hydrogels were placed between parallel rheometer plates (HR2, TA Instruments). The hydrogels were strained (0.4-5%) at a set frequency (10 rad s^{-1}). A minimum of six points within the linear range was averaged to obtain G' and reported for each hydrogel condition. Mesh size (ξ) was determined through the volumetric swelling ratio and storage moduli by Flory-Rehner calculation as previously described [11].

The swelling ratio, storage modulus, and mesh size were determined for alginate hydrogels gelled under different salinity conditions either within the polymer or cross-linking solutions using diH_2O or PBS^{++}. For this experiment, alginate (2% (w/v)) was cross-linked with a $CaCl_2$ (100 mM) solution kept around 2 ˚C. Thaw-induced gelation conditions were compared to a normal gelation method, where the alginate polymer was not frozen and gelled in the same cross-linking solution. Furthermore, the thawing rate effects were tested by altering the thawing solution temperatures (2 and 22.5 ˚C) under different calcium concentrations (50 and 200 mM). These extrema were chosen due to their ease of use for a temperature close to the freezing temperature and one that would induce rapid melting. The swelling and storage modulus was measured for these alginate hydrogels formed by thaw-induced gelation and compared to an alginate sponge formed by freezing-drying an alginate hydrogel.

3.2.3 Characterization of hydrogels with liquid-cores

For characterization of liquid-core hydrogel capsules, the shell thickness and mass of alginate gelled were determined. Shell thickness was calculated by subtracting the outer and inner diameters of the hydrogel disk and dividing by two. The amount of cross-linked material, mass gelled, was determined by measuring the dry weight of the capsules after freeze-drying. For the first characterization experiment, the shell thickness and mass gelled were calculated for the hydrogels formed with differing concentrations of $CaCl_2$ and alginate (50, 100, and 200 mM; and 1 and 2% (w/v), respectively) at 2 ˚C. Follow-up experiments tested shell thickness using 1% alginate and 100 mM $CaCl_2$. These experiments differed encapsulation volumes (10, 20, 30, 50, and 100 µL) thawed at approximately room temperature (22.5 ˚C) or tested the thawing rate by altering the temperature of the thawing solution (2 and 22.5 ˚C).

3.2.4 Cargo release from hydrogels formed by TIG

Release experiments were performed by loading cargo into solutions that were then frozen. The cargos were specifically chosen to encompass differing charges in a neutral pH and molecular weights: doxorubicin (Dox, 543 Da, Sigma), fluorescein isothiocyanate-dextran (FITC-dextran, 4 kDa, Sigma), and fluorescein isothiocyanate-albumin (FITC-albumin, 68 kDa, Sigma). These frozen solutions were loaded with either 0.2 µmol of Dox, 0.1 µmol of FITC-dextran, or 0.1 µmol of FITC-albumin. Despite hour efforts to keep the concentration of each cargo about the same, due to the magnitude changes in molecular weight, the use of high concentrations of doxorubicin presented an unnecessary health risk. Additionally, too low weights of albumin presented a challenge for accurate measurements. The frozen solutions include calcium chloride (Ca, 100 mM),

calcium with chitosan (CaC, 100mM and 1% (w/v), respectively), alginate (Al, 2% w/v), and alginate with chitosan (AC, 2% and 1% (w/v), respectively). Frozen solutions were formed into disks with a starting volume of 100 µL. The next day hydrogels were dropped and submerged in the thawing solutions. Samples thawed until the ice was no longer observable, typically less than a minute. The hydrogels were then placed in individual wells of a 24-well plate and immersed in PBS^{++} (500 µL, pH 7). The release experiment was carried out at room temperature. In addition, an experiment was performed to compare the release of FITC-dextran at room temperature and 37 °C. The sample media was extracted and placed into a clean 24-well plate. Fluorescence was measured by plate reader using known fluorescence spectra of FITC (excitation: 490 nm, emission: 525 nm) and doxorubicin (excitation: 485 nm; emission: 550 nm) (Spectramax I3, Molecular Devices). Standard curves were developed for each cargo. Wells were replenished with fresh media after each measurement. The release was measured over 4-weeks before samples were broken down and the remaining cargo measured. The relative release was calculated.

3.2.5 Statistical analysis

Results in this chapter are shown as mean values with standard deviations. Sample sizes are provided with each experiment and stated in the figure legends or shown in figures as individual data points. Statistical significance was asserted at $P < 0.05$. All analyses were performed using Graph-Pad Prism software (GraphPad Software Inc.).

3.3 Results

3.3.1 Thaw-induced gelation (TIG) of hydrogels

The TIG method utilizes a frozen solution of either alginate or ionic cross-linker, calcium, melted within the cross-linker or alginate solution, respectively (Figure 3.3A). Thawing cross-linker in an alginate polymer solution generates a liquid-core capsule with a hydrogel shell called alginate hydrogel capsules or just capsules. The hydrogel cross-links outwards from the frozen calcium as calcium can penetrate the growing hydrogel shell, but alginate polymer cannot. Similarly, thawing frozen alginate generates hydrogels in which polymer cannot diffuse through the cross-linked hydrogel. At the same time, calcium continues to diffuse inwards to cross-link the polymer and form what will be referred to as a TIG hydrogel to distinguish it from the control hydrogel and capsules. Chitosan was added to either the frozen solution or thawing bath for thaw-induced gelation hydrogels from alginate polymers ionically cross-linked with calcium ions.

The thaw-induced gelation process generated a solid hybrid hydrogel or liquid-core capsules with a hydrogel shell (Figure 3.3B). As the Orange II dye interacts with chitosan, the darker orange color represents areas with a higher localization of chitosan polymers. For the capsules, chitosan is localized around the hydrogel shell. In contrast, in the hybrid hydrogel where a solution of alginate and chitosan were frozen, the chitosan is in patches throughout the hydrogel. Furthermore, there appears to be no dense localization of chitosan when a frozen alginate solution is thawed in a calcium bath containing chitosan polymers. Interestingly, in the lyophilized sample cut in half, there is a distinct difference in polymer density from the outer edge of the hydrogel to the inner core, appearing denser around the edge and having larger pores in the center. SEM images were obtained to

investigate morphological changes in alginate networks between our control hydrogel and sponges versus the hydrogel formed by TIG (Figure 3.3C). Specifically, this hydrogel formed by TIG was only the one starting from a frozen alginate solution as the capsules collapsed. Overall, the alginate sponge contrasted the control and TIG hydrogel structure by having large micrometer-scale pores. Remarkably, smoother aggregated structures observed in the sponge are also visible in the TIG hydrogel and not the control hydrogel. Additionally, where the sponge is only made of the jagged-looking aggregated sheets, the TIG-formed hydrogel has softer features that resemble the control hydrogel.

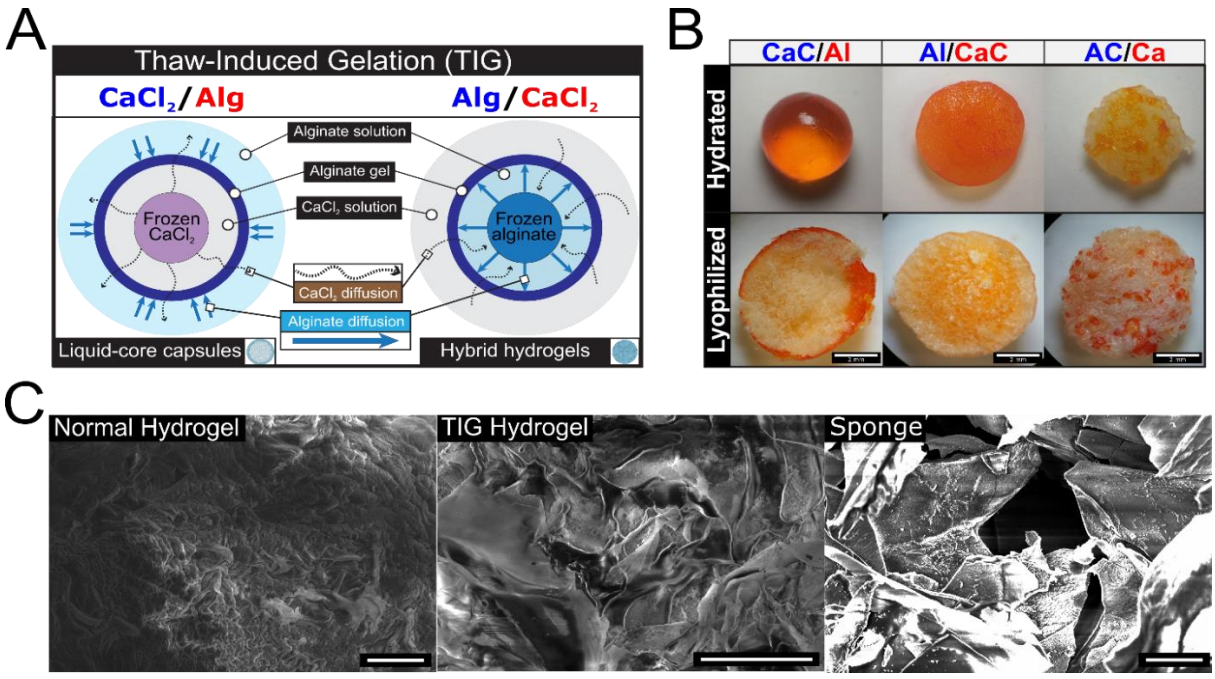

Figure 3.3 Fabrication of thaw-induced gelation (TIG) hydrogels. The TIG approach enables the creation of either liquid-core alginate hydrogel capsules or alginate hybrid hydrogels, depending on whether the alginate polymer or cross-linking is thawed or frozen. The hydrogel grows outwards for the capsules and inwards for the hydrogels through the diffusion of the calcium ions (A). Representative images of alginate and chitosan hydrogels formed by TIG were dyed with Orange II to visualize different regions (B). In these images, a shorthand is used: alginate (Al, 2% (w/v)), $CaCl_2$ (Ca, 100 mM), $CaCl_2$ and chitosan (CaC, 100 mM and 1% (w/v), respectively), and alginate and chitosan (AC, 2% and 1% (w/v), respectively). To differentiate condition of that solution, a frozen solution has its text in blue while the thawing solutions are in red. SEM images of 2% (w/v) constructs: normal hydrogel (the control hydrogel), TIG hydrogel, and alginate sponge; scale bar represents 50 µm (C).

3.3.2 Characterization of hydrogels formed by TIG of a frozen alginate solution

Characterization was performed to compare the TIG hydrogels to the control gelation scheme for generating alginate hydrogels and sponges. First, TIG was compared to standard ionic alginate gelation (normal) as a control group. In this normal gelation, hydrogels were formed without freezing and melting, but used the same solutions as the TIG hydrogels. In both methods, alginate and $CaCl_2$ were diluted in either a phosphate buffer solution with magnesium and calcium (PBS^{++} (1X)) or diH_2O, representing different osmolarities. The swelling ratios for hydrogels formed by TIG were comparable to the typical gelation techniques without freezing the alginate polymer, regardless of the salinity conditions (Figure 3.4A). There is a trend of alginate hydrogels formed via TIG to have a slightly lower swelling ratio. Aligning with this potential trend, the swelling ratio of an alginate sponge was approximately 26% less than the TIG hydrogel formed using the same concentrations of alginate, calcium, and gelation temperatures (Figure 3.4A & D). Additionally, the storage moduli of the TIG hydrogels were significantly stronger to control hydrogel formed through a more traditional gelation method ($p < 0.01$) (Figure 3.4B). Although there is no significant difference in swelling between salinity conditions, the elasticity of the TIG hydrogels was slightly improved in conditions where alginate was frozen in a phosphate buffer solution. In contrast, the control gelation method for generating alginate hydrogels decreased strength with phosphate buffer in the polymer solution. From the swelling and stiffness measurements, we obtained an estimate of the hydrogels' mesh size. TIG hydrogels' calculated mesh size was consistently smaller than the control alginate hydrogel (Figure 3.4C). Between the different salinity conditions, there was no significant difference in the measured properties.

Next, we measured the effect of slow and rapid thawing (2 ˚C and 22.5 ˚C calcium baths) using low and high calcium concentrations (50 and 200 mM). Briefly, the temperatures of the thawing bath defined the rate of heat transfer, and therefore the time it takes the alginate to melt. Additionally, the cross-linker concentrations define the rate of diffusion through different magnitudes of the concentration gradient. Together, these parameters control the melting and cross-linking rate and are being compared directly to alginate sponges. The swelling ratios and strength for hydrogels thawed at 2 ˚C were similar despite having different cross-linker concentrations. The TIG hydrogels formed via slow thawing in a 2 ˚C calcium bath had enhanced strength that was still less than the alginate sponges (Figure 3.4E). In contrast, when alginate polymer thaws rapidly at 22.5 ˚C, the resulting hydrogels were significantly less elastic and had greater swelling than the hydrogels formed with slow melting. Particularly, the 2% (w/v) alginate hydrogel cross-linked in a 50 mM calcium bath was barely coherent, resembling more of a sol gel.

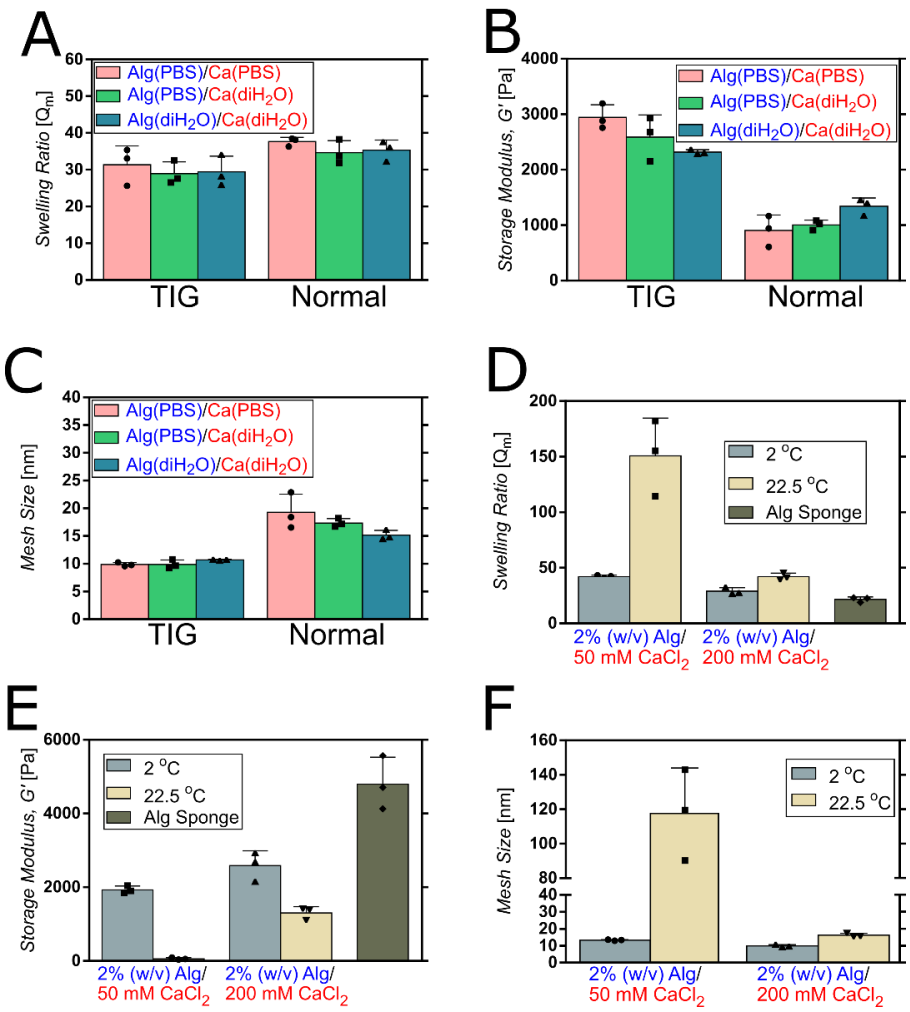

Figure 3.4 Physical characterization of alginate hydrogels. TIG hydrogels are compared to normal gelation methods via the swelling ratio (A), storage moduli (B), and mesh size (C). The dependence of thawing temperature (2˚C and 22.5˚C) and cross-linker concentration (50 and 200 mM) on 2% (w/v) alginate (Alg) was tested by the swelling ratio (D) storage moduli (E), and mesh size (F), and placed in comparison of alginate sponges. Frozen solutions and thawing solutions are represented through blue and red text, respectively. Bars with scatter plots represent the mean with individual measurements displayed and error bars representing standard deviation (A-F, n=3).

3.3.3 Liquid-core capsule fabrication and characterization

In addition to the hydrogels formed through thawing a frozen alginate polymer solution, starting with a frozen cross-linker solution that melts in an alginate polymer bath formed liquid-core capsules with an alginate hydrogel shell. Despite the different structural outcomes, similar factors of concentrations and temperature influence their formation. We tested three frozen concentrations of calcium chloride (50, 100, 200 mM) thawed in different alginate concentrations (1 and 2% (w/v)). Varying shell thicknesses were generated with these conditions. The slopes of shell thickness versus cross-linker concentration increase with higher alginate concentration from 3.409 μm mM^{-1} (R^2 = 0.7172) to 6.219 μm mM^{-1} (R^2 = 0.8897) from 1 to 2% (w/v) alginate, respectively (Figure 3.5A). This phenomenon is also observed in the slope for the dry mass of cross-linked hydrogel versus the cross-linker concentration, increasing from 15.17 μg mM^{-1} (R^2 = 0.9837) with 1% (w/v) alginate solution to 27.24 μg mM^{-1} (R^2 = 0.9771) with a 2% (w/v) alginate solution (Figure 3.5B). The slope of mass gelled approximately doubled from the doubling in alginate polymer concentration in the thawing bath within the range of tested calcium chloride concentrations. Interestingly, a similar shell thickness was generated from the various frozen volumes of calcium chloride tested (Figure 3.5C). However, it becomes increasingly challenging to prevent melting before submersion in the alginate bath the smaller the frozen solutions are. Because of this challenge, strings of liquid calcium solution generate these hydrogel tails, which can be seen in the inlet images on the bar graph. We combated this outcome by keeping the samples on dry ice before releasing the frozen samples from the mold, directly submerging them in the alginate polymer bath. Similar to the TIG hydrogels, there were temperature-dependent changes

in the hydrogel shells. Rapid thawing in an alginate bath at 22.5 ˚C led to hydrogel shells that were about half as thick as the capsule shells when using a thawing bath that was 2 ˚C (Figure 3.5D).

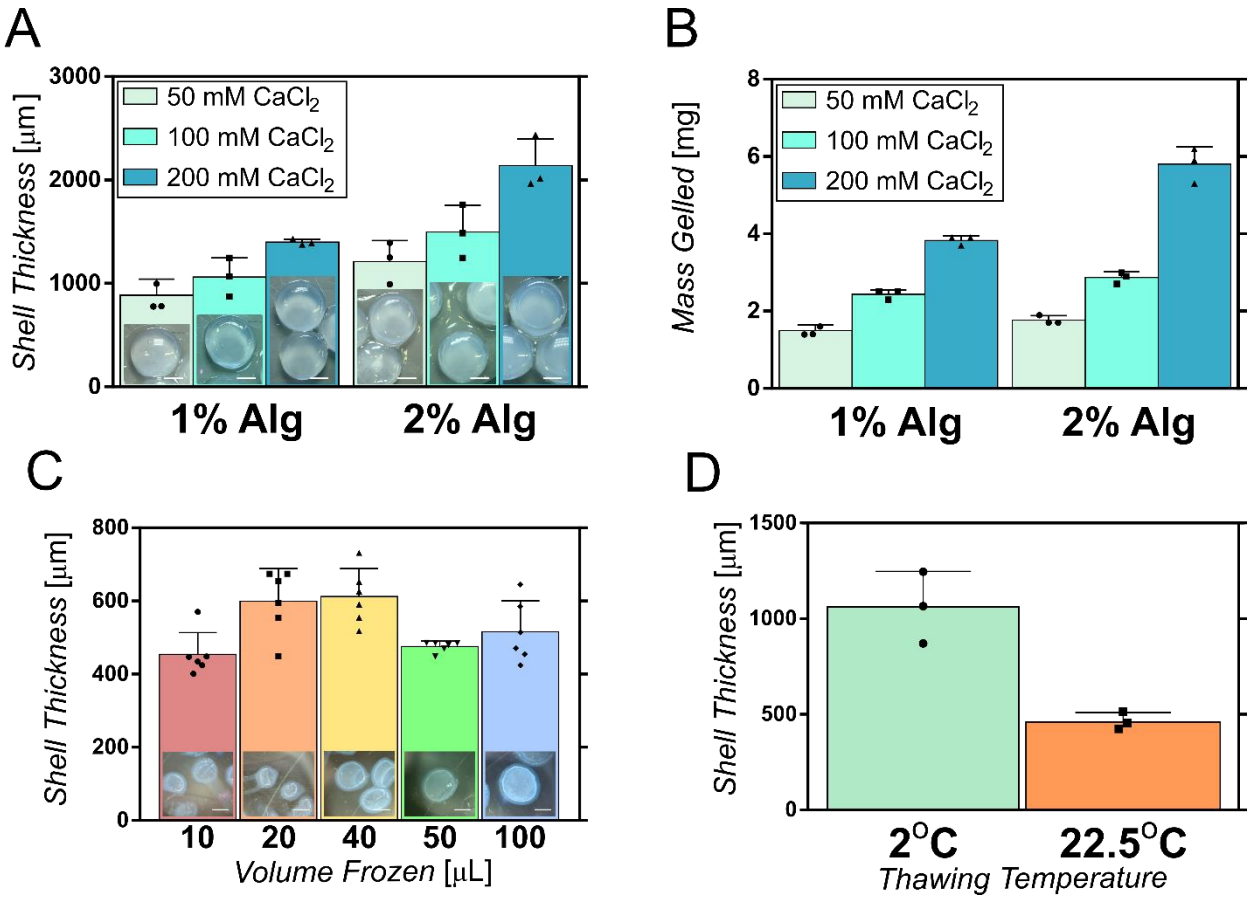

Figure 3.5 Characterization of liquid-core capsules gelation. Capsule shell thickness dependence on frozen cross-linker ($CaCl_2$) and alginate polymer (Alg) concentration at 2 ˚C with representative images (A). These capsules were lyophilized to measure the mass gelled (B). The shell thickness for different frozen cross-linker volumes with the same concentration was quantified with representative images of the capsules formed at 22.5 ˚C (C). Temperature-dependent changes in shell thickness were measured for 2 and 22.5 ˚C (D). Bars with scatter plots represent the mean with individual measurements displayed and error bars representing standard deviation (A, B, and D, n=3; and C, n=6). The scale bar in the images is 4 mm.

3.3.4 Release of Cargo from Alginate TIG Hydrogels and Liquid-Core Capsules

The influences of polymer aggregation and electrostatic interactions on release were interrogated using three distinct cargo molecules with different sizes and net charges in a neutral pH. Specifically, doxorubicin (dox; 543 Da), FITC-dextran (dextran; 4 kDa), and FITC-albumin (albumin; 66.5 kDa) were loaded into the frozen solutions, and TIG was performed by thawing the samples in the respective solution to induce ionic cross-linking of an alginate hydrogel. Additionally, to enable potential electrostatic interactions, chitosan was included as a polymer that would have a slight positive charge as a contrast to the negative charge of the alginate polymer. Generally, the release of this cargo from the various hydrogels formed by TIG followed a trend dependent on the cargo molecule's size (Figure 3.6A-E).

In all cases, dox was released more rapidly from the hydrogels than the albumin protein. However, when alginate polymers were frozen, the release rate of the dox molecule became slower than the larger dextran molecule (Figure 3.6A&B). The alginate hybrid hydrogels released 90% of dox after 72 hours, regardless of their chitosan content. Notwithstanding, dox in the liquid-core capsules, in which no alginate is frozen, rapidly released, with over 90% of the cargo diffusing out from the hydrogel within the first 24 hours (Figure 3.6D&E). The release profiles of dox from the liquid-core capsules were generally much faster than the TIG hydrogel, regardless of the additions of chitosan.

In contrast to the dependency of dox release profiles on whether the hydrogel resulted from frozen alginate, the release of dextran cargo was altered when it was frozen along with chitosan. Despite having the same chitosan containing thawing bath, the release of dextran was reduced only when chitosan was included in the frozen alginate

solution (Figure 3.6B&C). The result of this shift is most clearly observed in the shift of dextran from being released faster than dox in TIG hydrogels that did not include frozen chitosan to being released more slowly when the TIG hydrogel was formed from a frozen solution containing both alginate and chitosan. Similar differences resulting from frozen chitosan were observed with the liquid-core capsules. The release of dox and dextran is rapid from the liquid-core capsule with no chitosan, with over 90% of cargo released within 24 hours (Figure 3.6D). By using a frozen solution containing chitosan polymer, there is a reduction of release for dextran but not dox (Figure 4E). For liquid-core capsules, chitosan slowed the release of 90% of the dextran from 8 hours to 96 hours. In contrast, liquid-core capsules released 90% of dox within 8 hours, regardless of chitosan content.

These alterations in release profiles are more drastic with albumin. Generally, the addition of chitosan resulted in a slower release of albumin regardless of if it was frozen or not. Between TIG hydrogels where only the thawing bath differed through the addition of chitosan, there is a slight reduction in the release rate. However, if chitosan is frozen, the release of chitosan can be mostly prevented. For example, less than 20% of albumin was released after one week in liquid-core capsules and less than 30% in the TIG hydrogels when the frozen solution contains albumin and chitosan. Compared to the frozen solutions without chitosan, freezing albumin with chitosan significantly reduced the release rate of albumin. Lastly, we performed an additional experiment comparing the release of dextran at room temperature and 37˚C to observe how these release trends would be expected to change (Figure 3.7A-E). Generally, cargo is released faster at 37˚C than room temperature, with conserved differences between hydrogel groups.

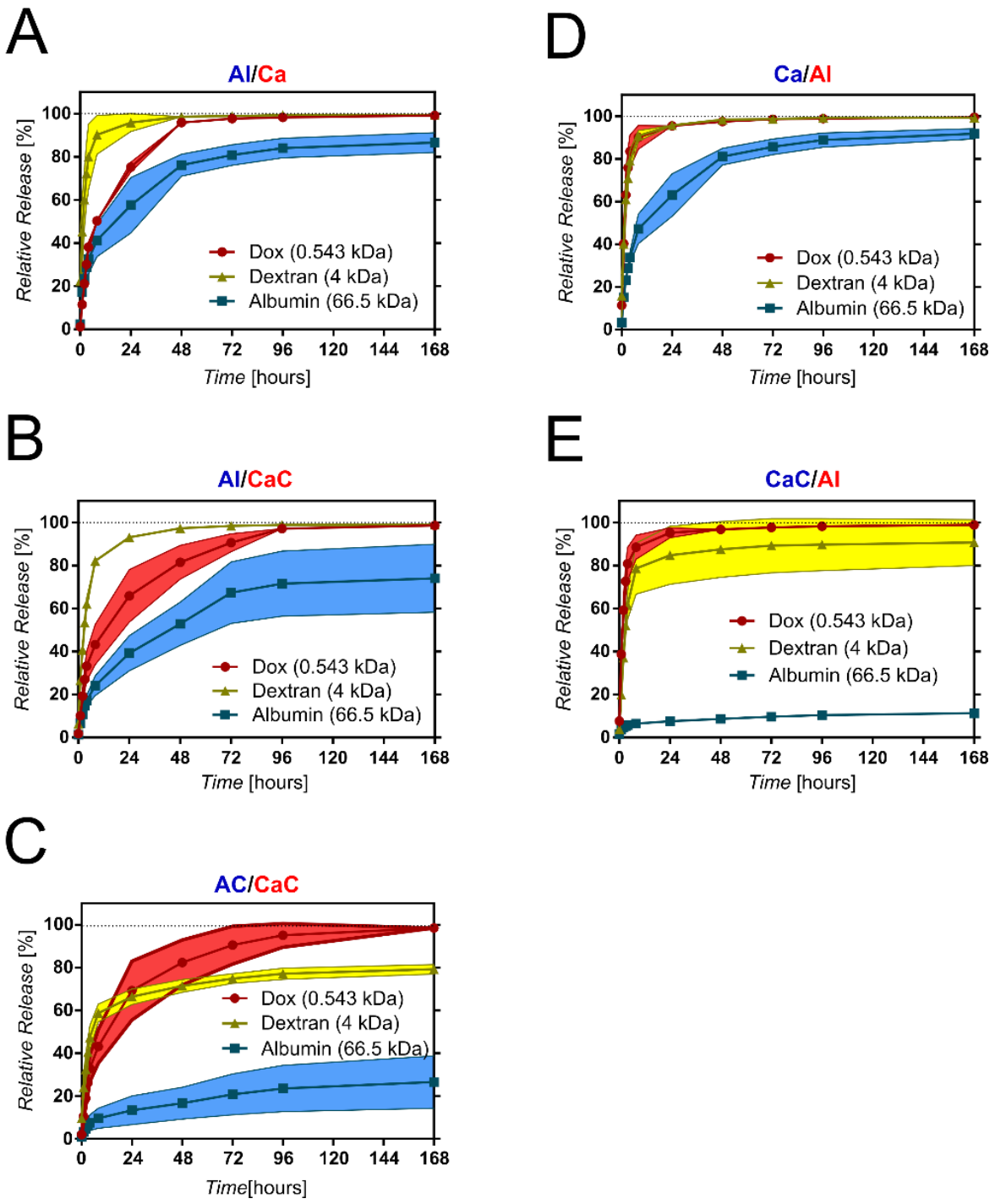

Figure 3.6 Relative release profiles of the cargo dextran, doxorubicin, and albumin. The shorthand is used to describe frozen solutions in blue and the thawing bath solutions in red: alginate (Al, 2% (w/v)), $CaCl_2$ (Ca, 100 mM), $CaCl_2$ and chitosan (CaC, 100 mM and 1% (w/v), respectively), and alginate and chitosan (AC, 2% and 1% (w/v)). Frozen

alginate was thawed in calcium (A) or calcium with chitosan solution (B). In addition, alginate and chitosan were thawed in calcium and chitosan solution (C). Calcium was frozen for liquid-core capsules without (D) or chitosan (E) and thawed in an alginate solution. Each cargo is represented by a line representing the mean, and shaded areas represent standard deviation (A-E, n=3).

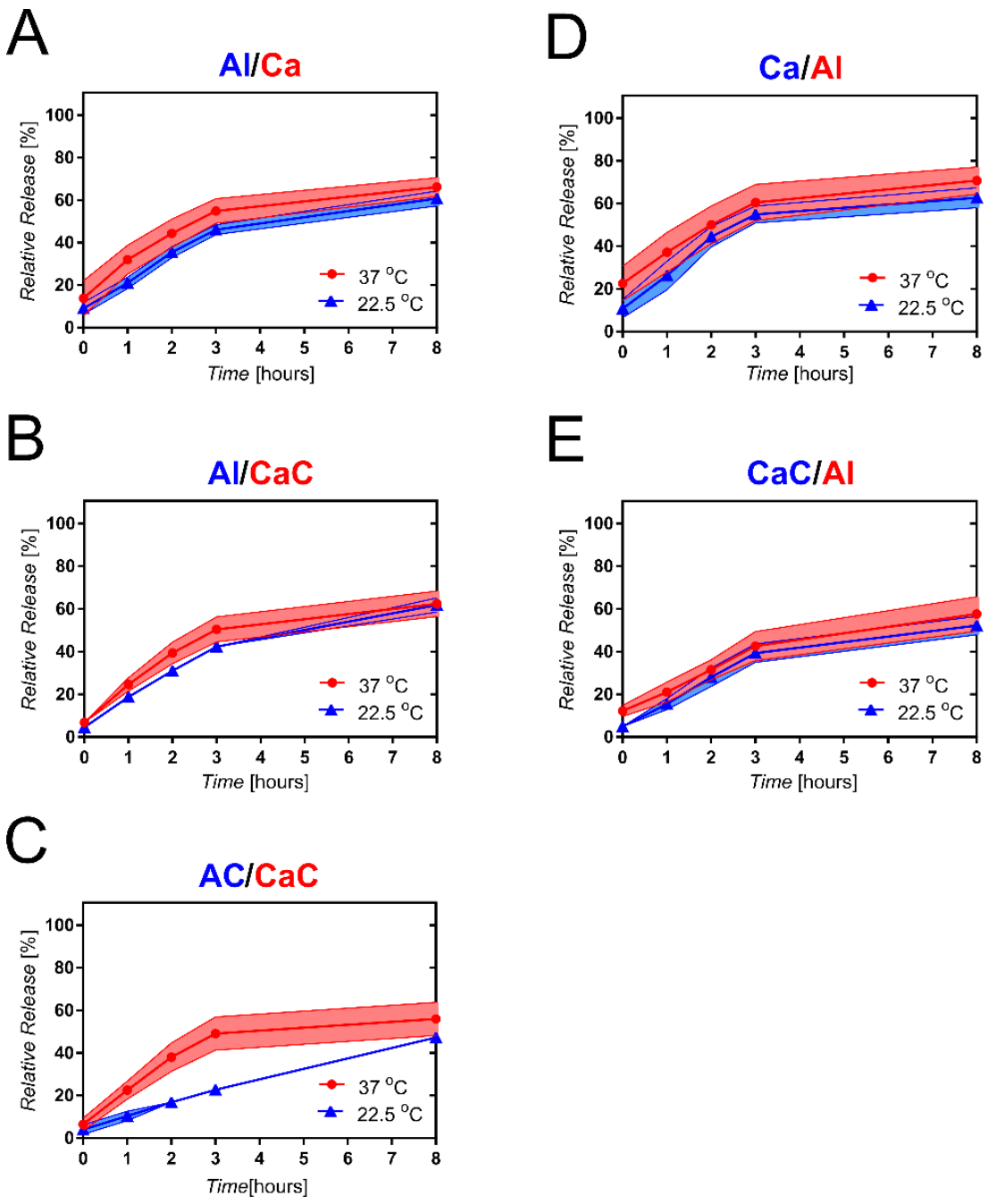

Figure 3.7 Relative release profiles of dextran at varying temperatures. Release of the dextran cargo from TIG hydrogels was performed in 22.5°C and 37°C solutions. The shorthand used to indicate hydrogel type is the same as Figure 3.7. Frozen alginate was thawed in calcium (A) or calcium with chitosan solution (B). In addition, alginate and chitosan were thawed in calcium and chitosan solution (C). Calcium was frozen for liquid-

core capsules without (D) or chitosan (E) and thawed in an alginate solution. Each cargo is represented by a line representing the mean, and shaded areas represent standard deviation (A-E, n=3).

3.4 Discussion

3.4.1 The formation of alginate hydrogels via TIG

The work in this chapter describes the gelation scheme that will be further tested for its utility in later chapters. This gelation scheme is dependent on the availability of alginate polymer or cross-linker to define the geometry and structure. This availability is the result of an irreversible thawing even that releases the polymer or cross-linker from a frozen state. Because this melting is the trigger for ionic cross-linking of alginate, we termed this scheme thaw-induced gelation (TIG). The process presented here resulted in two hydrogel structures: a TIG hydrogel and a liquid-core hydrogel capsule. While each of these will be explored in more depth in later chapters, additional hydrogels have been discovered why attempting to translate these hydrogels for cell cryopreservation applications.

Thawing alginate was hypothesized to partially dissolve aggregated polymer formed during freezing and ionically cross-link into the TIG hydrogels. The diffusion of calcium into the thawing alginate generated a hydrogel that approximately maintained the shape and size of the frozen disk. Notably, the hydrogels did swell up into a sphere despite the frozen alginate starting as a disk. Alternatively, melting frozen cross-linker in an alginate polymer solution produces a capsule with a hydrogel shell surrounding a liquid core approximately the volume of the initial frozen disk. Like the TIG hydrogel, the capsule also swelled to form something closer to a sphere. For alginate TIG hydrogels, we hypothesized aggregated polymer could improve electrostatic interactions between cargo and polymer. Similarly, liquid-core capsules would control release only through the mesh size of the hydrogel shell if there was no frozen polymer. Therefore, after the

characterization of the hydrogels, TIG strategies were validated for the delivery of therapeutic cargos smaller than the mesh size of alginate hydrogels. Consequently, the hydrogels demonstrated unique utility in enabling the controlled release of these cargos without chemical modifications to the hydrogels that have not been previously explored in the context of controlled delivery before.

3.4.2 Characterization of TIG hydrogels

The storage moduli and swelling ratios of alginate hydrogels formed by TIG are between the measured values of both an alginate sponge and hydrogel. While this could suggest a combination of physical features, these measurements alone do not directly answer that similar structures exist. Therefore, SEM was performed on the hydrogels, which further supports that the hydrogels formed by TIG had similar features of a hydrogel and sponge. Nonetheless, the hydrogels were significantly stiffer than the control alginate hydrogels for all salinity conditions and about 50% less than the alginate sponge group, suggesting a potential elasticity gain from non-ionically cross-linked polymer. Together these outcomes support our hypothesis that aggregated alginate polymer is partially preserved by TIG and results in a hydrogel that embodies some aspects of a sponge.

3.4.3 Hydrogels formed by TIG are distinctly different from cryogels

Importantly, these alginate hydrogels formed by TIG in this study are distinct from cryogels because the alginate hydrogel is being formed by ionic cross-linking following a thawing event rather than cross-linking during or due to a freezing event [28, 29]. Unlike

poly (vinyl alcohol) cryogels, alginate does not sustain the polymer aggregation from freezing [28, 30-32]. If the frozen alginate solutions were thawed in a bath of PBS without calcium, the alginate solution dissolved completely. Therefore, without ionic gelation during freezing or some other addition, a macroporous structure similar to cryogels or alginate sponges cannot be formed with frozen alginate. Altogether, the physical properties of the TIG hydrogels were between those of our control alginate hydrogels and alginate sponges. While it is unlikely that a macroporous structure is wholly preserved after thawing, our data suggest a dissociation of aggregated polymer within the alginate hydrogel. To interrogate the potential existence of persistent cryostructuring after thawing frozen polymer solution, chapter 4 describes work in which cryostructuring is modulated through various freezing rates. Appropriately, more hydrogel-like properties are beneficial for wound dressings, such as small pores having a lower tendency to adhere to an injury site and are less likely to harbor bacterial colonies [4, 21, 22, 33]. Additionally, a more elastic alginate hydrogel could provide a toughness that would better permit recovery after compression. Regardless of the application, the additional parameters of freezing and thawing already mimic processing steps used in cryogels, giving precedent to the feasibility of this gelation scheme for generating clinically relevant hydrogels where cryopreservation is needed.

3.4.4 Effects of buffer and pH when performing TIG

Interestingly, alginate TIG hydrogels were slightly stiffer, although not statistically significant, when the frozen polymer solutions contained a phosphate buffer instead of diH_2O. In contrast, the control alginate hydrogels were less stiff in phosphate buffers.

Generally, the use of phosphate buffers with divalent ionic cross-linking of alginate polymers would be expected to lead to weaker hydrogels because the phosphate ions can sequester calcium ions, which follows from the observed trends in our control hydrogels [12, 34]. However, the freezing of a phosphate solution can lead to a. acidic shift in pH. Specifically, previous studies have described a pH shift of a solution close to the pKa of alginate monomers when freezing PBS to -30˚C [32, 35, 36]. Thus, an acidic alginate solution has less electrostatic repulsion due to a loss of the negative charge from the carboxyl groups on the polymer. Consequently, aggregation of the polymers during freezing can be more efficient [31, 32]. However, while more effective aggregation would coincide with the increase in stiffness and agree with the hypothesis of persistent aggregations of alginate polymer after thawing, the overall magnitude of these differences is minuscule compared to the increase in stiffness from TIG hydrogels and out control hydrogels.

Furthermore, although the pH of a phosphate solution shifts when freezing, it is expected to return to neutral when thawing and would still impact calcium cross-linking, as with the control hydrogel. Therefore, although a notable change in pH can be expected when freezing polymers and should be considered in future studies, the potential changes to the resulting hydrogel remain unclear. Nevertheless, an acidic pH can potentially be detrimental to proteins that might be used as the target cargo [36]. Additionally, osmolarity shifts could also damage the cargo and alter hydrogel properties and will be discussed further in chapter 4.

3.4.5 Controlling hydrogel properties through thawing rates

The temperature of the thawing bath solution resulted in hydrogels with different properties, suggesting melting rate could be used to control alginate cross-linking during TIG. Interestingly, slower thawing had a comparable stiffness and swelling ratio as the hydrogels thawed four times the cross-linker concentration. In contrast, faster thawing of frozen alginate solution into 50 mM calcium solution resulted in the weakest gel and the largest swelling ratio. The reduced stiffness and increased swelling ratio observed with lower calcium concentrations are expected with alginate gelation [37]. However, the similarity of hydrogels that underwent slower thawing in different calcium concentrations could result from various factors. One possible explanation is that the rate of thawing was the limiting step for ionic cross-linking. That is, if calcium was able to diffuse to the edge where the alginate solution changed from a solid to a liquid, it could effectively cross-link the now available alginate polymers in the liquid phase. Nevertheless, further work is required to determine the interaction between thawing rate, the dissolving of aggregated alginate, and ionic cross-linking. Regardless, thawing rates were found to control swelling and stiffness properties of alginate TIG hydrogels. Given that high swelling and water retention in a wound are desired to support fluid transfer and wound dressings with smaller pores are often desired for their lower tendency to adhere to the wound, thawing rate provides an additional parameter for controlling alginate hydrogel properties [12, 21, 38]. These concepts are expanded upon in chapter 4, where the freezing rate is also modulated, which was hypothesized to alter aggregate wall thickness similar to alginate sponges [14, 22].

In contrast to alginate TIG hydrogels, dropping frozen cross-linker into alginate solution forms liquid-core capsules. Although TIG involves melting a frozen solution, the

dripping of a calcium solution into an alginate solution has been previously described as inverse gelation. Consequently, both TIG and inverse gelation have thicker alginate hydrogel shells with increased calcium concentrations, suggesting a similar calcium diffusion phenomenon [39, 40]. However, while inverse gelation resulted in thinner shells with a greater alginate concentration, TIG resulted in thicker capsules [40, 41]. The thawing event may slow calcium release compared to dropping liquid calcium into alginate during inverse gelation. The physical delay from thawing of the calcium solution is supported as the cause for this difference with TIG and inverse gelation because a faster thawing rate resulted in thinner hydrogel shells. Advantageously, while high alginate concentrations result in a highly viscous solution that can impede emulsion penetration with inverse gelation, the frozen solutions used in TIG preserved their form when submerging [42]. This characteristic of using a frozen element also permits different frozen amounts and shapes that are not possible with traditional inverse gelation.

3.4.6 Heat and particle diffusion perspectives for alginate capsules formed by TIG

Fundamentally, as the calcium diffuses away from the initial source, it will become diluted to a point where it cannot effectively cross-link alginate polymers. As described in Fick's 2nd law, the diffusion rate will depend on the local concentration gradient. Compared to inverse gelation, TIG controls the local concentration gradient by withholding calcium ions in the frozen state. Additionally, the differences between TIG and inverse gelation could be partially explained by a reduced ability for alginate cross-linking at lower temperatures [12]. Similar to particle diffusion, heat transfer also depends on the local

heat gradient. Together, the temperature gradients alter alginate gelation by modulating the diffusion rate and effectiveness for ionic cross-linking.

The parameters of diffusion and heat transfer altered how alginate cross-linking occurs. Notably, in the formation of capsules, alginate polymer cannot diffuse through the initially formed hydrogel shell. Therefore, the capsule's shell grows outwards as calcium ions diffuse down the concentration gradient. Importantly, the calcium ions are the diffusing element for hydrogel formation. When the calcium concentration in the frozen solution was increased from 50 to 200 mM, there was a greater change in the capsule's shell thickness between 1% and 2% (w/v) alginate. Specifically, there was a 15% increase in shell thickness with 50 mM $CaCl_2$ and a 50% increase with 200 mM. The larger gradient in calcium concentrations likely supported more efficient cross-linking further away despite the same change in local alginate concentrations. The thawing-dependent release of calcium could partially explain this discrepancy.

Although not directly explored in these experiments, the similar capsule shell thicknesses from different frozen volumes could also result from these heat transfer and diffusion effects. Because the shortest distance across the outer surfaces was the conserved 2 mm thickness from the rubber molds, this similar dimension of the geometry could have been the primary cause. Diffusion likely occurred over the shorter disk thickness until 1 mm was melted and diluted on each side. At that point, the entire samples would be melted regardless of volume. Overall, these parameters unique to TIG for liquid-core capsules lead to different outcomes than inverse gelation. These hydrogels should not be expected to follow the trends of inverse gelation when designing hydrogel-based cargo delivery vehicles [42, 43]. However, the use of a frozen solution to form an

encapsulating hydrogel has been employed in gastronomy by chefs and food scientists in a process called frozen reverse spherification [42-44]. Applications of this process have been patented for several uses with alcohol and to replicate the "pop" textures of caviar. While applying this technique within biomedical engineering applications is understudied, the integration of food science research and perspectives can be invaluable to medical applications of these materials.

3.4.7 Cargo delivery from alginate and chitosan hybrid hydrogels formed via TIG

The steric-based release of cargo is one of the primary considerations used when designing delivery vehicles. Unlike larger albumin, small cargos like dox and dextran were expected to encounter little physical hindrance while diffusing from the alginate hydrogels. In agreement with previous alginate hydrogel work, these smaller molecules were released within 24 hours in liquid-core capsules without chitosan [15, 23]. Moreover, the release of albumin from both TIG hydrogels and liquid-core capsules was similar without chitosan, suggesting phase-separation of alginate does not significantly affect albumin release. Importantly, however, these previously described combinations of hydrogels and cargos are not expected to interact electrostatically with each other except for alginate and dox. Dox is positively charged and would be expected to interact with negatively charged alginate [45]. Alternatively, the positive charge of chitosan is assumed to associate with the negative charge of the FITC attached to dextran [46, 47]. Consequently, the addition of chitosan led to a decrease in the release rate of albumin, which was more drastic in conditions where albumin was frozen within a chitosan-containing solution. In agreement with this outcome, previous work has described albumin

and chitosan forming a nanoparticle complex greater than 150 nm in diameter [48]. Previous studies have also suggested chitosan's ability to reduce the mesh size of alginate hydrogels by filling pores between cross-linked polymers [11, 13]. Compared to conditions without chitosan, reduced mesh size and possible nanoparticle complex formation would describe the diminished release rate of albumin from hydrogels with chitosan. The release rate of albumin within TIG hydrogels highlights how simple methods can adjust alginate hydrogel properties to improve delivery rate versatility. However, the drastic changes when the electrostatic complements of polymer and cargo are frozen together suggest an event beyond interactions of alginate and chitosan or polymer and the cargo.

3.4.8 Electrostatic phenomena are enhanced through freezing

When steric effects are ineffective at slowing release, electrostatics can provide additional cargo delivery control. The release kinetics between dox and dextran from alginate hydrogels suggest that the phase separation from freezing polymer, cryostructuring, provides further electrostatic interaction with the cargo. Specifically, positively charged dox would be expected to interact with negatively charged alginate, unlike the more neutral polysaccharide dextran with an attached FITC fluorescent tag [45, 49]. However, liquid-core capsules rapidly release dox and dextran within a day, suggesting insignificant steric or electrostatic control over release [11, 50]. This rapid release was also observed when the release experiment was carried out at 37 °C. In contrast, alginate TIG hydrogels without chitosan released the dox slower than dextran, suggesting these TIG hydrogels enhance electrostatic interactions between dox and the

alginate polymer. Similarly, the release of dextran plateaued before fully releasing cargo when the alginate freezing contained chitosan, which is potentially the result of alginate and chitosan electrostatically interactions entrapping dextran or chitosan having some interactions with the FITC fluorescent tag [15]. Altogether, the electrostatic effects on the diffusion of charged particles in hydrogels are still poorly understood, and models face increased complexity when working with pH-sensitive polymers and dynamic biological environments [17], the inhibition of release of albumin from hydrogel when starting from a frozen chitosan solution cannot be understated. Under conditions in which the net charge on polymers change, the TIG hydrogels could potentially be a pH-sensitive material ideal for oral delivery [51]. Therefore, TIG is an additive process for alginate hydrogels that could improve electrostatic interactions between charged polymers and cargo.

3.5 Conclusion

In summary, this chapter demonstrates how gelation by thawing alginate polymer in a calcium bath maintains desired hydrogel swelling properties, enhances elasticity, and suggests enhanced electrostatic interactions that are appealing for controlling the release of cargo. In addition, the liquid-core capsules presented defined shell thickness that also shows utility in encapsulating cargo. Although alginate TIG hydrogel results support the hypothesis of some maintained alginate aggregation, further work is needed to determine the structural effects of freezing and thawing rates explored in more depth within chapter 4.

3.6 References

[1] L. A. Wells and H. Sheardown, "Extended release of high pI proteins from alginate microspheres via a novel encapsulation technique," in *Eur J Pharm Biopharm*, vol. 65, no. 3). Netherlands, 2007, pp. 329-35.

[2] A. Haug and B. R. Larsen, "The solubility of alginate at low pH," *Acta Chem Scand,* vol. 17, no. 6, pp. 1653-62, 1963.

[3] Y. H. Lin, H. F. Liang, C. K. Chung, M. C. Chen, and H. W. Sung, "Physically crosslinked alginate/N,O-carboxymethyl chitosan hydrogels with calcium for oral delivery of protein drugs," (in eng), *Biomaterials,* vol. 26, no. 14, pp. 2105-13, May 2005, doi: 10.1016/j.biomaterials.2004.06.011.

[4] R. Jayakumar, M. Prabaharan, P. T. Sudheesh Kumar, S. V. Nair, and H. Tamura, "Biomaterials based on chitin and chitosan in wound dressing applications," (in eng), *Biotechnology advances,* vol. 29, no. 3, pp. 322-37, May-Jun 2011, doi: 10.1016/j.biotechadv.2011.01.005.

[5] J. Li and D. J. Mooney, "Designing hydrogels for controlled drug delivery," *Nature Reviews Materials,* Review Article vol. 1, p. 16071, 10/18/online 2016, doi: 10.1038/natrevmats.2016.71

https://www.nature.com/articles/natrevmats201671#supplementary-information.

[6] F. U. Momoh, J. S. Boateng, S. C. Richardson, B. Z. Chowdhry, and J. C. Mitchell, "Development and functional characterization of alginate dressing as potential protein delivery system for wound healing," (in eng), *International journal of biological macromolecules,* vol. 81, pp. 137-50, Nov 2015, doi: 10.1016/j.ijbiomac.2015.07.037.

[7] D. T. Brandau, L. S. Jones, C. M. Wiethoff, J. Rexroad, and C. R. Middaugh, "Thermal Stability of Vaccines," *Journal of Pharmaceutical Sciences,* vol. 92, no. 2, pp. 218-231, 2003/02/01/ 2003, doi: https://doi.org/10.1002/jps.10296.

[8] C. H. Saroja, P. K. Lakshmi, and S. Bhaskaran, "Recent trends in vaccine delivery systems: A review," *International Journal of Pharmaceutical Investigation,* vol. 1, no. 2, pp. 64-74, doi: 10.4103/2230-973X.82384.

[9] N. Cagol, W. Bonani, D. Maniglio, C. Migliaresi, and A. Motta, "Effect of Cryopreservation on Cell-Laden Hydrogels: Comparison of Different Cryoprotectants," *Tissue Engineering Part C: Methods,* vol. 24, no. 1, pp. 20-31, 2018/01/01 2017, doi: 10.1089/ten.tec.2017.0258.

[10] H. Gurruchaga *et al.*, "Advances in the slow freezing cryopreservation of microencapsulated cells," *Journal of Controlled Release,* vol. 281, pp. 119-138, 2018/07/10/ 2018, doi: https://doi.org/10.1016/j.jconrel.2018.05.016.

[11] P. A. Williams, K. T. Campbell, H. Gharaviram, J. L. Madrigal, and E. A. Silva, "Alginate-Chitosan Hydrogels Provide a Sustained Gradient of Sphingosine-1-Phosphate for Therapeutic Angiogenesis," *Annals of Biomedical Engineering,* journal article vol. 45, no. 4, pp. 1003-1014, April 01 2017, doi: 10.1007/s10439-016-1768-2.

[12] K. Y. Lee and D. J. Mooney, "Alginate: properties and biomedical applications," *Progress in polymer science,* vol. 37, no. 1, pp. 106-126, 2012, doi: 10.1016/j.progpolymsci.2011.06.003.

[13] O. Gaserod, O. Smidsrod, and G. Skjak-Braek, "Microcapsules of alginate-chitosan--I. A quantitative study of the interaction between alginate and chitosan," (in eng), *Biomaterials,* vol. 19, no. 20, pp. 1815-25, Oct 1998.

[14] H. L. Lai, A. Abu'Khalil, and D. Q. Craig, "The preparation and characterisation of drug-loaded alginate and chitosan sponges," (in eng), *International journal of pharmaceutics,* vol. 251, no. 1-2, pp. 175-81, Jan 30 2003.

[15] F.-L. Mi, H.-W. Sung, and S.-S. Shyu, "Drug release from chitosan–alginate complex beads reinforced by a naturally occurring cross-linking agent," *Carbohydrate Polymers,* vol. 48, no. 1, pp. 61-72, 2002/04/01/ 2002, doi: https://doi.org/10.1016/S0144-8617(01)00212-0.

[16] C. S. Brazel and N. A. Peppas, "Modeling of drug release from swellable polymers," (in eng), *European journal of pharmaceutics and biopharmaceutics : official journal of Arbeitsgemeinschaft fur Pharmazeutische Verfahrenstechnik e.V,* vol. 49, no. 1, pp. 47-58, Jan 2000.

[17] X. Zhang, J. Hansing, Roland R. Netz, and Jason E. DeRouchey, "Particle Transport through Hydrogels Is Charge Asymmetric," *Biophysical Journal,* vol. 108, no. 3, pp. 530-539, doi: 10.1016/j.bpj.2014.12.009.

[18] S. Zmora, R. Glicklis, and S. Cohen, "Tailoring the pore architecture in 3-D alginate scaffolds by controlling the freezing regime during fabrication," *Biomaterials,* vol. 23, no. 20, pp. 4087-4094, 2002/10/01/ 2002, doi: https://doi.org/10.1016/S0142-9612(02)00146-1.

[19] S.-H. Yu, F.-L. Mi, Y.-B. Wu, C.-K. Peng, S.-S. Shyu, and R.-N. Huang, "Antibacterial activity of chitosan–alginate sponges incorporating silver

sulfadiazine: Effect of ladder-loop transition of interpolyelectrolyte complex and ionic crosslinking on the antibiotic release," *Journal of Applied Polymer Science,* vol. 98, no. 2, pp. 538-549, 2005/10/15 2005, doi: 10.1002/app.21509.

[20] M. Dai *et al.*, "Chitosan-Alginate Sponge: Preparation and Application in Curcumin Delivery for Dermal Wound Healing in Rat," *Journal of Biomedicine and Biotechnology,* vol. 2009, p. 8, 2009, Art no. 595126, doi: 10.1155/2009/595126.

[21] I. Roy and M. N. Gupta, "Freeze-drying of proteins: some emerging concerns," *Biotechnology and Applied Biochemistry,* vol. 39, no. 2, pp. 165-177, 2004, doi: 10.1042/BA20030133.

[22] L. Shapiro and S. Cohen, "Novel alginate sponges for cell culture and transplantation," *Biomaterials,* vol. 18, no. 8, pp. 583-590, 1997/04/01/ 1997, doi: https://doi.org/10.1016/S0142-9612(96)00181-0.

[23] A. K. Anal and W. F. Stevens, "Chitosan-alginate multilayer beads for controlled release of ampicillin," (in eng), *International journal of pharmaceutics,* vol. 290, no. 1-2, pp. 45-54, Feb 16 2005, doi: 10.1016/j.ijpharm.2004.11.015.

[24] G. Maghami Ghobad and A. F. Roberts George, "Studies on the adsorption of anionic dyes on chitosan," *Die Makromolekulare Chemie,* vol. 189, no. 10, pp. 2239-2243, 1988/10/01 1988, doi: 10.1002/macp.1988.021891003.

[25] C. Ouwerx, N. Velings, M. M. Mestdagh, and M. A. V. Axelos, "Physico-chemical properties and rheology of alginate gel beads formed with various divalent cations," *Polymer Gels and Networks,* vol. 6, no. 5, pp. 393-408, 1998/10/01/ 1998, doi: https://doi.org/10.1016/S0966-7822(98)00035-5.

[26] T. Boontheekul, H. J. Kong, and D. J. Mooney, "Controlling alginate gel degradation utilizing partial oxidation and bimodal molecular weight distribution," (in eng), *Biomaterials,* vol. 26, no. 15, pp. 2455-65, May 2005, doi: 10.1016/j.biomaterials.2004.06.044.

[27] H. J. Kong, E. Wong, and D. J. Mooney, "Independent Control of Rigidity and Toughness of Polymeric Hydrogels," *Macromoleculeś,* vol. 36, no. 12, pp. 4582-4588, 2003/06/01 2003, doi: 10.1021/ma034137w.

[28] L. Shan *et al.*, "Fabrication and Use of Alginate-Based Cryogel Delivery Beads Loaded with Urea and Phosphates as Potential Carriers for Bioremediation," *Industrial & Engineering Chemistry Research,* vol. 55, no. 28, pp. 7655-7660, 2016/07/20 2016, doi: 10.1021/acs.iecr.6b01256.

[29] H. Zhang, F. Zhang, and J. Wu, "Physically crosslinked hydrogels from polysaccharides prepared by freeze–thaw technique," *Reactive and Functional Polymers,* vol. 73, no. 7, pp. 923-928, 2013/07/01/ 2013, doi: https://doi.org/10.1016/j.reactfunctpolym.2012.12.014.

[30] U. Fumio, Y. Hiroshi, N. Kumiko, N. Sachihiko, S. Kenji, and M. Yasunori, "Swelling and mechanical properties of poly(vinyl alcohol) hydrogels," *International journal of pharmaceutics,* vol. 58, no. 2, pp. 135-142, 1990/01/29/ 1990, doi: https://doi.org/10.1016/0378-5173(90)90251-X.

[31] Y. Zhao, W. Shen, Z. Chen, and T. Wu, "Freeze-thaw induced gelation of alginates," (in eng), *Carbohydr Polym,* vol. 148, pp. 45-51, Sep 5 2016, doi: 10.1016/j.carbpol.2016.04.047.

[32] Y. Zhao, Z. Chen, and T. Wu, "Cryogelation of alginate improved the freeze-thaw stability of oil-in-water emulsions," *Carbohydrate Polymers,* vol. 198, pp. 26-33, 2018/10/15/ 2018, doi: https://doi.org/10.1016/j.carbpol.2018.06.013.

[33] A. Tripathi and A. Kumar, "Multi-Featured Macroporous Agarose–Alginate Cryogel: Synthesis and Characterization for Bioengineering Applications," *Macromolecular Bioscience,* vol. 11, no. 1, pp. 22-35, 2011/01/10 2010, doi: 10.1002/mabi.201000286.

[34] O. Smidsrød and G. Skja˚k-Brˆk, "Alginate as immobilization matrix for cells," *Trends in Biotechnology,* vol. 8, pp. 71-78, 1990/01/01/ 1990, doi: https://doi.org/10.1016/0167-7799(90)90139-O.

[35] P. Kolhe, E. Amend, and K. S. Satish, "Impact of freezing on pH of buffered solutions and consequences for monoclonal antibody aggregation," *Biotechnology Progress,* vol. 26, no. 3, pp. 727-733, 2010/05/01 2009, doi: 10.1002/btpr.377.

[36] K. A. Pikal-Cleland, N. Rodríguez-Hornedo, G. L. Amidon, and J. F. Carpenter, "Protein Denaturation during Freezing and Thawing in Phosphate Buffer Systems: Monomeric and Tetrameric β-Galactosidase," *Archives of Biochemistry and Biophysics,* vol. 384, no. 2, pp. 398-406, 2000/12/15/ 2000, doi: https://doi.org/10.1006/abbi.2000.2088.

[37] K. Y. Lee, J. A. Rowley, P. Eiselt, E. M. Moy, K. H. Bouhadir, and D. J. Mooney, "Controlling Mechanical and Swelling Properties of Alginate Hydrogels Independently by Cross-Linker Type and Cross-Linking Density,"

Macromolecules, vol. 33, no. 11, pp. 4291-4294, 2000/05/01 2000, doi: 10.1021/ma9921347.

[38] Q. Xu *et al.*, "A hybrid injectable hydrogel from hyperbranched PEG macromer as a stem cell delivery and retention platform for diabetic wound healing," (in eng), *Acta Biomater,* vol. 75, pp. 63-74, Jul 15 2018, doi: 10.1016/j.actbio.2018.05.039.

[39] H. Tomida, C. Nakamura, H. Yoshitomi, and S. Kiryu, "Preparation of Theophylline-Loaded Calcium Alginate Gel Capsules and Evaluation of Their Drug Release Characteristics," *CHEMICAL & PHARMACEUTICAL BULLETIN,* vol. 41, no. 12, pp. 2161-2165, 1993, doi: 10.1248/cpb.41.2161.

[40] A. Blandino, M. Macías, and D. Cantero, "Immobilization of glucose oxidase within calcium alginate gel capsules," *Process Biochemistry,* vol. 36, no. 7, pp. 601-606, 2001/02/01/ 2001, doi: https://doi.org/10.1016/S0032-9592(00)00240-5.

[41] Y. Chai, L.-H. Mei, G.-L. Wu, D.-Q. Lin, and S.-J. Yao, "Gelation conditions and transport properties of hollow calcium alginate capsules," *Biotechnology and Bioengineering,* vol. 87, no. 2, pp. 228-233, 2004/07/20 2004, doi: 10.1002/bit.20144.

[42] E. Martins, D. Renard, Z. Adiwijaya, E. Karaoglan, and D. Poncelet, "Oil encapsulation in core–shell alginate capsules by inverse gelation. I: dripping methodology," *Journal of Microencapsulation,* vol. 34, no. 1, pp. 82-90, 2017/01/02 2017, doi: 10.1080/02652048.2017.1284278.

[43] E. Martins, D. Renard, J. Davy, M. Marquis, and D. Poncelet, "Oil core microcapsules by inverse gelation technique," *Journal of Microencapsulation,* vol. 32, no. 1, pp. 86-95, 2015/01/02 2015, doi: 10.3109/02652048.2014.985342.

[44] R. M. and L. S. J., "Water-Insoluble, Whey Protein- based Microspheres Prepared by an All-aqueous Process," *Journal of Food Science,* vol. 69, no. 1, pp. FEP50-FEP58, 2004, doi: doi:10.1111/j.1365-2621.2004.tb17867.x.

[45] J. Ruggiero, L. E. Xodo, A. Ciana, G. Manzini, and F. Quadrifoglio, "Charge effect in the interaction of doxorubicin and derivatives with polydeoxynucleotides," *Biochimica et Biophysica Acta (BBA) - Gene Structure and Expression,* vol. 1129, no. 3, pp. 294-302, 1992/02/11/ 1992, doi: https://doi.org/10.1016/0167-4781(92)90506-U.

[46] B. P. Koppolu, S. G. Smith, S. Ravindranathan, S. Jayanthi, T. K. Suresh Kumar, and D. A. Zaharoff, "Controlling chitosan-based encapsulation for protein and vaccine delivery," (in eng), *Biomaterials,* vol. 35, no. 14, pp. 4382-9, May 2014, doi: 10.1016/j.biomaterials.2014.01.078.

[47] C.-s. Hu, C.-h. Chiang, P.-d. Hong, and M.-k. Yeh, "Influence of charge on FITC-BSA-loaded chondroitin sulfate-chitosan nanoparticles upon cell uptake in human Caco-2 cell monolayers," *International Journal of Nanomedicine,* vol. 7, pp. 4861-4872, 08/10 2012, doi: 10.2147/IJN.S34770.

[48] M. Karimi, P. Avci, R. Mobasseri, M. R. Hamblin, and H. Naderi-Manesh, "The novel albumin–chitosan core–shell nanoparticles for gene delivery: preparation, optimization and cell uptake investigation," *J Nanopart Res,* vol. 15, no. 4, p. 1651, 04/24 2013, doi: 10.1007/s11051-013-1651-0.

[49] Y. Tabata, T. Kawai, Y. Murakami, and Y. Ikada, "Electric Charge Influence of Dextran Derivatives on their Tumor Accumulation After Intravenous Injection,"

Drug Delivery, vol. 4, no. 3, pp. 213-221, 1997/01/01 1997, doi: 10.3109/10717549709051895.

[50] K. T. Campbell, D. J. Hadley, D. L. Kukis, and E. A. Silva, "Alginate hydrogels allow for bioactive and sustained release of VEGF-C and VEGF-D for lymphangiogenic therapeutic applications," (in eng), *PloS one,* vol. 12, no. 7, p. e0181484, 2017, doi: 10.1371/journal.pone.0181484.

[51] A. W. Chan and R. J. Neufeld, "Tuneable semi-synthetic network alginate for absorptive encapsulation and controlled release of protein therapeutics," *Biomaterials,* vol. 31, no. 34, pp. 9040-9047, 2010/12/01/ 2010, doi: https://doi.org/10.1016/j.biomaterials.2010.07.111.

CHAPTER 4

Thaw-induced gelation improves alginate hydrogel mechanical stability while providing cryoprotective benefits for therapeutic cargo

4.1 Introduction

In chapter 3, the process of thaw-induced gelation (TIG) was described as a method to generate hydrogels disks or hydrogel capsules. While those previous experiments addressed electrostatic interactions between chitosan and alginate with select cargos, the frozen stage of TIG has utility as a hydrogel that incorporates the often-required cold storage of cargo and cells. This chapter will further describe the effects of cryostructuring, thaw-induced gelation, and the effects on bioactive cargo (vascular endothelial growth factor; VEGF). Specifically, only hydrogels formed by submerging a frozen alginate polymer solution into a cross-linker solution of calcium chloride will be discussed here. While we also attempted TIG with polymer and cells within a cryopreservation solution, the outcomes were a unique alginate cryogel formed by non-solvent induced phase separation rather than TIG. The utility of frozen alginate with cells will be described in the next chapter of the thesis.

Hydrogels have numerous roles in localizing cell and drug delivery [1-5]. For example, hydrogels have been used as drug carriers, dermal patches, and microgels for encapsulated cells [6-9]. However, few studies have addressed storage conditions when designing and validating novel hydrogel systems [10-14]. Nevertheless, cold storage could be a necessary step of the supply chain. Conceptually, it would be appealing if cold storage could also enhance the desired properties of therapeutic

hydrogels. Many polymers have been studied as a protective agent in cold storage of biologics, including alginate, polyvinyl alcohol, and polyethylene glycol [15-19]. Specifically, alginate has been widely used in biomedical applications due to its biocompatibility and ease in controlling physical and mechanical properties [6, 20]. Alginate is typically obtained from seaweed consisting of blocks of β-D-mannuronic acid (M) and α-L-guluronic acid (G) monomers [6]. The negatively charged G-blocks are permissive to ionic cross-linking with divalent cations, such as Ca^{2+} (forming an "egg-box" structure), allowing cells and therapeutic cargos to be encapsulated under mild conditions [21]. Therefore, alginate represents an appealing material for cold storage and subsequent encapsulation to overcome some clinical supply chain challenges.

Ionically cross-linked alginate hydrogels typically lack the mechanical stability of covalently cross-linked hydrogels due to calcium ions diffusing out the hydrogel over time [22]. This phenomenon can potentially be mitigated by forming an interpenetrating polymer network (IPN) [23]. An IPN is a material comprised of two or more interlaced networks or entangled on the molecular scale. Polymeric entanglements of IPNs typically result in enhanced mechanical stability and toughness, making them appealing materials for regenerative medicine and wound dressing applications [15, 16, 23-25]. While the networks are not cross-linked, IPNs still cannot be separated unless chemical bonds are broken.

IPNs can be classified in a couple of different ways. First, an IPN can be defined by how networks are entangled. For example, a semi-IPN differs from an IPN because the polymers can, in principle, be separated without breaking chemical bonds. IPNs can also be described by how they are formed; a sequential-IPN can be formed by

polymerizing an initial mixture of monomers, swelling the hydrogel with another monomer, and cross-linking that secondary monomer to form an IPN. Additionally, IPNs can be identified according to their molecular composition. An unusual IPN is the homo-IPN, where both polymers used in the networks are the same. They are usually sequential IPNs and were the first to be commercialized [26, 27]. Regardless of the type of IPN, it is similarly unclear how compliant any IPN hydrogels will be with low-temperature storage likely required in many clinical future applications [4, 7, 28].

In this chapter, we have two objectives. One objective was to elucidate the potential structure of hydrogels formed by the TIG method. The second objective was to determine the biocompatibility of the hydrogel by its cryoprotective capacity for frozen cargo. As previously described, TIG involves a frozen alginate polymer solution submerged in a bath of the ionic cross-linker, calcium. As the alginate solution melts, calcium ions cross-link the alginate polymer to form a hydrogel. This chapter tries to decipher the unique properties of these hydrogels produced by TIG compared to hydrogels created from a more standard ionic gelation scheme. Fundamentally, the rate the alginate solution is frozen alters the amount of polymer aggregated via cryostructuring [29-31]. Therefore, we hypothesize that TIG creates entanglements between a soluble aggregated polymer network and an ionically cross-linked network, generating a homo-IPN [32-35]. To test our hypothesis, we probed the effects of cryostructured alginate polymer through scanning electron microscopy (SEM), storage modulus, swelling, elasticity, and mesh size under varying freezing and thawing rate conditions.

Although the underlying molecular structure of each hydrogel might not be clear, we expect the polymer networks to differ by freezing and thawing rates because of cryostructuring and resolubilizing of aggregated polymers (Figure 4.1). Additionally, we characterized these hydrogels' stability, swelling, elasticity, and mesh size over three weeks to determine how well the potential entangled networks improve hydrogel stability. A subset of these samples was kept in a lab fridge for over a year to determine their stability in sterile, non-frozen cold storage. Furthermore, in addition to ensuring similarities of these hydrogels to other ionically cross-linked alginate hydrogels under varying osmolarity, cross-linker concentration, and solution acidity effects, we also characterized the potential cytotoxicity and cryoprotective potential of hydrogels produced by TIG. The data presented dramatically expands on the previous chapter's mechanical analysis data, which primarily focused on the feasibility of gelation and controlling the release of various cargos [36]. To our knowledge, the formation and characterization of an alginate hydrogel as a homo-IPN has not been previously described, suggesting TIG can produce a sequential-IPN with translational relevance for hydrogel systems to incorporate the clinical context of the cold storage chain.

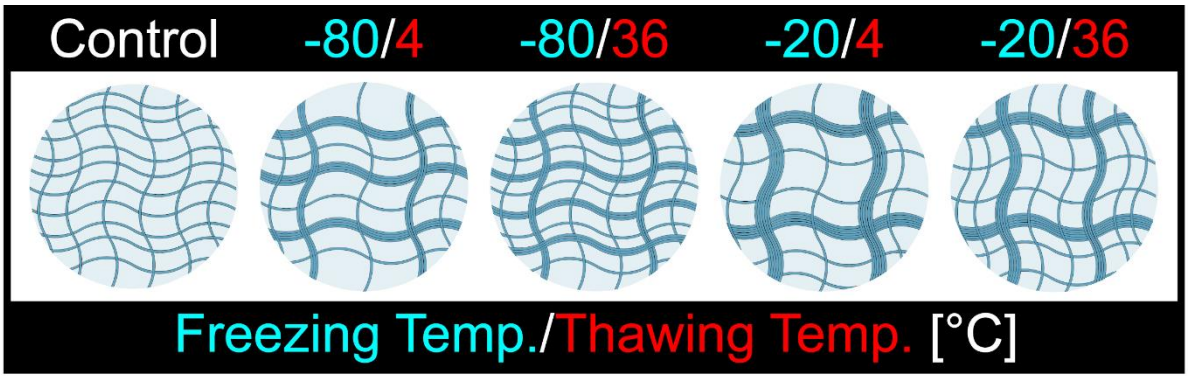

Figure 4.1 Theorized molecular structure of networks formed by TIG. TIG parallels the gelation schemes of an alginate hydrogel but starts with a frozen polymer solution. Here, the illustration shows lines of alginate polymer. Clusters of these lines represent aggregates resulting from cryostructuring. As faster freezing (-80) results in smaller ice crystals than slower freezing (-20), we anticipated correspondingly thicker aggregates in conditions that had slower freezing. In contrast, the control, not undergoing any cryostructuring, is not expected to have any aggregation. Notably, heat transfer precedes cross-linking with the TIG method. This heat transfer also enhances the solubility of the aggregated alginate polymer. Therefore, even after all the polymer has been melted and ionic cross-linking continues, we expect warmer thawing temperatures (36) to lead to more solubilized alginate polymer from the aggregated regions. Given that the initial stock of alginate polymers is in the aggregate formed by cryostructuring, the warmer thawing bath (36) is expected to result in a smaller mesh size than the colder thawing bath (4). However, if any aggregation exists, the mesh sizes of hydrogels formed by TIG should be larger than the control, regardless of thawing temperature.

4.2 Materials and methods

4.2.1 Hydrogel formation

The LF10/60 alginate polymer (molecular weight ~ 50 kDa and > 60% G-block) used in this study was purchased from FMC Biopolymers as the low molecular weight (LMW) polymer. Unless stated otherwise, all alginate polymer used in this study is the LMW variety. For an experiment with different molecular weight alginate polymers, an LF20/40 alginate polymer (molecular weight ~ 250 kDa and > 60% G-block; FMC Biopolymers) was used as the high molecular weight (HMW) polymer. Alginate was dissolved in a pH-neutral isotonic sodium chloride solution (0.9% (w/v); Sigma) unless stated otherwise. Alginate was prepared at various concentrations, 1% and 2% (w/v), by diluting from a 4% (w/v) stock. Calcium chloride (Sigma) was the divalent cation source for cross-linking alginate. The calcium solution was prepared at 100 mM with a pH of 7 unless stated otherwise.

All hydrogel groups were prepared by filling a rubber mold with 100 µL of the alginate polymer solution. The rubber mold is approximately 1.5 mm thick with circular cutouts 8 mm in diameter. For the control hydrogels, the rubber mold was covered with a porous membrane (Millipore) and carefully immersed into a calcium solution to induce ionic cross-linking, similar to a method previously used by our lab [37]. Throughout this chapter, the formation of a control hydrogel (control) will be referred to as following normal gelation (normal). TIG alginate hydrogels were formed as previously described [36] and in the previous chapter. Briefly, the rubber molds with the alginate solution were placed into either a -80 ˚C or -20 ˚C freezers until the solution froze, typically overnight. Importantly, all alginate solutions frozen at -20 ˚C were subsequently placed

in -80 ˚C freezers to ensure all samples were at the same temperature before thawing. For ionic gelation, the frozen alginate solution is submerged into the thawing solution of calcium chloride. Different temperatures of the calcium chloride solution were used to alter the thawing rate (4 ˚C, 20 ˚C, or 36 ˚C). These temperatures are above the melting point and represent what can be achieved with a lab refrigerator, room temperature, and a cell incubator. Once the frozen alginate is within the thawing solution, it melts and cross-links to form the hydrogel. After 10 minutes, the newly formed alginate hydrogels were removed and rinsed with a 0.9% (w/v) sodium chloride solution to remove the uncross-linked calcium chloride solution. We also characterized samples based on gelation time, including a set of samples that were only permitted to cross-link for 5 minutes after submersion. The calcium bath was placed in a larger beaker filled with water at the desired temperature to prevent temperature changes to the thawing solution.

4.2.2 Hydrogel stiffness and elasticity measurements

The stiffness and the viscoelasticity of hydrogels were measured via the shear storage modulus (G') and the damping factor (tan(δ)), respectively, via a rheometer (HR2, TA Instruments). After allowing hydrogels to swell in 0.9% (w/v) sodium chloride, excess fluid was wicked away, and the hydrogels were placed between parallel plates of the rheometer with an 8 mm head and applied with a 0.01 N axial force**.** The hydrogels were strained (0.01–1%) at a set frequency (6.3 rad s-1)**.** A minimum of 6 points within the linear range were averaged to obtain G' and tan(δ) for each hydrogel condition. The damping ratio (tan(δ)) is a ratio of the loss modulus (G") to the storage

modulus (G'), also known as the loss factor. This measurement represents the ratio of energy loss and storage. The closer this value is to zero, the more purely elastic the material acts.

4.2.3 Swelling ratio measurements

The volumetric swelling ratio (Q_v) of each hydrogel was determined using the wet weights (W_S) and dry weights (W_D). First, hydrogels were swollen in 0.9% (w/v) sodium chloride solution. Next, the dry weights for the same hydrogel samples were obtained after removing all moisture by lyophilization. The volumetric swelling ratio was then calculated via the following equation:

$$Q_V = \frac{\frac{W_S - W_D}{\rho_W} + \frac{W_D}{\rho_P}}{\frac{W_D}{\rho_P}},$$

Where ρ_W is the density of water and ρ_P is the polymer density (Alginate: 1.6 g/mL, [38, 39]).

4.2.4 Mesh size calculations

Mesh size (ξ) was estimated for the anionic hydrogels by Flory–Rehner calculation using swelling and Rheometry measurements, as previously described [36, 37, 40, 41]:

$$\xi = Q^{\frac{1}{3}} l \left(\frac{2M_c}{M_r}\right)^{1/2} C_n^{1/2}.$$

Here, l is the length of the repeating unit, or Kuhn length (5.15 Å), M_r is the molecular weight of the repeating unit (194 g/mol), and C_n is the characteristic ratio (21.1), which is a measure of chain stiffness. Q_v is the volumetric swelling ratio, which was defined in the previous section. M_C is the molecular weight between cross-links, which was determined via the following equation using the measurements of the shear storage modulus (G') and polymer concentration (C_P), the gas constant (R), and sample temperature (T):

$$M_C = \frac{C_P RT}{G'}.$$

4.2.5 Scanning electron microscopy (SEM) analysis

SEM images were obtained for the control alginate hydrogel and TIG alginate hydrogels. Alginate hydrogels were prepared as previously mentioned with TIG hydrogels being frozen at -80 ˚C or -20 ˚C and thawed in calcium solutions at 4 ˚C or 36 ˚C, representing faster or slower cooling and slow or rapid melting, respectively. After ionic gelation, hydrogels were left to swell in 0.9% (w/v) NaCl before being fixed with 2% (v/v) glutaraldehyde (GA) solution for four hours [42]. Subsequently, the hydrogels were immersed in ethanol solutions of increasing concentration up to 100%, as previously described [43]. To not induce ice formation that could act as a confounder for structures potentially created by TIG, cross-linked hydrogels underwent critical point drying (CPD) [36, 44-46]. The samples were then coated with gold and imaged with the Quattro S Scanning Electron Microscope (Thermo Fisher Scientific). During this process, extreme care was taken to prevent shrinkage of the samples. For example, we attempted to

minimize ambient air exposure by keeping the materials hydrated in the ethanol solvent immediately prior to CPD.

SEM images were taken at three different magnifications, 800x, 3,500x, and 25,000x, to observe larger structures and an alginate hydrogel's ionically cross-linked mesh structures. Importantly for experimental rigor, all TIG samples were frozen from room temperature and thawed for gelation from -80 ˚C to create consistent freezing and thawing rates regimes. Second, all hydrogels imaged were formed, swelled, fixed, and prepared for SEM imaging together as a batch to minimize hydrogel differences due to processing. Significant shrinkage could result from structural collapse, indicating SEM images might not recapitulate the structure as samples that retained their initial size. By preparing all samples as a batch, we expect structural differences will be compared based on their freezing and thawing treatments.

4.2.6 Freezing and thawing rate effects on hydrogel properties

To simultaneously interrogate the effect of freezing rates, thawing rates, and polymer concentration on TIG hydrogel mechanical properties and potential underlying structure, a full factorial design was employed to examine each combination of the various factor values. The three factors included freezing rate (-80 ˚C or -20 ˚C freezers), thawing rates (4 ˚C, 20 ˚C, or 36 ˚C thawing solutions), and polymer concentration (1% and 2% (w/v)). The thawing rates and polymer concentration conditions represent high, medium, and low values. Likewise, freezing conditions represent high and low values. Hydrogels were characterized by their storage modulus (G'), damping ratio (tan(δ)), swelling ratio, and the calculated mesh size. The results

were analyzed and plotted as contour plots, or surface maps, for each polymer concentration to visualize freezing and thawing effects on hydrogel properties using JMP software (SAS Institute).

4.2.7 Alginate hydrogel stability assay

Degradation of a control alginate hydrogel (2% (w/v)) and TIG alginate hydrogels (1% and 2% (w/v)) was measured over 21 days. All alginate hydrogels were formed using sterilized alginate, prepared as previously described [40, 41], cross-linked with sterile calcium chloride solution, and incubated in sterile sodium chloride solution. Sterile alginate stock was prepared by dissolving 1 gram of alginate 100 mL of deionized (DI) water. Next, 0.5 grams of activated charcoal (Sigma) was added and mixed with a magnetic stir bar for 30 minutes. The alginate solution was then sterile filtered (0.22 μm, Thermo Fisher Scientific), lyophilized, and stored in the freezer. TIG alginate hydrogels were formed from alginate solutions frozen at -80 ˚C and thawed at 36 ˚C. Alginate hydrogels were maintained in a sterile incubator at 36 ˚C to prevent microbial degradation of the hydrogels. Hydrogel stability was interrogated via their storage modulus, damping ratio, and swelling at days 0, 1, 2, 3, 7, and 21. Each data point represents a single hydrogel sample.

Additionally, 2% (w/v) alginate hydrogels formed using the same TIG conditions as our SEM experiments were stored in 0.9% (w/v) sodium chloride in 4 ˚C for over a year (383 days) before measurement. These hydrogels were characterized by their storage modulus, damping ratio, and swelling ratio to compare with similar hydrogels

measured on the day of gelation and the same hydrogel group used in the previous stability measurements. Each data point represents a single hydrogel sample.

4.2.8 Osmolarity effects on hydrogel formation

Osmolarity effects on gelation were examined by preparing cross-linking solutions of 225, 300, 375 mOsm/L by dissolving varying amounts of sodium chloride (0 mM, 37.5 mM, 75 mM, respectively) with 75 mM calcium chloride. Additionally, 300 mOsm/L cross-linking solutions were prepared with 50 mM, 75 mM, and 100 mM calcium chloride concentrations. Sodium chloride was added to make this solution 300 mOsm/L (75 mM, 37.5 mM, and 0 mM, respectively). In total, five different cross-linking solutions were used for forming alginate hydrogels, as the 300 mOsm/L groups with 75 mM $CaCl_2$ is shared between both groups. For TIG hydrogels, alginate was frozen in a -80 ˚C freezer and thawed using the various cross-linking solutions for gelation. The cross-linking solution was kept at room temperature (20 ˚C) in both the TIG method and the control. The storage modulus, damping ratio, and swelling ratio were measured for each of the hydrogels.

4.2.9 Buffer and pH effects on hydrogel formation

The freezing of phosphate solutions is known to generate an acidic pH [30, 31]. Given that TIG involves freezing the polymer solution, it is important to characterize how a pH change will affect hydrogel formation. Specifically, we used calcium chloride solutions (100 mM) at pH 5 and 7 to generate 2% (w/v) alginate hydrogels via TIG. Furthermore, the 2% (w/v) alginate solution was made by dissolving the polymer in

either 1X PBS (Sigma) or 0.9% (w/v) NaCl. Together, three groups were used: alginate dissolved in NaCl and cross-linked with a pH 7 calcium chloride solution, alginate dissolved in NaCl and cross-linked with a pH 5 calcium chloride solution, and alginate dissolved in PBS and cross-linked with a pH 5 calcium chloride solution. The alginate solution for TIG was frozen in the -80 ˚C freezer and thawed at room temperature (20 ˚C). The storage modulus, damping ratio, and swelling ratio were measured for each hydrogel.

4.2.10 MTT assay for cytotoxicity and proliferation analysis of HUVEC

Human umbilical vein endothelial cells (HUVECS; Lonza) from pooled donors were expanded in endothelial cell growth medium (EGM-2, Lonza) under standard conditions (37 ˚C and 5% CO_2), exchanging media every two days. EGM-2 was prepared as defined in the vendor's EGM-2 BulletKit™ medium with and without the addition of the growth factors, with N media being defined as the cell culture media without growth factors. HUVECs at passage 6 were seeded onto 12-well plates at a concentration of 10,000 cells/cm^2 using N media and allowed to attach for 24 hours. For the cytotoxicity assay, N media was replaced with EGM-2 with the supplemented growth factors or fresh N media for samples with no hydrogel, the control hydrogel, and the hydrogel formed through TIG. For interrogating potential cryoprotective nature, the vascular endothelial growth factor (VEGF) stock solution provided with the EGM-2 BulletKit™ medium was diluted to a 10X concentration within a 1% (w/v) alginate solution. The dilution in an alginate solution and the undiluted 100X stock were refrozen to their respective storage temperature (-20 ˚C). Frozen alginate was used to form

hydrogels as they thawed at 20 ˚C (TIG) or after completely thawing for the control hydrogel. Additionally, 100X stock was added to alginate to generate another control hydrogel group. The resulting concentrations of the VEGF-stock solution added to the cell culture wells was 1X, corresponding to a 100 µL hydrogel added 900 µL of N media in each well. Overall, this assay only characterizes the functionality of VEGF to promote proliferation after refreezing.

For both experiments, HUVECs were cultured for 72-hours under their respective condition before performing an MTT assay, a colorimetric assay for assessing cell metabolic activity in which NADH-dependent cellular oxidoreductase enzymes reduce tetrazolium dye MTT into insoluble formazan. The product has a purple color with an absorbance around 570 nm. Specifically, tetrazolium dye MTT (Sigma) diluted in PBS was added to each well at a final concentration of 0.5 mg/mL and incubated for three hours. The media was then replaced with 0.5 mL of isopropanol (Sigma), and plates were placed on a shaker for 15 minutes while being protected from light with aluminum foil. The total absorbance of formazan salt was quantified via the Spectramax ® i3 plate reader (Molecular Devices) at 570 nm, averaged per condition (n = 6), and normalized to the absorbance cells cultured in N media.

4.2.11 Statistical analysis

Results in this chapter are shown as mean values with standard deviations. Sample sizes are provided with each experiment and shown in figures as individual data points where applicable and listed in the figure legends. Statistical significance was asserted at $p < 0.05$ after performing Student's t-tests, ANOVAs, and Tukey's multiple

comparison tests where appropriate. All analyses were performed using Graph-Pad Prism software (GraphPad Software Inc.) and JMP software (SAS Institute).

4.3 Results

4.3.1 Formation of alginate hydrogels via TIG

In this chapter, TIG occurred when a frozen alginate polymer solution was thawed in a calcium bath, the ionic cross-linker of alginate. Ice crystals form between the polymers as the alginate solution freezes, known as cryostructuring (Figure 4.2). When melting, calcium ions cross-link the alginate polymer to form a hydrogel. Precisely, heat energy and calcium ions move towards the alginate polymer via the temperature and concentration gradients. The resulting hydrogel had an uncross-linked core if the frozen alginate solution were removed from the calcium bath before completely melting to the liquid phase. There was still a cross-linked hydrogel shell because any initially melted polymer on the outer surface becomes available for ionic cross-linking. Samples transitioned from solid ice to completely liquid within 100, 60, and 30 seconds for bath temperatures of 4, 20, and 36 ˚C, respectively, with no notable difference with 1 or 2% (w/v) alginate concentration. At a minimum, the thawing temperature would be expected to influence hydrogels due to the time it takes for frozen alginate to melt.

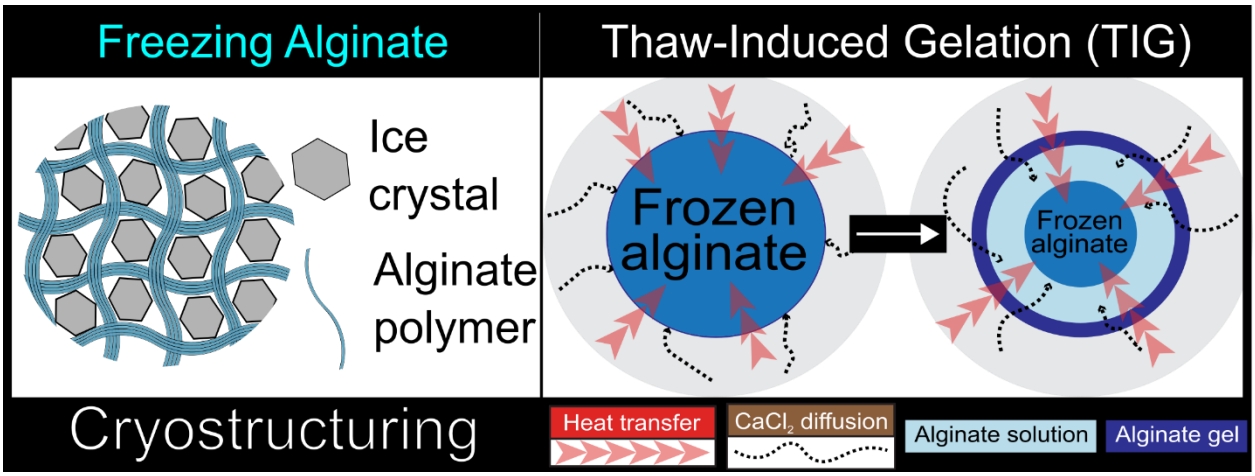

Figure 4.2 Thaw-induced gelation (TIG) involves cryostructuring followed by ionic cross-linking. The availability of alginate polymer to ionic cross-link could be altered by cryostructuring and the rate at which the frozen polymer solution melts. In practice, the solution wholly melted before being fully cross-linked. After the polymer solution is melted, ionic cross-linking will continue as the divalent cation diffuses into the previously frozen alginate solution.

4.3.2 The role of gelation time on hydrogel properties

The effects of gelation time on hydrogel properties were evaluated by measuring changes in the storage modulus, damping ratio, and swelling properties between 5- and 10-minutes after submersion. Consequently, the time for gelation was also limited by the melting rate due to the different thawing temperatures. Despite this, there was no clear trend in hydrogel properties concerning thawing temperature (Figure 4.3). With the -20 ˚C freezing condition, more time led to significantly stiffer hydrogels when thawed slowly at 4 ˚C. However, when the alginate solution was frozen in -80 ˚C undergoes TIG, more gelation time in a 36 ˚C cross-linker bath led to significantly stiffer hydrogels. Together, while these results indicate additional cross-linking, they also demonstrated how thawing's role on hydrogel properties could have additional influences.

4.3.3 The role of alginate molecular weight on hydrogel properties

Alginate molecular weight was evaluated for its influence on the storage modulus, damping ratio, and swelling ratio of hydrogels formed by TIG and the normal gelation method. For both gelation schemes, the increase in molecular weight led to increased stiffness, an increased damping ratio, and reduced swelling (Figure 4.4). TIG led to significantly stiffer hydrogels, less elastic, and had less swelling for each molecular weight. As a potential consequence, the storage modulus and damping ratio were significantly different between molecular weights with TIG but not the normal gelation scheme. Overall, these data reveal similar trends from polymer molecular weight and indicate expected differences between gelation methods described in this chapter.

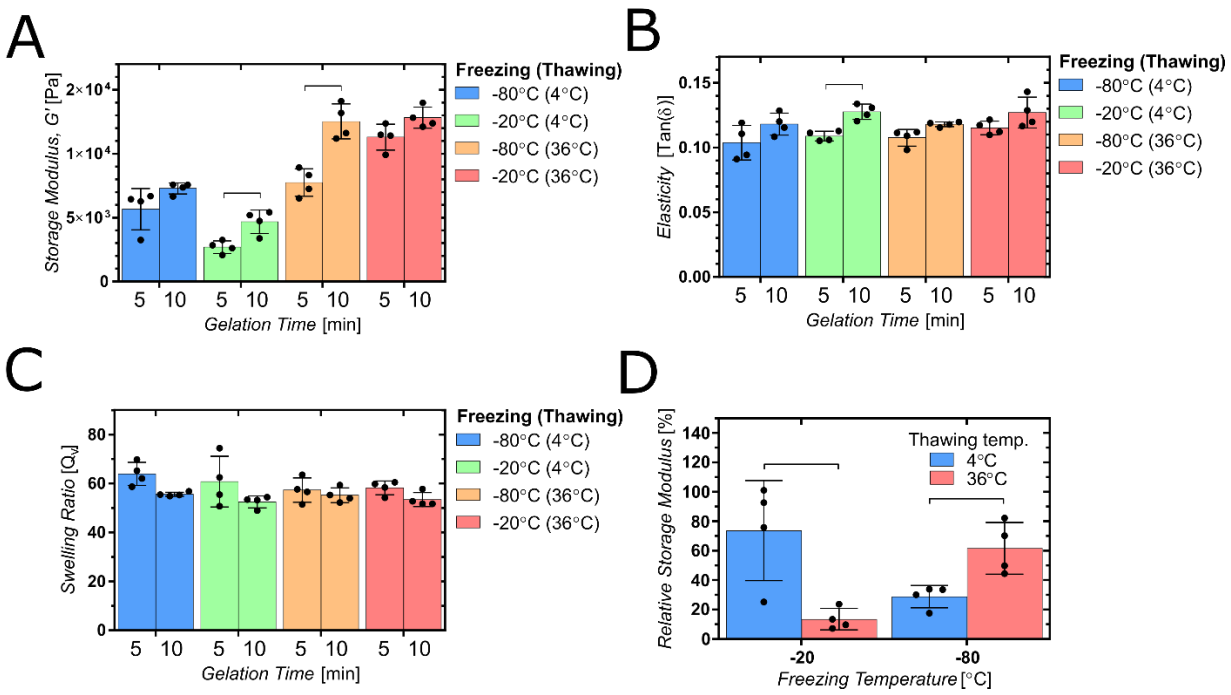

Figure 4.3 Effects of gelation time during TIG. Samples continue cross-linking between five and ten minutes, indicated by increasing trends in storage modulus (A) and elasticity (B) and a decreasing trend in the volumetric swelling ratio (C). While there was no significant difference in swelling ratio, hydrogels formed by freezing an alginate polymer in a -20 ˚C freezer and thawed in a 4 ˚C calcium bath and freezing in a -80 ˚C freezer and thawed in a 36 ˚C calcium bath were significantly stiffer with the additional five minutes. The relative change in storage modulus between five and ten minutes was also calculated to see which conditions were more likely to have significantly more cross-linking (D). Bar heights represent the group means, scatter dot plots display individual measurements, and error bars represent standard deviation (n = 4). A line between groups represents statistically significant differences ($P < 0.05$) between select comparisons after performing a two-way ANOVA and a Tukey's multiple comparison test.

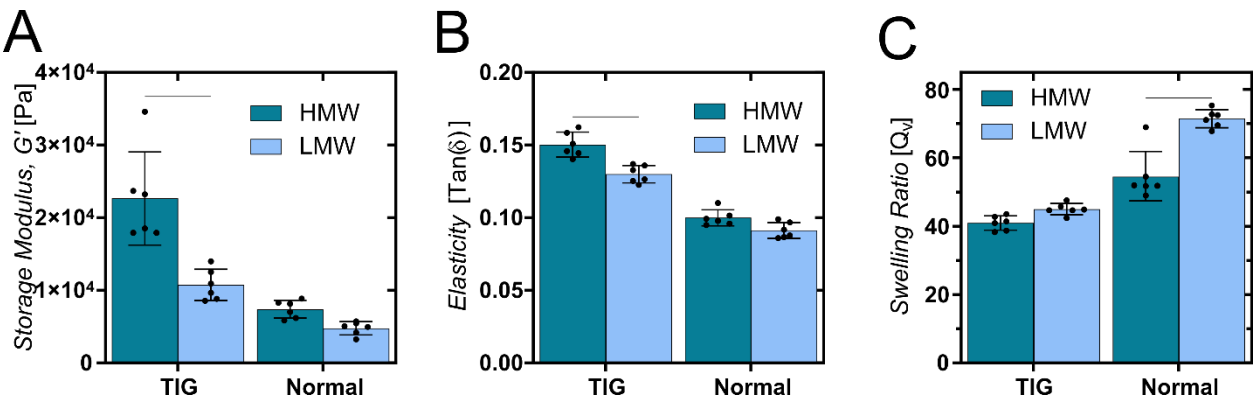

Figure 4.4 Molecular weight effect on hydrogels. Hydrogels formed via TIG or the normal gelation method (normal) are measured for their storage modulus (A), elasticity (B), and swelling ratio (C). Hydrogels formed via TIG and the control hydrogels (normal gelation) are significantly different with the same polymer molecular weight. High molecular weight (HMW) polymers led to stiffer and less elastic hydrogels than the low molecular weight (LMW) polymers. These differences were statistically significant for TIG hydrogels. Additionally, HMW polymers resulted in less swelling within hydrogels than LMW polymers, which was statistically significant for the control hydrogels. Bar heights represent the group means, scatter dot plots display individual measurements, and error bars represent standard deviation (n = 6). A line between select groups represents statistically significant differences ($P < 0.05$) between molecular weights of the same gelation method, assessed by performing a two-way ANOVA and a Tukey's multiple comparison test.

4.3.4 SEM analysis of TIG hydrogel polymer network morphology

SEM images investigated the polymer network's morphology for the alginate hydrogels formed via TIG and the control method (Figure 4.5A-O). Hydrogels forms with TIG are shown with a shorthand; for example, -80/4 represents a TIG hydrogel where alginate is frozen in a -80 ˚C freezer and thawed in a calcium bath at 4 ˚C (Figure 4.5D-F). Immediately, there is a clear distinction at 800x magnification, with the alginate network of all the hydrogels formed via TIG having larger pore structures not observed in the control group. Furthermore, TIG hydrogels have the most prominent pores when thawed in a 4 ˚C calcium bath (Figure 4.5D & J). Distinctly, the alginate polymer in both groups frozen in the -80 ˚C freezer aligns in a wave pattern that becomes discernable at the 3,500x magnification (Figure 4.5E & H). Of these two hydrogels, the group thawed more rapidly (-80/36) has denser folding and smaller pores (Figure 4.5L). In contrast to these wavy formations, the TIG hydrogels frozen in the -20 ˚C freezer have polymers that form thicker clusters (Figure 4.5K & N). Although the control hydrogel does not have these dense polymer structures seen at lower magnifications (Figure 4.5A & M), the -20/36 appears to be most like the control hydrogel at 25,000x magnification (Figure 4.5C & O). At 25,000x magnification, a mesh structure for TIG hydrogels is more evident. Mainly, with the -80/4 and -80/36 groups, there is a mesh structure within the wavy topography, with the mesh size being smaller with the -80/36 hydrogel (Figure 4.5F & L). Despite not guaranteeing the hydrogel's literal polymeric conformation, the SEM images demonstrate that the different freezing rates resulted in distinct structures, and the thawing rate might alter pore and mesh size.

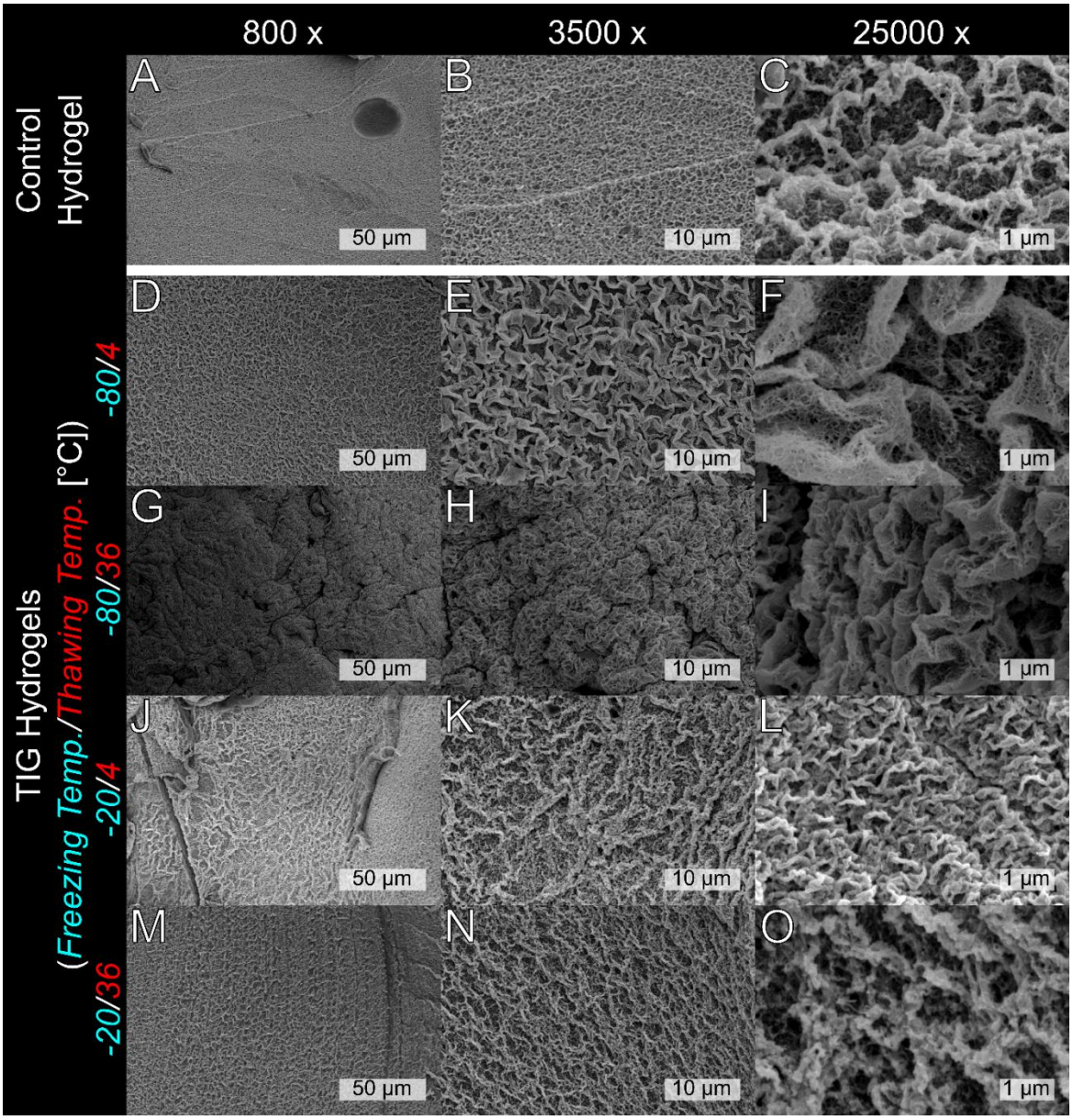

Figure 4.5 SEM images provide structural insight of hydrogels formed by TIG and the normal gelation scheme. Hydrogels formed by TIG appear distinct based on their combination of freezing and thawing rates (A-O). Four different hydrogels formed via TIG and one control hydrogel formed through the normal method were imaged at three different magnifications. The conditions of TIG represent either fast or slow freezing and fast or slow thawing, using -80 ˚C or -20 ˚C and 4 ˚C or 36 ˚C, respectively. The control hydrogel was cross-linked in a bath at 36 ˚C. Overall, all hydrogels appear to be

structurally distinct. Between the same TIG freezing condition, slower thawing (4 ˚C) resulted in larger pores. Similarly, between the same TIG thawing condition, slower freezing (-20 ˚C) had larger pores. For each hydrogel condition, different magnifications are representative of the same sample.

4.3.5 Full factorial analysis of freezing and thawing rates

Measurements of the mechanical and swelling properties of alginate hydrogels formed by TIG were obtained using the different combinations of polymer concentrations (1% and 2% (w/v)), alginate freezing temperatures (-20 ˚C and -80 ˚C), and calcium solution temperatures (4 ˚C, 20 ˚C, and 36 ˚C). The surface maps depict the trends in response to freezing and thawing temperatures (Figure 4.6). Consistently, the highest storage modulus for all alginate concentrations is in the bottom right of these surface maps, representing faster freezing at -80 ˚C and rapid thawing in a 36 ˚C calcium bath (Figure 4.6A). Specifically, hydrogels thawed at 36 ˚C with the 2% (w/v) polymer concentrations were significantly stiffer when frozen in -80 ˚C than at -20 ˚C. Furthermore, all hydrogels formed by freezing polymer at -80 ˚C had a statistically significant decrease in stiffness due to lower temperatures used in thawing. Overall, the colder freezing temperatures and warmer thawing temperatures result in higher hydrogel storage moduli, and the least stiff hydrogels were formed with slower freezing in the -20 ˚C freezer. The damping ratio represents the ratio of the loss modulus to the storage modulus. Interestingly, alginate hydrogels were more elastic when thawed slowly in a calcium solution at 4 ˚C (Figure 4.6B). Specifically, the 1% and 2% (w/v) alginate groups frozen at -80 ˚C were significantly more elastic when using the calcium solution at 4 ˚C than the warmer solution at 36 ˚C. Most notably, the largest damping ratios, indicating the least elastic hydrogels, were consistently by freezing in the -80 ˚C freezer and thawing in a 36 ˚C solution. The 2% (w/v) hydrogel prepared from freezing polymer in -80 ˚C had significantly more swelling when thawed slowly at 4 ˚C than if thawed rapidly at 36 ˚C (Figure 4.6C). However, there was no statistical difference in

the swelling ratio of 2% (w/v) hydrogels due to freezing rate changes. Regardless, the enhanced swelling ratios were consistently generated by the slowest thawing rate (4 ˚C) for all polymer concentrations. Across all alginate concentrations, the smallest mesh sizes were consistently within the area of rapid freezing (-80 ˚C) and thawing (36 ˚C), the same conditions that led to stiffer hydrogels with reduced swelling (Figure 4.6D). Strikingly, the largest mesh sizes were consistently formed when thawed at the intermediate room temperature (20 ˚C) from a polymer solution frozen in the -20 ˚C freezer. Together, these results elucidate the impact of freezing and thawing rates on the hydrogel properties.

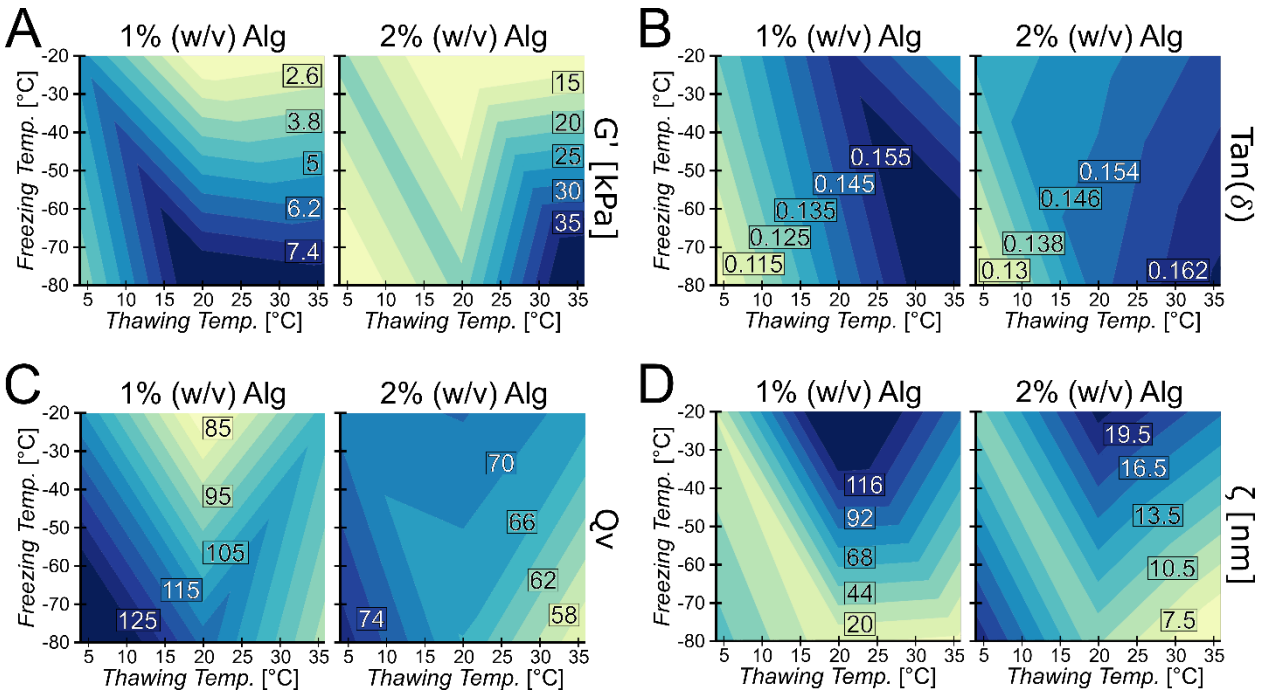

Figure 4.6 A full-factorial approach elucidated potential trends with TIG. Specifically, differing freezing and thawing conditions were used to form hydrogels of different polymer concentrations formed via TIG. The response surface maps of resulting hydrogel effect on storage moduli (A, G'), damping ratios (B, tan(δ)), swelling ratios (C, Qv), and mesh sizes (D, ξ). While altering polymer concentration does have expected effects on hydrogel properties, potential trends due to freezing and thawing temperatures were not always conserved across polymer concentration. However, a lower freezing temperature consistently led to stiffer hydrogels with a smaller mesh size. Additionally, a slower thawing rate led to more elastic hydrogels with more swelling, represented by a reduced tan(δ) value. Samples of varying alginate concentrations were generated using two freezing temperatures (-20 ˚C and -80 ˚C) and three thawing temperatures (4 ˚C, 20 ˚C, and 36 ˚C) (A-D, n = 6).

4.3.6 Alginate hydrogel stability

The stability of hydrogels was evaluated by measuring changes in the storage moduli, damping ratios, and swelling properties over three weeks. Additionally, various hydrogels prepared via TIG were measured after a year in non-frozen cold storage. Strikingly, all hydrogels produced by TIG showed an uncharacteristic increase in stiffness from day 0 to day 2, which did not occur in the control group (control) formed by normal gelation (Figure 4.7A). Coincidently, the 1% (w/v) hydrogel formed by TIG had a similar storage modulus as the 2% (w/v) control hydrogel during this time. After 21 days, only the control hydrogel had a statistically significant loss in stiffness (Figure 4.7B). However, this decrease appears to be primarily in the first week. Although not statistically significant, the hydrogels formed via TIG also had a downward trend in storage moduli over three weeks. Overall, the assay shows a time-dependent decrease in the stability of the hydrogels' storage moduli over time, with hydrogels formed via TIG being more resistant to these changes.

Paralleling changes in hydrogel storage moduli, TIG hydrogels had a statistically significant decrease in the damping ratio between days 0 and 2, representing an increase in elasticity (Figure 4.7C). In contrast, the control hydrogels had a significant loss in elasticity over this same period, as the damping ratio increased. Both 1% and 2% (w/v) alginate hydrogels produced by TIG became significantly more elastic over 21 days (Figure 4.7D). Notably, the hydrogels formed by TIG start significantly less elastic than the control hydrogel; however, with the opposing trends between the control and TIG methods, the TIG hydrogel became significantly more elastic after three days. Together these data indicate potential structural changes that initially occur with TIG

hydrogels that do not occur with the control hydrogels formed by the normal gelation method.

Despite initial fluctuations between all groups, only the control hydrogel significantly decreased swelling after three weeks (Figure 4.7E & F). Remarkably, TIG hydrogels had no statistically significant change in swelling after three weeks. Unlike the storage modulus and damping ratio, there is no significant difference in swelling over the initial two to three days between the TIG hydrogels. Furthermore, there is no clear indication that the hydrogels continue to swell to the equilibrium swelling ratio between the day of gelation and day one. Generally, these results point to TIG imparting more stability to the hydrogel's swelling than the control hydrogel.

Furthermore, a set of samples formed by TIG with differing freezing and thawing conditions was kept at 4 ˚C for over a year before being measured. Notably, the TIG hydrogel frozen in the -80 ˚C freezer and thawed in a 4 ˚C solution did not have a significant decrease in stiffness (Figure 4.8A). This hydrogel was the only condition that did not retain the increase in elasticity observed in the previous figure (Figure 4.8B). Additionally, after a year of cold storage, the swelling of TIG hydrogels significantly increased, except for that hydrogel formed by TIG with polymer frozen in the -80 ˚C freezer and thawed in a 4 ˚C solution (Figure 4.8C). Despite these mechanical and swelling properties changes, most hydrogels retained the surface topography they initially had after gelation (Figure 4.8D). The formation of these hydrogels from frozen alginate results in ridges from the ice, which can still be seen after a year. In contrast, hydrogels formed by the control method typically lost their integrity, swelled until they disintegrated in solution after a couple of months.

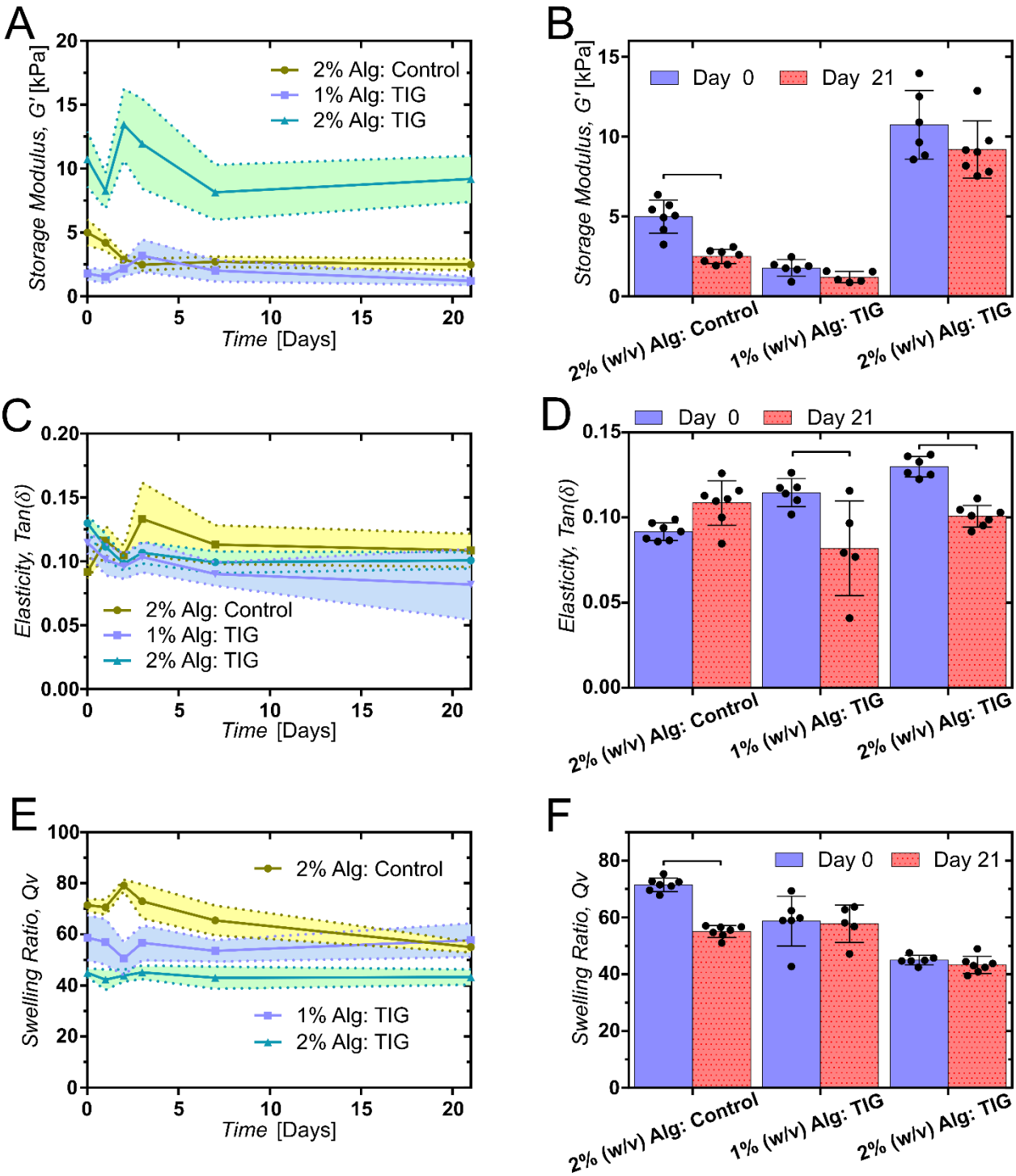

Figure 4.7 The stability of TIG hydrogels contrasted the control hydrogels. The degradation and subsequent change in hydrogel properties over three weeks were

characterized by measuring the storage moduli (A-B), damping ratios (C-D), and swelling ratios (E-F). Hydrogels formed by TIG were prepared by freezing polymer in the -80 ˚C freezer and thawing in a cross-linker solution that was 36 ˚C due to their contrasting damping ratio compared to the control hydrogels. The hydrogels prepared via TIG had better stability in storage modulus and swelling ratio than the control hydrogel. Additionally, changes in elasticity over time followed opposing trends between the control and TIG hydrogels. Lastly, all hydrogels formed via TIG had an uncharacteristic increase in stiffness and a decrease in damping ratio over the first three days. Data for figure panels A, C, and E represent the mean ± SD (indicated by shaded areas) over 21 days (n = 5 – 7). For figure panels B, D, and F, the bar represents mean, scatter dot plots display individual measurements, and error bars represent standard deviation (n = 5 – 7). A line between groups represents statistically significant differences ($P < 0.05$) between days 0 and 21 of the same hydrogels, assessed by a two-way ANOVA and a Tukey's multiple comparison test.

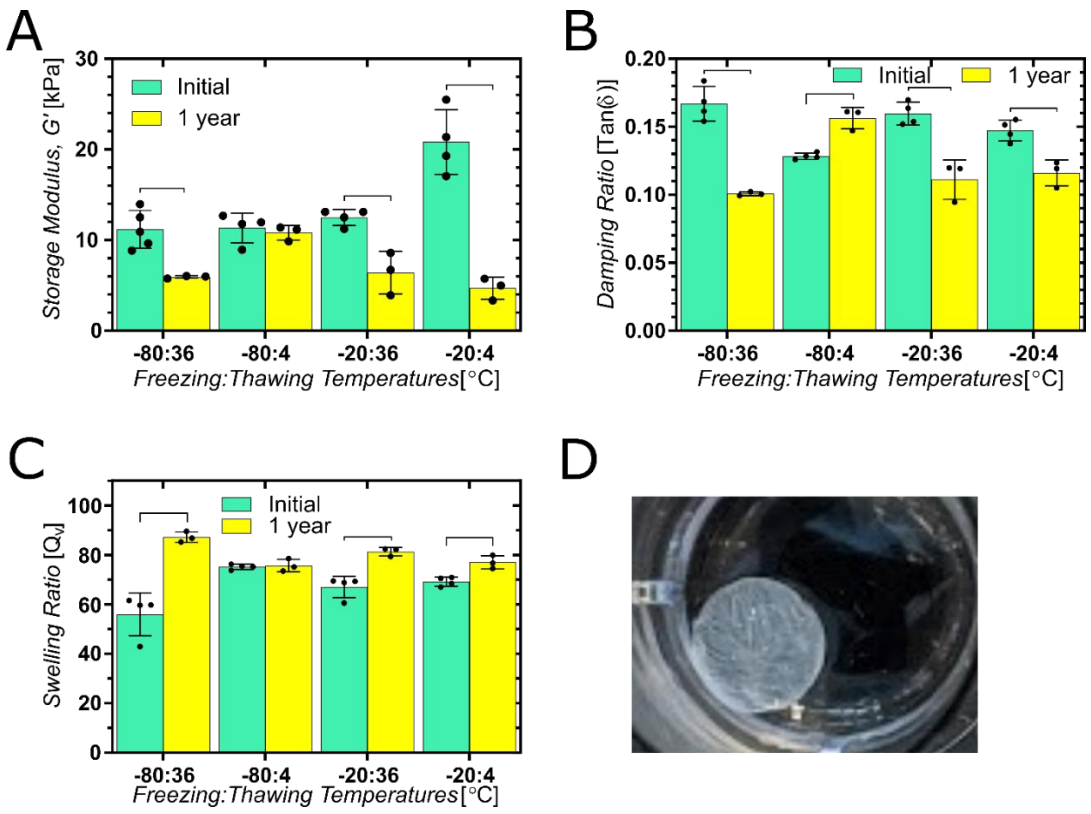

Figure 4.8 Stability of various TIG hydrogels over a year. TIG hydrogels formed by freezing in -20 ˚C and -80 ˚C and thawed in a solution at 4 ˚C and 36 ˚C were kept at 4 ˚C for over a year (383 days) in a saline solution, and their storage modulus (A), damping ratio (B), and swelling ratio (C) were measured. An image of a sample hydrogel displays ridges from the initial frozen polymer structure after over a year (D). While all hydrogels had some significant change in properties over a year, the hydrogel prepared by freezing in -80 ˚C and thawed in 4 ˚C had no significant change in stiffness or swelling. Additionally, the change in damping ratio for this group opposes the change observed in the other groups. The bar represents mean, scatter dot plots display individual hydrogel measurements, and error bars represent standard deviation (n = 3 – 4). Lines connecting groups represent statistically significant differences ($P < 0.05$) assessed by performing a two-way ANOVA and a Tukey's multiple comparison test.

4.3.7 Osmolarity effects on hydrogel formation

Hydrogels were evaluated by their storage modulus, damping ratio, and swelling ratios with different cross-linking solution osmolarities and cross-linker concentrations to examine potential variations in cross-linking behavior due to TIG. There were no statistical differences in stiffness due to differences in cross-linker solution osmolarity for both gelation methods (Figure 4.9A). Furthermore, both hydrogels were significantly more elastic with the isotonic cross-linker solution (Figure 4.9B). Lastly, there was significantly more swelling of the control hydrogel in the isotonic cross-linker solution (Figure 4.9C). Generally, hydrogels produced via TIG had similar trends as the control hydrogels for the varying osmolarity and cross-linker concentrations. Similarly, increasing the concentration of calcium ions led to significantly stiffer (Figure 4.9D) and less elastic (Figure 4.9E) hydrogels for both gelation methods (Figure 4.9D). However, the swelling properties trends differed between hydrogels formed via TIG and the control (Figure 4.9F). Regardless, the TIG method generally responded similarly to solution osmolarity and cross-linker concentration as the control.

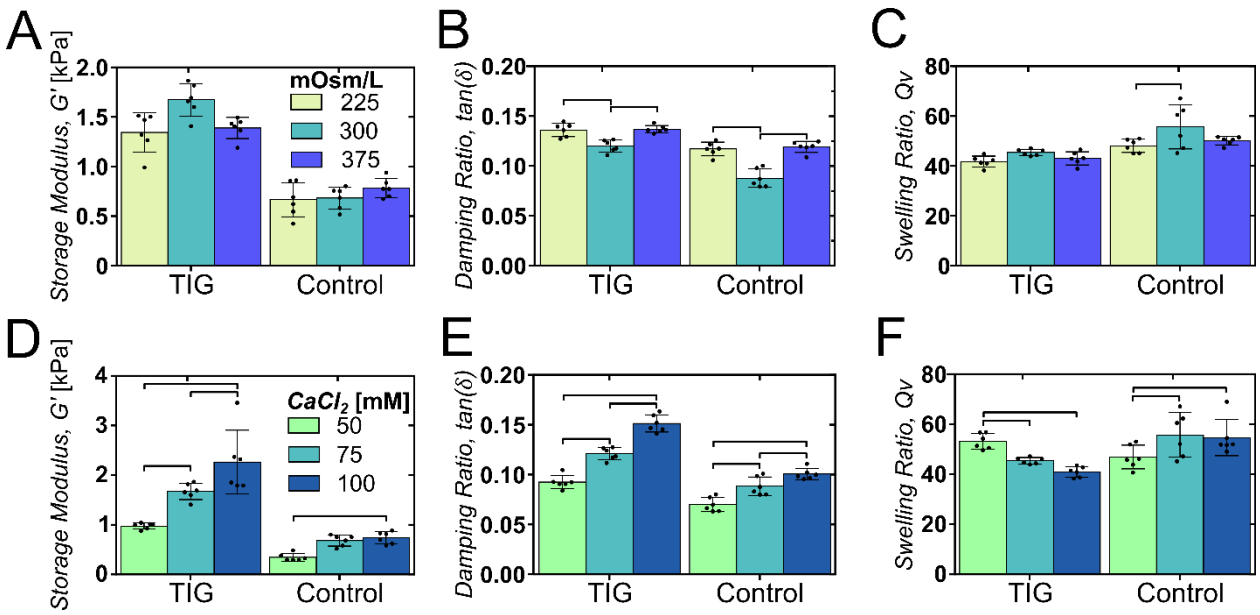

Figure 4.9 Alterations in osmolarity and cross-linker concentration had similar outcomes for hydrogels, regardless of gelation method. Hydrogels formed by TIG were prepared by freezing polymer in the -80 ˚C freezer and thawing in a cross-linker solution that was 20 ˚C. Specifically, both gelation methods had similar trends in stiffness with solution osmolarity (A) and cross-linker concentration (D). Furthermore, both groups had smaller damping ratios with an isotonic solution (B) and lower cross-linker concentrations (E). However, TIG did result in an opposing swelling trend with respect to cross-linker concentration, despite similar swelling trends with solution osmolarity. The bar represents mean, scatter dot plots display individual measurements, and error bars represent standard deviation (n = 6). A line between groups represents statistically significant differences ($P < 0.05$).

4.3.7 Buffer and pH effects on hydrogel formation

The effect of pH changes when freezing a phosphate solution and the role of pH of the cross-linker solution on the formation of hydrogels were assessed. Specifically, 2% (w/v) alginate solutions were prepared using a PBS or NaCl solution and cross-linked with an acidic or neutral calcium solution. These hydrogels were characterized for their stiffness, damping ratio, and swelling properties in line with previous experiments. Alginate hydrogels were significantly stiffer when formed with a neutral cross-linking solution (Figure 4.10A-C). TIG hydrogels appear stiffer with alginate dissolved in PBS, although this outcome was not statistically significant. Overall, these data do not indicate significant changes to hydrogel formation via TIG due to the buffers or solution pH used in this experiment.

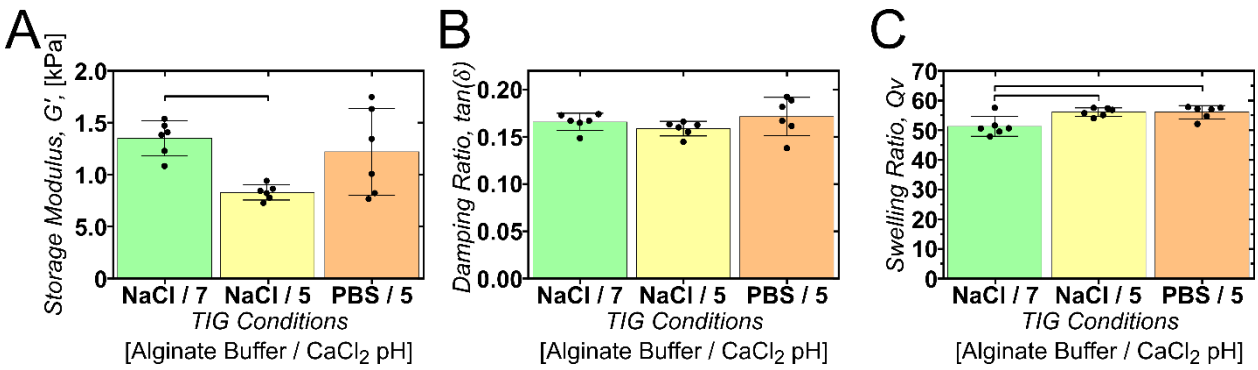

Figure 4.10 Buffer and pH changes are expected to alter hydrogel properties. Specifically, phosphate buffers change their pH when freezing, potentially impacting TIG. Hydrogels were formed via TIG with alginate polymer dissolved in NaCl or a phosphate-buffered saline (PBS) and frozen in a -80 ˚C freezer. These samples were thawed in a cross-linker solution that was 20 ˚C at pH 5 or 7. The acidity of the cross-linker solution had a significant impact on stiffness and swelling, but not the damping ratio. Similarly, the use of a phosphate solution did not significantly impact the resulting hydrogels. The bar represents mean, scatter dot plots display individual hydrogel measurements, and error bars represent standard deviation (n = 6). A line between groups represents statistically significant differences ($P < 0.05$).

4.3.9 Hydrogel cryoprotective outcomes

The potential cytotoxicity and cryoprotective capacity of the alginate hydrogels were investigated by using HUVECs. Influences on proliferation were determined by normalizing to cells culture in N media. The addition of hydrogels to the cell culture wells resulted in no significant difference with N media (Figure 4.11A). Although the addition of hydrogels to cells cultured in complete media led to a similar decrease in the resulting proliferation after three days, there was no difference in how the hydrogel was produced for both media conditions. Notably, with cells cultured in complete media, there were visibly fewer cells underneath the hydrogels. As expected, complete media led to significantly more proliferation than N media; overall, the thaw-induced gelation did not significantly reduce proliferation compared to the control hydrogel. Next, cells were exposed to a mitogenic factor, VEGF. Similar to proliferation in complete media, there was no significant difference between hydrogel conditions when VEGF-stock solution is frozen in an alginate solution (Figure 4.11B). Interestingly, there was significantly less proliferation if the VEGF-stock solution was not frozen in the polymer solution. When VEGF was refrozen in the stock vial, the resulting proliferation was comparable to the N media condition. These data indicate that alginate hydrogels formed via TIG are just as non-cytotoxic as more traditional gelation methods and that freezing the VEGF-stock solution in alginate led to more proliferation than refreezing the stock solution in the vial provided by the supplier's kit.

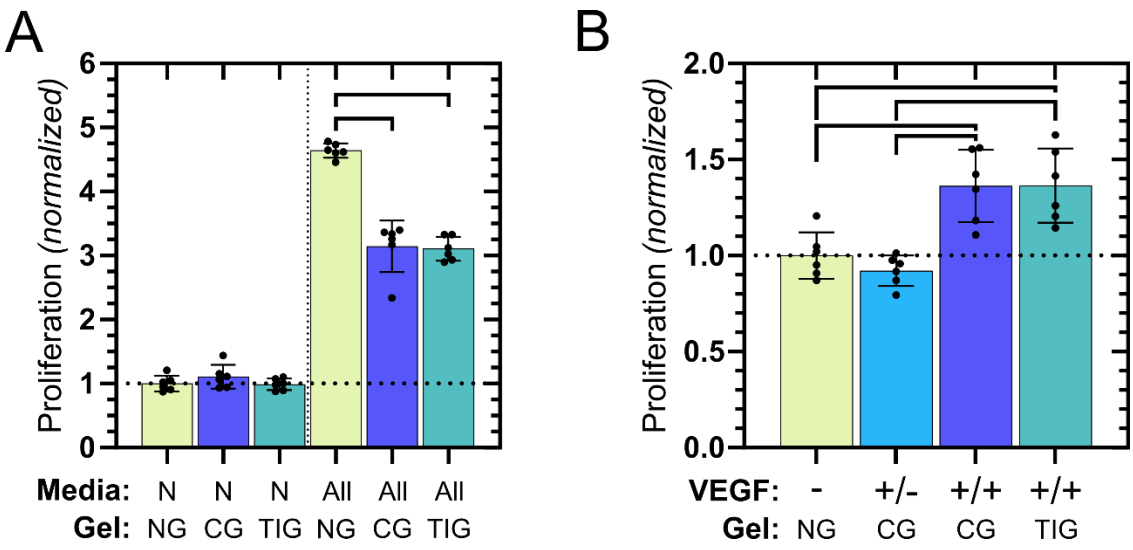

Figure 4.11 Alginate hydrogels formed via TIG had comparable metabolic activity per culture well as the control hydrogel. In N media (N), there was no significant difference in metabolic activity between no hydrogel (NG), control group (CG) hydrogel, and hydrogel formed by TIG (TIG) (A). However, using complete media (All), NG had significantly more metabolic activity than CG and TIG groups due to cell proliferation. Freezing the VEGF stock in an alginate solution (+/+) led to significantly more metabolic activity compared to no VEGF (-) and refrozen VEGF stock (+/-) (B). Data are normalized to the average untreated control cells cultured in N media (indicated by the dashed line). The bar represents mean, scatter dot plots display individual measurements, and error bars represent standard deviation (n = 6). A line between groups represents statistically significant differences ($P < 0.05$) assessed by performing a one-way ANOVA and a Tukey's multiple comparison test.

4.4 Discussion

4.4.1 The formation of a unique alginate hydrogel: a homo-IPN

This chapter demonstrates an enhancement of toughness and stability with the TIG strategy while displaying promising cryoprotective capacity. The hydrogel's mechanical properties indicate a dependence on the rate the polymer solution is frozen, which supports the soluble aggregation of eutectic structures via cryostructuring persists through the subsequent melting in the cross-linker solution [47, 48]. While aggregation of polymers from freezing a solution has been previously described as the mechanism for forming cryogels [49, 50], alginate does not form stable cryogels like polyvinyl alcohol [51-53]. Specifically, freezing alginate in a saline solution alone does not create a hydrogel; additional steps are required, such as ionic cross-linking. Additionally, the dependence of hydrogel stiffness and elasticity on thawing rate suggests the importance of ionic cross-linking and the potential impact this step might have on redissolving the potential aggregated eutectic structures. These dependencies freezing and thawing rates in the context of gelation time and altering molecular weight of the alginate polymer suggest the formation of hydrogels that embody gelation schemes and outcomes comparable to a semi-IPN that is sequentially formed [16, 24-26]. Specifically, within the context of TIG, the distinct structures formed from one polymer composition are representative of a homo-IPN [26, 33]. Furthermore, the formation of these previous homo-IPNs led to a decrease in swelling and increase in stiffness, paralleling the results observed in this chapter [26, 33]. To our knowledge, the formation of an alginate homo-IPN has not been previously described, suggesting the potential novelty TIG not only has for encapsulation and mechanical stability within the context for cold storage and

cryopreservation but also for forming a unique hydrogel structure with potential applications for interrogating cell responsiveness to IPNs from one polymer source.

4.4.2 SEM elucidates TIG impact on network structure

SEM images presented the structural differences between a conventional method to form alginate hydrogels, our control group, and TIG. While our control group hydrogel has a similar mesh structure observed in previous SEM images of alginate hydrogels [41, 43, 44, 54], all TIG hydrogels appear distinct from the control groups. Moreover, the wall thickness and pore size of TIG hydrogels were smaller than what was expected from alginate sponges [44, 55], suggesting the networks do not wholly replicate the cryostructuring observed in sponges. Notably, the networks formed by TIG were dependent on the utilized freezing and thawing rates. Compared to the control hydrogel group, the larger polymer clusters and pore sizes from the TIG hydrogels parallel previous studies with alginate sponges that described a slower freezing rate creating larger ice crystals that result in thicker polymer aggregations [29, 47, 55]. Adjacently, faster freezing leads to smaller amorphous ice crystals [56-58], potentially causing the wave patterns found in hydrogels formed by freezing in -80 ˚C but not in -20 ˚C. Broadly, these results suggest that the freezing rate alters the structure of the resulting hydrogel regardless of the thawing rate. Notwithstanding, the cross-linker solution temperature would affect the solubility of alginate, diffusion of calcium, and cross-linking efficiency of alginate [6, 59]. Succinctly, the thawing rate is expected to alter any aggregated alginate polymer's redissolving and ionic cross-linking. Therefore, the slower thawing rate leading to larger pores suggests thawing rate has a potential

role in preserving structures dependent on the freezing rate. Regardless, the SEM images suggest unique structures likely to influence the overall hydrogel's mechanical and physical properties.

4.4.3 Freezing and thawing rates impact hydrogel mechanical properties

TIG hydrogels had physical and mechanical properties depending on the freezing and thawing rates utilized. While larger alginate concentrations enhance stiffness and decrease swelling ratios agreed with many other alginate hydrogel studies [36, 41, 60-62], these hydrogels becoming stiffer with faster freezing rates matches a previous study with alginate sponges [29]. Moreover, the thawing rate also altered hydrogel properties, highlighting the importance of ionic cross-linking. Specifically, a warmer thawing temperature resulted in stiffer hydrogels consistent with previous reports where warmer gelation temperatures increase alginate calcium content [30, 59]. Correspondingly, hydrogels formed by TIG were more elastic and had more swelling when thawed slowly at 4 ˚C. While this outcome could result from the temperatures used in the thawing bath, these data could be described by the forming entanglements commonly associated with IPN [24, 26, 63]. Tentatively, if these TIG hydrogels could be described as a homo-IPN, an interpenetrating polymer network formed from polymers that are chemically identical [32, 34], it would be expected that this hydrogel would have different stiffness, elasticity, swelling, and mechanical stability compared to a hydrogel without reinforcing entanglements between networks formed by cryostructuring and ionic cross-linking.

As the process of TIG is sequential and each step appears to influence the hydrogel's network structure and the resulting mechanical properties, the results discussed previously support the formation of a homo-IPN. Specifically, the combination of data suggests the TIG hydrogel is distinct from using the normal gelation scheme. At a minimum, the overall decrease in temperature and phase transition would result in less ionic cross-linking in the same ten-minute period than the control gelation method [6, 64]. However, our results categorically illustration that TIG leads to stiffer, more elastic hydrogels where weaker, more viscous hydrogels would be expected. Notably, the increase in storage modulus and decreased elasticity with more gelation time and high molecular weight polymer indicate additional ionic cross-linking. The viscoelastic properties of an alginate hydrogel come from the ability to break and reform the ionic cross-links [65], and ionic cross-links represent anchor points where energy can be transferred to heat by breaking the bonds [66]. Furthermore, additional ionic cross-linking of alginate reduces swelling [36, 67-69]; however, TIG hydrogels would have less time and thermal energy for ionic cross-linking but have lesser swelling than the control hydrogel. Lastly, from SEM images of TIG hydrogels formed by freezing in -80 ˚C, the decrease in the mesh size when thawing at 36 ˚C further supports redissolving of alginate polymer by greater local concentration of polymer between aggregated regions. Fundamentally, these smaller meshes act as numerous small springs that, according to Hooke's law, are less capable of transmitting forces due to their short lengths than larger mesh sizes. Consequently, we confirm there were more elastic hydrogels formed with slower thawing rates. Therefore, the data support the existence of a cryostructured and an ionically cross-linked network entangled as an IPN.

4.4.4 TIG enhances mechanical stability of alginate hydrogels

The mechanical stability of hydrogels formed by TIG was superior to the control hydrogel group. This difference is expounded by the differences in mechanical properties and the swelling ratio between these hydrogels. Previous studies have shown that the damping ratio increases with increased ionic cross-linking of alginate polymers [62, 70]. Although TIG hydrogels initially had a greater damping ratio than the control hydrogel group, hydrogels formed by TIG had a striking increase in hydrogel stiffness and elasticity over the first three days. This outcome directly contrasted the decrease in stiffness and elasticity of the control hydrogels. This initial change in elastic behavior could represent the irreversible dissociation of aggregated polymers [66], resulting in entanglements that enhance the hydrogel's elasticity.

Additionally, the swelling of the control group decreased over three weeks, likely from the dissociation of alginate polymer from the hydrogel from salting-out [22]. Despite being exposed to the same favorable sterile conditions, hydrogels formed by TIG did not have a significant change in swelling. In the context of the previous data supporting cryostructured polymer, the dissociation of aggregated alginate would increase the swelling ratio [71, 72]. Countering this increase in swelling, additional entanglements, such as with an IPN, would be expected to reduce swelling [73-75]. Therefore, the entanglements within a hydrogel prepared via TIG could be reinforced during these first couple of days and reenforces the changes in stiffness and elasticity.

Moreover, physical entanglements are a characteristic attribute of materials with outstanding stability in stiffness and swelling properties [22, 24, 76, 77]. This longevity

of the TIG hydrogels (>1 year) occurs despite the expected thermodynamic loss of the divalent cation cross-linker [22], suggesting the existence of structures beyond ionic cross-linked polymer. Regardless of the underlying structure, the improved long-term elastic and swelling stability may prove advantageous for the therapeutic delivery of cells within a hydrogel that uses an alginate solution as an extracellular cryopreservation agent [19]. Together, these results suggest that the TIG method's compliance with frozen storage enables its stability for long-term cold storage.

4.4.5 TIG and control gelation scheme is similarly influenced by osmolarity, cross-linker concentration.

In this chapter, hydrogels prepared by TIG were consistently stiffer than the control gelation method under the same osmolarities, cross-linker concentration, and buffer acidities. Hydrogel trends due to osmolarity, cross-linker concentration, and solution acidity were consistent between the TIG and control gelation methods. Broadly, these observations between TIG and the control group hydrogels agree with enhancements observed in IPN hydrogels [15; 16; 69] and suggest similar mechanisms used to modulate alginate hydrogels applicable with TIG. However, it has been previously described that freezing a phosphate buffer makes the solution more acidic, and acidic solutions reduce the ionic cross-linking capacity for alginate polymers [51; 78; 79; 80; 81; 82]. While the significant decrease when using an acidic-calcium solution agrees with previous work [6; 83; 84], there appears to be little effect from freezing polymer in the phosphate buffer on the resulting hydrogel. Further work could

interrogate the amount of calcium bound to the hydrogels through a calcium-specific colorimetric assay.

4.4.6 TIG hydrogels are cryoprotective for VEGF

The function of TIG hydrogels for cells was assessed in two stages: metabolic activity during exposure to alginate hydrogels and proliferation with exposure to VEGF, a key factor for the mitogenic activity for vascular endothelial cells [43, 78, 79]. Specifically, an MTT assay was performed to determine cytotoxicity or enhancement of proliferation from the alginate hydrogel and the VEGF cargo [80, 81]. The alginate hydrogel prepared by TIG, like the control hydrogel, was not cytotoxic and agrees with previous research with alginate hydrogels [40, 43, 82]. The lower level of proliferation in complete media coinciding with fewer adherent cells between the culture well and hydrogel suggests the hydrogel could be sterically hindering proliferation, likely due to the lack of cell binding modalities on the alginate polymer [82-84]. Regardless, the alginate hydrogels had no detrimental effect on cell viability with N media.

Moreover, the potential cryoprotective nature of alginate is reinforced by the increased metabolic activity in the tissue culture wells in response to VEGF exposure, suggesting greater proliferation. Previously, freezing has been shown to have adverse degradation effects on VEGF protein [85]. Although the cryoprotective capacity of alginate has never been explicitly tested with VEGF, alginate has been described to promote the efficacy of vaccines and survival of cells as a cryoprotectant [18, 19, 86-88]. The overall mechanism of alginate preventing osmotic transients and ice formation would support the outcomes shown here and suggest the benefit of loading cargo in a

frozen polymer solution [19, 89-91]. Together, the lack of cytotoxicity with TIG and the cryoprotective outcome with the VEGF protein suggests the alginate hydrogels produced via TIG are biocompatible, maintaining the ability of the material to perform with an appropriate host response similar to the control hydrogel formed by the normal gelation scheme [92].

4.5 Conclusion

This chapter characterizes the alginate hydrogels produced by thaw-induced gelation (TIG) through the freezing and thawing rates utilized. Not only did the alginate hydrogel produced by TIG have enhanced stiffness and stability of its mechanical and swelling properties compared to the control hydrogel, but the gelation process has potential cryoprotective benefits for growth factor proteins. Overall, the expected cryostructuring and ionic cross-linking mechanisms are supported by the dependence on freezing and thawing rated during TIG and similar trends to the control group with changes in alginate and cross-linker concentration. With these two steps that structure the hydrogel, an aggregated polymer, and ionically cross-linked regions, we propose the hydrogel could represent a semi-IPN composed from the same initial alginate polymer solution, a homo-IPN. Advantageously, a homo-IPN formed by TIG represents a unique method for generating semi-IPNs from one polymer species. Regardless of the underlying structure, the gelation scheme could be applied ubiquitously to other ionically cross-linked polymeric hydrogel systems to enhance their mechanical and swelling stability and potentially provide some cryoprotective benefit. With the evidence of biocompatibility with TIG, further work could incorporate the cryopreservation and subsequent delivery of cells and growth factors with alginate acting as the cryopreservation agent and polymeric scaffold.

4.6 References

[1] S. E. Barnett and S. J. Varley, "The effects of calcium alginate on wound healing," (in eng), *Ann R Coll Surg Engl,* vol. 69, no. 4, pp. 153-5, Jul 1987.

[2] A. C. Daly, F. E. Freeman, T. Gonzalez-Fernandez, S. E. Critchley, J. Nulty, and D. J. Kelly, "3D Bioprinting for Cartilage and Osteochondral Tissue Engineering," *Advanced Healthcare Materials,* vol. 6, no. 22, p. 1700298, 2017/11/01 2017, doi: 10.1002/adhm.201700298.

[3] P. De Vos, G. H. J. Wolters, W. M. Fritschy, and R. Van Schilfgaarde, "Obstacles in the Application of Microencapsulation in Islet Transplantation," *The International Journal of Artificial Organs,* vol. 16, no. 4, pp. 205-212, 1993/04/01 1993, doi: 10.1177/039139889301600407.

[4] A. Mandal, J. R. Clegg, A. C. Anselmo, and S. Mitragotri, "Hydrogels in the clinic," *Bioengineering & Translational Medicine,* vol. 5, no. 2, p. e10158, 2020/05/01 2020, doi: 10.1002/btm2.10158.

[5] L. I. F. Moura, A. M. A. Dias, E. Carvalho, and H. C. de Sousa, "Recent advances on the development of wound dressings for diabetic foot ulcer treatment—A review," *Acta Biomaterialia,* vol. 9, no. 7, pp. 7093-7114, 2013/07/01/ 2013, doi: https://doi.org/10.1016/j.actbio.2013.03.033.

[6] K. Y. Lee and D. J. Mooney, "Alginate: Properties and biomedical applications," *Progress in Polymer Science,* vol. 37, no. 1, pp. 106-126, 1// 2012, doi: http://dx.doi.org/10.1016/j.progpolymsci.2011.06.003.

[7] R. C. Op 't Veld, X. F. Walboomers, J. A. Jansen, and F. A. D. T. G. Wagener, "Design Considerations for Hydrogel Wound Dressings: Strategic and Molecular

Advances," *Tissue Engineering Part B: Reviews,* vol. 26, no. 3, pp. 230-248, 2020/06/01 2020, doi: 10.1089/ten.teb.2019.0281.

[8] J. Li and D. J. Mooney, "Designing hydrogels for controlled drug delivery," (in eng), *Nature reviews. Materials,* vol. 1, no. 12, p. 16071, 2016, doi: 10.1038/natrevmats.2016.71.

[9] A. Camboni, A. Van Langendonckt, J. Donnez, J. Vanacker, M. M. Dolmans, and C. A. Amorim, "Alginate beads as a tool to handle, cryopreserve and culture isolated human primordial/primary follicles," in *Cryobiology*, vol. 67, no. 1). Netherlands: © 2013 Elsevier Inc, 2013, pp. 64-9.

[10] Y. H. Tu, M. L. Stiles, L. V. Allen, Jr., K. M. Olsen, C. I. Barton, and R. B. Greenwood, "Stability of amoxicillin trihydrate-potassium clavulanate in original containers and unit dose oral syringes," (in eng), *Am J Hosp Pharm,* vol. 45, no. 5, pp. 1092-9, May 1988.

[11] C. J. Hunt, "Technical Considerations in the Freezing, Low-Temperature Storage and Thawing of Stem Cells for Cellular Therapies," *Transfusion Medicine and Hemotherapy,* vol. 46, no. 3, pp. 134-150, 2019, doi: 10.1159/000497289.

[12] J.-D. Hecq *et al.*, "Doxorubicin-loaded drug-eluting beads (DC Bead®) for use in transarterial chemoembolization: A stability assessment," *Journal of Oncology Pharmacy Practice,* vol. 19, no. 1, pp. 65-74, 2013/03/01 2012, doi: 10.1177/1078155212452765.

[13] S. Ferber *et al.*, "Evaporative Cooling Hydrogel Packaging for Storing Biologics Outside of the Cold Chain," *Advanced Healthcare Materials,* vol. 7, no. 14, p. 1800220, 2018/07/01 2018, doi: https://doi.org/10.1002/adhm.201800220.

[14] S. J. Shire, "Formulation and manufacturability of biologics," *Current Opinion in Biotechnology,* vol. 20, no. 6, pp. 708-714, 2009/12/01/ 2009, doi: https://doi.org/10.1016/j.copbio.2009.10.006.

[15] F. Gnanaprakasam Thankam, J. Muthu, V. Sankar, and R. Kozhiparambil Gopal, "Growth and survival of cells in biosynthetic poly vinyl alcohol–alginate IPN hydrogels for cardiac applications," *Colloids and Surfaces B: Biointerfaces,* vol. 107, pp. 137-145, 2013/07/01/ 2013, doi: https://doi.org/10.1016/j.colsurfb.2013.01.069.

[16] X. Li *et al.*, "Strong, tough and mechanically self-recoverable poly(vinyl alcohol)/alginate dual-physical double-network hydrogels with large cross-link density contrast," *RSC Advances,* 10.1039/C8RA01302K vol. 8, no. 30, pp. 16674-16689, 2018, doi: 10.1039/C8RA01302K.

[17] K. Adebowale *et al.*, "Enhanced substrate stress relaxation promotes filopodia-mediated cell migration," *Nature Materials,* 2021/04/19 2021, doi: 10.1038/s41563-021-00981-w.

[18] X. Xiang, Z. Liu, and G. Zhao, "Sodium Alginate as a Novel Cryoprotective Agent for Cryopreservation of Endothelial Cells in a Closed Polytetrafluoroethylene Loop," *Biopreservation and Biobanking,* vol. 18, no. 4, pp. 321-328, 2020/08/01 2020, doi: 10.1089/bio.2020.0020.

[19] H. Gurruchaga *et al.*, "Advances in the slow freezing cryopreservation of microencapsulated cells," *Journal of Controlled Release,* vol. 281, pp. 119-138, 2018/07/10/ 2018, doi: https://doi.org/10.1016/j.jconrel.2018.05.016.

[20] O. Chaudhuri *et al.*, "Hydrogels with tunable stress relaxation regulate stem cell fate and activity," *Nature Materials,* vol. 15, no. 3, pp. 326-334, 2016/03/01 2016, doi: 10.1038/nmat4489.

[21] G. T. Grant, E. R. Morris, D. A. Rees, P. J. C. Smith, and D. Thom, "Biological interactions between polysaccharides and divalent cations: The egg-box model," *FEBS Letters,* vol. 32, no. 1, pp. 195-198, 1973/05/15 1973, doi: 10.1016/0014-5793(73)80770-7.

[22] C. K. Kuo and P. X. Ma, "Maintaining dimensions and mechanical properties of ionically crosslinked alginate hydrogel scaffolds in vitro," *Journal of Biomedical Materials Research Part A,* vol. 84A, no. 4, pp. 899-907, 2008/03/15 2008, doi: 10.1002/jbm.a.31375.

[23] Y. Zhang, J. Liu, L. Huang, Z. Wang, and L. Wang, "Design and performance of a sericin-alginate interpenetrating network hydrogel for cell and drug delivery," *Scientific Reports,* vol. 5, no. 1, p. 12374, 2015/07/24 2015, doi: 10.1038/srep12374.

[24] E. S. Dragan, "Design and applications of interpenetrating polymer network hydrogels. A review," *Chemical Engineering Journal,* vol. 243, pp. 572-590, 2014/05/01/ 2014, doi: https://doi.org/10.1016/j.cej.2014.01.065.

[25] S. Rehmani, M. Ahmad, M. U. Minhas, H. Anwar, M. I.-u.-d. Zangi, and M. Sohail, "Development of natural and synthetic polymer-based semi-interpenetrating polymer network for controlled drug delivery: optimization and in vitro evaluation studies," *Polymer Bulletin,* vol. 74, no. 3, pp. 737-761, 2017/03/01 2017, doi: 10.1007/s00289-016-1743-y.

[26] L. H. Sperling, "Interpenetrating Polymer Networks: An Overview," in *Interpenetrating Polymer Networks*, vol. 239, (Advances in Chemistry, no. 239): American Chemical Society, 1994, ch. 1, pp. 3-38.

[27] L. H. Sperling, "Interpenetrating Polymer Networks," *Encyclopedia of Polymer Science and Technology,* https://doi.org/10.1002/0471440264.pst170 2004/03/15 2004, doi: https://doi.org/10.1002/0471440264.pst170.

[28] H. Hu and F.-J. Xu, "Rational design and latest advances of polysaccharide-based hydrogels for wound healing," (in eng), *Biomaterials science,* vol. 8, no. 8, pp. 2084-2101, 2020/04// 2020, doi: 10.1039/d0bm00055h.

[29] L. Shapiro and S. Cohen, "Novel alginate sponges for cell culture and transplantation," *Biomaterials,* vol. 18, no. 8, pp. 583-590, 1997/04/01/ 1997, doi: https://doi.org/10.1016/S0142-9612(96)00181-0.

[30] C. Jeong, S. Kim, C. Lee, S. Cho, and S. B. Kim, "Changes in the Physical Properties of Calcium Alginate Gel Beads Under a Wide Range of Gelation Temperature Conditions," (in eng), *Foods,* vol. 9, no. 2, Feb 12 2020, doi: 10.3390/foods9020180.

[31] C. K. Kuo and P. X. Ma, "Ionically crosslinked alginate hydrogels as scaffolds for tissue engineering: Part 1. Structure, gelation rate and mechanical properties," *Biomaterials,* vol. 22, no. 6, pp. 511-521, 2001/03/15/ 2001, doi: https://doi.org/10.1016/S0142-9612(00)00201-5.

[32] T. V. Chirila, K. A. George, W. A. Abdul Ghafor, S. J. Pas, and A. J. Hill, "Sequential homo-interpenetrating polymer networks of poly(2-hydroxyethyl methacrylate): Synthesis, characterization, and calcium uptake," *Journal of*

Applied Polymer Science, vol. 126, no. S2, pp. E455-E466, 2012/11/25 2012, doi: 10.1002/app.36824.

[33] X. Lou, S. Vijayasekaran, T. V. Chirila, M. A. L. Maley, C. R. Hicks, and I. J. Constable, "Synthesis, physical characterization, and biological performance of sequential homointerpenetrating polymer network sponges based on poly(2-hydroxyethyl methacrylate)," *Journal of Biomedical Materials Research,* vol. 47, no. 3, pp. 404-411, 1999/12/05 1999, doi: 10.1002/(SICI)1097-4636(19991205)47:3<404::AID-JBM16>3.0.CO;2-F.

[34] D. L. Siegfried, D. A. Thomas, and L. H. Sperling, "A Reexamination of Polystyrene/Polystyrene Homo Interpenetrating Polymer Networks: Aspects of Relative Network Continuity and Internetwork Coupling," *Macromolecules,* vol. 12, no. 4, pp. 586-589, 1979/07/01 1979, doi: 10.1021/ma60070a009.

[35] J. V. Alemán *et al.*, "Definitions of terms relating to the structure and processing of sols, gels, networks, and inorganic-organic hybrid materials (IUPAC Recommendations 2007)," (in English), *Pure and Applied Chemistry,* vol. 79, no. 10, pp. 1801-1829, 01 Jan. 2007 2007, doi: https://doi.org/10.1351/pac200779101801.

[36] D. J. Hadley and E. A. Silva, "Thaw-Induced Gelation of Alginate Hydrogels for Versatile Delivery of Therapeutics," *Annals of Biomedical Engineering,* vol. 47, no. 8, pp. 1701-1710, 2019/08/01 2019, doi: 10.1007/s10439-019-02282-5.

[37] J. L. Madrigal, S. N. Sharma, K. T. Campbell, R. S. Stilhano, R. Gijsbers, and E. A. Silva, "Microgels produced using microfluidic on-chip polymer blending for

controlled released of VEGF encoding lentivectors," (in eng), *Acta biomaterialia,* vol. 69, pp. 265-276, 2018/03// 2018, doi: 10.1016/j.actbio.2018.01.013.

[38] M. L. Moya, M. Morley, O. Khanna, E. C. Opara, and E. M. Brey, "Stability of alginate microbead properties in vitro," (in eng), *Journal of materials science. Materials in medicine,* vol. 23, no. 4, pp. 903-912, 2012, doi: 10.1007/s10856-012-4575-9.

[39] B.-H. Lee, B. Li, and S. A. Guelcher, "Gel microstructure regulates proliferation and differentiation of MC3T3-E1 cells encapsulated in alginate beads," *Acta Biomaterialia,* vol. 8, no. 5, pp. 1693-1702, 2012/05/01/ 2012, doi: https://doi.org/10.1016/j.actbio.2012.01.012.

[40] K. T. Campbell, R. S. Stilhano, and E. A. Silva, "Enzymatically degradable alginate hydrogel systems to deliver endothelial progenitor cells for potential revasculature applications," (in eng), *Biomaterials,* vol. 179, pp. 109-121, 2018, doi: 10.1016/j.biomaterials.2018.06.038.

[41] K. T. Campbell, K. Wysoczynski, D. J. Hadley, and E. A. Silva, "Computational-Based Design of Hydrogels with Predictable Mesh Properties," *ACS Biomaterials Science & Engineering,* vol. 6, no. 1, pp. 308-319, 2020/01/13 2020, doi: 10.1021/acsbiomaterials.9b01520.

[42] J. T. Lee and K. L. Chow, "SEM sample preparation for cells on 3D scaffolds by freeze-drying and HMDS," (in eng), *Scanning,* vol. 34, no. 1, pp. 12-25, Jan-Feb 2012, doi: 10.1002/sca.20271.

[43] P. A. Williams, K. T. Campbell, H. Gharaviram, J. L. Madrigal, and E. A. Silva, "Alginate-Chitosan Hydrogels Provide a Sustained Gradient of Sphingosine-1-

Phosphate for Therapeutic Angiogenesis," *Annals of Biomedical Engineering,* vol. 45, no. 4, pp. 1003-1014, 2017/04/01 2017, doi: 10.1007/s10439-016-1768-2.

[44] R. Aston, K. Sewell, T. Klein, G. Lawrie, and L. Grøndahl, "Evaluation of the impact of freezing preparation techniques on the characterisation of alginate hydrogels by cryo-SEM," *European Polymer Journal,* vol. 82, pp. 1-15, 2016/09/01/ 2016, doi: https://doi.org/10.1016/j.eurpolymj.2016.06.025.

[45] J. Zhang and N. A. Peppas, "Morphology of poly(methacrylic acid)/poly(N-isopropyl acrylamide) interpenetrating polymeric networks," *Journal of Biomaterials Science, Polymer Edition,* vol. 13, no. 5, pp. 511-525, 2002/01/01 2002, doi: 10.1163/15685620260178373.

[46] H. I. Muri, L. Hoang, and D. R. Hjelme, "Mapping Nanoparticles in Hydrogels: A Comparison of Preparation Methods for Electron Microscopy," *Applied Sciences,* vol. 8, no. 12, 2018, doi: 10.3390/app8122446.

[47] A. M. Padilla, S. G. Chou, S. Luthra, and M. J. Pikal, "The Study of Amorphous Phase Separation in a Model Polymer Phase-Separating System Using Raman Microscopy and a Low-Temperature Stage: Effect of Cooling Rate and Nucleation Temperature," *Journal of Pharmaceutical Sciences,* vol. 100, no. 4, pp. 1362-1376, 2011/04/01/ 2011, doi: https://doi.org/10.1002/jps.22357.

[48] L. Bachmann and E. Mayer, "Physics of Water and Ice: Implications for Cryofixation," in *Cryotechniques in Biological Electron Microscopy*, R. A. Steinbrecht and K. Zierold Eds. Berlin, Heidelberg: Springer Berlin Heidelberg, 1987, pp. 3-34.

[49] V. I. Lozinsky *et al.*, "Study of cryostructurization of polymer systems VII. Structure formation under freezing of poly(vinyl alcohol) aqueous solutions," *Colloid and Polymer Science,* vol. 264, no. 1, pp. 19-24, 1986/01/01 1986, doi: 10.1007/BF01410304.

[50] U. Fumio, Y. Hiroshi, N. Kumiko, N. Sachihiko, S. Kenji, and M. Yasunori, "Swelling and mechanical properties of poly(vinyl alcohol) hydrogels," *International Journal of Pharmaceutics,* vol. 58, no. 2, pp. 135-142, 1990/01/29/ 1990, doi: https://doi.org/10.1016/0378-5173(90)90251-X.

[51] Y. Zhao, Z. Chen, and T. Wu, "Cryogelation of alginate improved the freeze-thaw stability of oil-in-water emulsions," (in eng), *Carbohydr Polym,* vol. 198, pp. 26-33, Oct 15 2018, doi: 10.1016/j.carbpol.2018.06.013.

[52] L. Shan *et al.*, "Fabrication and Use of Alginate-Based Cryogel Delivery Beads Loaded with Urea and Phosphates as Potential Carriers for Bioremediation," *Industrial & Engineering Chemistry Research,* vol. 55, no. 28, pp. 7655-7660, 2016/07/20 2016, doi: 10.1021/acs.iecr.6b01256.

[53] Y. Zhao, W. Shen, Z. Chen, and T. Wu, "Freeze-thaw induced gelation of alginates," in *Carbohydr Polym*, vol. 148. England: © 2016 Elsevier Ltd, 2016, pp. 45-51.

[54] D. Serp, M. Mueller, U. von Stockar, and I. W. Marison, "Low-temperature electron microscopy for the study of polysaccharide ultrastructures in hydrogels. II. Effect of temperature on the structure of Ca2+-alginate beads," *Biotechnology and Bioengineering,* vol. 79, no. 3, pp. 253-259, 2002/08/05 2002, doi: 10.1002/bit.10287.

[55] Y. Zhang, C. Wang, W. Jiang, W. Zuo, and G. Han, "Influence of Stage Cooling Method on Pore Architecture of Biomimetic Alginate Scaffolds," *Scientific Reports,* vol. 7, no. 1, p. 16150, 2017/11/23 2017, doi: 10.1038/s41598-017-16024-x.

[56] Y. Jiang, H. Hussain, and J. Kressler, "Poly(vinyl alcohol) Cryogel Formation Using Biocompatible Ice Nucleating Agents," *Macromolecular Materials and Engineering,* vol. 300, no. 2, pp. 181-190, 2015/02/01 2015, doi: 10.1002/mame.201400229.

[57] B. Wowk, "Thermodynamic aspects of vitrification," *Cryobiology,* vol. 60, no. 1, pp. 11-22, 2010/02/01/ 2010, doi: https://doi.org/10.1016/j.cryobiol.2009.05.007.

[58] P. Echlin, *Handbook of Sample Preparation for Scanning Electron Microscopy and X-Ray Microanalysis*, 1 ed. Springer US 2009, pp. XII, 332.

[59] J. L. Drury, R. G. Dennis, and D. J. Mooney, "The tensile properties of alginate hydrogels," *Biomaterials,* vol. 25, no. 16, pp. 3187-3199, 7// 2004, doi: http://dx.doi.org/10.1016/j.biomaterials.2003.10.002.

[60] E. A. Nunamaker, K. J. Otto, and D. R. Kipke, "Investigation of the material properties of alginate for the development of hydrogel repair of dura mater," *Journal of the Mechanical Behavior of Biomedical Materials,* vol. 4, no. 1, pp. 16-33, 2011/01/01/ 2011, doi: https://doi.org/10.1016/j.jmbbm.2010.08.006.

[61] H. J. Kong, E. Wong, and D. J. Mooney, "Independent Control of Rigidity and Toughness of Polymeric Hydrogels," *Macromolecules,* vol. 36, no. 12, pp. 4582-4588, 2003/06/01 2003, doi: 10.1021/ma034137w.

[62] B. E. Larsen, J. Bjørnstad, E. O. Pettersen, H. H. Tønnesen, and J. E. Melvik, "Rheological characterization of an injectable alginate gel system," (in eng), *BMC biotechnology,* vol. 15, pp. 29-29, 2015, doi: 10.1186/s12896-015-0147-7.

[63] R. C. Ball, M. Doi, S. F. Edwards, and M. Warner, "Elasticity of entangled networks," *Polymer,* vol. 22, no. 8, pp. 1010-1018, 1981/08/01/ 1981, doi: https://doi.org/10.1016/0032-3861(81)90284-6.

[64] C. Jeong, S. Kim, C. Lee, S. Cho, and S.-B. Kim, "Changes in the Physical Properties of Calcium Alginate Gel Beads Under a Wide Range of Gelation Temperature Conditions," (in eng), *Foods (Basel, Switzerland),* vol. 9, no. 2, p. 180, 2020, doi: 10.3390/foods9020180.

[65] X. Zhao, N. Huebsch, D. J. Mooney, and Z. Suo, "Stress-relaxation behavior in gels with ionic and covalent crosslinks," *Journal of Applied Physics,* vol. 107, no. 6, p. 063509, 2010/03/15 2010, doi: 10.1063/1.3343265.

[66] R. Bai, J. Yang, and Z. Suo, "Fatigue of hydrogels," *European Journal of Mechanics - A/Solids,* vol. 74, pp. 337-370, 2019/03/01/ 2019, doi: https://doi.org/10.1016/j.euromechsol.2018.12.001.

[67] K. Y. Lee, J. A. Rowley, P. Eiselt, E. M. Moy, K. H. Bouhadir, and D. J. Mooney, "Controlling Mechanical and Swelling Properties of Alginate Hydrogels Independently by Cross-Linker Type and Cross-Linking Density," *Macromolecules,* vol. 33, no. 11, pp. 4291-4294, 2000/05/01 2000, doi: 10.1021/ma9921347.

[68] H. W. Ooi, C. Mota, A. T. ten Cate, A. Calore, L. Moroni, and M. B. Baker, "Thiol–Ene Alginate Hydrogels as Versatile Bioinks for Bioprinting," *Biomacromolecules,*

vol. 19, no. 8, pp. 3390-3400, 2018/08/13 2018, doi: 10.1021/acs.biomac.8b00696.

[69] S. Zhao, M. Cao, H. Li, L. Li, and W. Xu, "Synthesis and characterization of thermo-sensitive semi-IPN hydrogels based on poly(ethylene glycol)-co-poly(epsilon-caprolactone) macromer, N-isopropylacrylamide, and sodium alginate," in *Carbohydr Res*, vol. 345, no. 3). Netherlands: 2009 Elsevier Ltd, 2010, pp. 425-31.

[70] M. A. LeRoux, F. Guilak, and L. A. Setton, "Compressive and shear properties of alginate gel: Effects of sodium ions and alginate concentration," *Journal of Biomedical Materials Research,* vol. 47, no. 1, pp. 46-53, 1999/10/01 1999, doi: 10.1002/(SICI)1097-4636(199910)47:1<46::AID-JBM6>3.0.CO;2-N.

[71] S. J. Kim, S. J. Park, and S. I. Kim, "Swelling behavior of interpenetrating polymer network hydrogels composed of poly(vinyl alcohol) and chitosan," *Reactive and Functional Polymers,* vol. 55, no. 1, pp. 53-59, 2003/02/01/ 2003, doi: https://doi.org/10.1016/S1381-5148(02)00214-6.

[72] E. S. Dragan and M. V. Dinu, "Advances in porous chitosan-based composite hydrogels: Synthesis and applications," *Reactive and Functional Polymers,* vol. 146, p. 104372, 2020/01/01/ 2020, doi: https://doi.org/10.1016/j.reactfunctpolym.2019.104372.

[73] D. Kim and K. Park, "Swelling and mechanical properties of superporous hydrogels of poly(acrylamide-co-acrylic acid)/polyethylenimine interpenetrating polymer networks," *Polymer,* vol. 45, no. 1, pp. 189-196, 2004/01/01/ 2004, doi: https://doi.org/10.1016/j.polymer.2003.10.047.

[74] W.-F. Lee and Y.-J. Chen, "Studies on preparation and swelling properties of the N-isopropylacrylamide/chitosan semi-IPN and IPN hydrogels," *Journal of Applied Polymer Science,* vol. 82, no. 10, pp. 2487-2496, 2001/12/05 2001, doi: 10.1002/app.2099.

[75] E. C. Muniz and G. Geuskens, "Compressive Elastic Modulus of Polyacrylamide Hydrogels and Semi-IPNs with Poly(N-isopropylacrylamide)," *Macromolecules,* vol. 34, no. 13, pp. 4480-4484, 2001/06/01 2001, doi: 10.1021/ma001192l.

[76] O. Jeon *et al.*, "Highly Elastic and Tough Interpenetrating Polymer Network-Structured Hybrid Hydrogels for Cyclic Mechanical Loading-Enhanced Tissue Engineering," *Chemistry of Materials,* vol. 29, no. 19, pp. 8425-8432, 2017/10/10 2017, doi: 10.1021/acs.chemmater.7b02995.

[77] Y. Qiu and K. Park, "Superporous IPN hydrogels having enhanced mechanical properties," *AAPS PharmSciTech,* vol. 4, no. 4, pp. 406-412, 2003/12/01 2003, doi: 10.1208/pt040451.

[78] C. E. Vorwald, K. C. Murphy, and J. K. Leach, "Restoring vasculogenic potential of endothelial cells from diabetic patients through spheroid formation," (in eng), *Cell Mol Bioeng,* vol. 11, no. 4, pp. 267-278, Aug 2018.

[79] K. T. Campbell, D. J. Hadley, D. L. Kukis, and E. A. Silva, "Alginate hydrogels allow for bioactive and sustained release of VEGF-C and VEGF-D for lymphangiogenic therapeutic applications," (in eng), *PloS one,* vol. 12, no. 7, pp. e0181484-e0181484, 2017, doi: 10.1371/journal.pone.0181484.

[80] M. C. Darnell *et al.*, "Performance and biocompatibility of extremely tough alginate/polyacrylamide hydrogels," (in eng), *Biomaterials,* vol. 34, no. 33, pp. 8042-8048, 2013, doi: 10.1016/j.biomaterials.2013.06.061.

[81] G. Fotakis and J. A. Timbrell, "In vitro cytotoxicity assays: comparison of LDH, neutral red, MTT and protein assay in hepatoma cell lines following exposure to cadmium chloride," *Toxicology letters,* vol. 160, no. 2, pp. 171-177, 2006.

[82] S. S. Ho, K. C. Murphy, B. Y. Binder, C. B. Vissers, and J. K. Leach, "Increased Survival and Function of Mesenchymal Stem Cell Spheroids Entrapped in Instructive Alginate Hydrogels," (in eng), *Stem Cells Transl Med,* vol. 5, no. 6, pp. 773-81, Jun 2016.

[83] C. E. Vorwald, S. S. Ho, J. Whitehead, and J. K. Leach, "High-Throughput Formation of Mesenchymal Stem Cell Spheroids and Entrapment in Alginate Hydrogels," in *Biomaterials for Tissue Engineering: Methods and Protocols*, K. Chawla Ed. New York, NY: Springer New York, 2018, pp. 139-149.

[84] M. M. Capeling *et al.*, "Nonadhesive Alginate Hydrogels Support Growth of Pluripotent Stem Cell-Derived Intestinal Organoids," *Stem Cell Reports,* vol. 12, no. 2, pp. 381-394, 2019/02/12/ 2019, doi: https://doi.org/10.1016/j.stemcr.2018.12.001.

[85] S. Balaiya, S. Grover, R. K. Murthy, and K. V. Chalam, "Freezing adversely affects measurement of vascular endothelial growth factor levels in human aqueous samples," (in eng), *Clinical ophthalmology (Auckland, N.Z.),* vol. 5, pp. 81-85, 2011, doi: 10.2147/OPTH.S15837.

[86] C. Saroja, P. Lakshmi, and S. Bhaskaran, "Recent trends in vaccine delivery systems: A review," (in eng), *International journal of pharmaceutical investigation,* vol. 1, no. 2, pp. 64-74, 2011, doi: 10.4103/2230-973X.82384.

[87] Y.-C. Lu *et al.*, "Scalable Production and Cryostorage of Organoids Using Core–Shell Decoupled Hydrogel Capsules," *Advanced Biosystems,* https://doi.org/10.1002/adbi.201700165 vol. 1, no. 12, p. 1700165, 2017/12/01 2017, doi: https://doi.org/10.1002/adbi.201700165.

[88] B. E. Christensen, "Alginates as biomaterials in tissue engineering," *Carbohydrate chemistry: chemical and biological approaches,* vol. 37, pp. 227-258, 2011.

[89] A. Patist and H. Zoerb, "Preservation mechanisms of trehalose in food and biosystems," *Colloids and Surfaces B: Biointerfaces,* vol. 40, no. 2, pp. 107-113, 2005/02/10/ 2005, doi: https://doi.org/10.1016/j.colsurfb.2004.05.003.

[90] C. M. Silva, A. J. Ribeiro, I. V. Figueiredo, A. R. Gonçalves, and F. Veiga, "Alginate microspheres prepared by internal gelation: Development and effect on insulin stability," *International Journal of Pharmaceutics,* vol. 311, no. 1, pp. 1-10, 2006/03/27/ 2006, doi: https://doi.org/10.1016/j.ijpharm.2005.10.050.

[91] M. C. Manning, K. Patel, and R. T. Borchardt, "Stability of Protein Pharmaceuticals," *Pharmaceutical Research,* vol. 6, no. 11, pp. 903-918, 1989/11/01 1989, doi: 10.1023/A:1015929109894.

[92] J. M. Anderson, "9.19 - Biocompatibility," in *Polymer Science: A Comprehensive Reference*, K. Matyjaszewski and M. Möller Eds. Amsterdam: Elsevier, 2012, pp. 363-383.

CHAPTER 5

Encapsulation of previously cryopreserved cells in alginate hydrogels via TIG and an alginate cryogel

5.1 Introduction

In the previous chapter, we discuss the formation of hydrogels formed by thaw-induced gelation (TIG) and its potential application as a carrier of protein therapeutic cargos that undergo frozen storage. We described the molecular structure of these hydrogels; however, utilizing TIG with cryopreserved cells necessitated the addition of a cryopreservation agent (CPA). Consequently, we expect the controlled slow freezing of cryopreservation to alter the molecular structure of the hydrogel, resulting in a different hydrogel than those described in the previous chapter. Interestingly, by incorporating one of the most widely used CPAs, dimethyl sulfoxide (Me_2SO), also abbreviated as DMSO, alginate hydrogels were formed without the calcium ionic cross-linker during TIG. Coincidently, this hydrogel could be considered an alginate cryogel formed.

The work in this brief chapter will mirror those in later chapters to address supply chain demands for future commercial cell therapy products. Some aspects of this supply chain are the mass production, transport, and storage of cellular products. Specifically, this work and those in later chapters will address the utility of cryopreservation for transporting and storing cells and potentially improving post-cryopreservation outcomes with instructive hydrogels. Critically, suboptimal freezing protocols can increase batch variability, reduce cell functionality and yield, and induce genetic drift [1]. For example, cryopreservation has repeatedly demonstrated negative consequences for MSC viability

and function [2, 3], diminished cadherin and integrin-binding efficacy [4], and remodeling of actin [5]. Despite this, over 80% of MSC clinical trial submissions were found to use cryopreservation as part of the manufacturing protocol [6]. Therefore, cryopreservation-induced changes to cell function should be addressed in research to prevent it from being a potential bottleneck during clinical trials.

One method to improve cellular outcomes from cryopreservation is using multiple cryoprotecting agents (CPAs) that enable different layers of protection of cells. For example, Me_2SO and alginate represent both intracellular and extracellular cryopreservation agents to protect against ice formation and osmotic shock [7]. Previous research has noted that the primary source of cell death after cryopreservation occurs via apoptosis [8-11]. Furthermore, this apoptosis can result from osmotic shock [12-15]. Therefore, this chapter explores the encapsulation of human embryonic kidney 293 cells (HEK-293) within alginate hydrogels in which alginate acts as a CPA. HEK-293 cells are an immortalized cell line of mesenchymal origin that can readily self-aggregate and form spheroids [16]. Here, we use this cell type with unmodified alginate to interrogate the effects of encapsulation via TIG and with the formation of a unique alginate cryogel.

As mentioned in previous chapters, TIG is a process that forms a hydrogel through ionic cross-linking that occurs when melting a frozen solution. Here, the frozen solution contains the alginate polymer, as well as HEK-293 cells and Me_2SO. When submerged in a calcium chloride bath, the frozen solution melts, calcium diffuses down the concentration gradient into the alginate polymer solution, and the alginate polymer is ionically cross-linked with calcium ions [17]. Alginate is a biocompatible polymer that

offers controllable mechanical properties, making it widely used in biomedical research and medicine [18]. Particularly important for the work presented in this chapter, alginate does not mediate cell attachment without chemical modifications [19-22]. Given the biocompatibility of alginate and its previous use as a cryoprotective agent [23-26], we hypothesized that HEK-293 cells could be encapsulated within alginate hydrogels while thawing from the cryopreserved state. HEK-293 cells were previously used in studies involving cryopreservation with alginate hydrogels [27, 28]. As part of this hypothesis, we expect the HEK-293 cells to grow within the alginate hydrogels as aggregates within the hydrogel. With this chapter, we start to lay the foundation of using post-cryopreservation gelation techniques to encapsulate cells using the methods described in chapters 3 and 4. The following chapters expand upon this work with cryopreservation with the alginate capsules described in chapter 3, pivoting away from a cryopreservation solution containing alginate.

5.2 Materials and methods

5.2.1 Cell culture and cryopreservation

Human embryonic kidney (HEK-293; ATCC) cells were cultured in Dulbecco's modified Eagle's medium (DMEM; Invitrogen) supplemented with 10% fetal bovine serum (FBS; Invitrogen) and 1% penicillin-streptomycin (Invitrogen) to form our complete media (DMEMc) as previously described [29]. Cells were cultured in tissue culture plates (12-well; Falcon) at 37 °C and under 5% CO_2. The cryopreservation of cells was performed using freezing solutions containing 10% (v/v) Me_2SO (also known as DMSO), 20% (v/v) FBS, and the complete media. With the addition of hydrogel formation, the freezing solutions also contained dissolved alginate polymer. All samples were frozen within a custom cryopreservation vessel made of Styrofoam. The Styrofoam vessel was first pre-chilled in a 4 °C refrigerator along with the cryopreservation solution. Cells were quickly added to the cryopreservation solution and placed in molds of approximately 100 µL to avoid prolonged exposure to the CPA and room temperatures. Next, the molds were placed in the vessel and moved to a -80 °C, where the cells underwent cryopreservation. Frozen disks were submerged in thawing solutions depending on whether the sample underwent TIG or not, breaking the cells out of cryopreservation. The temperatures of the thawing solutions were 4 or 36 °C to interrogate the impact of thawing rate on cell survival post-cryopreservation.

5.2.2 Hydrogel formation

The LF10/60 alginate polymer (molecular weight ~ 50 kDa and > 60% G-block) used in this study was purchased from FMC Biopolymers. Alginate was dissolved in

DMEMc used for culturing the HEK-293 cells. Alginate was prepared at 1% directly with the other components of the cryopreservation solution. Calcium chloride (Sigma) was the divalent cation source for cross-linking alginate, prepared at 100 mM with a pH of 7. The formation of alginate hydrogels via TIG parallels the process described for cryopreservation. As the cells are cryopreserved in the -80 °C freezer, the alginate solution transitions to a glassy solid, i.e., ice. The cryopreserved cells in the alginate-containing solution are submerged into a pre-warmed calcium chloride solution, starting TIG. During gelation, the 37 °C calcium chloride solution was periodically replaced to prevent cooling between samples. After gelation, samples were submerged in pre-warmed phosphate buffer solution (PBS) to remove excess calcium chloride from the hydrogel. Notably, the frozen solutions were moved directly from a -80 °C temperature to a thawing bath to induce rapid thawing. To help enable this process, dry ice near the biosafety cabinet kept samples at approximately -80 °C until the samples could be submerged and thawed.

5.2.3 Characterization of post-cryopreservation cell viability

100k HEK-293 cells were cryopreserved in 100 µL volumes within rubber wells. Rubber molds were the same as described in chapters 3 and 4. Conditions included cryopreservation solution without alginate, which was designated the control, and with alginate. A subset of alginate-containing samples also underwent TIG by submerging into a 100 mM $CaCl_2$ as described previously. Additionally, different thawing temperatures were utilized to challenge post-cryopreservation outcomes, 4 and 36 °C.

After 18 hours post-seeding, media was changed to remove residual cryopreservation agent solution.

Post-cryopreserved cells were imaged within the alginate hydrogels three days post-cryopreservation using phase-contrast microscopy (Zeiss Axio Vert A.4). HEK-293T cells that express GFP were used to visualize their position within the hydrogel better. Additionally, the metabolic activity within the ionically cross-linked alginate hydrogels or cell culture wells was measured via MTT (3-(4,5-dimethylthiazol-2-yl)-2,5-diphenyltetrazolium bromide) tetrazolium reduction assay (MTT assay) three days post-cryopreservation, with some modifications. Briefly, 25 µL of 5 mg/mL tetrazolium dye MTT was added for an approximate 0.5 mg/mL concentration per well. Cells were incubated for three hours within the hydrogel. Next, the media was replaced with isopropanol, and the hydrogels were mechanically destroyed within the wells. The plates were then agitated on a shaker for 15 minutes. The absorbance of the solubilized formazan was measured at 570 nm via the Spectramax ® i3 plate reader (Molecular Devices) and averaged per condition.

5.2.4 Statistical analysis

Results in this chapter are shown as mean values with standard deviations. Sample sizes are provided with each experiment and shown in figures as individual data points where applicable and listed in the figure legends. Statistical significance was asserted at $p < 0.05$ after performing a two-way ANOVA and Tukey's multiple comparison test. All analyses were performed using Graph-Pad Prism software (GraphPad Software Inc.) and JMP software (SAS Institute).

5.3 Results

5.3.1 Post-cryopreservation cell expansion in alginate hydrogels

This chapter briefly expands on the work in chapter 4 with the incorporation of cryopreserved cells. Specifically, cryopreservation agents were required to ensure the viability of the HEK-293 cells post-cryopreservation. Me_2SO was used as an intracellular cryopreservation agent. Additionally, alginate was utilized as an extracellular cryopreservation agent that is cross-linked when thawing the cryopreserved cells with TIG. One of the groups we included was a subset of cryopreserved cell samples in alginate that did not undergo TIG. To our surprise, this condition led to alginate that formed a hydrogel without the divalent cation, calcium. After three days, the cells within this hydrogel formed more prominent and numerous aggregates than the TIG hydrogel (Figure 5.1). Overall, all cells proliferated post-cryopreservation, with those in alginate forming small aggregates, like spheroids, within the hydrogels.

5.3.2 MTT assay of post-cryopreserved HEK-293 cells in TIG hydrogels

Three days after thawing the cryopreserved HEK-293 cells, an MTT assay was performed to visualize the location of cells within the tissue culture plates and quantify metabolic activity. From these images, purple formazan salt indicates that the control group successfully permitted the growth of cells on the bottom of the treated tissue culture plate (Figure 5.2A). Alternatively, both conditions with alginate have the dark purple localized to an area approximately the same size as the starting frozen disk of

the cryopreservation solution. Roughly, the hydrogels that underwent TIG were trended to be slightly smaller than those that did not experience ionic cross-linking. Notably, few cells escaped the hydrogels as the purple color is primarily within the hydrogels. After imaging, the formazan salt was solubilized, and absorbance was quantified for the control and TIG hydrogel samples thawed under 4 or 36 °C temperatures.

Interestingly, while thawing in a 4 °C bath led to significantly greater metabolic activity in the control group than the TIG hydrogel (alginate + Ca^{2+}), this temperature also had significantly greater metabolic activity than thawing at 36 °C (Figure 5.2B). In contrast, a thawing temperature of 36 °C led to a slight, non-significant, increase in metabolic activity for TIG hydrogels compared to 4 °C. Similarly, but not significantly, these TIG hydrogels formed at 36 °C appeared to have a slightly more metabolic activity than the control group. Together, the data indicate the formation of an unexpected hydrogel that could be better for post-cryopreserved cells than the ionically cross-crosslinked hydrogel. Moreover, the data suggest the hydrogel could be slightly advantageous for rapidly thawed cryopreserved cells.

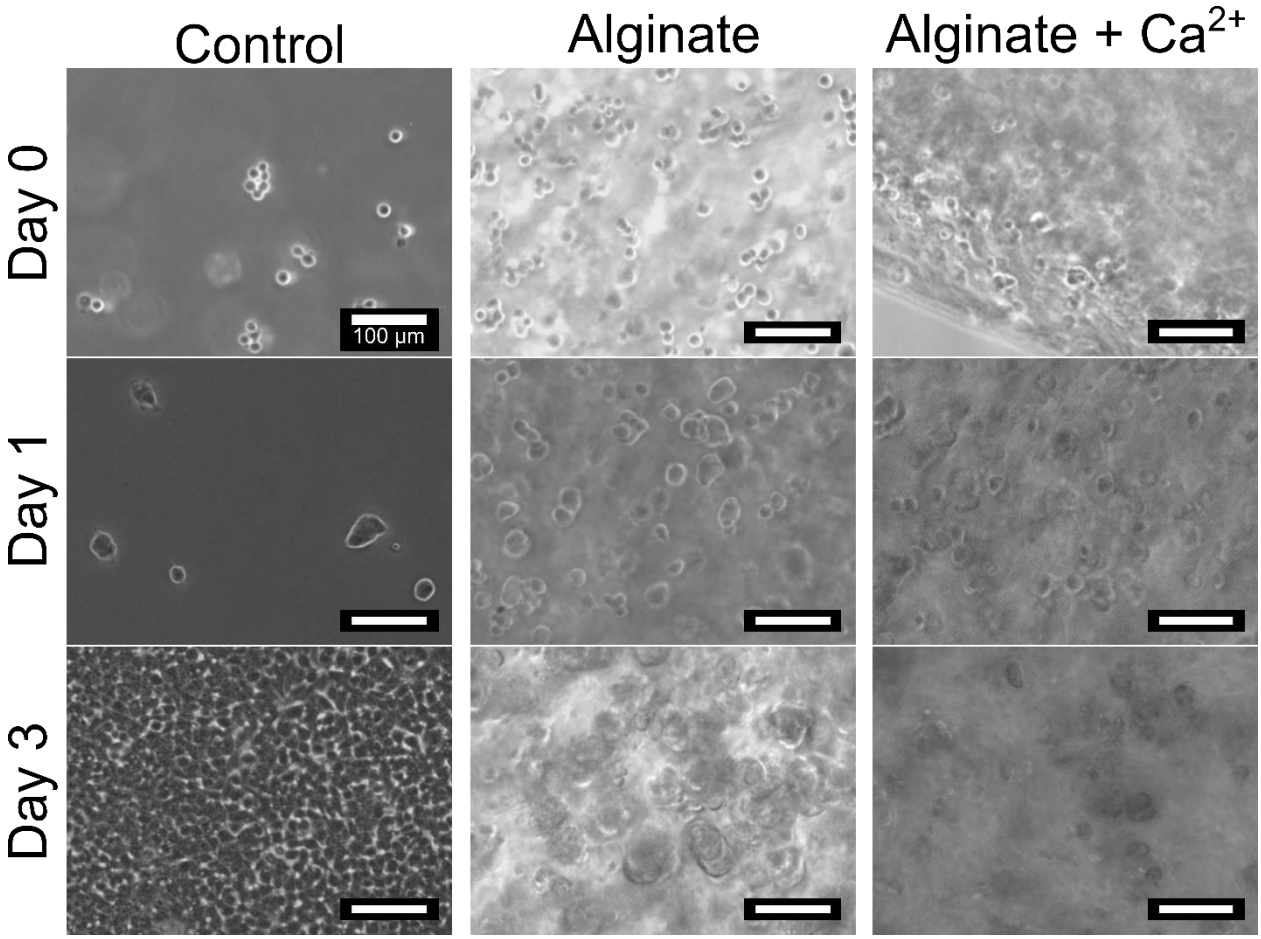

Figure 5.1 HEK-293 cells proliferate post-cryopreserved. Previously frozen cells were plated in 12-well plates and imaged over three days to observe proliferation on the tissue culture wells as well as in ionically cross-linked alginate hydrogels. Interestingly, the non-cross-linked alginate did not redissolve. Consequently, both alginate conditions resulted in small aggregates of HEK-293 cells by the third day. These aggregates appear larger and more numerous in the alginate condition without ionic cross-linking.

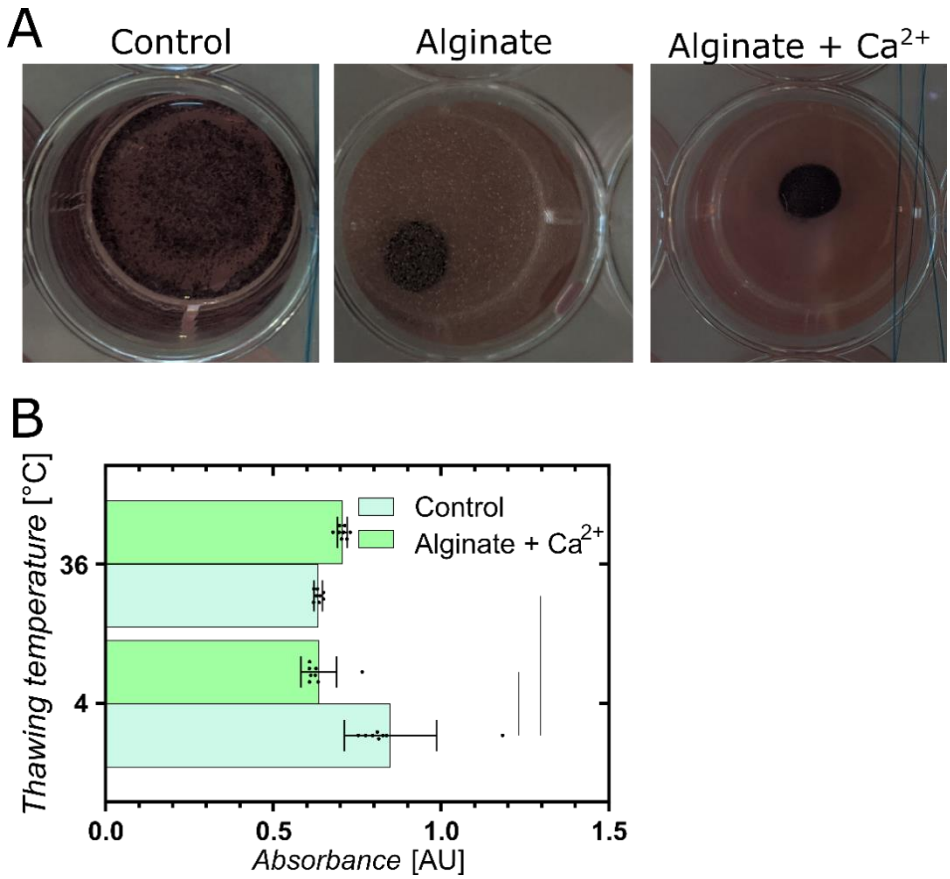

Figure 5.2 Cells are metabolic active within tissue culture wells 3-days post-cryopreservation. The thawing of cryopreserved cells occurred at 4 or 36 °C for the control group and ionically cross-linked hydrogel, but only 36 °C for the non-cross-linked alginate. Representative images of samples thawed at 36 °C after the addition of tetrazolium dye MTT indicated the location of cells via the production of purple formazan salts (A). Quantifying this MTT metabolite, there was significantly greater metabolic activity in the control group than ionically cross-linked alginate if thawed at 4 °C (B). In contrast, there was a non-significant trend of the ionically cross-linked alginate performing slightly better than the control. The bar represents mean, scatter dot plots display individual measurements, and error bars represent standard deviation (n = 8). A line between groups represents statistically significant differences ($P < 0.05$).

5.4 Discussion

5.4.1 Encapsulation of post-cryopreserved cells in an alginate hydrogel

The results in this chapter demonstrate the viability of post-cryopreserved cells encapsulated within alginate hydrogels formed by TIG. Concerning our hypothesis, the resulting hydrogel did encapsulate viable cells capable of proliferating within the hydrogel. Notably, the cells within the hydrogels formed aggregates, an expected observation considering that alginate does not support cell attachment without chemical modifications to the alginate polymer or the incorporation of other polymers [19-22]. While these results parallel those observed in previous research with alginate hydrogels and cryopreserved cells [23, 27, 28, 30-34], the overwhelming majority of these studies use alginate hydrogels that are already cross-crosslinked. Here, our results suggest that the ionic cross-linking of alginate might spatially hinder the proliferation of cells. Nevertheless, freezing an ionically cross-linked hydrogel could result in permeant cryostructuring that creates larger pores for cell proliferation [31]. Consequently, the previous studies using ionically cross-linked alginate hydrogels often reference the formation of a sponge or cryogel with large pores [35, 36]. In contrast to these studies that might seed cells onto the scaffold after forming the sponge or cryogel, the methods described here resulted in two different hydrogels where cells were distributed throughout. Fundamentally, this work promotes the additional utility of the hydrogels described in chapter 4, indicating TIG can be performed with cryopreserved cells. Specifically, this work suggests alginate hydrogels are biocompatible, supporting a specific response from the cells to aggregate and proliferate post-cryopreservation

within the hydrogel. Moreover, the work presented in this chapter also describes an additional hydrogel not formed by TIG but due to freezing and thawing.

5.4.2 The formation of a unique alginate cryogel

As previously mentioned, most studies using alginate with cryopreserved cells do by forming an alginate hydrogel, cryopreserving the encapsulated cells. Although there are some studies where alginate is only used as a cryoprotective agent, one publication appears to create a hydrogel post-cryopreservation by submerging a mold containing frozen cells and alginate in a solution containing calcium [30]. Notably, the alginate polymer was immersed in the calcium solution to cross-link for an hour, making the process similar to TIG, except the samples were within molds during gelation. Given the concentrations of calcium used and the timeframe of exposure, it should be expected that calcium could detrimentally affect cell viability [19], especially for post-cryopreserved cells [10, 11, 37]. Interestingly, despite having similar starting ingredients, this study did not describe the formation of an alginate hydrogel without calcium ions.

Notably, another study was able to form an alginate hydrogel without calcium ions and use Me_2SO [38]. Although this work was performed at room temperature and gelation was not as rapid as TIG, the group generated 2% (w/v) alginate hydrogels with similar elasticity and stiffness as those cross-linked with 100 mM $CaCl_2$. Their computational models show that Me_2SO cannot compensate for the repulsive forces between carboxylate groups of the alginate polymer; but rather, Me_2SO could stabilize the alginate networks through hydrogen bonding [38]. However, to accomplish gelation under these conditions, a 1% (w/v) alginate solution required a 50% (v/v) Me_2SO

concentration, an unfeasible concentration to use for the slow cooling cryopreservation techniques. Given the concerns of Me_2SO toxicity, a significant effort would need to be taken to ensure the intracellular cryopreservation agent is wholly removed [39].

In the context of the hydrogel formed here, the freezing results conditions that can improve the ability of Me_2SO to stabilize alginate polymers through hydrogen bonding. Mainly, the formation of a hydrogel during freezing through the stabilization of hydrogen bonds is the standard mechanism for forming cryogels with polyvinyl alcohol (PVA) solution [40-42]. Unlike PVA, the carboxylate groups of the alginate polymer prevent hydrogen bond stabilization alone [38]. However, with Me_2SO, freezing can similarly stabilize the hydrogen bonding of alginate polymers within the unfrozen regions during cryopreservation. Therefore, the hydrogel we describe here during the cryopreservation of HEK-293 cells in a cryopreservation solution containing alginate polymer would be classified as a cryogel. Strikingly, this appears to be the first description of alginate cryogel stabilized with Me_2SO without additional polymers or cross-linking with a divalent cation [31, 43, 44]. Together, these data presented in this chapter support that the hydrogel formed after freezing 1% (w/v) alginate solution with 10% (v/v) Me_2SO led to the formation of cryogels that can encapsulate post-cryopreserved cells and maintain their viability in culture. Combined with the work described in chapter 4, the TIG process could be cryoprotective for both cells and growth factors. Consequently, this process designed for cryopreservation can combine three aspects of tissue engineering: cells, signaling molecules, and material.

5.5 Conclusion

This chapter describes cryopreserved HEK-293 cells encapsulated within alginate hydrogels formed via TIG. Although the hydrogel formed via TIG was able to maintain cell viability and proliferation post-cryopreservation, the cells appear to perform better in the hydrogel we believe is an alginate cryogel. Consequently, this outcome raises essential questions regarding the properties of this potential alginate cryogel. Specifically, if Me_2SO and cryopreservation are fundamental for the hydrogel formation, is the Me_2SO retained within the hydrogel after thawing? Regardless of the potential construction of a cryogel, if it results in sequestered Me_2SO, this will also occur in the samples undergoing TIG. Future work in this area should address how Me_2SO is removed from the hydrogels and perform additional testing to determine how the polymer alters apoptosis post-cryopreservation. In future chapters, the use of TIG will be exclusively tested in the context of freezing the cryopreserved cells with the divalent cation cross-linker of alginate, calcium, which forms an alginate-hydrogel capsule. These liquid-core capsules can encapsulate cells that can form larger spheroids.

5.6 References

[1] C. J. Hunt, "Technical Considerations in the Freezing, Low-Temperature Storage and Thawing of Stem Cells for Cellular Therapies," *Transfusion Medicine and Hemotherapy,* vol. 46, no. 3, pp. 134-150, 2019, doi: 10.1159/000497289.

[2] S. Renzi, T. Lombardo, S. Dotti, S. S. Dessì, P. De Blasio, and M. Ferrari, "Mesenchymal stromal cell cryopreservation," (in eng), *Biopreserv Biobank,* vol. 10, no. 3, pp. 276-81, Jun 2012, doi: 10.1089/bio.2012.0005.

[3] D. Freimark *et al.*, "Systematic parameter optimization of a Me(2)SO- and serum-free cryopreservation protocol for human mesenchymal stem cells," in *Cryobiology*, vol. 63, no. 2). Netherlands: © 2011 Elsevier Inc, 2011, pp. 67-75.

[4] R. Chinnadurai *et al.*, "Actin cytoskeletal disruption following cryopreservation alters the biodistribution of human mesenchymal stromal cells in vivo," (in eng), *Stem Cell Reports,* vol. 3, no. 1, pp. 60-72, Jul 8 2014.

[5] S. B. Rizoli, O. D. Rotstein, J. Parodo, M. J. Phillips, and A. Kapus, "Hypertonic inhibition of exocytosis in neutrophils: central role for osmotic actin skeleton remodeling," (in eng), *Am J Physiol Cell Physiol,* vol. 279, no. 3, pp. C619-33, Sep 2000, doi: 10.1152/ajpcell.2000.279.3.C619.

[6] M. Mendicino, A. M. Bailey, K. Wonnacott, R. K. Puri, and S. R. Bauer, "MSC-based product characterization for clinical trials: an FDA perspective," in *Cell Stem Cell*, vol. 14, no. 2). United States: © 2014 Elsevier Inc, 2014, pp. 141-5.

[7] R. L. Levin and T. W. Miller, "An optimum method for the introduction or removal of permeable cryoprotectants: Isolated cells," *Cryobiology,* vol. 18, no. 1, pp. 32-48, 1981/02/01/ 1981, doi: https://doi.org/10.1016/0011-2240(81)90004-3.

[8] B. C. Heng *et al.*, "Loss of viability during freeze-thaw of intact and adherent human embryonic stem cells with conventional slow-cooling protocols is predominantly due to apoptosis rather than cellular necrosis," (in eng), *J Biomed Sci,* vol. 13, no. 3, pp. 433-45, May 2006, doi: 10.1007/s11373-005-9051-9.

[9] R. Martin-Ibañez, C. Unger, A. Strömberg, D. Baker, J. M. Canals, and O. Hovatta, "Novel cryopreservation method for dissociated human embryonic stem cells in the presence of a ROCK inhibitor," in *Hum Reprod*, vol. 23, no. 12). England, 2008, pp. 2744-54.

[10] M. A. Savitskaya and G. E. Onishchenko, "Apoptosis in cryopreserved eukaryotic cells," *Biochemistry (Moscow),* vol. 81, no. 5, pp. 445-452, 2016/05/01 2016, doi: 10.1134/S0006297916050023.

[11] X. Xu, S. Cowley, C. J. Flaim, W. James, L. Seymour, and Z. Cui, "The roles of apoptotic pathways in the low recovery rate after cryopreservation of dissociated human embryonic stem cells," (in eng), *Biotechnology progress,* vol. 26, no. 3, pp. 827-837, May-Jun 2010, doi: 10.1002/btpr.368.

[12] E. Casula, G. P. Asuni, V. Sogos, S. Fadda, F. Delogu, and A. Cincotti, "Osmotic behaviour of human mesenchymal stem cells: Implications for cryopreservation," *PLOS ONE,* vol. 12, no. 9, p. e0184180, 2017, doi: 10.1371/journal.pone.0184180.

[13] D. Gao and J. K. Critser, "Mechanisms of Cryoinjury in Living Cells," *ILAR Journal,* vol. 41, no. 4, pp. 187-196, 2000, doi: 10.1093/ilar.41.4.187.

[14] K. Muldrew and L. E. McGann, "The osmotic rupture hypothesis of intracellular freezing injury," *Biophysical Journal,* vol. 66, no. 2, Part 1, pp. 532-541, 1994/02/01/ 1994, doi: https://doi.org/10.1016/S0006-3495(94)80806-9.

[15] X. Xu, Y. Liu, Z. Cui, Y. Wei, and L. Zhang, "Effects of osmotic and cold shock on adherent human mesenchymal stem cells during cryopreservation," in *J Biotechnol*, vol. 162, no. 2-3). Netherlands: © 2012 Elsevier B.V, 2012, pp. 224-31.

[16] A. Blumlein, N. Williams, and J. J. McManus, "The mechanical properties of individual cell spheroids," *Scientific Reports,* vol. 7, no. 1, p. 7346, 2017/08/04 2017, doi: 10.1038/s41598-017-07813-5.

[17] D. J. Hadley and E. A. Silva, "Thaw-Induced Gelation of Alginate Hydrogels for Versatile Delivery of Therapeutics," *Annals of Biomedical Engineering,* vol. 47, no. 8, pp. 1701-1710, 2019/08/01 2019, doi: 10.1007/s10439-019-02282-5.

[18] K. Y. Lee and D. J. Mooney, "Alginate: properties and biomedical applications," (in eng), *Progress in polymer science,* vol. 37, no. 1, pp. 106-126, 2012, doi: 10.1016/j.progpolymsci.2011.06.003.

[19] S. S. Ho, K. C. Murphy, B. Y. Binder, C. B. Vissers, and J. K. Leach, "Increased Survival and Function of Mesenchymal Stem Cell Spheroids Entrapped in Instructive Alginate Hydrogels," (in eng), *Stem Cells Transl Med,* vol. 5, no. 6, pp. 773-81, Jun 2016.

[20] K. T. Campbell, R. S. Stilhano, and E. A. Silva, "Enzymatically degradable alginate hydrogel systems to deliver endothelial progenitor cells for potential

revasculature applications," (in eng), *Biomaterials,* vol. 179, pp. 109-121, 2018, doi: 10.1016/j.biomaterials.2018.06.038.

[21] M. M. Capeling *et al.*, "Nonadhesive Alginate Hydrogels Support Growth of Pluripotent Stem Cell-Derived Intestinal Organoids," *Stem Cell Reports,* vol. 12, no. 2, pp. 381-394, 2019/02/12/ 2019, doi: https://doi.org/10.1016/j.stemcr.2018.12.001.

[22] C. E. Vorwald, S. S. Ho, J. Whitehead, and J. K. Leach, "High-Throughput Formation of Mesenchymal Stem Cell Spheroids and Entrapment in Alginate Hydrogels," in *Biomaterials for Tissue Engineering: Methods and Protocols*, K. Chawla Ed. New York, NY: Springer New York, 2018, pp. 139-149.

[23] A. Camboni, A. Van Langendonckt, J. Donnez, J. Vanacker, M. M. Dolmans, and C. A. Amorim, "Alginate beads as a tool to handle, cryopreserve and culture isolated human primordial/primary follicles," in *Cryobiology*, vol. 67, no. 1). Netherlands: © 2013 Elsevier Inc, 2013, pp. 64-9.

[24] A. Herrler, S. Eisner, V. Bach, U. Weissenborn, and H. M. Beier, "Cryopreservation of spermatozoa in alginic acid capsules," *Fertility and Sterility,* vol. 85, no. 1, pp. 208-213, 2006/01/01/ 2006, doi: https://doi.org/10.1016/j.fertnstert.2005.06.049.

[25] X. Xiang, Z. Liu, and G. Zhao, "Sodium Alginate as a Novel Cryoprotective Agent for Cryopreservation of Endothelial Cells in a Closed Polytetrafluoroethylene Loop," *Biopreservation and Biobanking,* vol. 18, no. 4, pp. 321-328, 2020/08/01 2020, doi: 10.1089/bio.2020.0020.

[26] B. D. Giulio *et al.*, "Use of alginate and cryo-protective sugars to improve the viability of lactic acid bacteria after freezing and freeze-drying."

[27] V. Stensvaag, T. Furmanek, K. Lønning, A. J. Terzis, R. Bjerkvig, and T. Visted, "Cryopreservation of alginate-encapsulated recombinant cells for antiangiogenic therapy," (in eng), *Cell Transplant,* vol. 13, no. 1, pp. 35-44, 2004, doi: 10.3727/000000004772664879.

[28] H. Gurruchaga *et al.*, "Advances in the slow freezing cryopreservation of microencapsulated cells," *Journal of Controlled Release,* vol. 281, pp. 119-138, 2018/07/10/ 2018, doi: https://doi.org/10.1016/j.jconrel.2018.05.016.

[29] J. L. Madrigal, S. N. Sharma, K. T. Campbell, R. S. Stilhano, R. Gijsbers, and E. A. Silva, "Microgels produced using microfluidic on-chip polymer blending for controlled released of VEGF encoding lentivectors," (in eng), *Acta biomaterialia,* vol. 69, pp. 265-276, 2018/03// 2018, doi: 10.1016/j.actbio.2018.01.013.

[30] R. Chen, B. Wang, Y. Liu, R. Lin, J. He, and D. Li, "A study of cryogenic tissue-engineered liver slices in calcium alginate gel for drug testing," in *Cryobiology*, vol. 82. Netherlands: © 2018 Elsevier Inc, 2018, pp. 1-7.

[31] A. Katsen-Globa *et al.*, "Towards ready-to-use 3-D scaffolds for regenerative medicine: adhesion-based cryopreservation of human mesenchymal stem cells attached and spread within alginate-gelatin cryogel scaffolds," (in eng), *Journal of materials science. Materials in medicine,* vol. 25, no. 3, pp. 857-871, 2014, doi: 10.1007/s10856-013-5108-x.

[32] R. Malpique *et al.*, "Alginate Encapsulation as a Novel Strategy for the Cryopreservation of Neurospheres," *Tissue Engineering Part C: Methods,* vol. 16, no. 5, pp. 965-977, 2010/10/01 2009, doi: 10.1089/ten.tec.2009.0660.

[33] H. Huang *et al.*, "Alginate Hydrogel Microencapsulation Inhibits Devitrification and Enables Large-Volume Low-CPA Cell Vitrification," *Advanced Functional Materials,* https://doi.org/10.1002/adfm.201503047 vol. 25, no. 44, pp. 6839-6850, 2015/11/01 2015, doi: https://doi.org/10.1002/adfm.201503047.

[34] G. Bhakta *et al.*, "Cryopreservation of alginate-fibrin beads involving bone marrow derived mesenchymal stromal cells by vitrification," in *Biomaterials*, vol. 30, no. 3). Netherlands, 2009, pp. 336-43.

[35] J. Zhang *et al.*, "Cells behave distinctly within sponges and hydrogels due to differences of internal structure," (in eng), *Tissue engineering. Part A,* vol. 19, no. 19-20, pp. 2166-2175, 2013, doi: 10.1089/ten.TEA.2012.0393.

[36] P. Gurikov and I. Smirnova, "Non-Conventional Methods for Gelation of Alginate," *Gels,* vol. 4, no. 1, 2018, doi: 10.3390/gels4010014.

[37] A. Bissoyi, B. Nayak, K. Pramanik, and S. K. Sarangi, "Targeting cryopreservation-induced cell death: a review," (in eng), *Biopreserv Biobank,* vol. 12, no. 1, pp. 23-34, Feb 2014, doi: 10.1089/bio.2013.0032.

[38] M. M. Pérez-Madrigal, J. Torras, J. Casanovas, M. Häring, C. Alemán, and D. D. Díaz, "Paradigm Shift for Preparing Versatile M2+-Free Gels from Unmodified Sodium Alginate," *Biomacromolecules,* vol. 18, no. 9, pp. 2967-2979, 2017/09/11 2017, doi: 10.1021/acs.biomac.7b00934.

[39] F. C. Tan *et al.*, "Optimization of cryopreservation of stem cells cultured as neurospheres: comparison between vitrification, slow-cooling and rapid cooling freezing protocols," (in eng), *Cryo Letters,* vol. 28, no. 6, pp. 445-60, Nov-Dec 2007.

[40] V. Pazos, R. Mongrain, and J. C. Tardif, "Polyvinyl alcohol cryogel: Optimizing the parameters of cryogenic treatment using hyperelastic models," *Journal of the Mechanical Behavior of Biomedical Materials,* vol. 2, no. 5, pp. 542-549, 2009/10/01/ 2009, doi: https://doi.org/10.1016/j.jmbbm.2009.01.003.

[41] V. I. Lozinsky, "Cryotropic gelation of poly(vinyl alcohol) solutions," *Russian Chemical Reviews,* 10.1070/RC1998v067n07ABEH000399 vol. 67, no. 7, pp. 573-586, 1998, doi: 10.1070/RC1998v067n07ABEH000399.

[42] C. M. Hassan and N. A. Peppas, "Structure and Applications of Poly(vinyl alcohol) Hydrogels Produced by Conventional Crosslinking or by Freezing/Thawing Methods," in *Biopolymers · PVA Hydrogels, Anionic Polymerisation Nanocomposites*. Berlin, Heidelberg: Springer Berlin Heidelberg, 2000, pp. 37-65.

[43] X. Li *et al.*, "Strong, tough and mechanically self-recoverable poly(vinyl alcohol)/alginate dual-physical double-network hydrogels with large cross-link density contrast," *RSC Advances,* 10.1039/C8RA01302K vol. 8, no. 30, pp. 16674-16689, 2018, doi: 10.1039/C8RA01302K.

[44] L. Shan *et al.*, "Fabrication and Use of Alginate-Based Cryogel Delivery Beads Loaded with Urea and Phosphates as Potential Carriers for Bioremediation,"

Industrial & Engineering Chemistry Research, vol. 55, no. 28, pp. 7655-7660, 2016/07/20 2016, doi: 10.1021/acs.iecr.6b01256.

CHAPTER 6

Encapsulation of post-cryopreserved cells within alginate hydrogel capsules promotes the rapid formation of spheroids

6.1 Introduction

Chapter 5 described work with encapsulating cryopreserved HEK-293 cells. In parallel with this work, the alternative pathway of thaw-induced gelation (TIG) was performed to encapsulate cryopreserved cells within the liquid core of alginate hydrogel capsules. Inherent in how the components are prepared, the formation of capsules is fundamentally different from the TIG hydrogels presented in chapters 4 and 5. In contrast to submerging a frozen alginate solution in a calcium chloride bath to induce melting and cross-linking, capsules are formed by immersing a frozen calcium chloride solution into an alginate polymer-containing bath. This distinction is critical as calcium diffusion is away from the initial source, down the concentration gradient. This diffusion leads to rapid dilution of the cross-linker, as well as other elements that were in the frozen solution. This chapter will highlight that the alginate capsule gelation can be accomplished when thawing cryopreserved cells, the properties of these capsules can be modulated, and these cells form viable spheroids. One important finding was how cell survival and aggregation depended on the local concentration of cells within the hydrogel capsules.

The future commercial demands of cellular therapy products are expected to require cryopreservation to meet the regulatory requirements within manufacturing and transportation to clinics. Optimizing cryopreservation for novel cell therapies has been

suggested to be as important as improving cell culture [1]. Suboptimal freezing protocols can increase batch variability, reduce cell functionality and yield, and induce genetic drift independent of the optimized culture condition post-cryopreservation [1]. For example, for clinical trials with mesenchymal stromal cells (MSCs), cryopreservation has been shown to negatively impact cell viability and function [2, 3], binding efficacy [4], and cytoskeletal remodeling [5]. Nevertheless, the majority of MSC clinical trial submissions do not incorporate cryopreservation protocol as part of the manufacturing plans (> 80%) [6]. To address this potential challenge towards the success of cell therapies, research into new manufacturing protocols should integrate the cryopreservation perspectives.

One method to improve cellular function is using 3D aggregates of cells, known as spheroids, which better recapitulate the native *in vivo* environment through cadherin- and integrin-binding. Notably, using spheroids and organoids has been of growing interest within cellular therapy research. However, there have been relatively few studies in this area with respect to cryopreservation (< 150 studies when using search terms "cryopreservation" and "spheroid" on pubmed.gov). Nevertheless, there has been a recent growth in the number of published studies utilizing spheroids to improve the viability and function of the post-cryopreservation cell within the last five years. One of the earlier studies (2015) suggested spheroids promoted anti-apoptotic behavior from post-thawed human adipose-derived stem cells [7]. Despite not stating their cryopreservation protocol, the results from this study with cryopreserved spheroids match previous studies where cell-cell interactions generally improved cellular function [8-10]. Fundamentally, as apoptosis is the main pathway of cell death from

cryopreservation [11-14], the use of aggregated cells appears promising for reducing apoptosis and enhancing cellular-functional recovery. However, we hypothesize that when and how spheroids are used with cryopreservation matters and can be cell-type dependent. Notably, spheroids limit the diffusion of the cryopreservation agent (CPA) during cryopreservation and thawing. Not only can this impact cell viability, but residual CPA has been shown to have clinically significant side effects [1, 3, 15-18]. Furthermore, this diffusion limitation can cause an osmotic shock by increased CPA exposure [19]. These are the common challenges noted in the literature as previous studies improve the cryopreservation of whole spheroids, cellular aggregates, and tissues. Here, we present an alternative to cryopreserving spheroids, forming cell aggregates from previously cryopreserved cells. Although the TIG method described can be used with cryopreserved spheroids, the encapsulation of cells within hydrogel capsules provides a unique opportunity to instruct spheroid formation in a permeable membrane.

Chapter 3 characterized a process that simultaneously generates an alginate permeable hydrogel capsule by submerging and melting a frozen calcium chloride solution in a liquid alginate solution (Figure 6.1A) [20]. Alginate, a biocompatible polymer with easily controllable physical and mechanical properties, is widely used in biomedical research and medicine [21]. The alginate polymer is permissive to ionic cross-linking with divalent cations, rapidly cross-linking into an insoluble hydrogel with a calcium chloride solution [21, 22]. One significant feature relevant to this chapter is that cells do not adhere to the hydrogels. Consequently, previous studies using alginate hydrogels to encapsulate cells often bioconjugate an RGD-peptide sequence to the

alginate polymer [23, 24]. However, with the application of TIG, these hydrogels encourage cell-cell interactions from the absence of cell-environment binding sites [8, 23, 25, 26], potentially forming spheroids. Therefore, we hypothesize that spheroids can be formed from cryopreserved cells within these alginate capsules by utilizing a cellular freezing solution that contains calcium chloride (Figure 6.1B) without inducing significant cryopreservation-induced damage. To explore this hypothesis, we examine the ability of post-cryopreserved HEK-293 cells to aggregate. HEK-293 cells are a commonly utilized cell line for *in vitro* model systems because they are low maintenance, metabolically active, and rapidly dividing, previously used in studies involving spheroid mechanics, cryopreservation, and alginate hydrogels [27, 28]. First, the influence of the modified cryopreserving solution on hydrogel formation was characterized. Next, the effect of calcium on cell cryopreservation viability was interrogated. Lastly, hydrogel properties and cell concentration were optimized for spheroid formation. Together, the simultaneous thawing of cryopreserved cells while encapsulating within a permeable capsule represents a novel approach for potentially incorporating hydrogels with the cryopreservation of cell therapies.

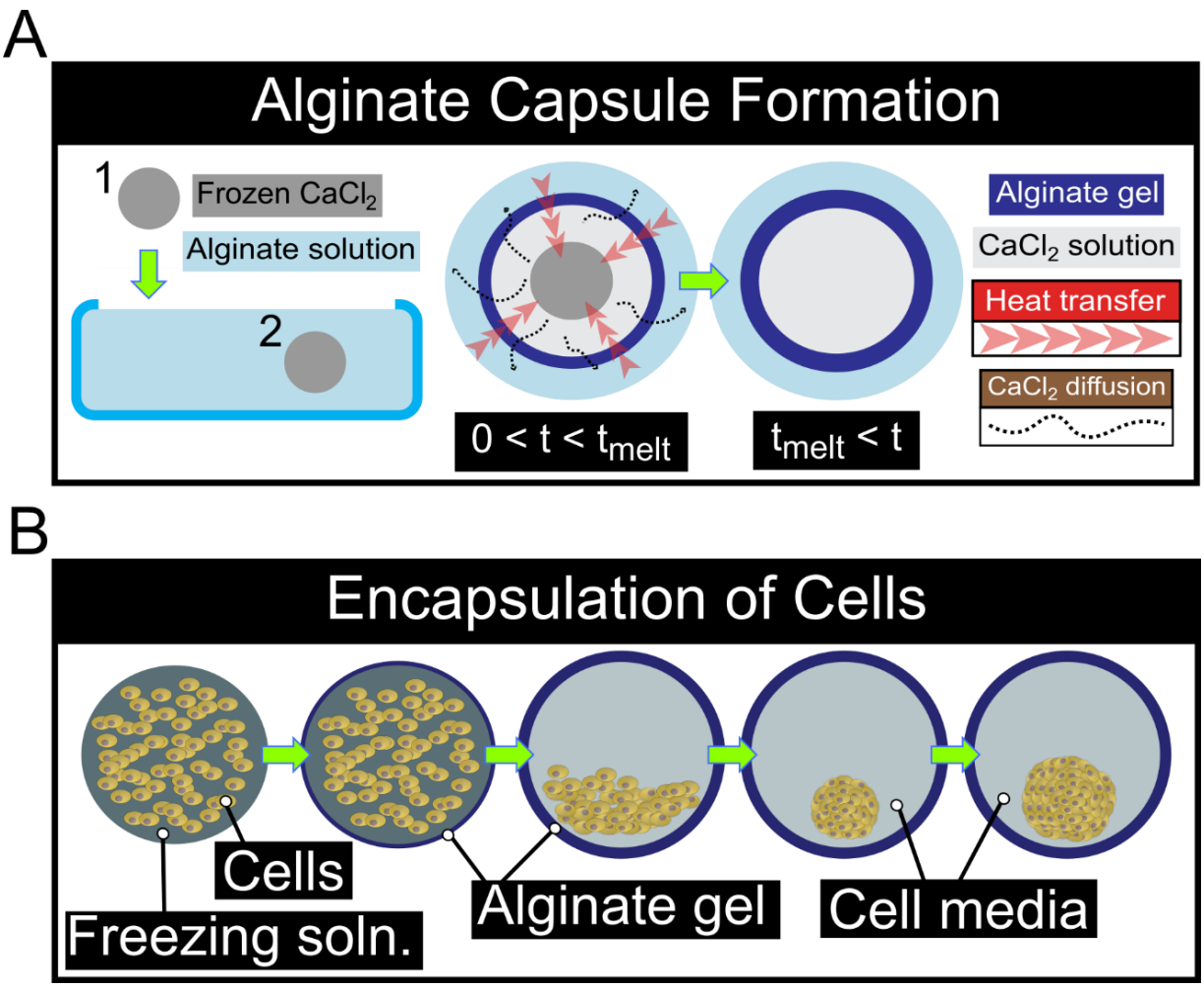

Figure 6.1 Alginate capsule formation via TIG. The gelation scheme to form alginate hydrogel capsules involves a frozen cross-linker solution thawed in a polymer-containing solution. Specifically, in this application, a frozen cryopreservation solution containing calcium chloride is submerged in a warmed alginate solution leading to heat to transfer into the frozen solution causing it to melt (A). In the liquid state, the calcium ions diffuse down the concentration gradient into the alginate solution. Consequently, ionic cross-linking occurs around the previously frozen solution to create a capsule. Notably, thawing a frozen solution containing cryopreserved cells would encapsulate them within the hydrogel capsule (B). Once the capsule forms, the contained cells can consolidate and preferentially aggregate together.

6.2 Materials and methods

6.2.1 Hydrogel capsule formation

LF10/60 alginate polymer (molecular weight ~ 120-150 kDa and >60% G-block; purchased from FMC Biopolymers) was used in this work. All alginate hydrogels were formed with purified and sterile filtered alginate polymer, prepared as previously described [23, 29]. Briefly, one gram of alginate was dissolved in 100 mL of deionized (DI) water. Next, 0.5 grams of activated charcoal (Sigma) was added and mixed for 30 minutes via a magnetic stirrer. Then, the alginate solution is sterile filtered (0.22 μm, Thermo Fisher Scientific), lyophilized, and stored in a freezer. A 2% (w/v) alginate solution was prepared by mixing the dry polymer in an isotonic saline solution (0.9% (w/v) NaCl). This alginate solution was then diluted to 0.5% and 1% (w/v) if needed. The standard-cryopreserving solution contains calcium chloride (Sigma), dimethyl sulfoxide (Me_2SO; Sigma), also commonly abbreviated as DMSO, fetal bovine serum (FBS; Invitrogen), and cell media (Dulbecco's Modified Eagle Medium (DMEM); Invitrogen). As the baseline, 10% (v/v) Me_2SO and 20% (v/v) FBS were added to DMEM to generate the cellular freezing solution recommended for human embryonic kidney (HEK-293) cells. In experiments, 5, 10, and 20% (v/v) Me_2SO and 0, 20, 40, and 80% (v/v) FBS were also used to interrogate cryopreservation agent (CPA) effects on hydrogel formation and cryopreservation of cells. Calcium chloride was added to the cellular freezing solution from a 6 M stock to create final concentrations ranging from 75 mM to 300 mM.

Gelation of the alginate hydrogel capsules was performed as previously described using TIG [20]. Briefly, the modified cryopreserving solution containing

calcium chloride, FBS, and Me_2SO was pipetted into wells formed from circular-cut rubber holes placed onto a glass plate. The rubber molds had holes with diameters 3, 6, and 8 mm, representing final freezing solution volumes of 10, 50, or 100 µL, respectively. The filled molds were then placed in a custom cryopreservation vessel made from Styrofoam and moved to a -80 ºC freezer overnight. A 37 ºC alginate solution in a wide-mouthed beaker was used to thaw the cryopreservation solution (> 50 mL). First, the rubber mold was removed from the glass backing using a sliding motion to ensure the frozen disks remained in the rubber mold. Then, the rubber mold was flexed over the alginate solution to release multiple frozen disks. Once in the alginate solution, ionic cross-linking of the hydrogel capsules begins. We briefly swirled the alginate-containing beaker with a circular motion by grasping the beaker or with a spatula to sink the frozen disk. If samples are not entirely submerged, the hydrogel will not be sealed and form a bowl structure. The solution is typically finished melting and cross-linking after two minutes. Completed melting can be visualized by increasing transparency throughout the sample. Successful encapsulation was judged on whether the samples remained intact when lifted with a spatula. The capsules were then scooped out of the beaker and placed in prewarmed media to remove uncross-linked alginate polymer from the outer surface and promote dilution of the cryopreservation agents. Notably, the thawing of multiple frozen samples will cool the alginate solution, primarily if small volumes (< 50 mL) were used. We reduced this change by placing the alginate-containing beaker in a larger container with warm water (> 200 mL; 37 °C).

6.2.2 Cell culture and cryopreservation

Human embryonic kidney (HEK-293; ATCC) cells were cultured in Dulbecco's modified Eagle's medium (DMEM; Invitrogen) supplemented with 10% fetal bovine serum (FBS; Invitrogen) and 1% penicillin-streptomycin (Invitrogen) to form our complete media (DMEMc) as previously described [30]. Cells were cultured in tissue culture plates at 37 °C and under 5% CO_2. The cryopreservation of cells was performed as described in the previous section and using a freezing solution containing only 10% (v/v) Me_2SO, 20% (v/v) FBS, and the complete media. For experiments without hydrogels, cells were frozen within cryopreservation vials placed into a Mr. Frosty™ (Thermo Fisher). These vials were filled with 500 µL at a concentration of 200,000 cells/mL.

6.2.3 Alginate hydrogel characterization

Alginate hydrogel capsules were characterized under varying concentrations of the polymer, cross-linker, FBS, and Me_2SO. First, the capsule shell thickness was measured from microscope images using ImageJ software (NIH). After being stored in saline for 24 hours, the hydrogels' storage moduli and swelling ratios were measured. Wet weights were obtained after draining the capsule's liquid core by slicing the capsules in half with a scalpel. Next, rheology was performed on a sectioned half of the hydrogel samples placed between parallel plates of an HR3 rheometer (TA instruments). The samples were strained from 0.5 - 5% at a frequency of 10 rad s^{-1}. A minimum of six points within the linear range was averaged to obtain the storage modulus, G'. Lastly, the hydrogel samples were lyophilized to acquire the dry weight. The volumetric swelling ratio was calculated using the following equation:

$$Q_V = \frac{\frac{W_S - W_D}{\rho_W} + \frac{W_D}{\rho_P}}{\frac{W_D}{\rho_P}},$$

where ρ_W is the density of water and ρ_P is the polymer density (Alginate: 1.6 g/mL, [31, 32]). W_S and W_D represent the hydrogel's swollen and dry weight, respectively.

Mesh size (ξ) was estimated for the anionic hydrogels by Flory–Rehner calculation using swelling ratio and storage modulus, as previously described [20, 23, 29, 30]:

$$\xi = Q^{\frac{1}{3}} l \left(\frac{2M_c}{M_r}\right)^{1/2} C_n^{1/2}.$$

Here, l is the length of the repeating unit, or Kuhn length (5.15 Å). M_r is the molecular weight of the repeating unit (194 g/mol). C_n is the characteristic ratio (21.1), which is a measure of chain stiffness. Q is the volumetric swelling ratio, which was defined in the previous section. M_C is the molecular weight between cross-links, which was determined via the following equation using the measurements of the shear storage modulus (G') and polymer concentration (C_P), the gas constant (R), and sample temperature (T):

$$M_C = \frac{C_P RT}{G'}.$$

Lastly, a solution containing 200 nmol of fluorescein isothiocyanate (FITC) and 100 mM calcium chloride solution, 10% Me_2SO, and 20% FBS was loaded into 50 µL molds. TIG was performed with a 1% (w/v) alginate polymer thawing bath, and after two minutes of gelation, samples were moved to the washing bath for 5 or 10 minutes. The timing of the gelation and removal from the washing bath was performed such that the release of FITC from hydrogel capsules into 1 mL saline solutions began at approximately the same time. The fluorescence of FITC in each well was measured via the Spectramax ® i3 plate reader (Molecular Devices) every five minutes for an hour. The saline solution

was replaced after each measurement. Together, these measurements provide details on the capsule size, stiffness, water content, and permeability.

6.2.4 Post-cryopreservation cell viability

After thawing cryopreserved cells, cell viability was determined with a trypan blue exclusion assay, and metabolic activity was evaluated via an MTT (3-(4,5-dimethylthiazol-2-yl)-2,5-diphenyltetrazolium bromide) tetrazolium reduction assay (MTT assay) three days post-cryopreservation. The effects of $CaCl_2$ and FBS on cell survival were interrogated by altering their concentration in the modified cryopreserving solution. Specifically, cell freezing solution groups included 0, 75, 100, 150, and 300 mM $CaCl_2$ with 20% (v/v) FBS. Additionally, groups with 100 mM $CaCl_2$ were made with varying FBS concentrations of 0, 20, and 80% (v/v). For both experiments, HEK-293 cells (200,000 cells/mL) were cryopreserved using cryopreservation vials within a Mr. Frosty™. Cells were thawed in a hot water bath at 37 °C and underwent a $1/10^{th}$ dilution once thawed by placing the cell-containing solution into cell media. For initial cell viability, cells were equilibrated for ten minutes at 37 °C before starting the trypan blue exclusion assay. Cell viability percentage was averaged per condition (n = 6) from measurements determined by a Countess automated cell counter (Life Technologies).

HEK-293 cells were seeded at 2,000 cells per well (20,000 cells/mL) in 96-well tissue culture plates for the metabolic activity assay. Before cell seeding, the number of viable cells post-cryopreservation was calculated via the Countess automated cell counter. Uncryopreserved cells were obtained from a confluent cell culture dish; the cells were detached with a 0.05% Trypsin-EDTA (Invitrogen) solution and seeded into

the 96-well tissue culture plates. After three days post-seeding, 10 µL of 5 mg/mL tetrazolium dye MTT (Sigma) was added to each well and incubated for three hours. The media was then aspirated away and replaced with100 µL of isopropanol (Sigma). Next, the plates were placed on a shaker for 15 minutes, protected from light by covering plates with aluminum foil. The total absorbance of formazan salt was quantified via the Spectramax ® i3 plate reader at 570 nm and averaged per condition (n = 8). From these values, a percentage of reduced metabolic activity from cryopreserved cells was calculated. Specifically, the absorbance from the unfrozen groups was subtracted from the cryopreserved group. This value was divided by the absorbance of the uncryopreserved control group. Succinctly,

$$Absorbance\ Reduction\ (\%) = \frac{Uncryopreserved\ Group - Cryopreserveed\ Group}{Uncryopreserved\ Group} * 100\% \ .$$

6.2.5 Spheroid characterization

The characterization of spheroid formation within alginate capsules was performed under various conditions, including different alginate polymer concentrations, calcium chloride concentrations, capsule volumes, and cell concentrations. Specifically, the effect of alginate concentration on spheroid formation was assessed with 0.5, 1, and 2% (w/v) alginate polymer solutions. Second, calcium chloride concentrations of 75, 100, and 150 mM were used to examine its effect on cryopreservation and spheroid formation from the HEK-293 cells. For experiments altering the alginate and calcium chloride concentrations, 10k cells were cryopreserved in 50 µL volumes. This number of cells was chosen from values used in hanging drop and agarose microwell techniques [10, 33, 34]. Lastly, cell concentration was adjusted by altering the number of cells

frozen per disk and the volume of the frozen disk. Groups include 10k cells in 10, 50, and 100 µL volumes and 5k cells in 50 µL volume. These groups compare different cell concentrations, a different number of cells (5k and 10k cells) within the same 50 µL volume, and the same cell concentration (100 cells/µL) with 50 and 100 µL volumes.

Spheroids were imaged within the alginate capsules three days post-cryopreservation using phase-contrast microscopy (Zeiss Axio Vert A.4). Spheroid diameters were then measured using ImageJ (NIH) and summarized in histograms with fitted Gaussian curves to characterize size distribution. The overall metabolic activity within the alginate capsule was determined via an MTT assay with some modification. Briefly, 25 µL of 5 mg/mL tetrazolium dye MTT was added for an approximate concentration of 0.5 mg/mL per well. Cells were incubated for three hours within the hydrogel capsule. Next, the media was carefully removed from the hydrogel capsules and the wells and replaced with isopropanol. The plates were then agitated on a shaker for 15 minutes. The absorbance of the solubilized formazan was measured at 570 nm via the Spectramax ® i3 plate reader and averaged per condition (n = 2 - 6). These values were then normalized to the initial number of cells frozen and the initial volume of frozen solution within the rubber wells.

6.2.6 Statistical analysis

Results are shown as mean values with standard deviations. Sample sizes are provided with each experiment, displayed in figures as individual data points where applicable, and listed in the figure legends. Statistical significance was asserted at $p < 0.05$ after performing t-tests, ANOVAs, and Tukey's multiple comparison tests where

appropriate. All analyses were performed using Graph-Pad Prism software (GraphPad Software Inc).

6.3 Results

6.3.1 Alginate hydrogel capsule formation is tunable

The alginate hydrogels were characterized by their swelling ratio, stiffness, mesh size, and capsule shell thickness. Expectedly, the doubling of the alginate solution concentration from 1% to 2% (w/v) led to an increase in the shell thickness (12%; Figure 6.2A) and a decrease in mesh size (46%; Figure 6.2B) that were both statistically significant. Although there was a statistically significant increase in stiffness by doubling the alginate polymer concentration (Figure 6.3A), the swelling ratio did not significantly change (Figure 6.3B). Furthermore, all calcium concentrations tested had statistically different capsule thicknesses (Figure 6.2C). Specifically, there was an approximately linear trend with shell thickness (R^2 = 0.9650). Similarly, calcium concentrations also significantly decreased mesh size as the concentration increased from 75 mM,100 mM, and 300 mM (Figure 6.2D). However, hydrogel mesh size did not have a strong trend with $CaCl_2$ concentrations (R^2 = 0.6832). Additionally, the stiffness (Figure 6.3C) and swelling ratio (Figure 6.3D) were statistically different between 75 and 300 mM $CaCl_2$. Notably, it was difficult to recover intact capsules using lower calcium concentrations (< 50 mM). Together, the hydrogel capsules' controllability of shell thickness and mesh size is demonstrated by changing the polymer and calcium concentrations.

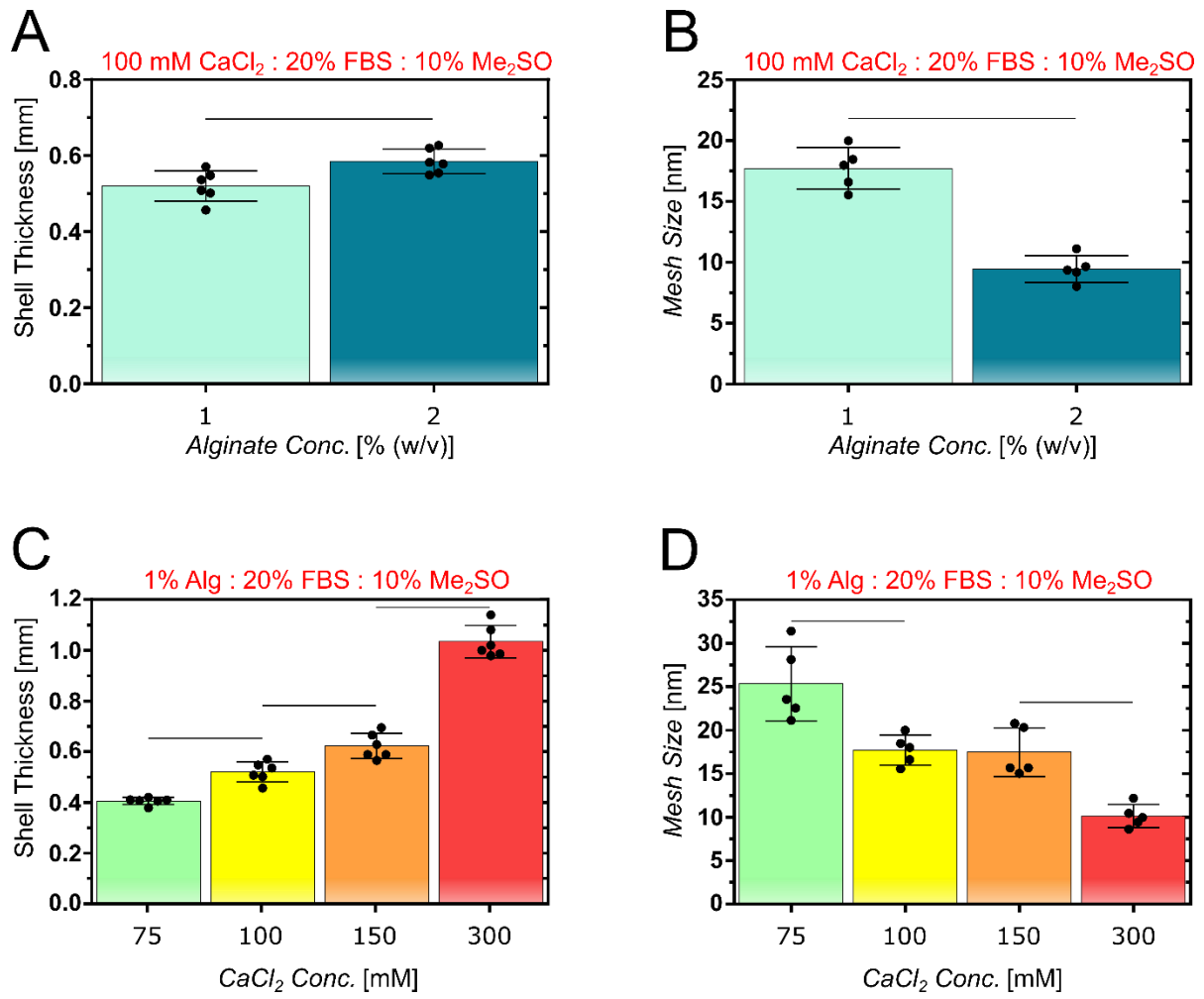

Figure 6.2 Hydrogel capsules can be controlled through polymer and cross-linker concentrations. Specifically, when using a cell freezing solution containing 20% (v/v) FBS, 10% (v/v) Me_2SO, and 100 mM $CaCl_2$, the shell thickness increases slightly with a doubling in alginate concentration from 1% (w/v) to 2% (w/v) (A), and also results in a significantly smaller mesh size (B). Similarly, as the calcium concentration increased, the capsule's shell thickness increased (C), and mesh size decreased (D). Bar graphs represent the mean ± SD with individual data points shown (n = 6 for shell thickness and n = 5 for mesh size measurements). Lines between groups represent select statistically significant differences ($P < 0.05$) assessed by performing a one-way ANOVA and a Tukey's multiple comparison test.

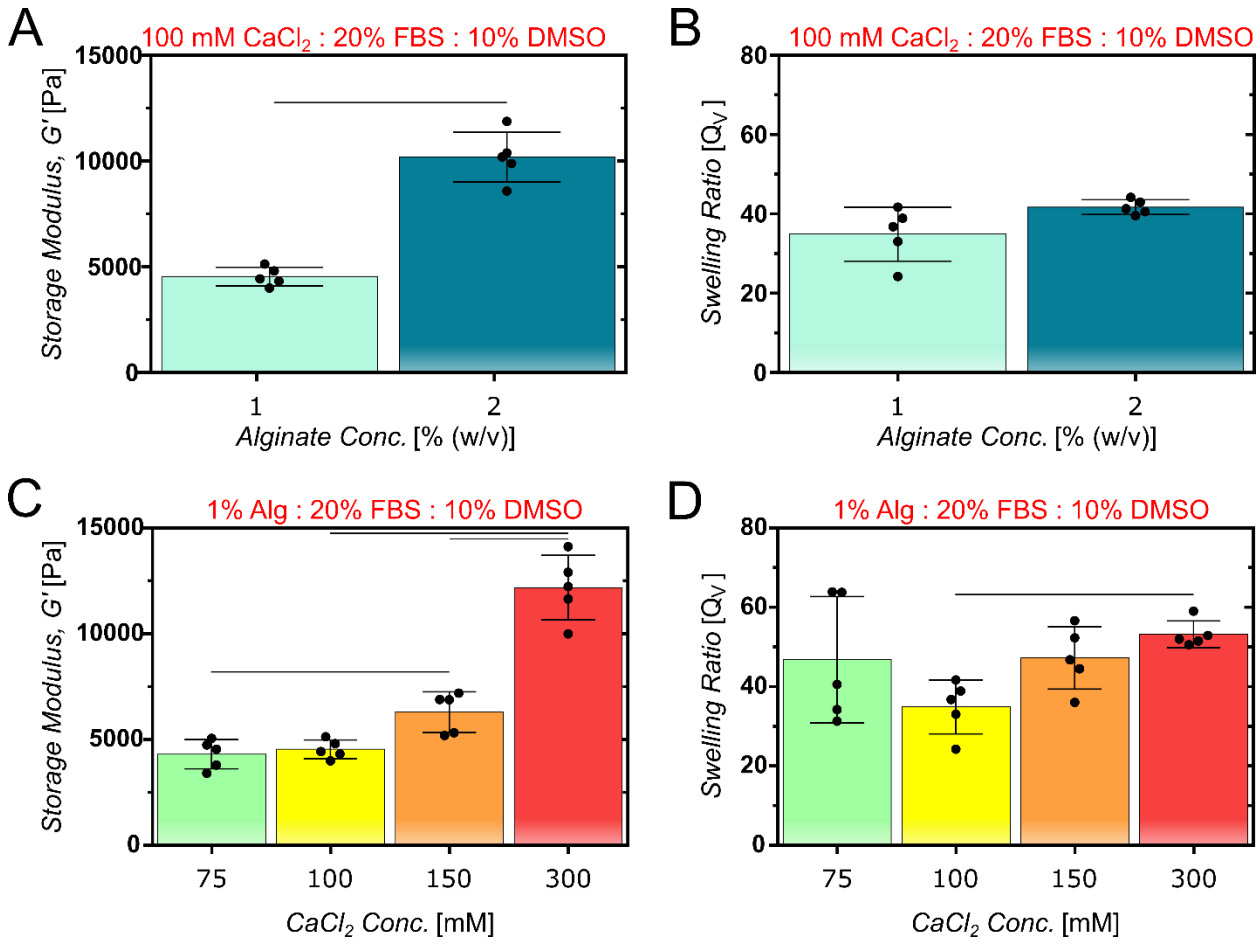

Figure 6.3 Alginate polymer and calcium chloride concentrations alter hydrogel properties. With a cell freezing solution containing 20% (v/v) FBS, 10% (v/v) Me_2SO, and 100 mM $CaCl_2$, the storage modulus approximately doubles with a doubling in alginate concentration from 1% (w/v) to 2% (w/v) (A); however, there was no significant change in swelling (B). As the calcium concentration increased, so did the capsule's storage modulus (C). Furthermore, a higher calcium concentration, increasing from 100 mM to 300 mM, led to a significant increase in swelling (D). Bar graphs represent the mean ± SD with individual data points shown (n = 5). Lines between groups represent select statistically significant differences ($P < 0.05$) assessed by performing a one-way ANOVA and a Tukey's multiple comparison test.

6.3.2 Permeable alginate capsules support dilution of the cryopreservation solution

The washing bath enables the diffusion of previously frozen molecules out of the hydrogel capsules, leading to their dilution. Mainly, doubling the amount of time the capsules were in the washing solution (5 and 10 minutes) led to a significant increase in the initial amount of FITC released from the capsules after 1 minute (Figure 6.4). Specifically, the FITC released was approximately 50 and 70% for the 5- and 10-minute times, respectively. Notably, both rinse times led to over 90% of the FITC being released after one hour. This experiment highlights the permeability of the hydrogel capsules for enabling the release of relatively small molecules (< 400 Da).

6.3.3 Alginate hydrogel formation is affected by the cryopreservation agents

The mechanical and physical properties of the hydrogel capsule were measured for the potential effect of Me_2SO and FBS in the modified cryopreserving solution on alginate cross-linking. The 20% (v/v) Me_2SO concentration resulted in statistically thinner capsule shells than the lower concentration (5% v/v), but with a similar mesh size (Figure 6.5A-B). Interestingly, the 20% (v/v) Me_2SO concentration that resulted in slightly thinner shells led to significantly stiffer hydrogels that had more swelling than the lower concentration (5% (v/v)) (Figure 6.6A-B). Generally, there were no significant differences in shell thickness, stiffness, swelling, or mesh size between no FBS and 20% (v/v) (Figure 6.5C-D and 6.6C-D). However, 80% (v/v) FBS led to a significant decrease in shell thickness, increased mesh size, and a decrease in storage moduli compared to no FBS. These data indicate that Me_2SO and FBS influence hydrogel properties but do not prevent hydrogel formation.

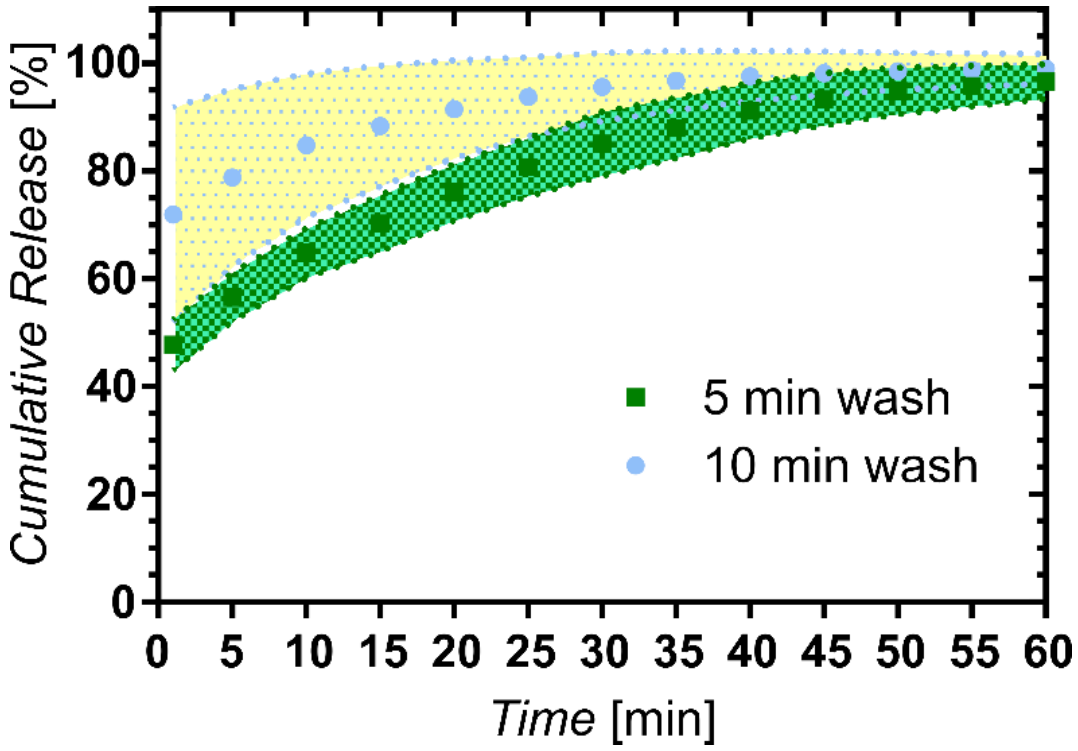

Figure 6.4 Release of FITC from alginate hydrogel capsules. 200 nmol of fluorescein isothiocyanate (FITC) was frozen in a 50 µL mold. Gelation in alginate occurred for 2 minutes before being moved into the washing-saline buffer for 5 or 10 minutes. About 200 mL of wash buffer was used to solubilize the high concentration of FITC before hydrogel capsules were moved to individual wells containing 1 mL of saline. Overall, most of the fluorescent molecule was removed from the capsules after a total elapsed time of 12 minutes (2 minutes for gelation, 5 minutes in the wash bath, and 5 minutes in 1 mL saline). Additionally, over 90% of FITC was removed within an hour. Data represent the mean ± SD (indicated by shaded areas) (n = 8).

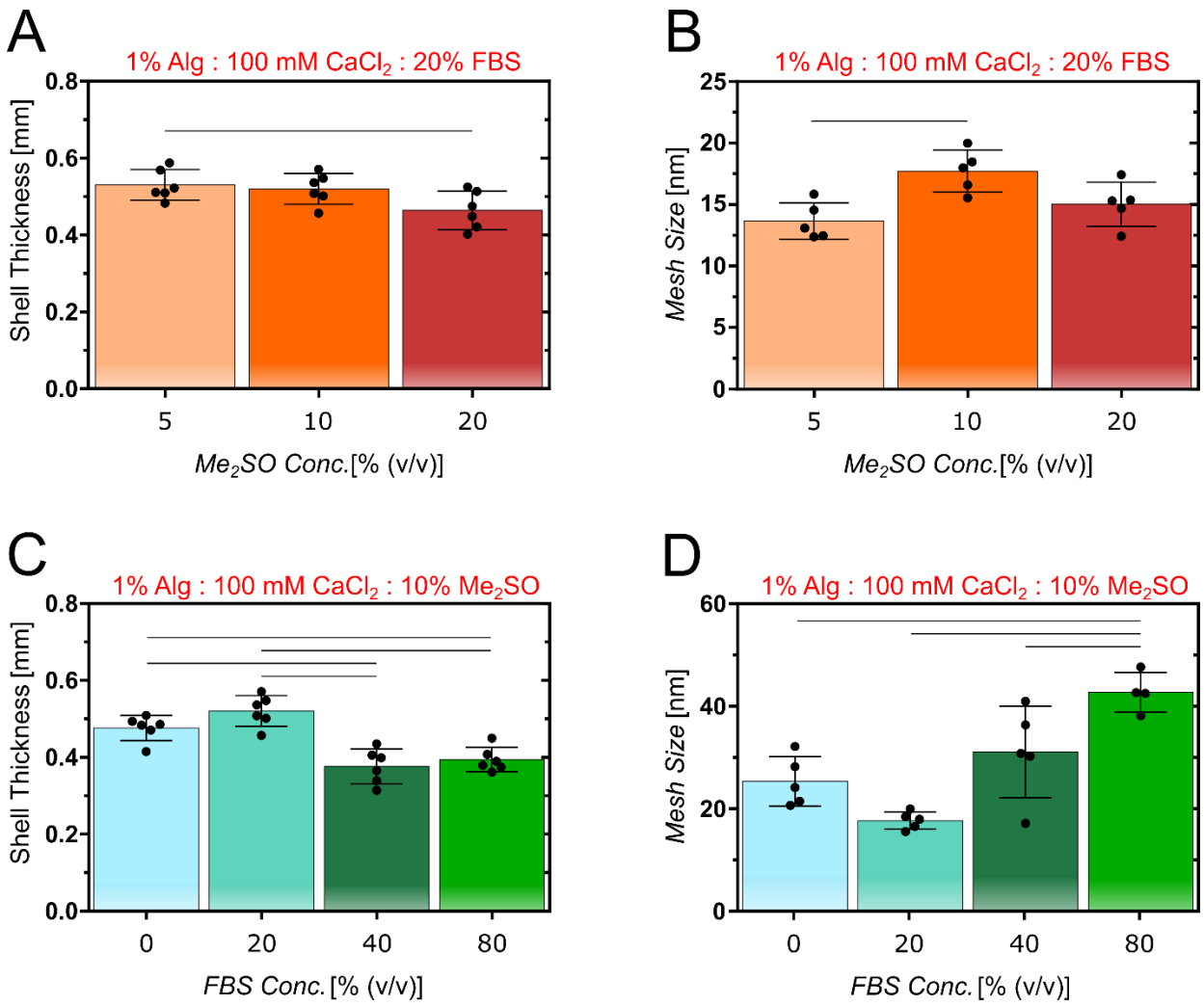

Figure 6.5 CPAs, Me_2SO and FBS, indicate some influence over hydrogel capsule formation. A 100 mM $CaCl_2$ solution and a 1% (w/v) alginate solution were used as the frozen and thawing solutions, respectively. First, the intracellular cryopreservation agent, Me_2SO, did not have a significant effect on capsule shell thickness (A) or the hydrogel mesh size (B). Similarly, the extracellular cryopreservation agent fetal bovine serum (FBS) did not have a statistically significant impact on shell thickness (C) or mesh size (D) at a concentration of 20% (v/v) compared to no FBS. However, higher concentrations of FBS led to a significant change in gelation. Specifically, 80% (v/v) had a significantly larger mesh size than the other concentrations. Furthermore, the 40%

and 80% (v/v) FBS concentrations had a significantly thinner shell than the 0% and 20% (v/v) FBS concentrations. Bars graphs represent the mean ± SD with individual data points (n = 6 for shell thickness and n = 5 for mesh size measurements). Lines between groups represent statistically significant differences ($P < 0.05$) assessed by performing a one-way ANOVA and a Tukey's multiple comparison test.

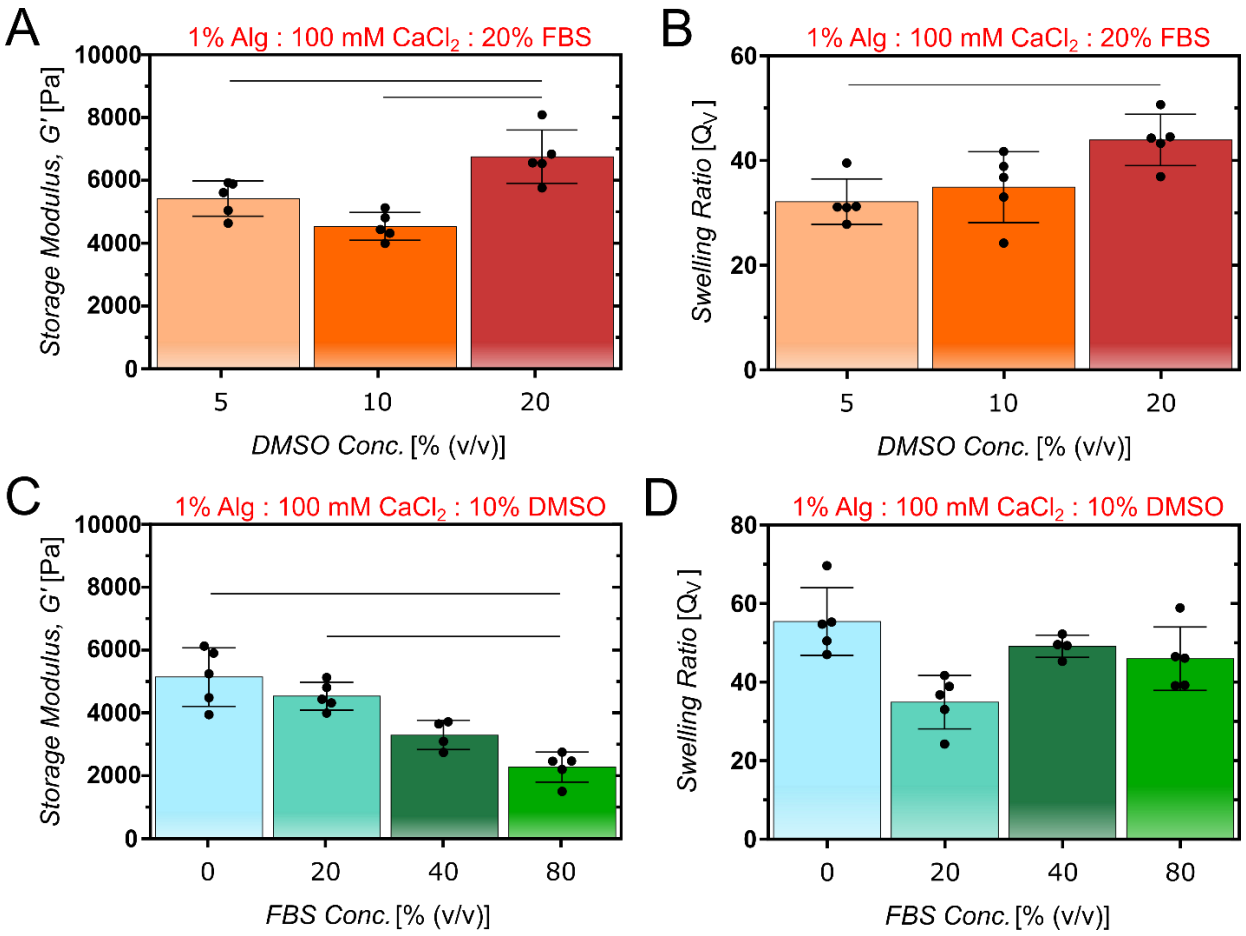

Figure 6.6 Me2SO and FBS affect swelling ratios and storage moduli of capsules.

A 100 mM CaCl2 solution was used in the freezing solution and a 1% (w/v) alginate solution as the thawing solution for each group. Both the storage modulus (A) and swelling ratios (B) of the hydrogel significantly increased between 5% and 20% (v/v) Me_2SO concentrations. There was a significant decrease in the storage modulus of hydrogels formed with a freezing solution containing 80% FBS compared to no FBS and 20% FBS. However, there was no significant difference in swelling with the different concentrations of FBS. Bar graphs represent the mean ± SD with individual data points shown (n = 5). Lines between groups represent statistically significant differences ($P < 0.05$) assessed by performing a one-way ANOVA and a Tukey's multiple comparison test.

6.3.4 Modified cryopreserving solutions can augment post-cryopreservation cell viability

Comparable to the cryopreservation agents Me_2SO and FBS affecting hydrogel formation, the alginate cross-linker, calcium, could influence the post-cryopreservation viability of the HEK-293 cells. Therefore, initial cellular viability and day-3 metabolic activity were measured post-cryopreservation using various calcium and FBS concentrations in the modified cryopreservation solution. Adding calcium chloride did not have a statistically significant effect on initial viability (Figure 6.7A). Similarly, there was no statistically significant difference in initial viability from increasing the FBS concentration (Figure 6.7B). However, concentrations of $CaCl_2$ above 100 mM had significantly less metabolic activity than concentrations at and below 100 mM (Figure 6.7C). Notably, a cryopreserving solution of 100 mM $CaCl_2$,10% (v/v) Me_2SO, and 20% (v/v) FBS was more metabolically active compared to no FBS and 80% (v/v) FBS (Figure 6.7D). Overall, the influence of calcium in the freezing solution on post-cryopreservation cell viability appears marginal if below 150 mM and might be augmented by FBS concentration.

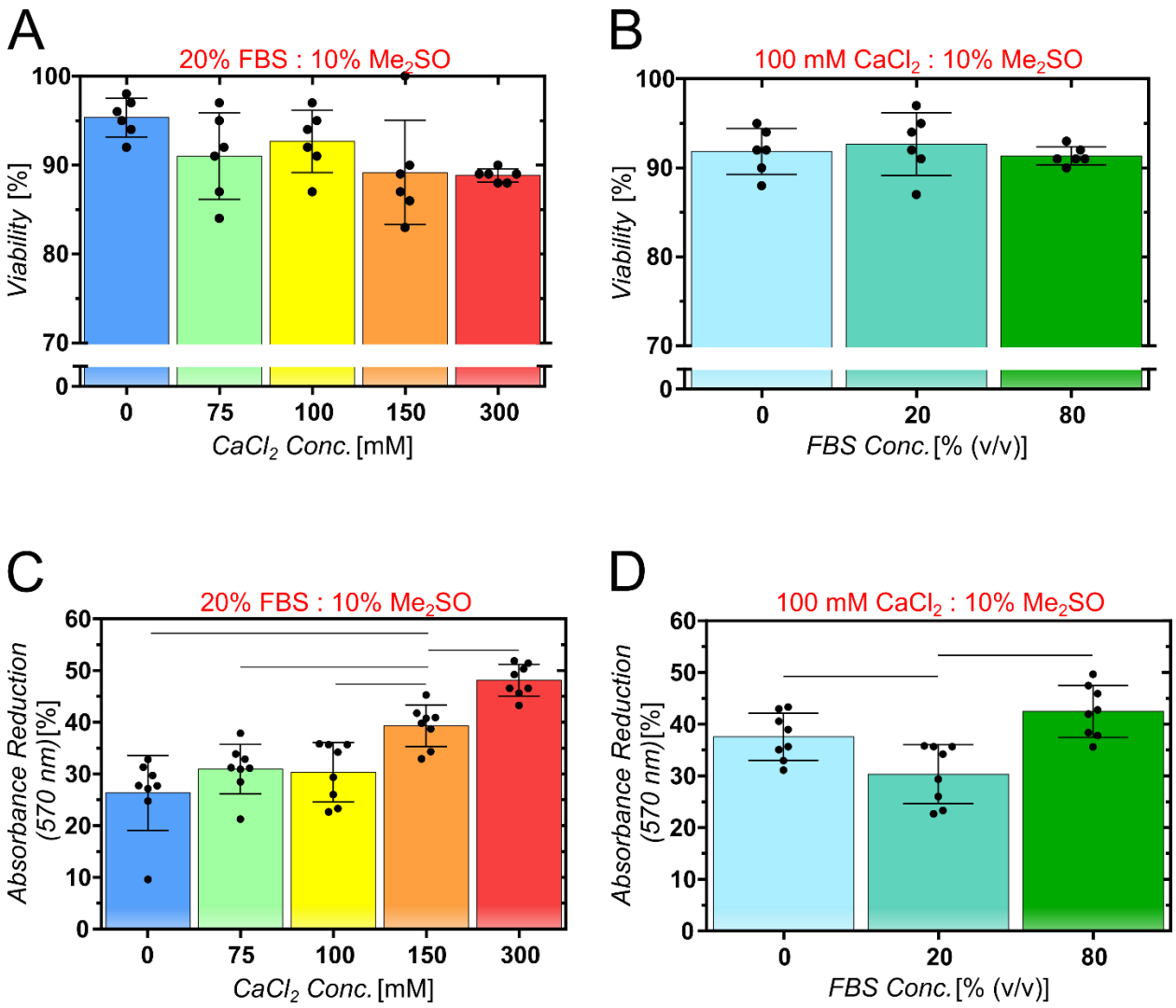

Figure 6.7 The addition of higher calcium concentrations into the freezing solution had an impact on cells post-cryopreservation. Specifically, initial cell viability post-cryopreservation, via a trypan blue exclusion assay, and metabolic activity 3-days post-cryopreservation, via an MTT assay, was measured for cells whose freezing solution had supplemental concentrations of calcium chloride (A and C) and fetal bovine serum (FBS) (B and D). Cell recovery was measured as the reduction in metabolic activity with respect to a control group that was not cryopreserved. Interestingly, there was no significant change in initial cell viability due to changing calcium concentrations (A) and FBS (B), with average viability being above 85%. There

is a ubiquitous decrease in cellular metabolism because of cryopreservation (C and D). Although the higher concentrations of calcium hindered the cell recovery, 75 mM and 100 mM concentrations of calcium chloride were not significantly different from the control group (C). Furthermore, with a freezing solution containing 100 mM calcium chloride, the addition of FBS did have a significant benefit to cell recovery, but only at the lower concentration (20% (v/v)) (D). Bar graphs represent the mean ± SD with individual data points (n = 6 for viability, and n = 8 for metabolic activity). Lines between groups represent statistically significant differences ($P < 0.05$) assessed by performing a one-way ANOVA and a Tukey's multiple comparison test.

6.3.5 Alginate polymer concentration augments spheroid formation

Three concentrations of alginate polymer in the thawing bath were examined for the resulting capsules' ability to promote aggregation of post-cryopreserved cells into spheroids. Overall, the ability of the HEK-293 cells to form spheroids within the alginate capsules was enhanced by higher concentrations of alginate in the thawing-bath solution. The average diameter of spheroids increased from an average of 75.75 µm with 0.5% (w/v) alginate solution to 91.73 µm with 2% (w/v) alginate solution (Figure 6.8A-C). Additionally, the spheroid formation appeared to follow an approximately normal distribution. While 0.5% and 1% (w/v) alginate concentrations had stronger correlating distributions than the 2% (w/v) concentration, this higher concentration had a few spheroids over 3-times larger than the average. Representative images from the inside of the capsules show spheroids with irregular shapes, indicating a consolidation of multiple spheroids into these larger aggregates (Figure 6.8D). Furthermore, these images highlight that spheroids form from single cells at the bottom of the alginate capsule after three days post-cryopreservation.

6.3.6 Cross-linker concentration within the cryopreservation solution modifies spheroid formation

Spheroid formation from post-cryopreserved cells was interrogated from different cryopreservation solutions containing $CaCl_2$. Similar to the results with different alginate polymer concentrations, multiple spheroids formed per capsule in Gaussian-like distributions (Figure 6.9A-C). While the average spheroid diameter formed from the modified cryopreserving solution containing 75 mM $CaCl_2$ was significantly smaller than

those produced with 100 and 150 mM, the coefficient of determination was superior (R^2 = 0.96). Additionally, there was evidence of aggregates consolidating into larger spheroids three days after thawing (Figure 6.9D). Overall, these data suggest that calcium impacts post-cryopreserved cells' ability to form spheroids within the alginate capsules.

6.3.7 Cellular concentration dictates the effectiveness of spheroid formation

The capability of cells to form aggregates was defined by the cell concentration in the cryopreserved solution. Specifically, the largest observed spheroids were in capsules formed from 10k cells within the 10 and 50 µL frozen volumes (Figure 6.10A-D). Additionally, on average, only 13 spheroids were generated within the 100 µL volume. In contrast, 38 and 118 spheroids developed within the 10 and 50 µL volumes, respectively. Consequently, the metabolic activity per hydrogel capsules was enhanced using the smaller volumes of the cryopreserved cells (Figure 6.10E). Next, the starting concentration of the cells was maintained constant (100 cells per µL) for different sized alginate capsules (50 and 100 µL). Although the cell concentration was the same, the smaller volume of 50 µL had more than five times the spheroids as the larger volume of 100 µL (Figure 6.10F) and significantly larger spheroids (Figure 6.10D & G). However, there was no significant difference in metabolic activity (Fig 8H). However, doubling the initial number of cells frozen, from 5k to 10k in 50 µL, resulted in an almost 4-fold increase in metabolic activity per cell (Figure 6.10I). Strikingly, the doubling in initial cells did not lead to a significant difference in average spheroid diameters (Figure 6.10C & G). Furthermore, although the number of cells initially frozen doubled from 5k to 10k,

the number of spheroids formed after three days only increased by about 64%, from 72 spheroids to 118. Together, these data indicate that a higher concentration of cells results in better cellular outcomes via aggregation and metabolic activity.

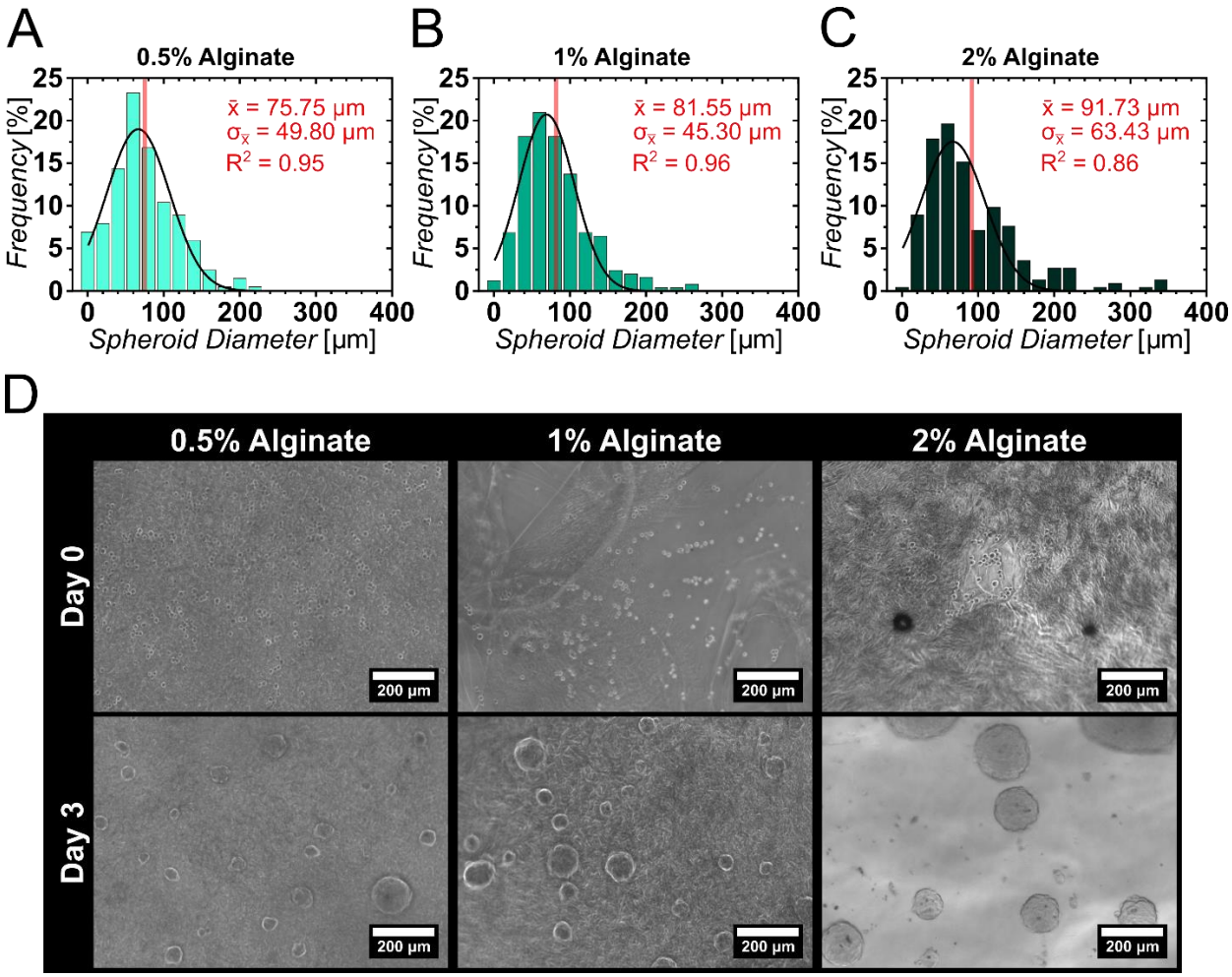

Figure 6.8 Post-cryopreserved cells formed spheroids within 72 hours inside alginate capsules. Alginate capsules were formed by submerging frozen cell solutions within 0.5% (A), 1% (B), and 2% (C) (w/v) alginate solutions. There is an apparent trend of increasing spheroid diameters with increasing alginate concentration. The difference in the average spheroid diameters is statistical significance between 0.5% and 2% (w/v) alginate. Importantly, a few larger spheroids are formed within the 2% alginate group (C), indicating consolidation of smaller spheroids (D). Images highlight how the capsules facilitate the formation of multiple spheroids along the bottom inner surface of capsules. Spheroid diameters were measured from images within the capsules. Histograms represent over 200 individual spheroids with bin centers every 20 µm. Red

text lists the mean diameter ($\bar{x}$), standard deviation ($\sigma_{\bar{x}}$), and coefficient of determination (R^2) about a Gaussian curve, shown in black. A vertical red line also displays the mean diameter. Statistically significant differences between groups were assessed using a one-way ANOVA and a Tukey's multiple comparison test.

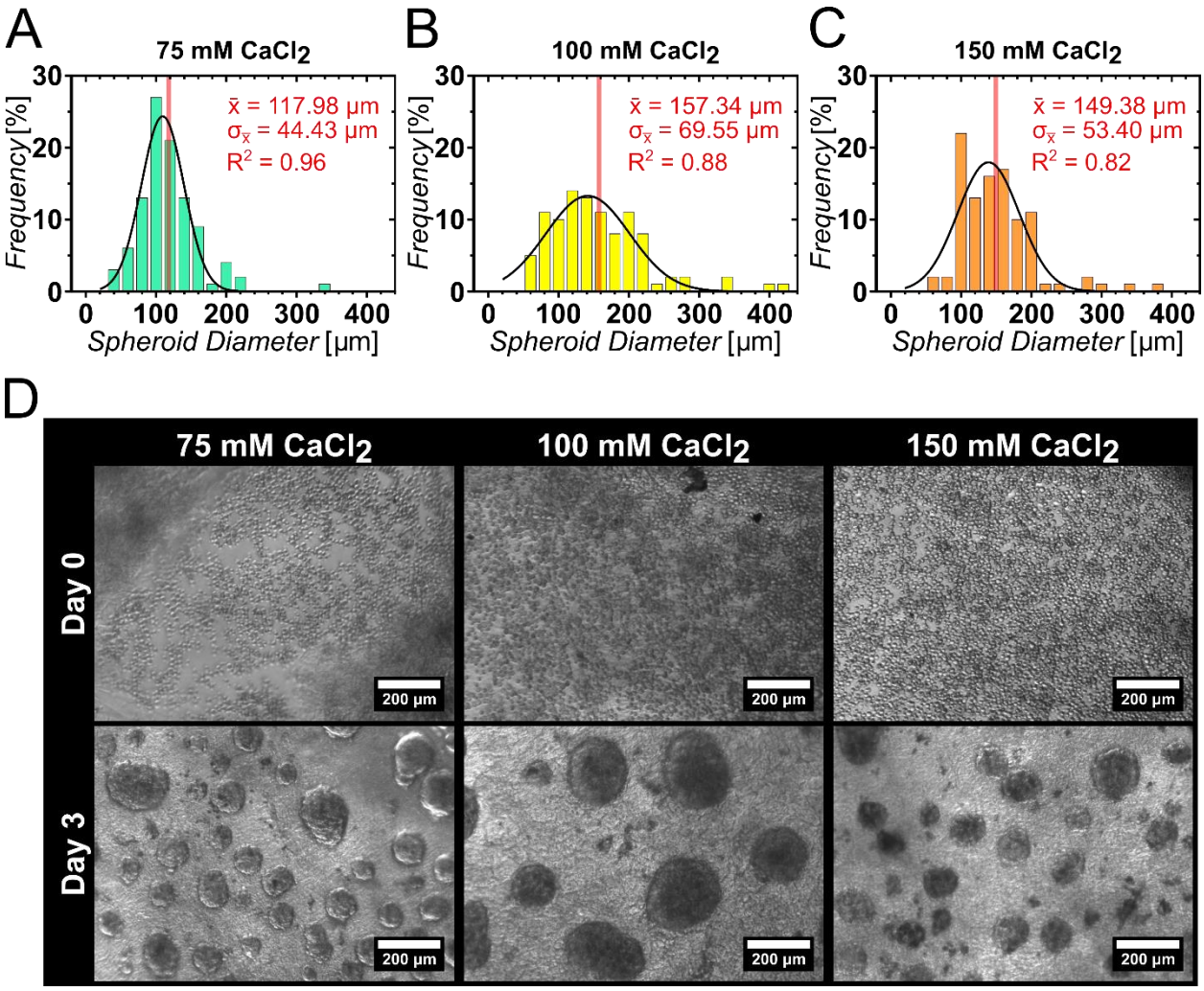

Figure 6.9 The formation of spheroids was impacted by the concentration of calcium chloride within the freezing solution. Alginate capsules were formed by submerging frozen cell solutions containing either 75 (A), 100 (B), or 150 (C) mM calcium chloride into a 1% (w/v) alginate solution. While there was a statistical difference in spheroid diameters between 75 mM and the other two concentrations of calcium chloride, these groups had a lower coefficient of determination. The consolidation and aggregation of multiple spheroids occurred more often in the group using 100 mM calcium chloride, as observed by the oblong spheroids at day 3 (D). Spheroid diameters were measured from images within the capsules. Histograms

represent 100 individual spheroids with bin centers every 20 μm. Red text lists the mean diameter ($\bar{x}$), standard deviation ($\sigma_{\bar{x}}$), and coefficient of determination (R^2) about a Gaussian curve, shown in black. A vertical red line also displays the mean diameter. Statistically significant differences between groups were assessed using a one-way ANOVA and a Tukey's multiple comparison test.

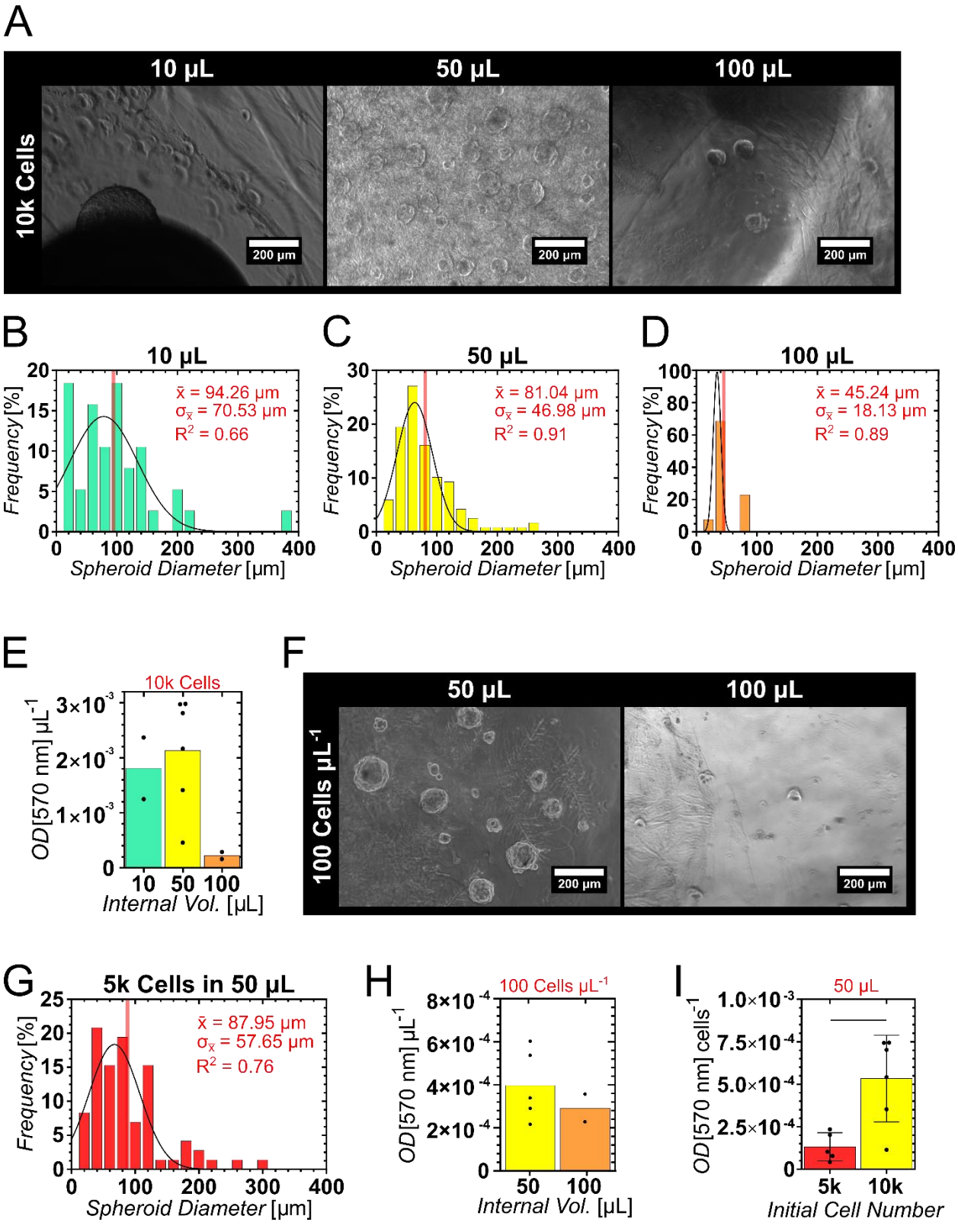
A
10 µL
50 µL
100 µL
10k Cells
200 µm
B
10 µL
x̄ = 94.26 µm
σx̄ = 70.53 µm
R2 = 0.66
Frequency [%]
Spheroid Diameter [µm]
C
50 µL
x̄ = 81.04 µm
σx̄ = 46.98 µm
R2 = 0.91
D
100 µL
x̄ = 45.24 µm
σx̄ = 18.13 µm
R2 = 0.89
E
10k Cells
OD[570 nm] µL-1
Internal Vol. [µL]
F
100 Cells µL-1
G
5k Cells in 50 µL
x̄ = 87.95 µm
σx̄ = 57.65 µm
R2 = 0.76
H
100 Cells µL-1
I
50 µL
OD[570 nm] cells-1
5k
10k
Initial Cell Number

Figure 6.10 Spheroid formation is impacted by the proximity of neighboring cells. The proximity of neighboring cells was controlled by either changing the internal volume of the alginate capsule (10, 50, and 100 µL) or by altering the number of cells cryopreserved (5k and 10k cells). The number of spheroids and their size were impacted by capsule volume (A-E). With the smallest internal volume of 10 µL, the largest spheroids were formed (B). Furthermore, capsules with a 50 µL internal volume had more spheroids formed, 118 spheroids, and a more normal distribution of the spheroid sizes than the other volumes (C). In contrast, the 100 µL not only had the smallest spheroids but the least formed in the capsule, 13 spheroids (D). The metabolic activity per capsule, indicating the optical density from an MTT assay normalized to the initial number of cryopreserved cells, indicates how the 100 µL volume had substantially less activity than the other two volumes (E). This loss of cellular activity is further shown in images inside the capsules where the same initial cell concentration is used with between 50 and 100 µL volumes (F). Similarly, a halving of cells within the 50 µL volumes led to 72 spheroids within the capsule (G). Despite this apparent effect from capsule volume, the impact on metabolic activity is unclear (H). Interestingly, the metabolic activity per cell more than doubles with a doubling in initial cell number from 5k to 10k cells within a 50 µL volume capsule after normalizing to initial cell number (I). Spheroid diameters were measured from images within the capsules. Histograms represent total spheroids in a representative capsule with bin centers every 20 µm with the mean diameter ($\bar{x}$), standard deviation ($\sigma_{\bar{x}}$), and coefficient of determination (R^2) about a Gaussian curve, listed in red. A vertical red line also displays the mean diameter. Metabolic activity measurements represent the activity per capsule

normalized to the initial cell number prior to cryopreservation or the internal capsule volume. Bar graphs represent the mean ± SD with individual data points. Lines between groups represent statistically significant differences ($P < 0.05$) assessed by performing a one-way ANOVA and a Tukey's multiple comparison test or a Student's t-test. Similarly, average spheroid sizes between data presented as histograms were assessed via a one-way ANOVA and a Tukey's multiple comparison test.

6.4 Discussion

6.4.1 Formation of encapsulating alginate hydrogel capsules via TIG

The work described in this chapter is the application of the hydrogel capsules presented in chapter 3 with cryopreserved cells. The alginate hydrogels used in the experiments reported in this chapter are formed by melting a frozen cross-linker solution into a liquid. Once in the liquid state, the cross-linker and other components of the freezing solution can diffuse into an alginate solution. This process of forming alginate capsules by submerging a calcium solution into alginate has previously been characterized as inverse gelation and reverse spherification [35-37]. While in agreement with our previous work where hydrogel capsule thickness increased with higher polymer concentrations, studies with inverse gelation showed a contrasting decrease in shell thickness with higher polymer concentrations [20, 38, 39]. However, this discrepancy could be explained by inverse gelation not using a frozen calcium solution. Therefore, TIG maintains its distinct hydrogel formation, despite the addition of CPAs.

6.4.2 Influences of the cryoprotectants on hydrogel gelation

Given the similar trends with and without Me_2SO and FBS, we do not expect these CPAs to impact alginate hydrogel gelation detrimentally. Me_2SO and FBS represent common CPAs utilized in the cryopreservation of cells [40-42]; however, if other CPAs or hydrogels are to be used, they would need to be tested for their impact with TIG. Specifically, in Appendix B, we briefly describe the dual gelation of alginate hydrogel capsules with a fibrin core. Despite the evidence of a fibrin hydrogel formation within the capsules, Me_2SO has been shown to hinder fibrin formation [43]. Regardless,

the release of FITC from the capsules suggests that molecules smaller than the FITC would similarly be released from the capsules. Specifically, Me_2SO would be expected to diffuse down the concentration gradient, reducing the concentration within the capsules. The dilution of Me_2SO could be essential for reducing osmotic shock and bringing the Me_2SO concentration to non-cytotoxic levels more quickly than traditional post-cryopreservation techniques [3, 16, 40, 44-49]. Collectively, these results suggest that the hydrogel properties can be controlled with minimal impact from the addition of Me_2SO and FBS and supports that the CPAs might be diluted during the gelation and washing steps. Additionally, trends in stiffness, swelling, and mesh size with polymer and cross-linker concentrations are in agreement with other alginate hydrogel studies [21, 29, 30, 50]. Nevertheless, the calcium added to the freezing solution and hydrogel formation can still impact cell survival post-cryopreservation.

6.4.3 Effects of alginate hydrogel formation via TIG on post-cryopreserved cells

We showed that the alginate cross-linker did influence the recovery of cryopreserved cells; however, cell viability and metabolic recovery remained relatively unchanged between 75 and 100 mM $CaCl_2$ compared to the control without any $CaCl_2$. Previous studies have employed similar calcium concentrations for producing an alginate hydrogel to encapsulate viable cells [8, 23, 26]. However, cryopreserved cells can be more sensitive to changes in local ion concentrations due to the exposure to osmotic shifts inherent with cryopreservation [51-54]. Contextually, the calcium chloride is added to an already hypertonic solution designed to promote cellular dehydration when cooling [42, 55, 56]. When freezing, cell damage can result from dehydration,

intracellular ice formation, and cryopreserving agent cytotoxicity [16, 55, 57]. Generally, membrane disruption from ice leads to necrosis, while osmotic shock and dehydration could follow apoptosis pathways [3, 58, 59]. The trypan blue exclusion assay used in this study does not suggest additional necrosis, even from adding 300 mM of $CaCl_2$. Nevertheless, the metabolic activity reduction three days post-cryopreservation with 300 mM $CaCl_2$ in the freezing solution was nearly double that of the unmodified freezing solution, suggesting more moribund cells post-cryopreservation [60]. The addition of calcium might be worsening osmotic shock or over dehydrating the cells [55, 57, 59]. Therefore, while calcium added to the cell freezing solution might not cause initial necrosis, it is expected to impact cell recovery in culture. Together, these results motivate the importance of future work to explore the role of calcium and cryopreservation on cell-cell binding and recovery from cryopreservation-induced damage [12, 53, 54, 61, 62].

6.4.4 Formation of spheroids from post-cryopreserved cells within hydrogel capsules

Cryopreserved cells encapsulated within alginate capsules formed multiple spheroids after three days. Higher polymer density hydrogels resulted in larger spheroids. These results agree with previous work that produced human intestinal organoids with alginate hydrogels [25]. Likewise, the optimal concentration of $CaCl_2$ being 100 mM $CaCl_2$ suggests a balance between the effects of calcium on cryopreservation and how the resulting hydrogel capsule supports cell survival and aggregation. Together, altering the polymer and cross-linker concentrations change the hydrogel's permeability for cryopreservation agents, cell debris, and media [20, 30].

Appropriately, previous studies suggest osmotic shock can be lessened by imposing additional drag forces on the solutes and solvent [57, 63-65]. We directly observed this non-instantaneous release with FITC diffusing out of the alginate capsules over an hour. Therefore, the alginate hydrogel could potentially reduce the risk and damage of osmolarity shock, similar to the common practice of multiple dilution steps during thawing [11, 19, 66]. Moreover, this dilution would be continuous in a large enough thawing bath, as the capsules trap the cells inside.

6.4.5 Comparison of cryopreserved and post-cryopreserved hydrogels

In previous chapters, we discussed cryostructuring as a method to generate aggregates of alginate polymer during freezing. Particularly in chapter 5, we discuss how the combination of cryostructuring and Me_2SO led to an alginate cryogel. Notably, this cryostructuring can be a detrimental process for cryopreserved cell viability. [56, 57, 59, 67-69]. Slow freezing cryopreservation protocols represent a balance between dehydration and ice formation, and although a hydrogel can reduce extracellular ice damage to post-cryopreserved cells, the ice that does form can structurally damage the hydrogel [70-72]. Additionally, the drag forces preventing large shifts in osmolarity when thawing also prevent the CPAs from diffusing into hydrogels to be cryopreserved. The cryopreservation of larger tissue-engineered constructs with hydrogels will need to consider the challenges of cryopreserving large tissue samples [58, 69, 73]. In contrast, cells encapsulated in hydrogels while thawing bypass these effects of freezing the hydrogel: no cryostructuring of the polymer or limitations to CPA permeability during cryopreservation. Overall, future work should explore and optimize how changes to the

capsule's shape and hydrogel mesh size will influence how cells aggregate within the hydrogel due to effects on solution osmolarity and diffusion of intra-capsular components [74, 75].

6.4.6 Spheroid formation is dependent on cell concentration

Both the size of the alginate capsules and the number of cells affected the efficiency of spheroid formation. Specifically, larger spheroids were created with a higher cell concentration. These results are in agreement with previous studies that describe larger spheroids resulting from more cells being available to aggregate [26, 33, 76]. Moreover, our data suggest that too low cell concentrations resulted in cells being unable to aggregate efficiently, indicated by the reduced number and size of spheroids in the 100 µL capsules than the 50 µL capsules with the same cell concentration. Although there could be some confounding effects on the effectiveness of cryopreservation with the different solution volumes and the resulting cell viability [1], the freeze-thawing of cells has also been shown to reduce cell-binding efficiency and lead to apoptosis [4, 12, 62]. Therefore, we suspect that cells within the alginate capsules at low concentrations became apoptotic from being unable to form cell-cell contact [12, 62], resulting in fewer and smaller spheroids after three days. Notably, the enhancement of cell-cell interactions has been previously described as improving cell survival post-cryopreservation [77-80]. Overall, these results suggest that using an appropriate cell concentration to promote cell aggregation post-cryopreservation is critical.

6.4.7 TIG enables unique internal geometries of hydrogel capsules

The internal geometry of capsules formed in this chapter closely replicates the shape of the frozen solution, i.e., a flat disk. Consequently, multiple spheroids are formed per capsule as cells aggregate with their nearest neighboring cells at the bottom of the capsule's internal surface. Previously, we have found that TIG enables the use of a wide variety of shapes. For example, tubes can be created from frozen sticks and hollow donut-like structures from frozen toruses. Using a convex shape generates a concave well, similar to hanging-drop and round-bottom wells [26, 81, 82], reducing the cell concentration required for spheroid formation within the alginate capsules. Therefore, controlling the geometry of the frozen solution is an appealing parameter for controlling spheroid formation in future work.

6.5 Conclusion

This chapter described the formation of spheroids from post-cryopreserved HEK-293 cells within an encapsulating alginate hydrogel. To our knowledge, this is the first description of a technique to encapsulate cryopreserved cells in an alginate hydrogel while thawing. Therefore, we established the procedures for controlling the hydrogel capsule and optimizing cell viability by adjusting a modified cryopreserving solution and the alginate-containing thawing solution. Overall, the modified cryopreserving solution led to viable cells that formed metabolically active spheroids from HEK-293 cells post-cryopreservation. Unlike traditional spheroid formation techniques, this method uses a permeable alginate hydrogel that not only isolates the cells but, importantly, enables the diffusion of waste and nutrients [75, 83-85]. Additionally, cells aggregating within a hydrogel post-cryopreservation bypasses damages caused by freezing whole spheroids or cells encapsulated within hydrogels [15, 72]. The work in this chapter also suggests substantial opportunities for using instructive hydrogels to improve post-cryopreserved cell function in clinical therapies requiring frozen storage, thereby addressing a potential bottleneck in cell therapies caused by cryopreservation-induced damages.

6.6 References

[1] C. J. Hunt, "Technical Considerations in the Freezing, Low-Temperature Storage and Thawing of Stem Cells for Cellular Therapies," *Transfusion Medicine and Hemotherapy,* vol. 46, no. 3, pp. 134-150, 2019, doi: 10.1159/000497289.

[2] S. Renzi, T. Lombardo, S. Dotti, S. S. Dessì, P. De Blasio, and M. Ferrari, "Mesenchymal stromal cell cryopreservation," (in eng), *Biopreserv Biobank,* vol. 10, no. 3, pp. 276-81, Jun 2012, doi: 10.1089/bio.2012.0005.

[3] D. Freimark *et al.*, "Systematic parameter optimization of a Me(2)SO- and serum-free cryopreservation protocol for human mesenchymal stem cells," in *Cryobiology*, vol. 63, no. 2). Netherlands: © 2011 Elsevier Inc, 2011, pp. 67-75.

[4] R. Chinnadurai *et al.*, "Actin cytoskeletal disruption following cryopreservation alters the biodistribution of human mesenchymal stromal cells in vivo," (in eng), *Stem Cell Reports,* vol. 3, no. 1, pp. 60-72, Jul 8 2014.

[5] S. B. Rizoli, O. D. Rotstein, J. Parodo, M. J. Phillips, and A. Kapus, "Hypertonic inhibition of exocytosis in neutrophils: central role for osmotic actin skeleton remodeling," (in eng), *Am J Physiol Cell Physiol,* vol. 279, no. 3, pp. C619-33, Sep 2000, doi: 10.1152/ajpcell.2000.279.3.C619.

[6] M. Mendicino, A. M. Bailey, K. Wonnacott, R. K. Puri, and S. R. Bauer, "MSC-based product characterization for clinical trials: an FDA perspective," in *Cell Stem Cell*, vol. 14, no. 2). United States: © 2014 Elsevier Inc, 2014, pp. 141-5.

[7] X. Guo, S. Li, Q. Ji, R. Lian, and J. Chen, "Enhanced viability and neural differential potential in poor post-thaw hADSCs by agarose multi-well dishes and spheroid culture," in *Hum Cell*, vol. 28, no. 4). Japan, 2015, pp. 175-89.

[8] S. S. Ho, K. C. Murphy, B. Y. Binder, C. B. Vissers, and J. K. Leach, "Increased Survival and Function of Mesenchymal Stem Cell Spheroids Entrapped in Instructive Alginate Hydrogels," (in eng), *Stem Cells Transl Med,* vol. 5, no. 6, pp. 773-81, Jun 2016.

[9] K. C. Murphy, S. Y. Fang, and J. K. Leach, "Human mesenchymal stem cell spheroids in fibrin hydrogels exhibit improved cell survival and potential for bone healing," (in eng), *Cell Tissue Res,* vol. 357, no. 1, pp. 91-9, Jul 2014.

[10] C. E. Vorwald, K. C. Murphy, and J. K. Leach, "Restoring vasculogenic potential of endothelial cells from diabetic patients through spheroid formation," (in eng), *Cell Mol Bioeng,* vol. 11, no. 4, pp. 267-278, Aug 2018.

[11] B. C. Heng *et al.*, "Loss of viability during freeze-thaw of intact and adherent human embryonic stem cells with conventional slow-cooling protocols is predominantly due to apoptosis rather than cellular necrosis," (in eng), *J Biomed Sci,* vol. 13, no. 3, pp. 433-45, May 2006, doi: 10.1007/s11373-005-9051-9.

[12] R. Martin-Ibañez, C. Unger, A. Strömberg, D. Baker, J. M. Canals, and O. Hovatta, "Novel cryopreservation method for dissociated human embryonic stem cells in the presence of a ROCK inhibitor," in *Hum Reprod*, vol. 23, no. 12). England, 2008, pp. 2744-54.

[13] M. A. Savitskaya and G. E. Onishchenko, "Apoptosis in cryopreserved eukaryotic cells," *Biochemistry (Moscow),* vol. 81, no. 5, pp. 445-452, 2016/05/01 2016, doi: 10.1134/S0006297916050023.

[14] X. Xu, S. Cowley, C. J. Flaim, W. James, L. Seymour, and Z. Cui, "The roles of apoptotic pathways in the low recovery rate after cryopreservation of dissociated

human embryonic stem cells," (in eng), *Biotechnology progress,* vol. 26, no. 3, pp. 827-837, May-Jun 2010, doi: 10.1002/btpr.368.

[15] B. C. Heng, H. Yu, and S. C. Ng, "Strategies for the cryopreservation of microencapsulated cells," *Biotechnology and Bioengineering,* https://doi.org/10.1002/bit.10837 vol. 85, no. 2, pp. 202-213, 2004/01/20 2004, doi: https://doi.org/10.1002/bit.10837.

[16] G. M. Fahy, "The relevance of cryoprotectant “toxicity” to cryobiology," *Cryobiology,* vol. 23, no. 1, pp. 1-13, 1986/02/01/ 1986, doi: https://doi.org/10.1016/0011-2240(86)90013-1.

[17] M. Benekli, B. Anderson, D. Wentling, S. Bernstein, M. Czuczman, and P. McCarthy, "Severe respiratory depression after dimethylsulphoxide-containing autologous stem cell infusion in a patient with AL amyloidosis," *Bone Marrow Transplantation,* vol. 25, no. 12, pp. 1299-1301, 2000/06/01 2000, doi: 10.1038/sj.bmt.1702452.

[18] M. A. Higman, J. D. Port, N. J. Beauchamp, and A. R. Chen, "Reversible leukoencephalopathy associated with re-infusion of DMSO preserved stem cells," *Bone Marrow Transplantation,* vol. 26, no. 7, pp. 797-800, 2000/10/01 2000, doi: 10.1038/sj.bmt.1702589.

[19] R. L. Levin and T. W. Miller, "An optimum method for the introduction or removal of permeable cryoprotectants: Isolated cells," *Cryobiology,* vol. 18, no. 1, pp. 32-48, 1981/02/01/ 1981, doi: https://doi.org/10.1016/0011-2240(81)90004-3.

[20] D. J. Hadley and E. A. Silva, "Thaw-Induced Gelation of Alginate Hydrogels for Versatile Delivery of Therapeutics," *Annals of Biomedical Engineering,* vol. 47, no. 8, pp. 1701-1710, 2019/08/01 2019, doi: 10.1007/s10439-019-02282-5.

[21] K. Y. Lee and D. J. Mooney, "Alginate: properties and biomedical applications," (in eng), *Progress in polymer science,* vol. 37, no. 1, pp. 106-126, 2012, doi: 10.1016/j.progpolymsci.2011.06.003.

[22] G. T. Grant, E. R. Morris, D. A. Rees, P. J. C. Smith, and D. Thom, "Biological interactions between polysaccharides and divalent cations: The egg-box model," *FEBS Letters,* vol. 32, no. 1, pp. 195-198, 1973/05/15 1973, doi: 10.1016/0014-5793(73)80770-7.

[23] K. T. Campbell, R. S. Stilhano, and E. A. Silva, "Enzymatically degradable alginate hydrogel systems to deliver endothelial progenitor cells for potential revasculature applications," (in eng), *Biomaterials,* vol. 179, pp. 109-121, 2018, doi: 10.1016/j.biomaterials.2018.06.038.

[24] J. A. Rowley and D. J. Mooney, "Alginate type and RGD density control myoblast phenotype," in *J Biomed Mater Res*, vol. 60, no. 2). United States: 2002 Wiley Periodicals, Inc. J Biomed Mater Res 60: 217-223, 2002; DOI 10.1002/jbm.1287, 2002, pp. 217-23.

[25] M. M. Capeling *et al.*, "Nonadhesive Alginate Hydrogels Support Growth of Pluripotent Stem Cell-Derived Intestinal Organoids," *Stem Cell Reports,* vol. 12, no. 2, pp. 381-394, 2019/02/12/ 2019, doi: https://doi.org/10.1016/j.stemcr.2018.12.001.

[26] C. E. Vorwald, S. S. Ho, J. Whitehead, and J. K. Leach, "High-Throughput Formation of Mesenchymal Stem Cell Spheroids and Entrapment in Alginate Hydrogels," in *Biomaterials for Tissue Engineering: Methods and Protocols*, K. Chawla Ed. New York, NY: Springer New York, 2018, pp. 139-149.

[27] A. Blumlein, N. Williams, and J. J. McManus, "The mechanical properties of individual cell spheroids," *Scientific Reports,* vol. 7, no. 1, p. 7346, 2017/08/04 2017, doi: 10.1038/s41598-017-07813-5.

[28] V. Stensvaag, T. Furmanek, K. Lønning, A. J. Terzis, R. Bjerkvig, and T. Visted, "Cryopreservation of alginate-encapsulated recombinant cells for antiangiogenic therapy," (in eng), *Cell Transplant,* vol. 13, no. 1, pp. 35-44, 2004, doi: 10.3727/000000004772664879.

[29] K. T. Campbell, K. Wysoczynski, D. J. Hadley, and E. A. Silva, "Computational-Based Design of Hydrogels with Predictable Mesh Properties," *ACS Biomaterials Science & Engineering,* vol. 6, no. 1, pp. 308-319, 2020/01/13 2020, doi: 10.1021/acsbiomaterials.9b01520.

[30] J. L. Madrigal, S. N. Sharma, K. T. Campbell, R. S. Stilhano, R. Gijsbers, and E. A. Silva, "Microgels produced using microfluidic on-chip polymer blending for controlled released of VEGF encoding lentivectors," (in eng), *Acta biomaterialia,* vol. 69, pp. 265-276, 2018/03// 2018, doi: 10.1016/j.actbio.2018.01.013.

[31] M. L. Moya, M. Morley, O. Khanna, E. C. Opara, and E. M. Brey, "Stability of alginate microbead properties in vitro," (in eng), *Journal of materials science. Materials in medicine,* vol. 23, no. 4, pp. 903-912, 2012, doi: 10.1007/s10856-012-4575-9.

[32] B.-H. Lee, B. Li, and S. A. Guelcher, "Gel microstructure regulates proliferation and differentiation of MC3T3-E1 cells encapsulated in alginate beads," *Acta Biomaterialia,* vol. 8, no. 5, pp. 1693-1702, 2012/05/01/ 2012, doi: https://doi.org/10.1016/j.actbio.2012.01.012.

[33] K. C. Murphy, J. Whitehead, P. C. Falahee, D. Zhou, S. I. Simon, and J. K. Leach, "Multifactorial Experimental Design to Optimize the Anti-Inflammatory and Proangiogenic Potential of Mesenchymal Stem Cell Spheroids," (in eng), *Stem Cells,* vol. 35, no. 6, pp. 1493-1504, Jun 2017.

[34] K. C. Murphy *et al.*, "Measurement of oxygen tension within mesenchymal stem cell spheroids," (in eng), *J R Soc Interface,* vol. 14, no. 127, Feb 2017.

[35] E. Martins, D. Renard, Z. Adiwijaya, E. Karaoglan, and D. Poncelet, "Oil encapsulation in core-shell alginate capsules by inverse gelation. I: dripping methodology," (in eng), *J Microencapsul,* vol. 34, no. 1, pp. 82-90, Feb 2017, doi: 10.1080/02652048.2017.1284278.

[36] A. Blandino, M. Macías, and D. Cantero, "Immobilization of glucose oxidase within calcium alginate gel capsules," *Process Biochemistry,* vol. 36, no. 7, pp. 601-606, 2001/02/01/ 2001, doi: https://doi.org/10.1016/S0032-9592(00)00240-5.

[37] P. Lee and M. A. Rogers, "Effect of calcium source and exposure-time on basic caviar spherification using sodium alginate," *International Journal of Gastronomy and Food Science,* vol. 1, no. 2, pp. 96-100, 2012/06/01/ 2012, doi: https://doi.org/10.1016/j.ijgfs.2013.06.003.

[38] A. Foglio Bonda, L. Regis, L. Giovannelli, and L. Segale, "Alginate/maltodextrin and alginate/shellac gum core-shell capsules for the encapsulation of peppermint

essential oil," in *Int J Biol Macromol*, vol. 162. Netherlands: © 2020 Elsevier B.V, 2020, pp. 1293-1302.

[39] E. Martins, D. Poncelet, R. C. Rodrigues, and D. Renard, "Oil encapsulation techniques using alginate as encapsulating agent: applications and drawbacks," (in eng), *J Microencapsul,* vol. 34, no. 8, pp. 754-771, Dec 2017, doi: 10.1080/02652048.2017.1403495.

[40] A. B. Sultani, L. A. Marquez-Curtis, J. A. Elliott, and L. E. McGann, "Improved Cryopreservation of Human Umbilical Vein Endothelial Cells: A Systematic Approach," (in eng), *Sci Rep,* vol. 6, p. 34393, Oct 6 2016.

[41] J. Zhao, H. N. Hao, R. L. Thomas, and W. D. Lyman, "An efficient method for the cryopreservation of fetal human liver hematopoeitic progenitor cells," (in eng), *Stem Cells,* vol. 19, no. 3, pp. 212-8, 2001, doi: 10.1634/stemcells.19-3-212.

[42] D. E. Pegg, "Principles of Cryopreservation," in *Cryopreservation and Freeze-Drying Protocols*, J. G. Day and G. N. Stacey Eds. Totowa, NJ: Humana Press, 2007, pp. 39-57.

[43] T. R. Henderson, R. F. Henderson, and J. L. York, "Effects of dimethyl sulfoxide on subunit proteins," (in eng), *Ann N Y Acad Sci,* vol. 243, pp. 38-53, Jan 27 1975, doi: 10.1111/j.1749-6632.1975.tb25342.x.

[44] F. C. Tan *et al.*, "Optimization of cryopreservation of stem cells cultured as neurospheres: comparison between vitrification, slow-cooling and rapid cooling freezing protocols," (in eng), *Cryo Letters,* vol. 28, no. 6, pp. 445-60, Nov-Dec 2007.

[45] S. L. Ebertz and L. E. McGann, "Cryoinjury in endothelial cell monolayers," (in eng), *Cryobiology,* vol. 49, no. 1, pp. 37-44, Aug 2004, doi: 10.1016/j.cryobiol.2004.04.003.

[46] G. D. Elliott, S. Wang, and B. J. Fuller, "Cryoprotectants: A review of the actions and applications of cryoprotective solutes that modulate cell recovery from ultra-low temperatures," *Cryobiology,* vol. 76, pp. 74-91, 2017/06/01/ 2017, doi: https://doi.org/10.1016/j.cryobiol.2017.04.004.

[47] B. J. Fuller, "Cryoprotectants: the essential antifreezes to protect life in the frozen state," *Cryoletters,* vol. 25, no. 6, pp. 375-388, // 2004.

[48] E. Casula, G. Traversari, S. Fadda, O. V. Klymenko, C. Kontoravdi, and A. Cincotti, "Modelling the osmotic behaviour of human mesenchymal stem cells," *Biochemical Engineering Journal,* vol. 151, p. 107296, 2019/11/15/ 2019, doi: https://doi.org/10.1016/j.bej.2019.107296.

[49] X. Xu, Y. Liu, Z. Cui, Y. Wei, and L. Zhang, "Effects of osmotic and cold shock on adherent human mesenchymal stem cells during cryopreservation," in *J Biotechnol*, vol. 162, no. 2-3). Netherlands: © 2012 Elsevier B.V, 2012, pp. 224-31.

[50] M. Davidovich-Pinhas and H. Bianco-Peled, "A quantitative analysis of alginate swelling," *Carbohydrate Polymers,* vol. 79, no. 4, pp. 1020-1027, 2010/03/17/ 2010, doi: https://doi.org/10.1016/j.carbpol.2009.10.036.

[51] M. J. Berridge, M. D. Bootman, and P. Lipp, "Calcium - a life and death signal," *Nature,* vol. 395, no. 6703, pp. 645-648, 1998/10/01 1998, doi: 10.1038/27094.

[52] L. Waters, M. P. Padula, D. C. Marks, and L. Johnson, "Cryopreserved platelets demonstrate reduced activation responses and impaired signaling after agonist stimulation," *Transfusion,* https://doi.org/10.1111/trf.14310 vol. 57, no. 12, pp. 2845-2857, 2017/12/01 2017, doi: https://doi.org/10.1111/trf.14310.

[53] L. Waters, M. P. Padula, D. C. Marks, and L. Johnson, "Calcium chelation: a novel approach to reduce cryopreservation-induced damage to frozen platelets," (in eng), *Transfusion,* vol. 60, no. 7, pp. 1552-1563, Jul 2020, doi: 10.1111/trf.15799.

[54] J. C. Kim, Y. Li, S. Lee, Y. J. Yi, C. S. Park, and S. H. Woo, "Effects of cryopreservation on Ca2+ signals induced by membrane depolarization, caffeine, thapsigargin and progesterone in boar spermatozoa," in *Mol Cells*, vol. 26, no. 6). Korea South, 2008, pp. 558-65.

[55] P. Mazur, "Kinetics of water loss from cells at subzero temperatures and the likelihood of intracellular freezing," (in eng), *The Journal of general physiology,* vol. 47, no. 2, pp. 347-369, 1963, doi: 10.1085/jgp.47.2.347.

[56] P. Mazur, S. P. Leibo, and E. H. Y. Chu, "A two-factor hypothesis of freezing injury: Evidence from Chinese hamster tissue-culture cells," *Experimental Cell Research,* vol. 71, no. 2, pp. 345-355, 1972/04/01/ 1972, doi: https://doi.org/10.1016/0014-4827(72)90303-5.

[57] K. Muldrew and L. E. McGann, "The osmotic rupture hypothesis of intracellular freezing injury," *Biophysical Journal,* vol. 66, no. 2, Part 1, pp. 532-541, 1994/02/01/ 1994, doi: https://doi.org/10.1016/S0006-3495(94)80806-9.

[58] J. O. M. Karlsson and M. Toner, "Long-term storage of tissues by cryopreservation: critical issues," *Biomaterials,* vol. 17, no. 3, pp. 243-256, 1996/01/01/ 1996, doi: https://doi.org/10.1016/0142-9612(96)85562-1.

[59] D. Gao and J. K. Critser, "Mechanisms of Cryoinjury in Living Cells," *ILAR Journal,* vol. 41, no. 4, pp. 187-196, 2000, doi: 10.1093/ilar.41.4.187.

[60] A. Bissoyi, B. Nayak, K. Pramanik, and S. K. Sarangi, "Targeting cryopreservation-induced cell death: a review," (in eng), *Biopreserv Biobank,* vol. 12, no. 1, pp. 23-34, Feb 2014, doi: 10.1089/bio.2013.0032.

[61] H. G. Wang *et al.*, "Ca2+-induced apoptosis through calcineurin dephosphorylation of BAD," (in eng), *Science,* vol. 284, no. 5412, pp. 339-43, Apr 9 1999, doi: 10.1126/science.284.5412.339.

[62] X. Li, G. Meng, R. Krawetz, S. Liu, and D. E. Rancourt, "The ROCK inhibitor Y-27632 enhances the survival rate of human embryonic stem cells following cryopreservation," (in eng), *Stem Cells Dev,* vol. 17, no. 6, pp. 1079-85, Dec 2008, doi: 10.1089/scd.2007.0247.

[63] J. Li and D. J. Mooney, "Designing hydrogels for controlled drug delivery," (in eng), *Nature reviews. Materials,* vol. 1, no. 12, p. 16071, 2016, doi: 10.1038/natrevmats.2016.71.

[64] B. Amsden, "Solute Diffusion within Hydrogels. Mechanisms and Models," *Macromolecules,* vol. 31, no. 23, pp. 8382-8395, 1998/11/01 1998, doi: 10.1021/ma980765f.

[65] A. D. Drozdov, A. A. Papadimitriou, J. H. M. Liely, and C. G. Sanporean, "Constitutive equations for the kinetics of swelling of hydrogels," *Mechanics of*

Materials, vol. 102, pp. 61-73, 2016/11/01/ 2016, doi: https://doi.org/10.1016/j.mechmat.2016.08.012.

[66] W. J. Armitage, "Cryopreservation of animal cells," (in eng), *Symposia of the Society for Experimental Biology,* vol. 41, pp. 379-393, 1987 1987.

[67] J. P. Acker, A. Larese, H. Yang, A. Petrenko, and L. E. McGann, "Intracellular ice formation is affected by cell interactions," in *Cryobiology*, vol. 38, no. 4). Netherlands: 1999 Academic Press., 1999, pp. 363-71.

[68] K. Muldrew and L. E. McGann, "Mechanisms of intracellular ice formation," (in eng), *Biophys J,* vol. 57, no. 3, pp. 525-32, Mar 1990.

[69] L. L. Kuleshova, S. S. Gouk, and D. W. Hutmacher, "Vitrification as a prospect for cryopreservation of tissue-engineered constructs," *Biomaterials,* vol. 28, no. 9, pp. 1585-1596, 2007/03/01/ 2007, doi: https://doi.org/10.1016/j.biomaterials.2006.11.047.

[70] G. Zhao, X. Liu, K. Zhu, and X. He, "Hydrogel Encapsulation Facilitates Rapid-Cooling Cryopreservation of Stem Cell-Laden Core–Shell Microcapsules as Cell–Biomaterial Constructs," *Advanced Healthcare Materials,* https://doi.org/10.1002/adhm.201700988 vol. 6, no. 23, p. 1700988, 2017/12/01 2017, doi: https://doi.org/10.1002/adhm.201700988.

[71] H. Huang *et al.*, "Alginate Hydrogel Microencapsulation Inhibits Devitrification and Enables Large-Volume Low-CPA Cell Vitrification," *Advanced Functional Materials,* https://doi.org/10.1002/adfm.201503047 vol. 25, no. 44, pp. 6839-6850, 2015/11/01 2015, doi: https://doi.org/10.1002/adfm.201503047.

[72] H. Gurruchaga *et al.*, "Advances in the slow freezing cryopreservation of microencapsulated cells," *Journal of Controlled Release,* vol. 281, pp. 119-138, 2018/07/10/ 2018, doi: https://doi.org/10.1016/j.jconrel.2018.05.016.

[73] E. Umemura, Y. Yamada, S. Nakamura, K. Ito, K. Hara, and M. Ueda, "Viable cryopreserving tissue-engineered cell-biomaterial for cell banking therapy in an effective cryoprotectant," (in eng), *Tissue Eng Part C Methods,* vol. 17, no. 8, pp. 799-807, Aug 2011, doi: 10.1089/ten.tec.2011.0003.

[74] N. A. Peppas and A. S. Hoffman, "1.3.2E - Hydrogels," in *Biomaterials Science (Fourth Edition)*, W. R. Wagner, S. E. Sakiyama-Elbert, G. Zhang, and M. J. Yaszemski Eds.: Academic Press, 2020, pp. 153-166.

[75] J. A. Brassard and M. P. Lutolf, "Engineering Stem Cell Self-organization to Build Better Organoids," *Cell Stem Cell,* vol. 24, no. 6, pp. 860-876, 2019/06/06/ 2019, doi: https://doi.org/10.1016/j.stem.2019.05.005.

[76] H. J. Kim, R. Castañeda, T. H. Kang, S. Kimura, M. Wada, and U.-J. Kim, "Cellulose hydrogel film for spheroid formation of human adipose-derived stemcells," *Cellulose,* vol. 25, no. 4, pp. 2589-2598, 2018/04/01 2018, doi: 10.1007/s10570-018-1732-4.

[77] J. N. Harvestine, N. L. Vollmer, S. S. Ho, C. A. Zikry, M. A. Lee, and J. K. Leach, "Extracellular Matrix-Coated Composite Scaffolds Promote Mesenchymal Stem Cell Persistence and Osteogenesis," (in eng), *Biomacromolecules,* vol. 17, no. 11, pp. 3524-3531, Nov 14 2016, doi: 10.1021/acs.biomac.6b01005.

[78] A. I. Hoch, V. Mittal, D. Mitra, N. Vollmer, C. A. Zikry, and J. K. Leach, "Cell-secreted matrices perpetuate the bone-forming phenotype of differentiated mesenchymal stem cells," (in eng), *Biomaterials,* vol. 74, pp. 178-87, Jan 2016.

[79] K. C. Murphy, A. I. Hoch, J. N. Harvestine, D. Zhou, and J. K. Leach, "Mesenchymal Stem Cell Spheroids Retain Osteogenic Phenotype Through α2β1 Signaling," (in eng), *Stem Cells Transl Med,* vol. 5, no. 9, pp. 1229-37, Sep 2016.

[80] M. W. Laschke and M. D. Menger, "Life is 3D: Boosting Spheroid Function for Tissue Engineering," *Trends in Biotechnology,* vol. 35, no. 2, pp. 133-144, 2017/02/01/ 2017, doi: https://doi.org/10.1016/j.tibtech.2016.08.004.

[81] R. Foty, "A simple hanging drop cell culture protocol for generation of 3D spheroids," (in eng), *J Vis Exp,* no. 51, May 6 2011.

[82] M. A. Gionet-Gonzales and J. K. Leach, "Engineering principles for guiding spheroid function in the regeneration of bone, cartilage, and skin," *Biomedical Materials,* vol. 13, no. 3, p. 034109, 2018/03/21 2018, doi: 10.1088/1748-605x/aab0b3.

[83] R. J. McMurtrey, "Roles of Diffusion Dynamics in Stem Cell Signaling and Three-Dimensional Tissue Development," *Stem Cells and Development,* vol. 26, no. 18, pp. 1293-1303, 2017/09/15 2017, doi: 10.1089/scd.2017.0066.

[84] S. A. Ruiz and C. S. Chen, "Emergence of Patterned Stem Cell Differentiation Within Multicellular Structures," *STEM CELLS,* https://doi.org/10.1634/stemcells.2008-0432 vol. 26, no. 11, pp. 2921-2927, 2008/11/01 2008, doi: https://doi.org/10.1634/stemcells.2008-0432.

[85] R. Mori, Y. Sakai, and K. Nakazawa, "Micropatterned organoid culture of rat hepatocytes and HepG2 cells," in *J Biosci Bioeng*, vol. 106, no. 3). Japan, 2008, pp. 237-42.

CHAPTER 7

Cell cycle evaluation during the multicellular spheroid formation of previously cryopreserved cells

7.1 Introduction

This chapter describes a transition of the internal geometry of the alginate hydrogel capsules from chapter 6. Specifically, we shifted from using a rubber mold that created frozen disks to a PDMS mold that enabled the formation of a convex frozen disk. When this frozen disk is used with thaw-induced gelation (TIG), the alginate hydrogel capsule recapitulates the convex ice as a concave microwell, more analogous to the typical geometries used for spheroid formation [1-3]. To interrogate the formation of spheroids from post-cryopreserved cells within capsules and microwells, we incorporate a unique evaluation system, fluorescence ubiquitination cell cycle indicator (FUCCI) expressing human embryonic kidney cells (HEK-293T). Specifically, we hypothesized that the capsules could improve metabolic recovery due to the ability of the capsules to promote steady diffusion of cryopreservation agents (CPAs). Therefore, we evaluate the changes in spheroid formation, metabolic activity, and cell cycle stage for post-cryopreserved cells that were immediately plated in microwells, diluted after pelleting via centrifugation and encapsulated within alginate hydrogel capsules using TIG. While the results in this chapter suggest the HEK-293T cells are robust to potential damage from post-cryopreservation osmotic stress, this chapter highlights a method for forming spheroids in capsules formed by TIG analogous to microwell, hanging drop, and Aggrewell™ systems typically employed in spheroid formation.

Multicellular spheroids have been utilized as models of the 3D tissue environment for several decades, ranging from tumor models to brain organoids [4-8]. However, the formation of spheroids from cryopreserved cells remains understudied. Most studies investigate methods to cryopreserve spheroids, including employing hydrogels [9, 10]. Regardless, these studies often highlight the need to address the same challenge to industrial and clinical applications: the need for large-scale culture and cryopreservation of organoids and spheroids. One challenge these studies might address is how the spheroid size, and any accompanying encapsulating hydrogel, become an obstacle to the successful diffusion and saturation of the cryoprotectant [11]. Contrarily, encapsulating the organoids in a polymeric material can also be cryoprotective by reducing intracellular and extracellular ice formation [9, 12, 13]. Therefore, in addition to the balance between ice formation and cell dehydration, the cryopreservation of spheroids and cells in hydrogels also involves a balance between CPA penetration and ice formation.

One alternative to cryopreserving spheroids is to form spheroids post-cryopreservation. Similarly, the alternative to cryopreserving cells encapsulated in a hydrogel would be to encapsulate them after thawing. Notably, cryopreservation is known to reduce cadherin binding and reduce the deposition of extracellular matrix proteins [14], indicating a pertinent challenge in developing spheroids from previously cryopreserved cells. Despite this challenge, cell-cell adhesion initiates survival and proliferation for anchorage-dependent cells [15]; therefore, post-cryopreservation formation of spheroids might offer unique advantages for post-cryopreserved cell

function recovery compared to 2D culture. Furthermore, this perspective could represent an appealing alternative to cryopreserving tissue-engineered constructs.

In this chapter, we postulate that the FUCCI system can provide information on the recovery of cells from the cryopreserved state. FUCCI is a set of red and green fluorescence probes tagging Cdt1 and geminin, respectively [16-18]. These degrade at different cell cycle phases, resulting in cell nuclei appearing red in G1 and green in the S/G2/M phase [19]. Using FUCCI-expressing HEK-293T cells, we further interrogate the ability of post-cryopreserved cells to form spheroids within alginate hydrogel capsules that are crosslinked when thawing. While the utility of FUCCI-expressing cells with spheroids has been briefly explored, this is the first instance of this method being extended to study changes in cell cycle from previous cryopreserved cells.

7.2 Methods

7.2.1 Cell culture

Human embryonic kidney cells, specifically HEK-293T cells, were cultured in Dulbecco's modified Eagle's medium (DMEM, Invitrogen) supplemented with 10% fetal bovine serum (FBS, Gibco) and 1% penicillin-streptomycin (Invitrogen), forming our complete media (DMEMc) as previously described [3]. Cells were expanded in tissue culture plates at 37 °C and under 5% CO_2. An initial experiment was carried out to compare the formation of spheroids on tissue culture plates (TCP), agarose, and the alginate hydrogel capsules formed by TIG. These agarose and capsule conditions will be described below. Additionally, cell-adherent tissue culture plates and ultra-low attachment surface round-bottom 96-well plates (Corning) were used for 2D and spheroid culture, respectively. For brevity, the round bottom 96-well plates will be referred to as microwells (µWells). Cells were cryopreserved using a freezing solution containing 10% (v/v) dimethyl sulfoxide (Me_2SO, Sigma) and 20% (v/v) fetal bovine serum (FBS; Invitrogen). For conditions where cells were encapsulated in alginate hydrogel capsules, the freezing solution also contained 100 mM $CaCl_2$.

7.2.2 Transduction of HEK-293T cells with a FUCCI encoding lentivector

Transduction of cells with FUCCI encoding lentivectors was specifically performed with HEK-293T (ATCC) as previously described [16]. Briefly, HEK-293T cells were seeded into a 24-well plate (3×10^4 cells/well) and cultured in DMEM. Next, HEK-293T cells were cultured with approximately 9000 TU (MOI 0.3) of FUCCI lentivectors for four hours before the vector-loaded media was aspirated and replaced with fresh

media. Cell media was changed every day until cells were confluent. FUCCI transduced HEK-293T cells were then passaged and underwent a serial dilution protocol as previously described for selecting a pure FUCCI expressing HEK-293T line [20]. FUCCI-positive wells were determined via fluorescent microscopy (Axio Vert.A1; Zeiss) and chosen for expansion. These FUCCI-positive wells received media changes every other day until confluent. After which, the cells were passaged and seeded on 24-well plates. This process was repeated sequentially for a 6-well plate and finally a T75 flask. Cells were continually monitored in culture for both FUCCI activity and morphological stability.

7.2.3 Agarose-coated plates for spheroid formation

HEK-293T spheroids were formed in agarose-coated 96-well plates as previously described [21]. Following the liquid overlay method, a thin film of autoclaved 1% (w/v) agarose (Sigma) was used to coat the bottom of 96-well plates. Agarose was warmed to achieve a liquid state. Next, 75 µL of sterile agarose was dispensed into the 96-well plates to form a slightly concave shape. These plates were then allowed to cool and stored in the fridge before use. Before being seeded with cells, plates were exposed to UV light for 15 minutes to sterilize the plates further. Ten thousand cells were seeded per well with 100 µL of cell media. Spheroids were formed from post-cryopreserved cells over three days before analysis.

7.2.4 Alginate hydrogel capsule formation via TIG

LF10/60 alginate polymer (molecular weight ~ 120-150 kDa and >60% G-block; purchased from FMC Biopolymers) was used in this chapter for hydrogel formation via TIG. All alginate hydrogels were purified, and sterilized alginate polymer was prepared as previously described [22, 23]. Briefly, one gram of alginate was dissolved in 100 mL of deionized (DI) water. Next, 0.5 grams of activated charcoal (Sigma) was added and mixed for 30 minutes via a magnetic stirrer. Then, the alginate solution is sterilized using a filter (0.22 µm, Thermo Fisher Scientific), lyophilized, and stored in a freezer. A 1% (w/v) alginate solution was prepared by mixing the dry polymer in an isotonic saline solution (0.9% (w/v) NaCl). The modified-cryopreserving solution contained 100 mM calcium chloride (Sigma), 10% (v/v) Me_2SO, 20% (v/v) FBS, and DMEM, unless stated otherwise. Only one other condition was used, in which a 75 mM calcium chloride concentration was used. Calcium chloride was added to the cellular freezing solution from a 6 M stock to create the final concentrations.

Gelation of the alginate hydrogel capsules was performed using TIG, as described in previous chapters [24], with some modification. Specifically, the freezing solution was pre-chilled to 4 °C prior to mixing with cells to minimize cytotoxic exposure to Me_2SO. Next, the cell-containing cryopreservation solution was pipetted into wells. Wells were formed from either rubber molds placed on a glass plate or wells made from polydimethylsiloxane (PDMS; Sylgard). The rubber mold was made by cutting out holes 6 mm in diameter, resulting in a mold that held 50 µL. The PDMS mold was designed by 3D printing a positive mold with the geometry of each well being a cylinder topped with a cylinder. The 6 mm in diameter cylinder met with the base of the cone. The height of the cylinder and cone was 1.5 and 1 mm, respectively, for a total of 2.5 mm.

Consequently, the PDMS negative mold could hold 50 µL. Once frozen, the cryopreservation solution matched the shape of the positive mold's geometry.

Cells were encapsulated with the alginate hydrogels through TIG. Gelation was initiated by submersion and melting the cryopreserved cell solution within a 1% (w/v) alginate solution at 37 ºC. After melting and crosslinking (approximately 2 minutes), the capsules were then scooped out of the beaker and placed in prewarmed cell media to remove excess alginate polymer and promote dilution of the CPA. Subsequently, hydrogel capsules were moved to tissue culture plates filled with DMEM.

7.2.5 Fabrication of PDMS molds used as cryopreservation vessels

The 3D printed negative mold used to fabricate the positive mold made of PDMS was designed in Autodesk Fusion 360 (Autodesk). The geometry that will hold the ice was spaced out a minimum distance of 2 mm. The layer height was approximately 0.1mm. The walls to hold in the uncured PDMS were a minimum of 5 mm. We printed the design in polylactic acid (PLA) at a flow temperature of 190 °C. A 9:1 mixture of polymer to curing agent was created, placed under a vacuum to remove bubbles, and poured over the 3D printed negative mold. Samples were cured overnight at 40 °C to prevent warping of the 3D-printed mold at higher temperatures. PDMS positive molds were removed from the PLA container using a surgical knife and spatula. PDMS molds were then placed back in an oven at 70 °C to continue curing. After curing, PDMS molds were washed, dried, and autoclaved before use. During use, PDMS molds loaded with cells to be cryopreserved were placed in Petri dishes (Corning) to prevent contamination and then moved to our custom cryopreservation vessel.

7.2.6 Post-cryopreservation characterization of cells

Metabolic activity of post-cryopreserved cells was performed via an MTT assay and measuring spheroid diameter where appropriate. For all experiments, 10,000 post-cryopreserved cells were seeded per well or within the hydrogel capsules. MTT assays were performed three days post-cryopreservation. Specifically, 10 µL of 5 mg/mL tetrazolium dye MTT (Sigma) to each well and incubating for three hours. Next, 100 µL of a solubilizing solution was added. The solubilizing solution contained 40% (v/v) dimethylformamide (DMF; Sigma), 2% (v/v) glacial acetic acid (Sigma), and 16% (w/v) sodium dodecyl sulfate (SDS; Sigma) [25]. Samples were protected from light by covering plates with aluminum foil and placed on a shaker for one hour. The total absorbance of formazan salt was quantified via the Spectramax ® i3 plate reader (Molecular Devices) at 570 nm and averaged per condition (n = 8). The spheroid formation was characterized by measuring the diameters of cell aggregates over three days. Spheroids were imaged within the microwells or alginate capsules using phase-contrast microscopy (Zeiss Axio Vert A.4) and measured using ImageJ (NIH) (n = 8).

7.2.7 Quantitative analysis of FUCCI-expressing HEK-293T cells

Estimation of proliferation within spheroids was quantified via the fluorescence of FUCCI-expressing HEK-293T cells. Specifically, the mean gray fluorescence value was obtained from images taken with a phase-contrast microscope and calculated with ImageJ. The mean gray value represents the average gray value between 0-255 of each pixel within the selection. The selection used is a field of view that was 1.02 x 0.77

mm. Furthermore, the focus was adjusted to maximize the mean gray value for green fluorescence. The same exposure of 4095 ms was used for both red and green fluorescence.

7.2.8 Statistical analysis

Sample sizes are provided with each figure legend and visualized in figures as individual data points, where applicable. Results are presented as mean values with standard deviations. Statistical significance was asserted at $p < 0.05$ after performing a Student's t-test, one-way ANOVA, two-way ANOVA, and Tukey's multiple comparison tests where appropriate. All analyses were performed using Graph-Pad Prism software (GraphPad Software Inc).

7.3 Results

7.3.1 Post-cryopreserved cells on different culture substrates

We used a frozen disk with TIG which generated a flat surface with multiple spheroids formed from post-cryopreserved cells. Notably, while cells adhere to TCP, allowing for media changes without disturbing the cells, it is challenging to change media with the agarose wells without disturbing the spheroids. Consequently, there was noticeable debris surrounding cellular aggregated in the agarose wells than in other conditions (Figure 7.1A). Although the alginate capsules formed by TIG did not have this debris, the geometry does not have the lowest point for cells to settle. Regardless, spheroids continue to grow over time (Figure 7.1B), even aggregating together into large spheroids (Figure 7.1C). Although the aggregation and growth of cells suggest their viability, cells on these non-adherent surfaces had less absorbance from an MTT assay than cells cultured on TCP (Figure 7.1D). However, we noticed spheroids did not completely break apart and solubilize the formazan salt during the MTT assay. Together, these data raise two concerns: 1) alginate capsules formed via TIG are not as analogous to non-adherent microwell systems often used for spheroid formation, and 2) MTT assays face challenges with solubilizing the signal with aggregated cells.

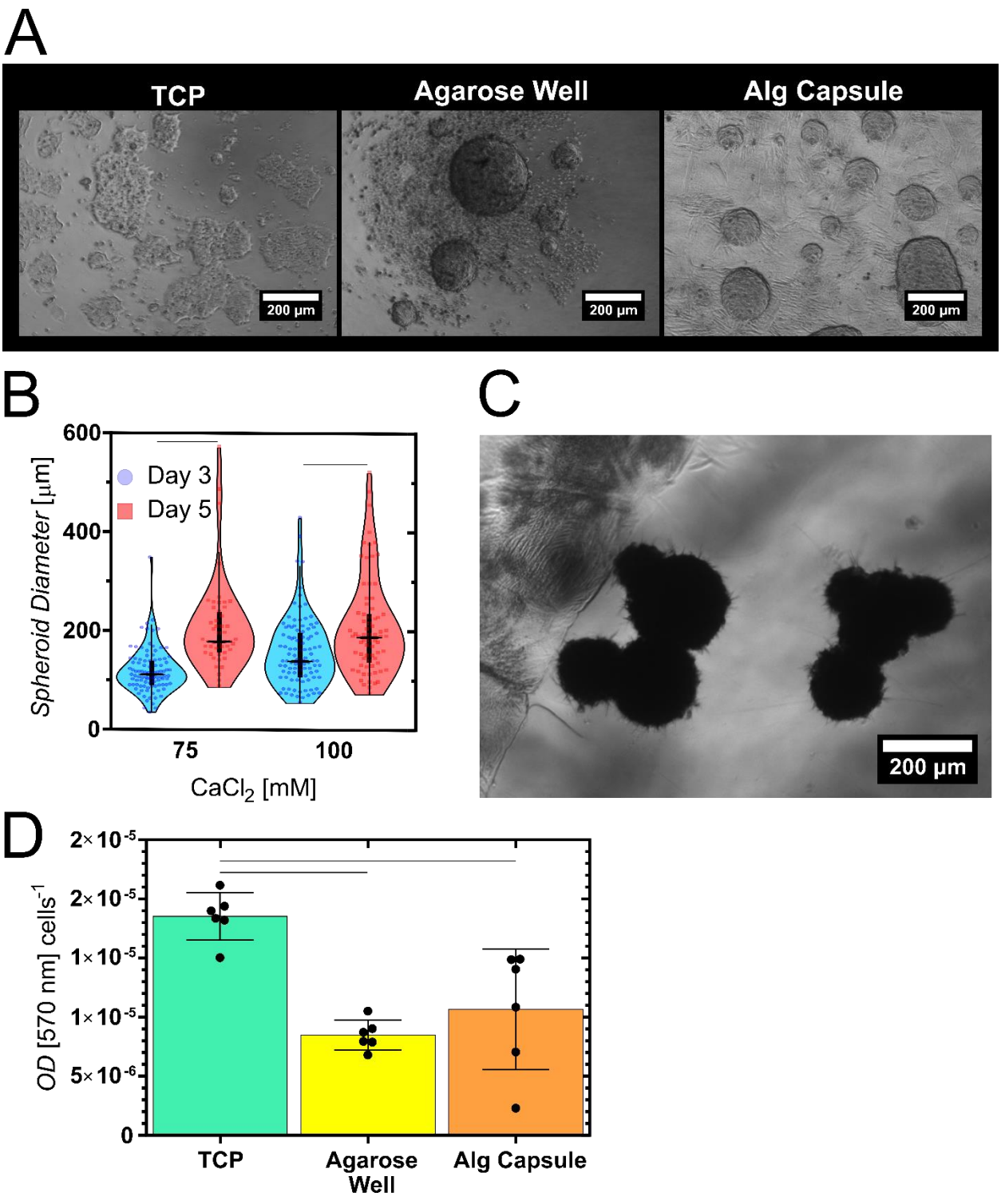

Figure 7.1 Metabolic activity of post-cryopreserved cells on various culture surfaces. Post-cryopreserved cells were seeded in tissue culture plates (TCP), wells containing agarose, or encapsulated in an alginate (Alg) hydrogel capsule. Over three

days, cells within the agarose well and capsules formed multiple spheroids (A). There is noticeable debris in the agarose wells surrounding the spheroids, which is not apparent in the alginate capsules. Spheroids in alginate capsules grew over time (B), often through the aggregation of multiple spheroids (C). Three days post-cryopreservation, an MTT assay was performed. The TCP condition was significantly more metabolically active than the other conditions (n = 6) (D). Violin plot presents the mean, interquartile range, whiskers, and individual data points. The bar graph presents the mean ± SD with individual data points. Lines between groups represent select statistically significant differences ($P < 0.05$) assessed by performing a one-way ANOVA and a Tukey's multiple comparison test.

7.3.2 TIG of capsules with a microwell structure

To generate the hydrogel capsules via TIG that better recapitulate the microwell structure, commonly utilized in spheroid-forming techniques, we modified the geometry of the frozen cryopreservation solution. The new ice geometry was accomplished by first 3D printing a mold for PDMS (Figure 7.2A). Notably, infill percentage, layer height, and PDMS curing temperature were essential in maintaining the cone geometry with a fused deposition modeling (FDM) 3D printer. Specifically, too much infill (>40%) led to destructive warping when curing at temperatures above 50 °C. Alternatively, too little infill (<10%) led to pillowing that would not necessarily damage the mold but could cause leakage of the uncured PDMS. We found a balance with low initial curing temperatures (35 – 40 °C), 20% infill, and 0.0875 mm layer heights. These conditions created smooth-surfaced PDMS molds that held cryopreserved cells (Figure 7.2B). Incredibly, the 3D printed mold layers were copied over to the PDMS mold and then onto the inner surface of the alginate hydrogel capsule (Figure 7.2C). Furthermore, after TIG, the capsules had a shell thickness between 550 and 650 nm (Figure 7.2D), which was not statistically different from the capsules formed using the rubber molds with the same solution volume containing the identical concentrations of alginate and calcium. Importantly for our objective, the new internal geometry of the capsules facilitated the formation of a single primary spheroid similar to the condition we observed with the agarose wells (Figure 7.2E), despite the visible layers from the 3D-printed mold. Furthermore, these capsules did not have debris surrounding the spheroids, as was observed with the agarose wells. These new capsules were used for all following conditions using TIG.

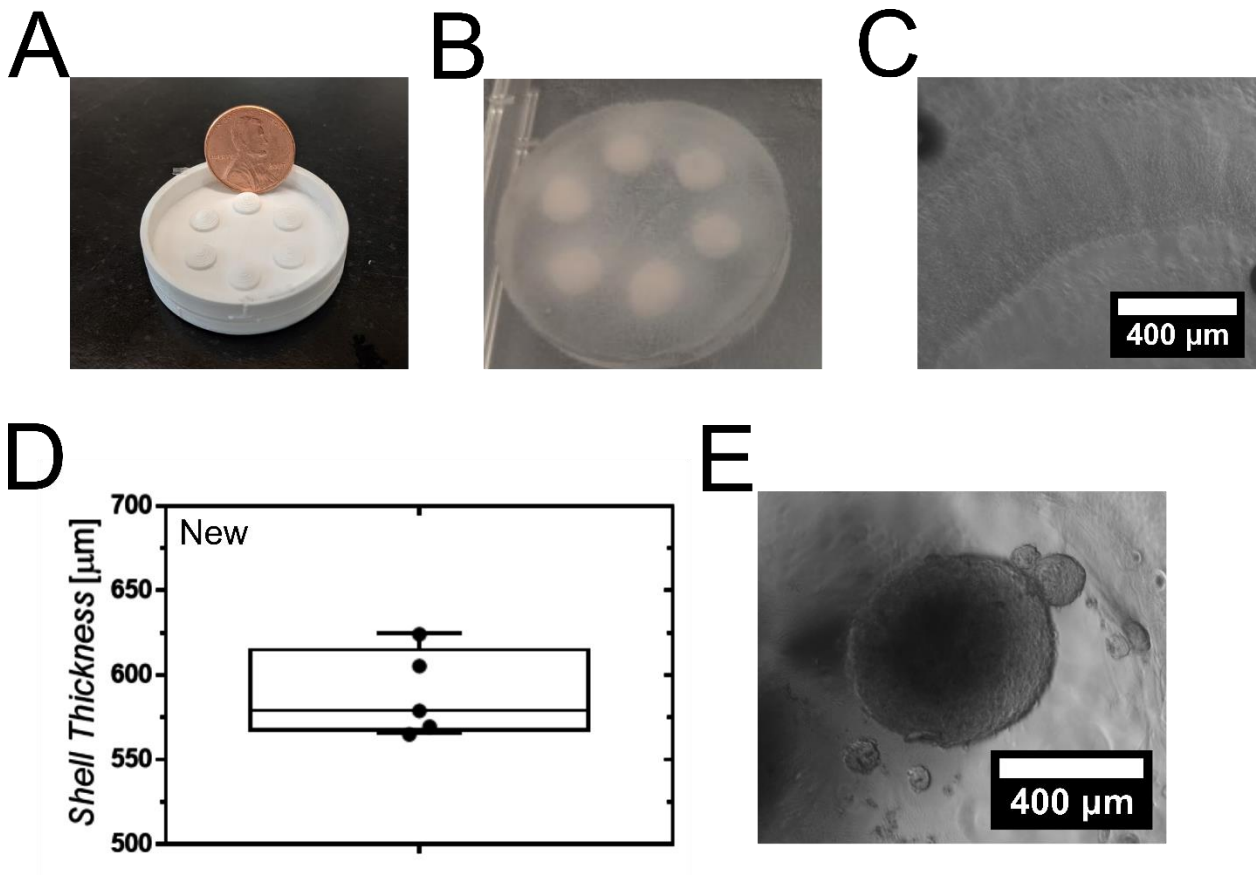

Figure 7.2 New mold for alginate capsules generates a single primary spheroid. Using a 3D printed positive mold (A), a PDMS negative mold can be generated and used as the vessel for cryopreserving cells (B). The alginate capsule accurately recapitulates the geometry of the 3D printed positive mold, seen by the ridges on the inner surface of the hydrogel capsule, representing the individual 3D-printed layers (C). Overall, these capsules had a shell thickness between 550 and 650 µm (D). Three days post-cryopreservation and encapsulation, a single large spheroid was formed (E). Box plot represents the mean, interquartile range, and range of individual capsules, whose specific values are also shown.

7.3.3 Characterization of FUCCI-expressing HEK-293T cells

After transduction of the FUCCI-expressing HEK-293T cells, we set out to characterize the signal they produced. First, we confirm that the transduction did not significantly impact the metabolic activity of these cells compared to non-transduced cells of a similar passage (Figure 7.3A). Next, we cultured these cells for a week, measuring the fluorescence from fields of view full of cells. The magnitude of green and red fluorescence did not greatly change over this period. Specifically, green fluorescence increased by about 17% after thawing, and red fluorescence increased by about 11% from day one to day four. However, there was a dip in green fluorescence when the cells became about 80% confluent (Figure 7.3B). Representative images of the cells at different times post-cryopreservation indicate the cell-cycle state of individual cells (Figure 7.3C). Most cells initially expressed red fluorescence, which became green as cells proliferated. As the cell culture became about 80% confluent, more cells fluoresced red. Notably, the green fluorescence was much brighter than the red under identical conditions. The brightness for images was adjusted, but no adjustments were made for quantitative analysis.

Next, we attempted to quantitatively compare fluorescence signal over three days between HEK-293T cells on TCPs and microwells. There was no significant difference in either red or green fluorescence over these three days for cells on TCP. However, there was a significant increase in green fluorescence for cells in microwells, where spheroids formed. Interestingly, there was a significant difference in green fluorescence on day two between microwells initially loaded with 5k cells versus 10k cells. Specifically, there was brighter green fluorescence with the lower initial cell

number. Nevertheless, there was no significant difference between the initial seeded number of cells by the third day.

7.3.4 Post-cryopreservation dilution of CPA for HEK-293T cells in microwells

To compare assessment strategies of post-cryopreserved cells, we interrogated the role of CPA dilution via centrifugation after thawing cells into DMEMc. Spheroids formed in microwells had comparable spheroid diameters of similar structures over three days (Figure 7.4A & B). Despite this similarity, cells centrifuged to replace the media containing Me_2SO with fresh DMEMc and resuspended were significantly more metabolically active than cells seeded directly into the microwells (Figure 7.4C). Additionally, microwells containing cells that underwent this dilution had significantly more red fluorescence at day two than cells directly seeded (Figure 7.4D). The directly seeded cells also had significantly more green fluorescence at day three post-cryopreservation than the diluted cells. Together, this data indicates that despite similar spheroid formation, dilution of CPA led to slightly more metabolic cells that, on the third day, were potentially less proliferative than the directly seeded cells.

7.3.5 Spheroid formation from post-cryopreserved cells

Spheroid formation was assessed by their size and metabolic activity from an MTT assay three days post-cryopreservation in microwells and alginate hydrogel capsules formed by TIG. Each condition resulted in significantly different spheroid sizes (Figure 7.5A). Within microwells, cells that were not cryopreserved resulted in the smallest spheroids in microwells, and the largest spheroids were formed from

cryopreserved cells. Cryopreserved cells within the hydrogel capsules were of intermediate size with the other two conditions. The metabolic activity in the microwells or alginate capsules reflected the trends observed with spheroid size (Figure 7.5B). When normalizing this data to the average spheroid volume, both cryopreserved cell conditions are significantly less metabolically active than the group with cells that were previously passaged. Overall, these data indicate uncertainty due to cell density in spheroids and the resulting metabolic activity due to cryopreservation.

7.3.6 FUCCI-expression of post-cryopreserved HEK-293T spheroids

HEK-293T cells transduced with the FUCCI system were seeded into microwells or encapsulated in alginate hydrogel capsules post-cryopreservation. Overall, capsules had greater fluorescence from cells than microwells, a statistically significant trend at days one and three for red fluorescence and days two and three for green fluorescence (Figure 7.6A & B). Similar to the previous measurement of FUCCI signal from spheroids, spheroids in capsules had a significant increase in green fluorescence between days one and three. Unlike the MTT assay, the difference in green fluorescence was amplified when normalized to average spheroid volume (Figure 7.6B). After normalization, the brightness of green fluorescence was over two times greater in the capsules than in the microwells. From the representative images, both conditions creased similarly round spheroids (Figure 7.6D). Spheroids within the capsules were smaller but had localized areas of bright green fluorescence that the spheroids in the microwells did not. Together, these data highlight how FUCCI-systems can be used to measure cell states of spheroids post-cryopreservation.

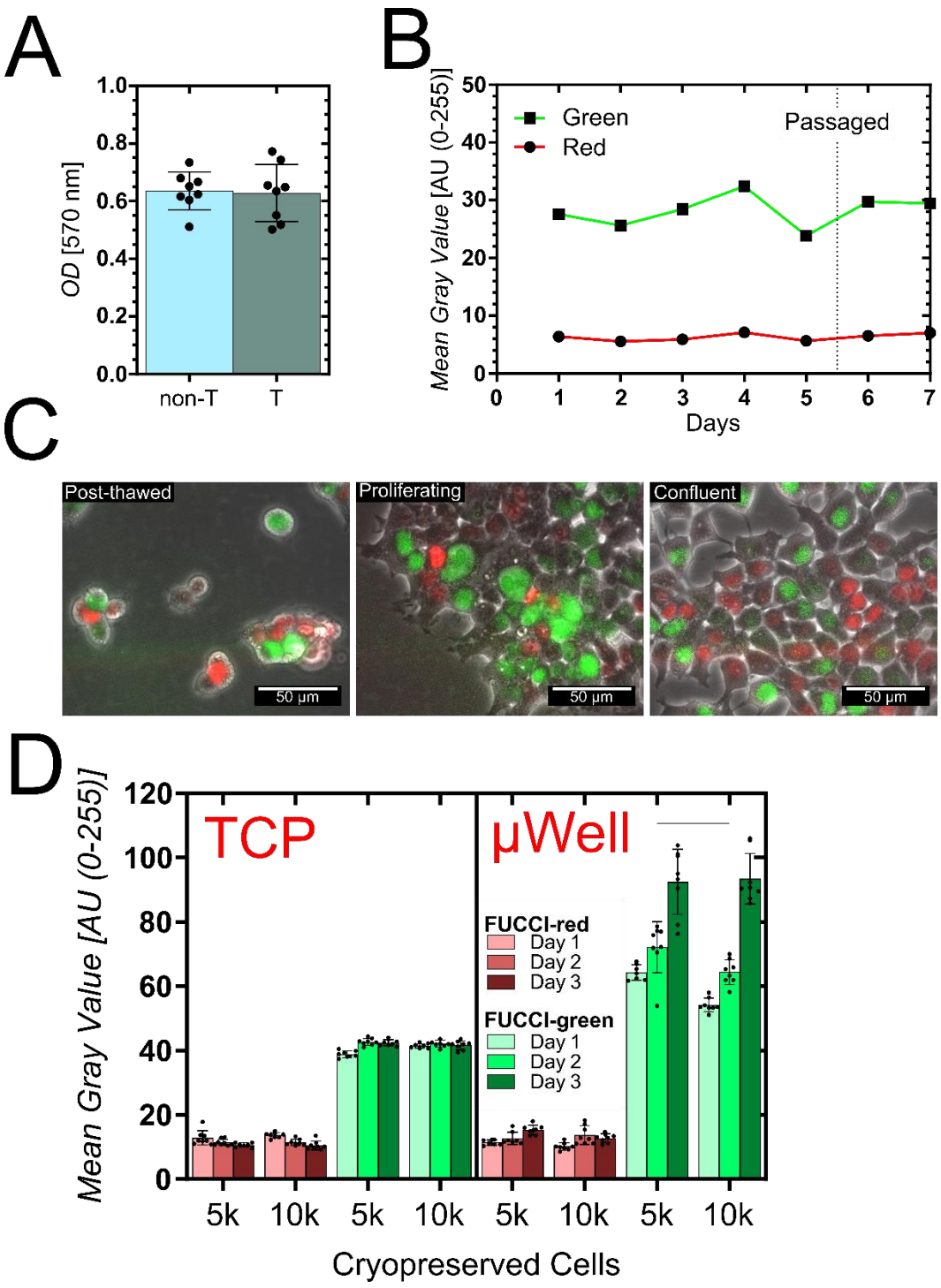

Figure 7.3 FUCCI-expressing cells reveal their state in the cell cycle. After transducing HEK-293T cells to express the FUCCI system (T), the metabolic activity of these cells was similar to non-transduced (non-T) cells of a similar passage (A). When

culturing these cells, they could adhere to the surface of culture dishes, reaching confluency around day five. Interestingly, around the time of confluency, there was an appreciable increase and dip in the measure mean absorbance value of green fluorescence (B). At the level of individual cells, post-thawed from a cryopreserved state, most cells appear to present red fluorescence, representing the G1 phase (C, left). As cells proliferated (middle) to confluency (right), cells transitioned from mainly S, G2, and M phases (green) back to the G1 phase (red). There was little difference between cell number and fluorescence (D). There was a significant difference between 5k and 10k cells only on the second day. Although cells on tissue culture plates (TCP) did not have a change in fluorescence magnitude over time, cells within non-adherent microwells (μWell) did have a significant increase in green fluorescence between the first and last day for both 5k and 10k cell conditions. Bar graphs represent the mean ± SD with individual data points shown (n = 8). Lines between groups represent select statistically significant differences ($P < 0.05$) assessed by performing a Student's t-test (A) or a two-way ANOVA and a Tukey's multiple comparison test (D).

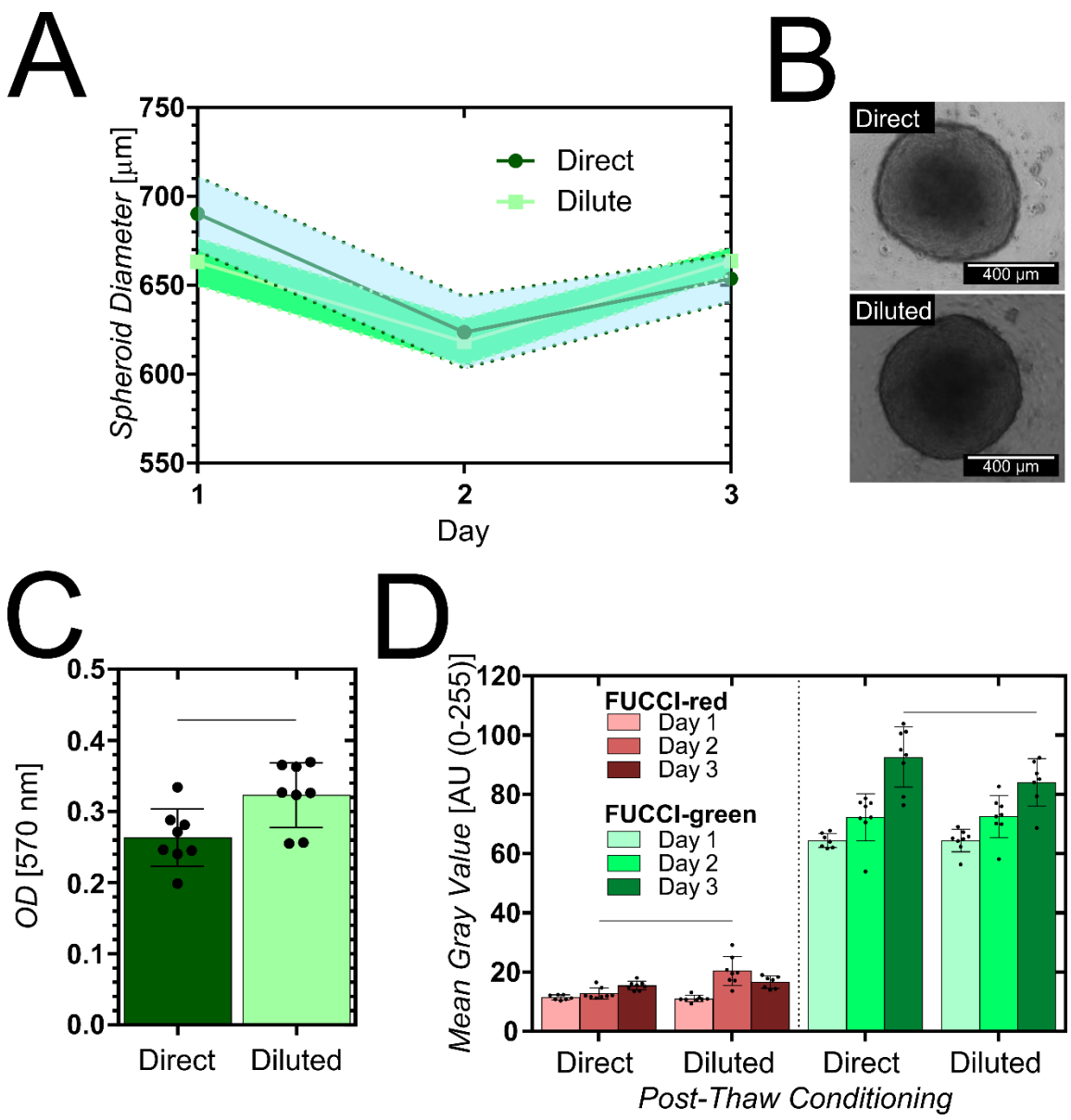

7.4 Post-cryopreservation dilution of CPA effects on spheroid formation. There was no significant difference in spheroid diameters over three days for post-cryopreserved cells that were either directly seeded (Direct) on non-adherent microwells or diluted via centrifugation (Diluted) (A). Spheroid characteristics also appear similar in roundness and a lack of cell debris in the microwell (B). However, directly plating the cells did result in a significant decrease in metabolic activity compared to diluted conditions. Fluorescence from FUCCI indicate the diluted condition had significantly

more cells in G1 phase (red) at day 2 and less cells in S, G2, and M phases (green) at day 3 compared to directly seeded cells. Bar graphs represent the mean ± SD with individual data points shown (n = 8). Lines between groups represent select statistically significant differences ($P < 0.05$) assessed by performing a student's t-test (C) or a two-way ANOVA and a Tukey's multiple comparison test (D).

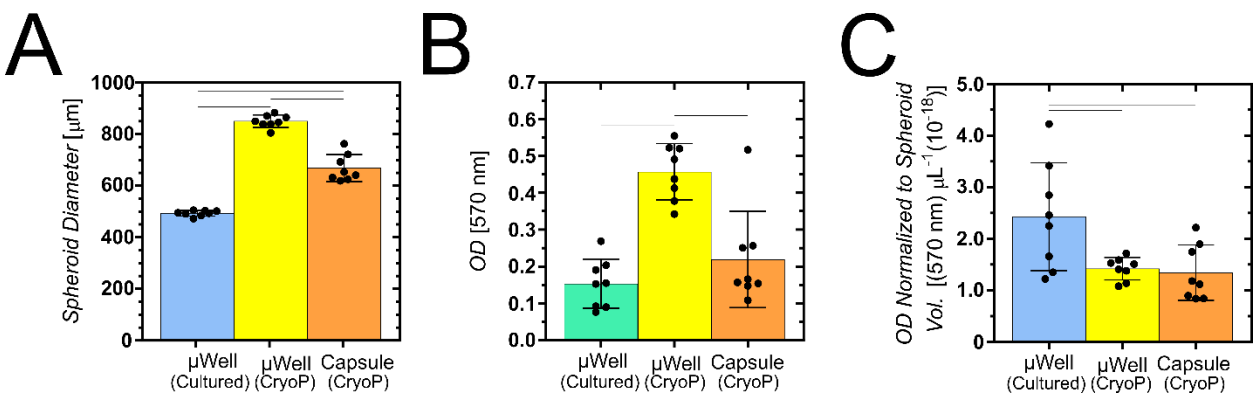

7.5 Post-cryopreserved cells in microwells appear to have similar metabolic activity as alginate capsules. Three days post-cryopreservation (CryoP), the spheroids in microwells (µWell) were significantly larger than those formed from uncryopreserved cells (Cultured) and post-cryopreserved cells in alginate capsules (Capsules). Additionally, these previously cryopreserved cells seeded in microwells appear more metabolically active via an MTT assay (B), but when normalized to the spheroid volume, the condition with uncryopreserved cells appear more metabolically active than the cryopreserved cell groups. Bar graphs represent the mean ± SD with individual data points shown (n = 8). Lines between groups represent select statistically significant differences ($P < 0.05$) assessed by a one-way ANOVA and a Tukey's multiple comparison test (D).

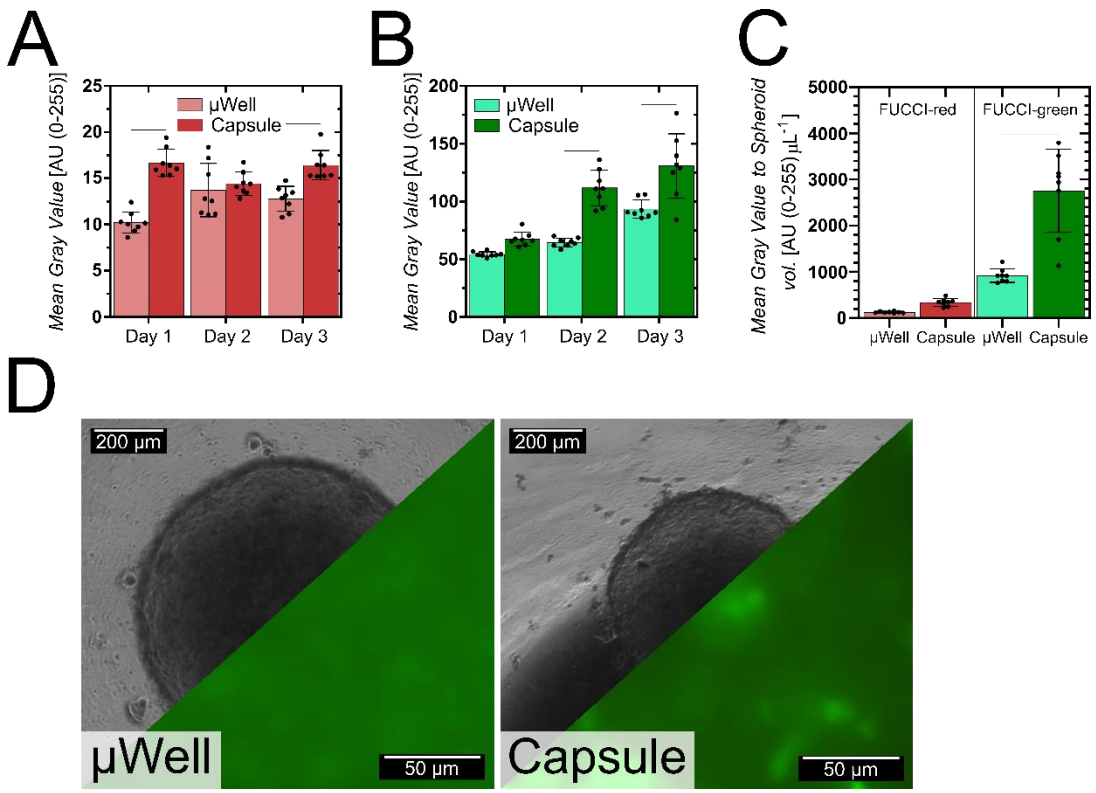

Figure 7.6 Post-cryopreserved cells in microwells displayed less FUCCI-derived fluorescence than cells in alginate capsules. Although both culture conditions had similar trends over three days post-cryopreservation, cells within the alginate capsules (Capsule) had significantly greater fluorescence signal than microwells (μWell) at day one (red), day two (green), and day three (red and green) (A & B). When normalized to spheroid volume at day three, these differences were amplified (C). Images of spheroids and a composite image of fluorescence signal at a higher magnification focused on the center of the spheroid highlight localized bright green fluorescence in the alginate capsules (D). Bar graphs represent the mean ± SD with individual data points shown (n = 8). Lines between groups represent select statistically significant differences ($P < 0.05$) assessed by a multiple t-tests for each day between conditions (A & B) or for each fluorescence color (C). Not shown is the ANOVA and Tukey's multiple comparison test between days for the same condition and fluorescence.

7.4 Discussion

7.4.1 Alginate capsules were comparable to microwell systems

In this chapter, we compare the alginate hydrogel capsules to microwell systems for their ability to form spheroids. To start, we compare the geometry of alginate capsules described in chapter 6 to microwell made from agarose in a 96-well TCP. Although both formed multiple spheroids, those in the agarose wells had one primary spheroid because of the rounded bottom that forms [26, 27]. Notably, although multiple spheroids were formed, the overall metabolic activity of the non-adherent conditions was similar. Referencing the work in the previous chapter, we recognized that a sufficient number of cells was required for spheroid formation. Here, the mechanistic cause of that point is emphasized by the filipodia-like structures of the cells linking spheroids together as they aggregate into a larger spheroid. Regardless, the technique cannot make single spheroids of similar size in each capsule, like microwells or hanging drop methods [2, 28]. Although it should be able to maintain an encapsulated cryopreserved spheroid as a single aggregated, modifying the geometry of the frozen disk was explored as an alternative. Moving forward, we plan to use alginate hydrogel capsules as a condition to understand optimal processes to obtain spheroids post-cryopreservation. Therefore, it was essential to enable the technique to have a similar geometry as the more commonly used microwell systems, like 96-well plates, hanging drop, AggreWell^{TM}, and custom designs [2, 3, 29-32].

7.4.2 Formation of specialized capsule geometries using PDMS

Starting with the same initial geometry with a PDMS mold, we compared the initial viability of cells cryopreserved in cryopreservation tubes and PDMS. In a preliminary experiment, we found no significant loss in viability from using the PDMS vessel with human umbilical vein endothelial cells (HUVECs). In agreement, in a recent study, a research group used PDMS as a heat transfer fluid for cryopreserving and thawing biological tissues [33]. The computational simulations described in that study found that PDMS enables rapid cooling and thawing, highlighting its potential use as a cryopreservation vessel. The use of Me_2SO has not had a thorough investigation for its capacity as a cryopreservation vessel, with only about a dozen studies used cryopreservation and PDMS (pubmed.gov, 2021). Of these approximatley twelve studies, the research objective is to determine if cells can be cryopreserved within microfluidic devices [34, 35], rather than interrogating the use of PDMS. Regardless, Me_2SO has low solubility with PDMS, being considered compatible and recommended for microreactor systems [36]. Therefore, PDMS shows promise as a cryopreservation-vessel material that we can use for TIG.

7.4.3 Using FDM 3D printers for rapid prototyping of cryopreservation vessels

Next, we set out to make patterned capsules using the easily accessible tools at our disposal. Using an FDM 3D printer, we printed the negative mold for the cryopreservation vessels. FDM 3D printers work by bringing a thermoplastic to a flow temperature and patterning the melted material on a surface, stacking the layers. The PDMS and frozen cryopreservation solution were able to maintain the features due to the resolution of the 3D printer, highlighted by the lines between the individual layers

showing up in the alginate hydrogel capsule. Overall, we were able to create microwell-like structures holding a volume of about 50 µL. While testing the feasibility of shaping the internal and external features of the capsules, we were also able to generate long tubes (about 20 mm in length), hollow donuts, and cubes. Generally, the outer geometry is rounded due to the outwards diffusion of the calcium ions. While we suspect this outcome represents a promising method for micropatterning tissue constructs, we focus on the formation or maintenance of spheroids for these initial studies.

7.4.4 Limitations and benefits encountered with 3D printing

As with much of rapid prototyping, the quality of the outcome is dependent on the equipment available. Our personal FDM 3D printer was used to create the negative molds. Distinctly, the FDM 3D printer deposits multiple layers to create a cone geometry. Consequently, the cone had a step structure that also could warp due to the relatively low flow temperature of PLA. We went through several iterations until we settled on the geometry of the 3D printed negative mold and curing temperature for PDMS. Although previous studies have used FDM 3D printers to generate complex features in PDMS or as microfluidics themselves [37, 38], refined angles are challenging to accomplish. While other 3D printing methods, such as stereolithography (SLA), could result in less of a step structure and warping, the true advantage of 3D printing is simplistic, fast, and efficient prototyping [39, 40]. The prototypes we created were modeled, printed, and used to make a PDMS cryopreservation vessel within the same working day.

Similarly, the process could be expanded to design specialized cryopreservation vessels for TIG to create specialized cell constructs post-cryopreservation. Utilizing thermal changes to create 3D structures is the fundamental basis for FDM 3D printers. Additionally, alginate has been an appealing material for bioinks in tissue engineering 3D printers [41]. Together, using alginate to create 3D tissue constructs could be expanded with the use of TIG. For now, this process represents a potential budding technique that needs further validation with cryopreserved cells.

7.4.5 *Motivation for using FUCCI-expressing HEK-293T cells to study cryopreservation*

To interrogate the formation of spheroids from post-cryopreserved cells, we employed real-time cell cycle imaging techniques. Specifically, we used FUCCI-expressing cells to study spheroids, a process that at the time was performed in less than a dozen other studies [16, 42, 43]. Likewise, no studies have incorperated FUCCI-expressing cells to investigate cryopreservation. Here, the use of these cells indicates cell state and recovery of metabolic processes post-cryopreservation. In the previous chapter, we have noted in previous studies and our own how the metabolic activity is reduced post-cryopreservation. Therefore, we suspected the fluorescence from FUCCI-expressing cells would change in both colors with cell state and magnitude with the recovery of metabolic activity. Given the objective of cryopreservation to maintain cell function after being frozen, FUCCI-expression in cells has promise in studying novel methods for improving post-cryopreservation cell proliferation and spheroid cell packing. While we did not observe a change in fluorescence intensity over time post-cryopreservation with the HEK-293T cells on TCP, there was an increase in microwells,

suggesting its potential use could extend beyond individual cell states via FACS or confocal microscopy [44].

7.4.6 FUCCI-expression in post-cryopreserved cells

We investigated the role of CPA dilution post-cryopreservation in microwell systems using FUCCI-expressing cells. Despite similar spheroid size and shape, the spheroids formed from diluted cells were slightly more metabolically active at day three than the directly plated cells. Seemingly in contrast, the cells directly plated had significantly more green fluorescence than the diluted groups. However, in spheroids that are 500-600 μm in diameter, proliferation is primarily limited to the cells on the surface of spheroids [45]. Similarly, diffusion limitations through the spheroid could impair analytes from working as intended with aggregates of cells. Consequently, procedures such as an MTT assay might not release all of the metabolized analytes during solubilizing and could be impacted by cell packing density. Alternatively, as cell confinement alters cell division by constricting mitotic spindle formation, the arrest in the S/G2/M phase would also leave FUCCI-transduced cells expressing the green fluorescence [17]. Therefore, a combination of real-time cell imaging with post hoc metabolic activity and DNA quantification could provide essential information on post-cryopreservation cell recovery. With both techniques combined, the data could indicate independent information that the CPA-diluted cells are more metabolically active and are not proliferating as much as the cells seeded directly into the microwells. Meaningfully, the FUCCI-expressing cells permit observation of the spheroids without disruption before destructive testing.

7.4.7 Spheroid formation in capsules versus microwells

Lastly, we use these FUCCI-expressing cells to determine if there is any significant detriment to using TIG for encapsulating post-cryopreserved cells in alginate capsules compared to the more traditional microwell systems. Overall, the combinatory results represent information on overall cellular recovery post-cryopreservation. Spheroids formed in microwells were larger and appeared more metabolically active than even the uncryopreserved control, a result that does not agree with the loss in metabolic activity observed in the previous chapter. However, this result could be due to the density of cells in the spheroid, enabling better solubilization of the metabolized MTT. After normalizing to spheroid volume, both cryopreservation conditions were less than the unfrozen group. After this normalization, the spheroids in the microwells were similar to the capsules. Previously, studies either cryopreserve the whole spheroid or culture on 2D tissue culture plates for three days before seeding in microwells [46]. While previous work has shown a reduced capacity for cell-cell interactions post-cryopreservation [14], the utility of spheroids is derived by an organization that better recapitulates the native *in vivo* environment. These influences on cell adhesion and actin formation from cryopreservation could impact the structuring of spheroids.

Further interrogation with fluorescence from the FUCCI-expressing cells showed that the spheroids formed within capsules had greater fluorescence than those in microwells. While this could indicate better metabolic recovery, we have substantial reservations about any conclusion. Specifically, without a significant difference from the MTT assay, it would be unclear what differences would be expected in fluorescence.

Therefore, the FUCCI data in this chapter determined that the green fluorescence of FUCCI-expressing cells is expected to increase over time post-cryopreservation, showing promise for future evaluation of cryopreserved cells if used in combination with metabolic activity, apoptosis, and DNA quantification assays [47, 48].

7.5 Conclusion

This chapter presents the formation of unique internal geometries of alginate hydrogel capsules formed by TIG and suggests that the FUCCI expression can be informative of cell aggregation post-cryopreservation. Specifically, post-cryopreserved cells were proliferative while having an increase in both red and green fluorescence on TCP. Furthermore, as post-cryopreserved cells aggregated into spheroids, green fluorescence increased for both microwells and the alginate capsules. While the work in this chapter breaks ground on the utilization of 3D printing to create PDMS cryopreservation vessels and the use of the FUCCI-system to interrogate cryopreserved cells, the development of new geometries for TIG-formed constructs with 3D printing enables creativity for research into post-cryopreservation cell encapsulation.

7.6 References

[1] K. C. Murphy, J. Whitehead, D. Zhou, S. S. Ho, and J. K. Leach, "Engineering fibrin hydrogels to promote the wound healing potential of mesenchymal stem cell spheroids," (in eng), *Acta biomaterialia,* vol. 64, pp. 176-186, 2017, doi: 10.1016/j.actbio.2017.10.007.

[2] M. A. Gionet-Gonzales and J. K. Leach, "Engineering principles for guiding spheroid function in the regeneration of bone, cartilage, and skin," *Biomedical Materials,* vol. 13, no. 3, p. 034109, 2018/03/21 2018, doi: 10.1088/1748-605x/aab0b3.

[3] C. E. Vorwald, S. S. Ho, J. Whitehead, and J. K. Leach, "High-Throughput Formation of Mesenchymal Stem Cell Spheroids and Entrapment in Alginate Hydrogels," in *Biomaterials for Tissue Engineering: Methods and Protocols*, K. Chawla Ed. New York, NY: Springer New York, 2018, pp. 139-149.

[4] N. Gjorevski *et al.*, "Designer matrices for intestinal stem cell and organoid culture," in *Nature*, vol. 539, no. 7630). England, 2016, pp. 560-564.

[5] M. E. Wechsler, M. Shevchuk, and N. A. Peppas, "Developing a Multidisciplinary Approach for Engineering Stem Cell Organoids," *Annals of Biomedical Engineering,* vol. 48, no. 7, pp. 1895-1904, 2020/07/01 2020, doi: 10.1007/s10439-019-02391-1.

[6] J. A. Brassard and M. P. Lutolf, "Engineering Stem Cell Self-organization to Build Better Organoids," *Cell Stem Cell,* vol. 24, no. 6, pp. 860-876, 2019/06/06/ 2019, doi: https://doi.org/10.1016/j.stem.2019.05.005.

[7] R. Malpique *et al.*, "Alginate Encapsulation as a Novel Strategy for the Cryopreservation of Neurospheres," *Tissue Engineering Part C: Methods,* vol. 16, no. 5, pp. 965-977, 2010/10/01 2009, doi: 10.1089/ten.tec.2009.0660.

[8] D. Khaitan, S. Chandna, M. B. Arya, and B. S. Dwarakanath, "Establishment and characterization of multicellular spheroids from a human glioma cell line; Implications for tumor therapy," *Journal of Translational Medicine,* vol. 4, no. 1, p. 12, 2006/03/02 2006, doi: 10.1186/1479-5876-4-12.

[9] Y.-C. Lu *et al.*, "Scalable Production and Cryostorage of Organoids Using Core–Shell Decoupled Hydrogel Capsules," *Advanced Biosystems,* vol. 1, no. 12, p. 1700165, 2017/12/01 2017, doi: https://doi.org/10.1002/adbi.201700165.

[10] H. Gurruchaga *et al.*, "Advances in the slow freezing cryopreservation of microencapsulated cells," *Journal of Controlled Release,* vol. 281, pp. 119-138, 2018/07/10/ 2018, doi: https://doi.org/10.1016/j.jconrel.2018.05.016.

[11] X. Yu, G. Chen, and S. Zhang, "A model to predict the permeation kinetics of dimethyl sulfoxide in articular cartilage," (in eng), *Biopreserv Biobank,* vol. 11, no. 1, pp. 51-6, Feb 2013, doi: 10.1089/bio.2012.0050.

[12] E. S. Dragan and M. V. Dinu, "Advances in porous chitosan-based composite hydrogels: Synthesis and applications," *Reactive and Functional Polymers,* vol. 146, p. 104372, 2020/01/01/ 2020, doi: https://doi.org/10.1016/j.reactfunctpolym.2019.104372.

[13] R. Chen, B. Wang, Y. Liu, R. Lin, J. He, and D. Li, "A study of cryogenic tissue-engineered liver slices in calcium alginate gel for drug testing," in *Cryobiology*, vol. 82. Netherlands: © 2018 Elsevier Inc, 2018, pp. 1-7.

[14] R. Chinnadurai *et al.*, "Actin cytoskeletal disruption following cryopreservation alters the biodistribution of human mesenchymal stromal cells in vivo," (in eng), *Stem Cell Reports,* vol. 3, no. 1, pp. 60-72, Jul 8 2014.

[15] C. S. Chen, M. Mrksich, S. Huang, G. M. Whitesides, and D. E. Ingber, "Geometric Control of Cell Life and Death," *Science,* vol. 276, no. 5317, p. 1425, 1997, doi: 10.1126/science.276.5317.1425.

[16] L. Spoerri, K. A. Beaumont, A. Anfosso, and N. K. Haass, "Real-Time Cell Cycle Imaging in a 3D Cell Culture Model of Melanoma," (in eng), *Methods Mol Biol,* vol. 1612, pp. 401-416, 2017, doi: 10.1007/978-1-4939-7021-6_29.

[17] R. A. Moriarty and K. M. Stroka, "Physical confinement alters sarcoma cell cycle progression and division," (in eng), *Cell Cycle,* vol. 17, no. 19-20, pp. 2360-2373, 2018.

[18] S.-B. Koh *et al.*, "A quantitative FastFUCCI assay defines cell cycle dynamics at a single-cell level," *Journal of Cell Science,* vol. 130, no. 2, pp. 512-520, 2017, doi: 10.1242/jcs.195164.

[19] A. Sakaue-Sawano *et al.*, "Visualizing Spatiotemporal Dynamics of Multicellular Cell-Cycle Progression," *Cell,* vol. 132, no. 3, pp. 487-498, 2008/02/08/ 2008, doi: https://doi.org/10.1016/j.cell.2007.12.033.

[20] P. A. Longo, J. M. Kavran, M.-S. Kim, and D. J. Leahy, "Chapter Fourteen - Single Cell Cloning of a Stable Mammalian Cell Line," in *Methods in Enzymology*, vol. 536, J. Lorsch Ed.: Academic Press, 2014, pp. 165-172.

[21] A. Blumlein, N. Williams, and J. J. McManus, "The mechanical properties of individual cell spheroids," *Scientific Reports,* vol. 7, no. 1, p. 7346, 2017/08/04 2017, doi: 10.1038/s41598-017-07813-5.

[22] K. T. Campbell, R. S. Stilhano, and E. A. Silva, "Enzymatically degradable alginate hydrogel systems to deliver endothelial progenitor cells for potential revasculature applications," (in eng), *Biomaterials,* vol. 179, pp. 109-121, 2018, doi: 10.1016/j.biomaterials.2018.06.038.

[23] K. T. Campbell, K. Wysoczynski, D. J. Hadley, and E. A. Silva, "Computational-Based Design of Hydrogels with Predictable Mesh Properties," *ACS Biomaterials Science & Engineering,* vol. 6, no. 1, pp. 308-319, 2020/01/13 2020, doi: 10.1021/acsbiomaterials.9b01520.

[24] D. J. Hadley and E. A. Silva, "Thaw-Induced Gelation of Alginate Hydrogels for Versatile Delivery of Therapeutics," *Annals of Biomedical Engineering,* vol. 47, no. 8, pp. 1701-1710, 2019/08/01 2019, doi: 10.1007/s10439-019-02282-5.

[25] in *Assay Guidance Manual*, S. Markossian *et al.* Eds. Bethesda MD, 2004.

[26] J. Dahlmann *et al.*, "The use of agarose microwells for scalable embryoid body formation and cardiac differentiation of human and murine pluripotent stem cells," *Biomaterials,* vol. 34, no. 10, pp. 2463-2471, 2013/03/01/ 2013, doi: https://doi.org/10.1016/j.biomaterials.2012.12.024.

[27] X. Guo, S. Li, Q. Ji, R. Lian, and J. Chen, "Enhanced viability and neural differential potential in poor post-thaw hADSCs by agarose multi-well dishes and spheroid culture," in *Hum Cell*, vol. 28, no. 4). Japan, 2015, pp. 175-89.

[28] K. C. Murphy, S. Y. Fang, and J. K. Leach, "Human mesenchymal stem cell spheroids in fibrin hydrogels exhibit improved cell survival and potential for bone healing," (in eng), *Cell Tissue Res,* vol. 357, no. 1, pp. 91-9, Jul 2014.

[29] D. M. Dean, A. P. Napolitano, J. Youssef, and J. R. Morgan, "Rods, tori, and honeycombs: the directed self-assembly of microtissues with prescribed microscale geometries," *The FASEB Journal,* vol. 21, no. 14, pp. 4005-4012, 2007/12/01 2007, doi: https://doi.org/10.1096/fj.07-8710com.

[30] K. Lee *et al.*, "Gravity-oriented microfluidic device for uniform and massive cell spheroid formation," *Biomicrofluidics,* vol. 6, no. 1, p. 014114, 2012/03/01 2012, doi: 10.1063/1.3687409.

[31] B. C. Gettler, J. S. Zakhari, P. S. Gandhi, and S. K. Williams, "Formation of Adipose Stromal Vascular Fraction Cell-Laden Spheroids Using a Three-Dimensional Bioprinter and Superhydrophobic Surfaces," *Tissue Engineering Part C: Methods,* vol. 23, no. 9, pp. 516-524, 2017/09/01 2017, doi: 10.1089/ten.tec.2017.0056.

[32] H. J. Kim, R. Castañeda, T. H. Kang, S. Kimura, M. Wada, and U.-J. Kim, "Cellulose hydrogel film for spheroid formation of human adipose-derived stemcells," *Cellulose,* vol. 25, no. 4, pp. 2589-2598, 2018/04/01 2018, doi: 10.1007/s10570-018-1732-4.

[33] S. E. Lauk-Dubitskiy *et al.*, "Porcine heart valve, aorta and trachea cryopreservation and thawing using polydimethylsiloxane," *Cryobiology,* vol. 93, pp. 91-101, 2020/04/01/ 2020, doi: https://doi.org/10.1016/j.cryobiol.2020.02.003.

[34] Y. Nagahara, H. Sekine, M. Otaki, M. Hayashi, and N. Murase, "Use of high concentrations of dimethyl sulfoxide for cryopreservation of HepG2 cells adhered to glass and polydimethylsiloxane matrices," (in eng), *Cryobiology,* vol. 72, no. 1, pp. 53-9, Feb 2016, doi: 10.1016/j.cryobiol.2015.11.004.

[35] Y. Zou, T. Yin, S. Chen, J. Yang, and W. Huang, "On-chip cryopreservation: a novel method for ultra-rapid cryoprotectant-free cryopreservation of small amounts of human spermatozoa," (in eng), *PLoS One,* vol. 8, no. 4, p. e61593, 2013.

[36] J. N. Lee, C. Park, and G. M. Whitesides, "Solvent compatibility of poly(dimethylsiloxane)-based microfluidic devices," (in eng), *Anal Chem,* vol. 75, no. 23, pp. 6544-54, Dec 1 2003, doi: 10.1021/ac0346712.

[37] G. Gaal *et al.*, "Simplified fabrication of integrated microfluidic devices using fused deposition modeling 3D printing," *Sensors and Actuators B: Chemical,* vol. 242, pp. 35-40, 2017/04/01/ 2017, doi: https://doi.org/10.1016/j.snb.2016.10.110.

[38] V. Saggiomo and A. H. Velders, "Simple 3D Printed Scaffold-Removal Method for the Fabrication of Intricate Microfluidic Devices," *Advanced Science,* vol. 2, no. 9, p. 1500125, 2015/09/01 2015, doi: https://doi.org/10.1002/advs.201500125.

[39] C. M. B. Ho, S. H. Ng, K. H. H. Li, and Y.-J. Yoon, "3D printed microfluidics for biological applications," *Lab on a Chip,* 10.1039/C5LC00685F vol. 15, no. 18, pp. 3627-3637, 2015, doi: 10.1039/C5LC00685F.

[40] A. Waldbaur, H. Rapp, K. Länge, and B. E. Rapp, "Let there be chip—towards rapid prototyping of microfluidic devices: one-step manufacturing processes,"

Analytical Methods, 10.1039/C1AY05253E vol. 3, no. 12, pp. 2681-2716, 2011, doi: 10.1039/C1AY05253E.

[41] T. Gonzalez-Fernandez, A. J. Tenorio, K. T. Campbell, E. A. Silva, and J. K. Leach, "Alginate-Based Bioinks for 3D Bioprinting and Fabrication of Anatomically Accurate Bone Grafts," (in eng), *Tissue Eng Part A,* vol. 27, no. 17-18, pp. 1168-1181, Sep 2021.

[42] K. A. Beaumont, A. Anfosso, F. Ahmed, W. Weninger, and N. K. Haass, "Imaging- and Flow Cytometry-based Analysis of Cell Position and the Cell Cycle in 3D Melanoma Spheroids," (in eng), *J Vis Exp,* no. 106, p. e53486, Dec 28 2015.

[43] Y. Onozato, A. Kaida, H. Harada, and M. Miura, "Radiosensitivity of quiescent and proliferating cells grown as multicellular tumor spheroids," (in eng), *Cancer Sci,* vol. 108, no. 4, pp. 704-712, Apr 2017, doi: 10.1111/cas.13178.

[44] N. Zielke and B. A. Edgar, "FUCCI sensors: powerful new tools for analysis of cell proliferation," *WIREs Developmental Biology,* vol. 4, no. 5, pp. 469-487, 2015/09/01 2015, doi: https://doi.org/10.1002/wdev.189.

[45] J. Laurent, C. Frongia, M. Cazales, O. Mondesert, B. Ducommun, and V. Lobjois, "Multicellular tumor spheroid models to explore cell cycle checkpoints in 3D," (in eng), *BMC Cancer,* vol. 13, p. 73, Feb 8 2013.

[46] H.-J. Kim *et al.*, "Three-Dimensional Spheroid Formation of Cryopreserved Human Dental Follicle-Derived Stem Cells Enhances Pluripotency and Osteogenic Induction Properties," (in eng), *Tissue engineering and regenerative medicine,* vol. 16, no. 5, pp. 513-523, 2019, doi: 10.1007/s13770-019-00203-0.

[47] S. S. Ho, K. C. Murphy, B. Y. Binder, C. B. Vissers, and J. K. Leach, "Increased Survival and Function of Mesenchymal Stem Cell Spheroids Entrapped in Instructive Alginate Hydrogels," (in eng), *Stem Cells Transl Med,* vol. 5, no. 6, pp. 773-81, Jun 2016.

[48] C. E. Vorwald, K. C. Murphy, and J. K. Leach, "Restoring vasculogenic potential of endothelial cells from diabetic patients through spheroid formation," (in eng), *Cell Mol Bioeng,* vol. 11, no. 4, pp. 267-278, Aug 2018.

CHAPTER 8

Optimal conditions for obtaining HUVEC and MSC spheroids post-cryopreservation

8.1 Introduction

In this chapter, we transition to using cells with therapeutic potential with proper cryopreservation to determine optimal conditions for acquiring spheroids post-cryopreservation systematically. In previous chapters, we discuss the alternative to the common practice of cryopreserving spheroids, organoids, and tissue fragments forming cell aggregates from post-cryopreserved cells [1-7]. Although we had success with the human embryonic kidney cells (HEK-293 and HEK-293T), this cell line of mesenchymal origin would be expected to behave differently from primary endothelial cells. Therefore, verifying post-cryopreservation cell encapsulation via TIG was viable in instructing spheroid formation. The work described in this chapter attempts to determine whether spheroids should be formed pre- or not post-cryopreservation from human umbilical cord endothelial cells (HUVECs). Expanding on this work, we also incorporate primary mesenchymal cells, human mesenchymal stromal cells (MSCs) to broaden our understanding of how different cell types respond to cryopreservation. Fascinatingly, these two primary cells had flipped responses to pre- or post-cryopreservation spheroid formation. Therefore, the work in this chapter highlights the importance of understanding and optimizing cryopreservation strategies for the cell type.

The use of spheroids as a model of 3D tissue has been widely adopted as it is accepted as better recapitulating the native *in vivo* environment better than tissue

culture plastics [8-15]. Moreover, spheroids have been suggested to improve the efficacy of potential cell therapies. Spheroids can act as functional building blocks to build tissue or repair damaged tissue [14]. Regardless, clinical-minded perspectives typically address large-scale culture and cryopreservation as a challenge to be overcome [16-18].

By cryopreserving cells, their shelf-life of cell therapies can be expanded through decades. Moreover, the technology enables cell therapies to reach clinics outside of research settings as treatments can be produced off-site, stored, and transported [19]. Specifically, biobanking of cell samples could enable cells taken during birth, such as HUVECs, to be used to repair tissue at later stages of life or act as a model system to study prospective treatments [20, 21]. With these perspectives, the use of spheroids is an appealing approach for developing functional units for research and cell therapies, making a woven motivation for studying cryopreservation in the context of spheroids. Significantly, cryopreservation is known to reduce cadherin binding and deposition of extracellular matrix proteins [22]. This inhibition could counter the improved survival and proliferation cell-cell interactions have for anchorage-dependent cells [23]. Nevertheless, the alternative being cryopreservation of preformed spheroids could result in structural damage from intracellular and extracellular ice formation, osmotic shock, and cryopreservation agent cytotoxicity [24-28].

In this chapter, we take a step back from studying hydrogel encapsulation of cryopreserved cells to address another aspect of cryobiology that has not been previously studied: the optimal procedure for obtaining spheroids post-cryopreservation. While we postulate that MSCs will form aggregates from post-cryopreserved cells, like

the HEK-293T cells in previous chapters, we expected to face challenges with forming HUVEC spheroids from previously frozen cells. Therefore, we also include in the work presented in this chapter the cryopreservation of spheroids. Succinctly, we have two hypotheses that might only be appropriate for specific cells or their combinations: 1) cryopreserved spheroids recover faster from cryopreservation than dispersed cells, and 2) the formation of spheroids post-cryopreservation results in less cryodamage to cells than cryopreserved spheroids. While studies typically study the impact of cryopreservation on preformed spheroids or post-cryopreservation formation of spheroids, this work represents one of the first instances of comparing both processes together. The knowledge gained by this work could be applied to TIG-based encapsulation.

8.2 Methods

8.2.1 Cell culture

Human umbilical vein endothelial cells (HUVECS; Lonza) from pooled donors were expanded in endothelial cell growth medium (EGM-2, Lonza) under standard conditions (37 ˚C and 5% CO_2), exchanging media every two days. EGM-2 was prepared as defined in the vendor's EGM-2 BulletKit™ medium with and without the addition of the growth factors, with N media being defined as the cell culture media without growth factors. Cells were used between passages 4 – 6. Human mesenchymal stromal cells (MSCs; Lonza) were also expanded in EGM-2 under the same conditions as the HUVECs. These cells were also used between passages 5 – 8 with, at most, one passage after thawing. Expansion and initial experiments were carried out on tissue culture plates (TCP). Additional experiments were primarily carried out using ultra-low attachment surface round-bottom 96-well plates (Corning), which will be referred to as microwells. We also carried out a brief experiment with TIG to form alginate hydrogel capsules.

Cells were cryopreserved using a freezing solution with a final composition of 10% (v/v) dimethyl sulfoxide (Me_2SO, Sigma) and 20% (v/v) fetal bovine serum (FBS; Invitrogen), and 70% (v/v) EBM-2. To avoid potential confusion, Me_2SO is more commonly abbreviated as DMSO outside the field of cryobiology. For all conditions except for samples undergoing TIG, cells were cryopreserved in cryovials (VWR) at a concentration of 10^6 cells per mL. After thawing cryopreserved cells to a 1:10 dilution, the cell solution was centrifuged at 300 RCF for 5 minutes to pellet the cells. The supernatant was replaced with fresh media to minimize the remaining Me_2SO. 100 µL of

cell solution was pipetted into each microwell at a concentration of 10^5 cells per mL. The same concentration and volume were used to seed cells on 96-well tissue culture plates. For conditions in which MSCs and HUVECs are used together, cells are either cryopreserved separately and seeded into wells or cryopreserved together. Under both conditions, each cell type was used at the same concentration and volume, a 1:1 ratio. For conditions where spheroids are cryopreserved, previously passaged cells were seeded at a concentration of 10^5 cells per mL into the microwells. Spheroids were formed over three days, then cryopreserved using the same freezing solution described above. Notably, ten spheroids were cryopreserved per cryovial. For post-cryopreservation seeding of spheroids on microwells, steps followed those described above, except single spheroids, which were pipetted into each well individually.

8.2.2 Alginate hydrogel capsule formation via TIG

LF10/60 alginate polymer (molecular weight ~ 120-150 kDa and >60% G-block; purchased from FMC Biopolymers) was used in this chapter for hydrogel formation via TIG. All alginate hydrogels were purified, and sterilized alginate polymer was prepared as previously described [29, 30]. Briefly, one gram of alginate was dissolved in 100 mL of deionized (DI) water. Next, 0.5 grams of activated charcoal (Sigma) was added and mixed for 30 minutes via a magnetic stirrer. Then, the alginate solution is sterilized using a filter (0.22 µm, Thermo Fisher Scientific), lyophilized, and stored in a freezer. A 1% (w/v) alginate solution was prepared by mixing the dry polymer in an isotonic saline solution (0.9% (w/v) NaCl). The modified-cryopreserving solution contained 75- or 100-mM calcium chloride (Sigma), 10% (v/v) Me_2SO, 20% (v/v) FBS, and EMB-2. Calcium

chloride was added to the cellular freezing solution from a 6 M stock to create the final concentrations.

Gelation of the alginate hydrogel capsules was performed using TIG from polydimethylsiloxane (PDMS; Sylgard) molds used in chapter 7. Specifically, the freezing solution was pre-chilled to 4 °C prior to mixing with cells to minimize cytotoxic exposure to Me_2SO. Next, the cell-containing cryopreservation solution was pipetted into wells. The PDMS mold was designed by 3D printing a positive mold using a geometry of a 6 mm in diameter cylinder topped with a cone. The height of the cylinder and cone was 1.5 and 1 mm, respectively, for a total of 2.5 mm. Consequently, the PDMS negative mold held 50 µL. Once frozen, the cryopreservation solution matched the shape of the positive mold's geometry. Cells were encapsulated with the alginate hydrogels through TIG. Gelation was initiated by submersion and melting the cryopreserved cell solution within a 1% (w/v) alginate solution at 37 ºC. After melting and crosslinking (approximately 2 minutes), the capsules were scooped out of the beaker and placed in pre-warmed cell media. Subsequently, hydrogel capsules were moved to 12-well tissue culture plates filled with EMB-2.

8.2.3 Cell imaging and staining

Phase-contrast microscopy was used to image cells using an inverted fluorescence microscope (Zeiss Axio Vert A.4) and processed with ImageJ (NIH). From brightfield images, spheroid diameters were measured by the Feret diameter from perimeter traces around each spheroid. Notably, Feret diameter can become biased for samples that have low circularity. Cell viability was assessed with live/dead staining for

HUVECs encapsulated in alginate hydrogel capsules. 12-well plates containing EBM-2 and cell-containing capsules were replaced with a 1x phosphate buffer solution (PBS; Life Technologies) and placed back in the cell incubator for thirty minutes. Next, calcein AM (1 µM, live cells, Fisher Scientific) and ethidium homodimer-1 (EthD-1, 2.5 µM, Marker Gene Technologies) were added to each well, incubating for thirty minutes in the cell incubator. After incubation, PBS containing calcein AM and EthD-1 was replaced with fresh PBS. Cells were imaged with a fluorescence microscope. Composite images of each channel and brightfield were made in ImageJ.

8.2.4 Cell viability and proliferation

Cell viability was determined through a trypan blue exclusion test. This assay also was used to determine viable cell concentration for cryopreservation and cell seeding. An aliquot of cell suspension was mixed with 0.4% trypan blue (Sigma) at a 1:1 ratio. Quantification occurred using the Countess automated cell counter (Life Technologies). Proliferation was determined using the change in DNA content. Specifically, the Quant-iT PicoGreen DNA Assay Kit (Invitrogen) was used to determine the DNA content of cells after forming a calibration curve from known cell concentrations determined with the Countess. To acquire DNA from samples, cells were lysed in a 1x passive lysis buffer (Promega). Samples were then pipetted to centrifugation tubes and centrifuged to pellet cell debris at 5000 RCF for five minutes. A sampling of DNA was taken from the supernatant and mixed with the PicoGreen working solution. Fluorescence was measured at 485 nm (excitation)/ 528 nm (emission). For one experiment, a ROCK inhibitor, Y-27632 (STEMCELL Technologies),

was added to each microwell at a final concentration of 10 µM, as previously utilized [31-34].

8.2.5 Cell metabolic activity and caspase 3/7 activity

Metabolic activity of post-cryopreserved cells was performed via an MTT (3-(4,5-dimethylthiazol-2-yl)-2,5-diphenyltetrazolium bromide) tetrazolium reduction assay (MTT assay) three days post-cryopreservation. Specifically, 10 µL of 5 mg/mL tetrazolium dye MTT (Sigma) to each well of a 96-well plate and incubating for three hours. Next, 100 µL of a solubilizing solution was added. The solubilizing solution contained 40% (v/v) dimethylformamide (DMF; Sigma), 2% (v/v) glacial acetic acid (Sigma), and 16% (w/v) sodium dodecyl sulfate (SDS; Sigma) [35]. Samples were protected from light by covering plates with aluminum foil and placed on a shaker for one hour. The total absorbance of formazan salt was quantified via the Spectramax ® i3 plate reader (Molecular Devices) at 570 nm.

Additionally, metabolic activity was assessed via an Alamar Blue (Invitrogen) and normalized to DNA content. Alamar Blue was added at a 1:1 ratio from the manufacturer's supplied stock solution to cell solution. This combinatory solution was incubated for three hours in the cell incubator. Next, the fluorescence was detected on the Spectramax ® i3 plate reader and normalized to DNA content from the same samples using the Quant-iT PicoGreen DNA Assay Kit. In contrast to proliferation, the normalization of metabolic activity was done per nanogram of DNA. Normalization to DNA content was determined using a standard curve from the supplied DNA stock provided by the manufacturer.

Apoptosis was quantitatively measured by analyzing 50 µL of lysate per sample using a Caspase-Glo 3/7 assay (Promega), as described previously [36]. This cell lysate was the same used for the DNA quantification used to normalize the metabolic activity. Luminescence was detected on a microplate reader and normalized to the DNA content, as described earlier. Notably, the same DNA content was used to normalize both the metabolic activity and apoptosis.

8.2.6 Statistical analysis

Sample sizes are provided with each figure legend and visualized in figures as individual data points, where applicable. Results are presented as mean values with standard deviations. Statistical significance was asserted at $p < 0.05$ after performing a Student's t-test, one-way ANOVA, two-way ANOVA, and Tukey's multiple comparison tests where appropriate. All analyses were performed using Graph-Pad Prism software (GraphPad Software Inc).

8.3 Results

8.3.1 Effects of cryopreservation on HUVECs

HUVECs were cryopreserved (cryo) with various concentrations of calcium chloride and compared to non-cryopreserved cells (passaged). These cells were seeded into microwells simultaneously, allowing each to form cellular aggregates from the same individual cell suspensions. Unsurprisingly, cryopreserved cells had significantly less metabolic activity than the previously passaged cell group (Figure 8.1A). This difference is exemplified in the approximate doubling in measured absorbance with twice the initial seeded number of passaged HUVECs, but only about a 50% increase with the cryopreserved cells. Regardless, the addition of calcium chloride to the cellular freezing solution did not significantly impact post-cryopreservation viability, determined via a trypan blue exclusion assay (Figure 8.1B), nor spheroid size 3-days after seeding (Figure 8.1C). However, there was a significant difference in spheroid size when comparing passaged cells to cryopreserved cells without calcium. Interestingly, adding calcium chloride to the freezing solution might have resulted in a positive trend in spheroid diameters. Spheroids' representative images with a live/dead stain have a similar distribution of live and dead cells. Together, these data indicate that cryopreservation does influence HUVEC cell metabolic activity and capacity to form spheroids. The influences of calcium ions could still impact metabolic activity but do not detrimentally impact post-thaw viability nor prevent spheroid formation.

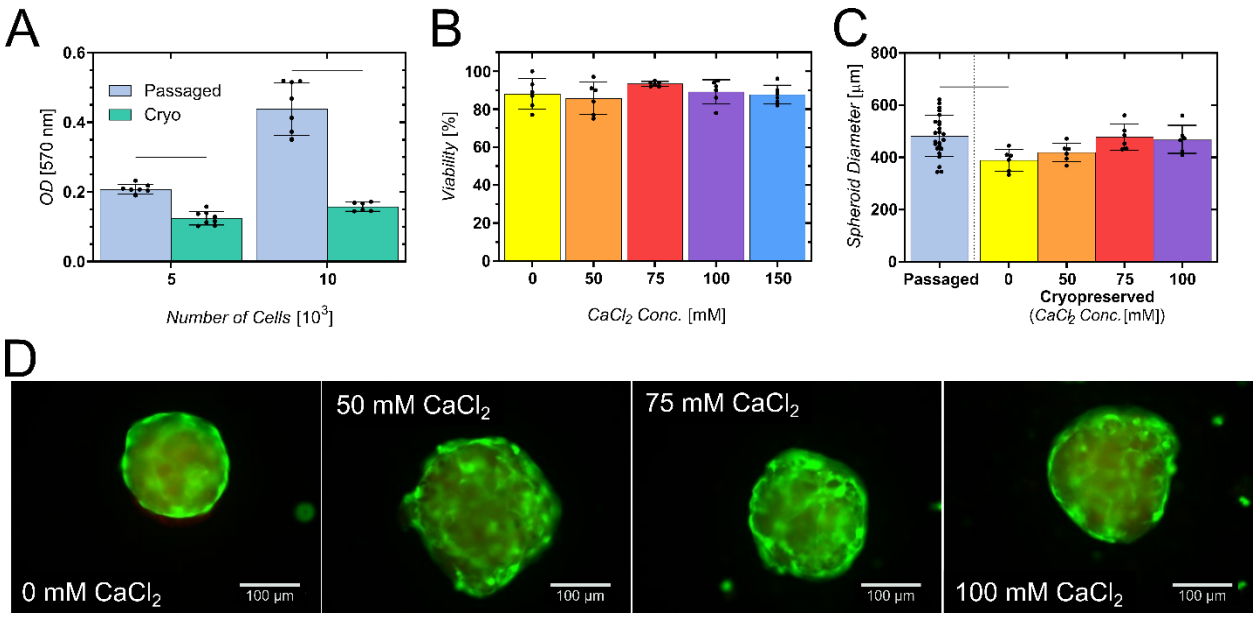

Figure 8.1 Effect of cryopreservation solutions containing calcium for HUVECs. Post-cryopreserved and passaged cells were seeded into microwells to characterize the influence of cryopreservation of spheroid formation. Cryopreservation resulted in significantly reduced metabolic activity in microwells (A; n = 6 – 8). However, adding calcium chloride to the freezing solution did not significantly impact initial cell viability for concentrations up to 150 mM (B; n = 6). Although cryopreserving cells resulted in a significantly smaller spheroid with no calcium, the addition of calcium chloride to the freezing solution led to a non-statistically significant increase in spheroid diameter. Regardless, HUVECs did form aggregates from post-cryopreserved cells with the addition of calcium, seen in live/dead stained spheroids (D). Bar graphs present the mean ± SD with individual data points. Lines between groups represent statistically significant differences ($P < 0.05$) assessed by performing a one-way ANOVA and a Tukey's multiple comparison test.

8.3.2 TIG encapsulation of HUVECs resulted in loss aggregates

Spheroid formation by HUVECs encapsulated in alginate hydrogel capsules via TIG was briefly evaluated for its feasibility. First, the cryopreservation process was assessed for cells cryopreserved in cryovials versus the custom PDMS vessels described in chapter 7. Astonishingly, cells cryopreserved on PDMS performed vastly better than with the cryovial (Figure 8.2A). Notably, cells within cryovials are thawed until a sliver of ice is left. In contrast, frozen samples in the PDMS vessels are immediately dislodged and melted via submersion in fresh pre-warmed cell media. After culturing for three days, the resulting aggregates did not form a sphere shape (Figure 8.2B). Regardless, DNA content suggests greater proliferation in hydrogels crosslinked by a cryopreservation solution containing 100 mM $CaCl_2$ (Figure 8.2C). Although not statistically significant, cells from the 100 mM $CaCl_2$ conditions had a slightly higher trend of metabolic activity (Figure 8.2D). Together, the DNA content and metabolic activity normalized to DNA suggest better recovery with the greater concentration of calcium used. This outcome is emphasized by the lower average caspase activity (Figure 8.2E). Nevertheless, the data indicate challenges for the formation of spheroids from post-cryopreserved HUVECs.

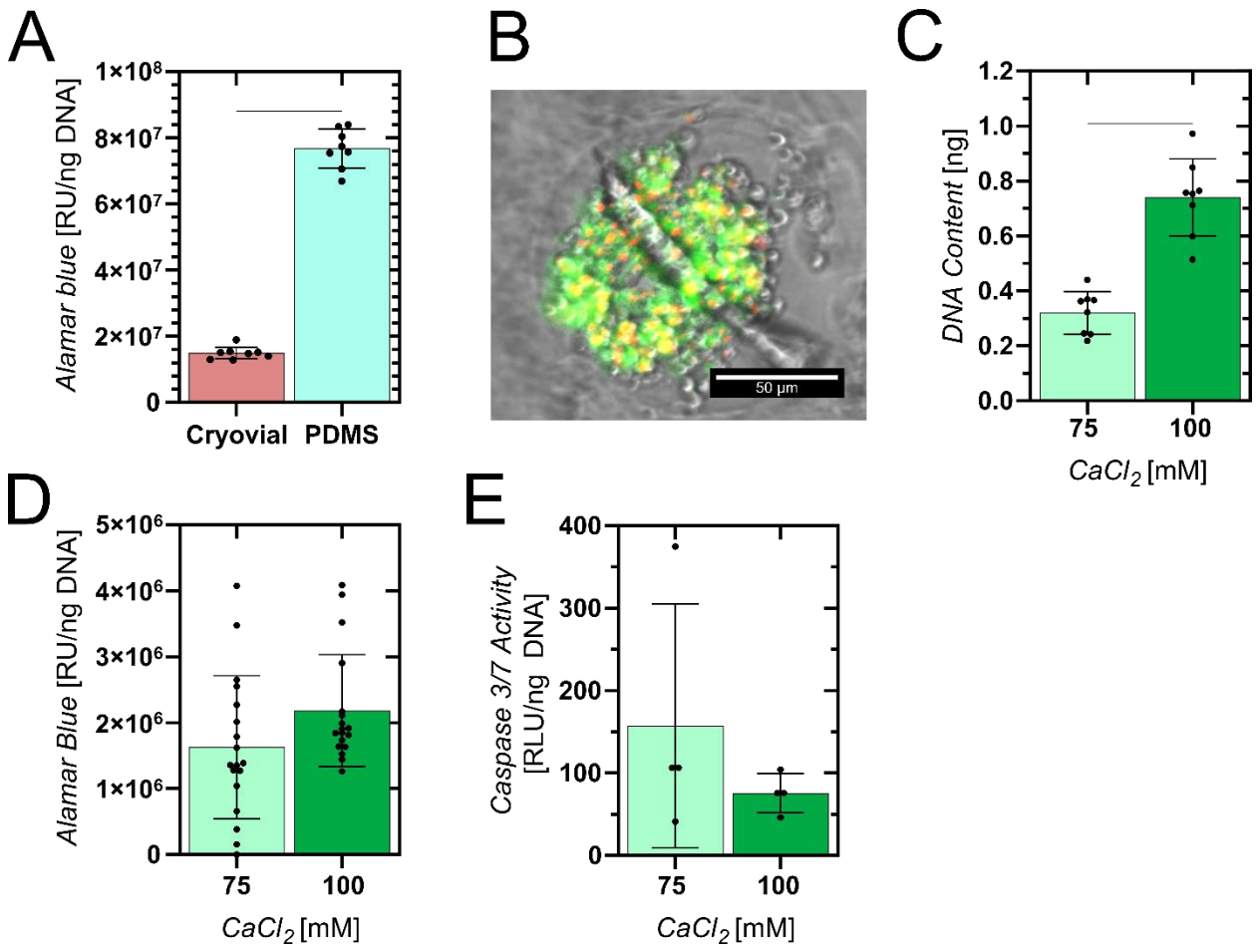

Figure 8.2 HUVECs could form aggregates after encapsulation via TIG. Despite the promising increase in metabolic activity for cells cryopreserved in PDMS compared to cryovials (A; n = 8), only loose aggregates formed in the alginate hydrogel capsules (B). Regardless, as we compared DNA content (C; n = 8), metabolic activity (D; n = 18), and apoptosis activity (E; n = 4) between capsules formed with cryopreservation solutions containing 75- or 100- mM $CaCl_2$, the higher concentration of the salt appears to lead to better outcomes. The bar graph presents the mean ± SD with individual data points. Lines between groups represent statistically significant differences ($P < 0.05$) assessed by performing a Student's t-test.

8.3.3 Characterizing HUVEC spheroids from post-cryopreserved cells

To better understand the optimal conditions for obtaining spheroids from cryopreserved cells, we cryopreserved either individual HUVECs in suspension or whole spheroids. These cryopreserved conditions were compared to individual cells previously cultured on TCP. After two days post-seeding, neither cryopreserved cells nor the passaged cells formed one cohesive aggregated (Figure 8.3A). Meanwhile, the cryopreserved HUVEC spheroid remained aggregated, appearing to shrink slightly over two days. Attempting to measure the largest spheroids formed three days post-seeding, the aggregates formed by previously cryopreserved cells in suspension were significantly smaller than the cryopreserved spheroid (Figure 8.3B). The cryopreserved spheroids had a similar diameter after three days, possibly maintaining the size through cryopreservation. However, the metabolic activity of the previously cryopreserved spheroid was greater than the other two conditions (Figure 8.3C). Unsurprisingly, between individual cells in suspension, the cryopreserved cells had a significantly lower metabolic activity than the unfrozen cells. Despite this, both individual HUVECs in suspension conditions had a significantly greater caspase activity. Overall, these data suggests that HUVECs formed more viable spheroids post-cryopreservation if they were cryopreserved as spheroids.

The effects of cryopreservation of HUVECs were further interrogated using a rho-associated kinase (ROCK) inhibitor, Y-27632, to determine if post-cryopreservation outcomes were consequential of apoptosis from dissociated HUVECs. Indeed, proliferation was significantly increased when the inhibitor was used with previously frozen dissociated cells but not in cryopreserved spheroids (Figure 8.4A). Interestingly,

these data also indicate how these dissociated cells were more proliferative than the cryopreserved spheroid group. Notably, the cryopreserved spheroids were significantly smaller than the HUVECs that formed spheroids post-cryopreservation (Figure 8.4B), a result inconsistent with the previous figure. However, each experiment represents its batch from a later passage. More importantly, previously cryopreserved spheroids have a much smaller variance than spheroids formed from cryopreserved cells, a result that is consistent with data in Figure 8.3. Although there was no other statistically significant difference with using Y-27632, cryopreserved spheroids had significantly greater metabolic activity (Figure 8.4C) and less caspase activity (Figure 8.5D) than the cryopreserved individual cells in suspension. Together, the addition of Y-27632 might increase proliferation slightly. However, overall, the results between experiments consistently suggest HUVEC spheroids are likely to be more active and undergo less apoptosis if from a previously cryopreserved spheroid.

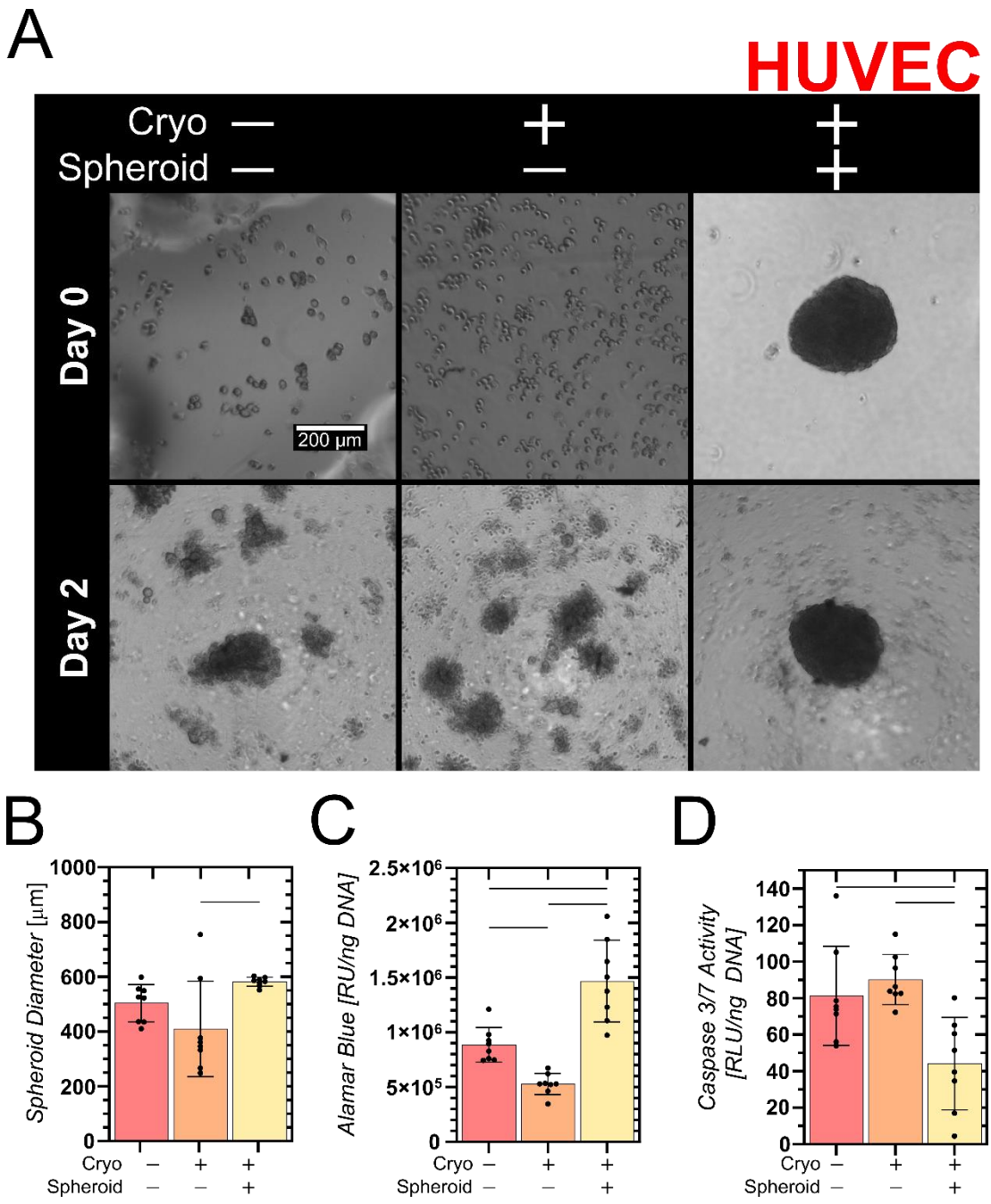

Figure 8.3 Preformed HUVEC spheroids enabled healthier spheroids post-cryopreservation than forming spheroids from post-cryopreserved cells. Two days after seeding into microwells, neither dispersed cell conditions (Spheroid -) resulted in spheroid formation (A). Alternatively, the cryopreserved spheroid (Spheroid +) remained aggregated, although the boundaries appear less smooth. The spheroids

formed after three days from the non-cryopreserved cells were similar to the cryopreserved spheroid (B). However, the pre-aggregated cells had significantly greater metabolic activity (C) and less caspase activity (D) than the dispersed cells. Brightfield images were taken via an inverted phase-contrast microscope. Bar graphs present the mean ± SD with individual data points (n = 8). Lines between groups represent statistically significant differences ($P < 0.05$) assessed by performing a one-way ANOVA followed by a Tukey's multiple comparison test.

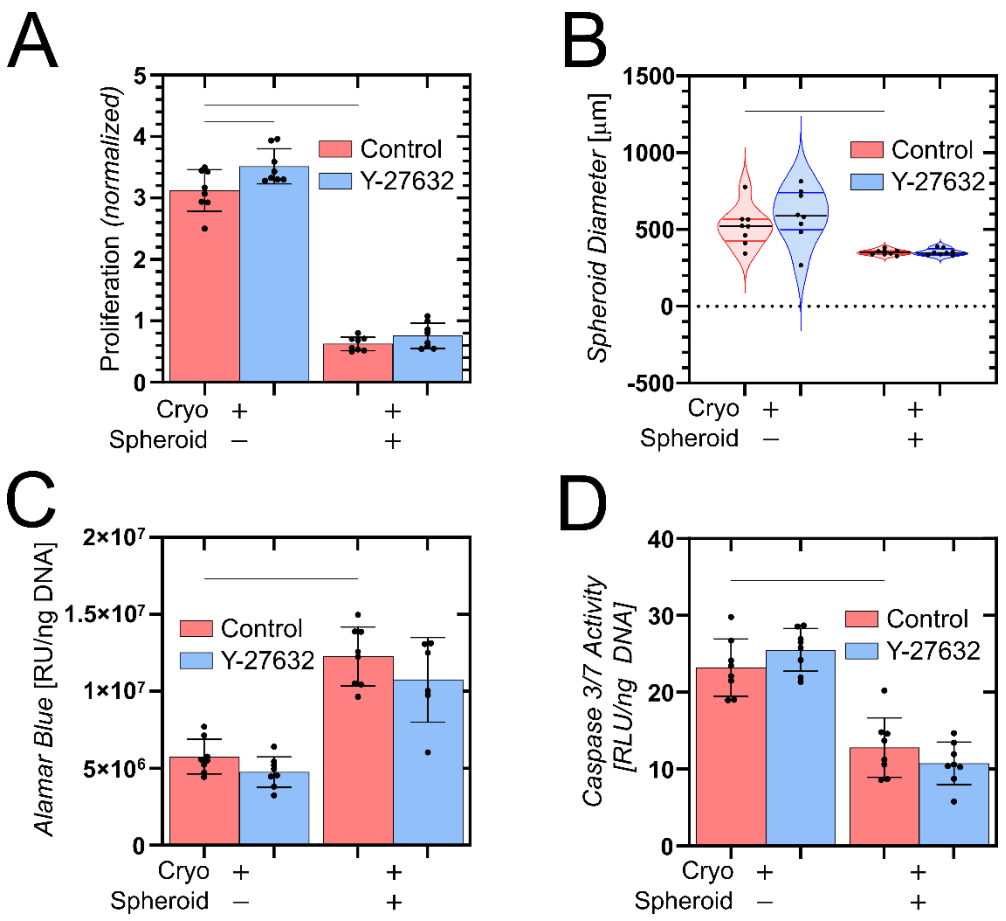

Figure 8.4 Treatment of cryopreserved HUVECs with a ROCK inhibitor, Y-27632, did not significantly impact post-cryopreservation outcomes. Only the proliferation of dispersed cells (Spheroid -) had a statistically significant change due to the addition of 10 µM Y-27632 (A). Additionally, proliferation was much higher in the dispersed cell groups than in the preformed spheroids. Preformed spheroids had less spheroid size variance (B), more metabolic activity (C), and less caspase activity (D) than the dispersed cells that formed spheroids. Bar graphs present the mean ± SD with individual data points. The violin plot displays the mean, quartiles, and individual points. Lines between groups represent select statistically significant differences ($P < 0.05$) assessed by performing a one-way ANOVA and a Tukey's multiple comparison test.

8.3.4 Characterizing MSC spheroids from post-cryopreserved cells

In contrast to HUVECs having difficulty forming spheroids two days after seeding in a microwell, dispersed MSCs could form spheroids, regardless of whether the cells were cryopreserved or not (Figure 8.5A). Although the cryopreserved spheroid remains intact after thawing, it appears to lose the defined boundary. Overall, spheroids had similar sizes, although the variance of spheroid sizes was much larger than the HUVEC spheroids (Figure 8.5B). Crucially, the cryopreservation of MSC spheroids led to a significant reduction in metabolic activity, whereas there was not a significant decrease in metabolic activity between dispersed cell conditions (Figure 8.5C). Caspase activity appears elevated in previously cryopreserved cells, but there is no apparent difference between the groups (Figure 8.5D). These data indicate potentially opposing trends in what is optimal for post-cryopreserved MSCs versus the HUVECs.

8.3.5 Comparing effects of cryopreservation between MSCs and HUVECs

MSCs and HUVECs were directly compared to understand the differences in spheroid formation after cryopreservation. Fundamentally, the MSCs are more metabolically active than the HUVECs (Figure 8.6A) when quantified via an MTT assay. As a potential consequence, the MSC spheroids tended to be larger than HUVEC spheroids; however, this trend was only statistically significant for the non-cryopreserved cells (Figure 8.6B). For cryopreserved cells, MSCs had more metabolic activity and less caspase activity than HUVECs when cryopreserved as individually dispersed cells (Figure 8.6C & E). Nonetheless, HUVECs had greater metabolic activity

than MSCs when preformed spheroids were cryopreserved (Figure 8.6D). Although HUVEC caspase activity was less in preformed spheroids than spheroids formed post-cryopreservation, caspase activity between MSCs and HUVECs was similar with preformed spheroids.

8.3.6 Altering post-cryopreservation outcomes by combining MSCs

With the diverging outcomes from cryopreserved MSCs and HUVECs, we next combined both cells after being cryopreserved or cultured separately. Immediately, the data indicates that with both cell types, spheroids can effectively form two days after seeding with dispersed cells (Spheroid -) (Figure 8.7A). Notably, after two days, the cryopreserved spheroids did not aggregate together post-cryopreservation, remaining of similar size and placement. Specifically, the smaller spheroid was made from HUVECs, and the larger spheroid was made from MSCs. The HUVEC spheroid retained a sharp contrasting boundary, but the MSCs lost their initially defined boundary. These outcomes were consistent with what was observed with each spheroid in isolation (Figure 8.3A & Figure 8.5A). Despite the representative images suggesting that between dispersed cells forming spheroids, cryopreserved cells formed smaller spheroids, no significant difference was found in our study. However, the combination of two preformed spheroids did have a larger diameter than the other two conditions (Figure 7.7B). More revealing, with the combination of both cell types, cryopreservation led to less metabolic activity and less caspase activity (Figure 8.7C & D). Overall, the combination of MSCs and HUVECs reduced the differences in metabolic activity, caspase activity, and spheroid formation due to cryopreservation.

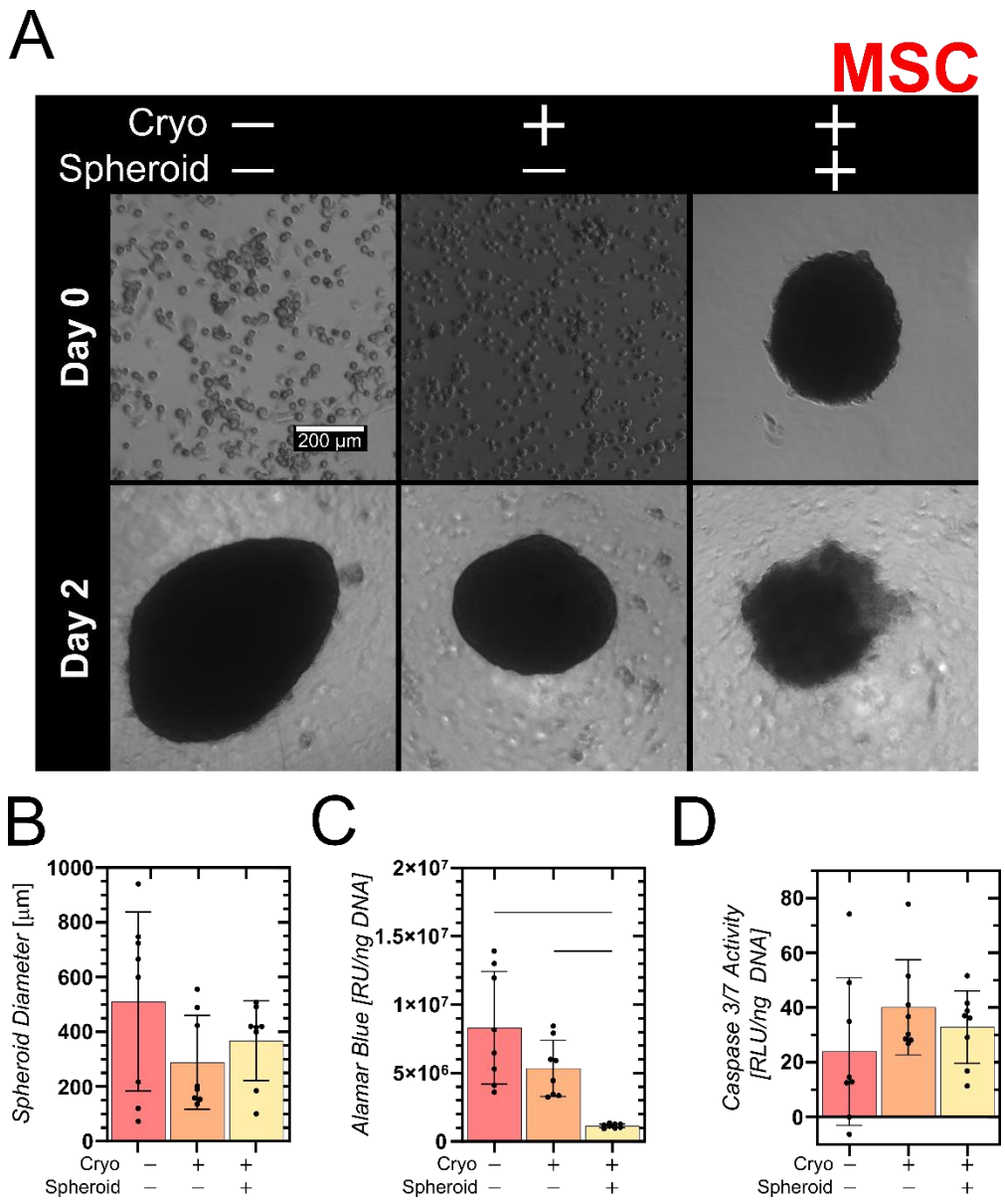

Figure 8.5 MSCs formed healthier spheroids from post-cryopreserved cells compared to cryopreserved spheroids. Dispersed cells seeded into microwells formed spheroids within two days (A). While the cryopreserved spheroid initially had a high contrasting boundary as the spheroids formed from dispersed cells, the boundaries became less sharp after two days. There was no significant difference in spheroid diameters (B) or caspase activity (D). Metabolic activity was significantly lower in the

condition where a spheroid was cryopreserved (C). Brightfield images were taken via an inverted phase-contrast microscope. Bar graphs present the mean ± SD with individual data points (n = 8). Lines between groups represent statistically significant differences ($P < 0.05$) assessed by performing a one-way ANOVA followed by a Tukey's multiple comparison test.

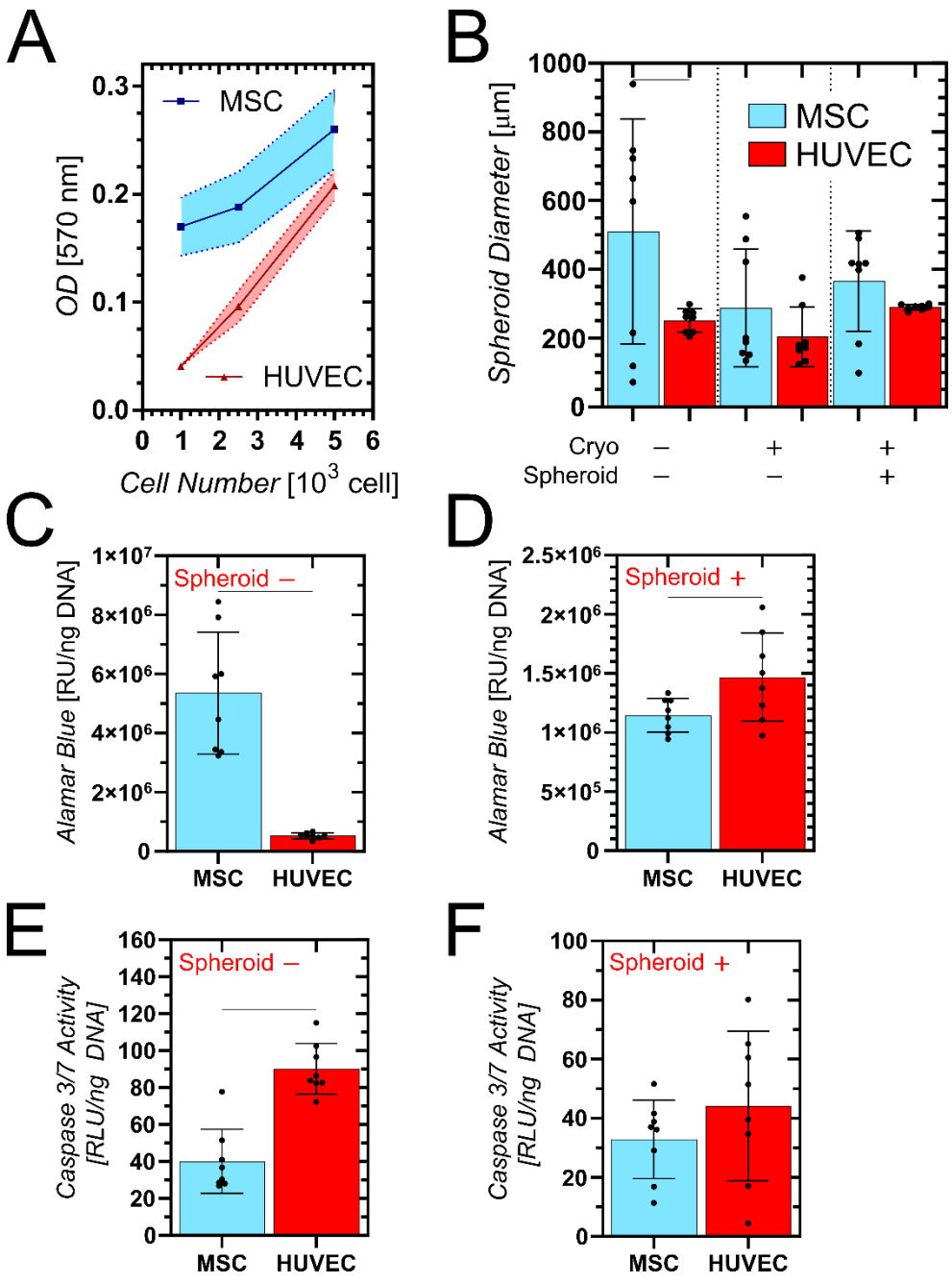

Figure 8.6 MSCs and HUVECs respond differently to being cryopreserved as single cells or as spheroids. Generally, the MSCs had greater metabolic activity than the HUVECs (A), also forming larger spheroids when not cryopreserved (Cryo -) (B). As a potential consequence, cryopreserved MSC had more metabolic activity than HUVECs when seeded as dispersed cells in microwells (Spheroid -) (C). However,

when spheroids were cryopreserved, the HUVEC spheroids had greater metabolic activity than the MSC spheroids (D). Caspase activity was significantly lower in MSCs than HUVECs when seeded as dispersed cells (E); however, both cell types had similar apoptosis activity when cryopreserved as spheroids. The line graph presents the mean value as middle points connected via a line. Standard deviations are represented through the shaded area, connecting these values between each number of cells (n = 8). Bar graphs present the mean ± SD with individual data points (n = 8). Lines between groups represent statistically significant differences ($P < 0.05$) assessed by performing Student's t-tests.

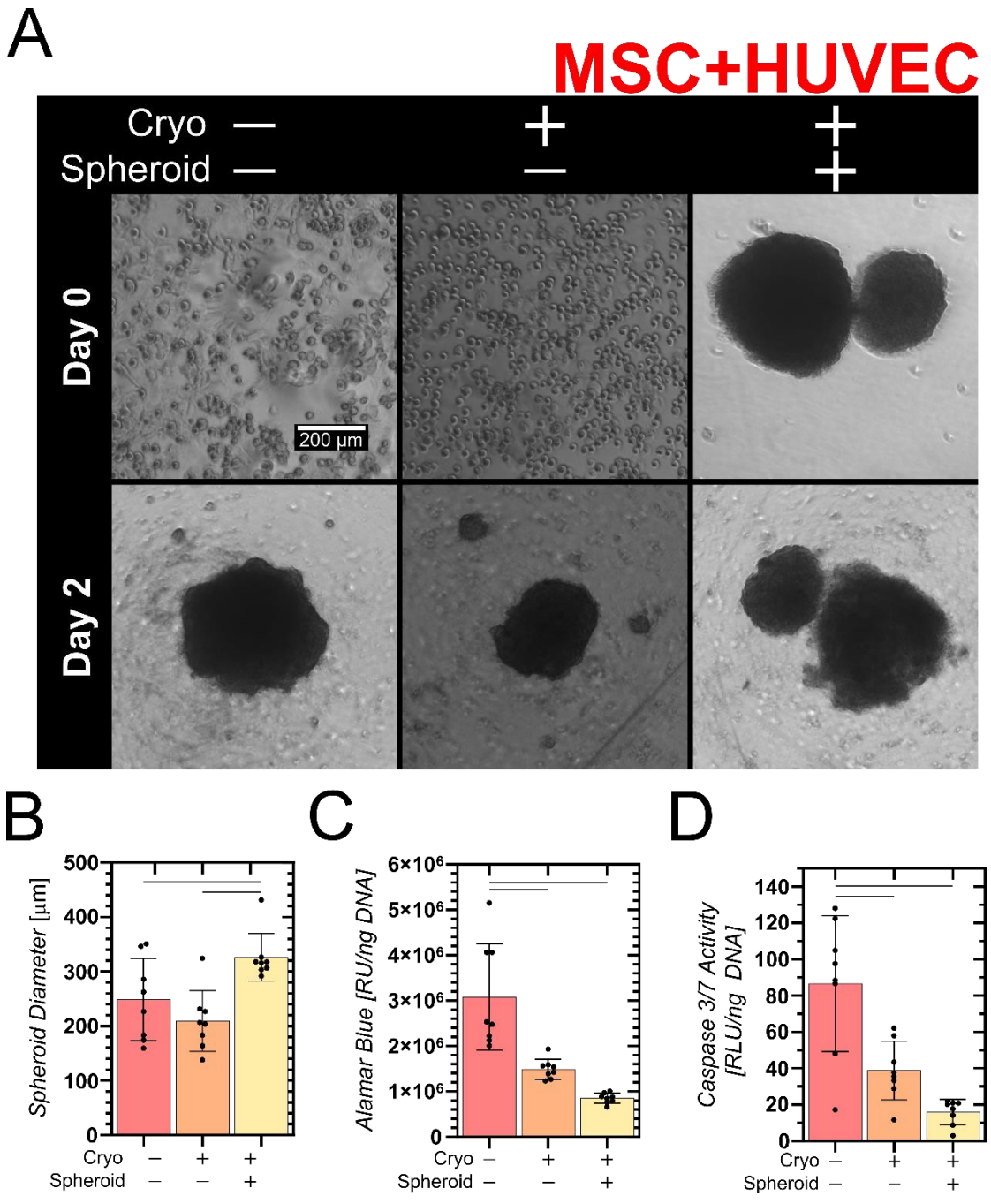

Figure 8.7 The combination of MSCs and HUVECs enabled the spheroid formation of post-cryopreserved cells in microwells. Similar to MSCs, dispersed cells seeded into microwells formed spheroids within two days (A). While the cryopreserved spheroids initially had a high contrasting boundary as the spheroids formed from

dispersed cells, after two days, the boundaries became less sharp in the larger MSC spheroid. Cryopreserved spheroids were significantly larger than the other conditions (B). Interestingly, as metabolic activity decreased between conditions (C), so did caspase activity (D). Notably, non-cryopreserved cells had significantly more metabolic activity and caspase activity. Brightfield images were taken via an inverted phase-contrast microscope. Bar graphs present the mean ± SD with individual data points (n = 8). Lines between groups represent statistically significant differences ($P < 0.05$) assessed by performing a one-way ANOVA followed by a Tukey's multiple comparison test.

8.3.7 Assessing the effects of cryopreserving MSCs and HUVECs together

We next assessed the outcomes from cryopreserving solutions or spheroids containing both MSCs and HUVECs. These cells were additionally cultured in EBM-2 media without the supplemental growth factors. As a baseline, the combination of MSCs and HUVECs was compared to cryopreserved HUVECs. Similar to previous experiments (Figure 8.4A), HUVECs were more proliferative from dispersed cryopreserved cells than cryopreserved spheroids (Figure 8.8A). The addition of MSCs reduced the difference between these conditions, but the decrease with cryopreserved cells was still statistically significant. Interestingly, the addition of MSCs led to a decrease in proliferation with dispersed cells but an increase with cryopreserved spheroids. Additionally, dispersed HUVECs had a similarly large variance in spheroid diameters that did not occur with the addition of MSCs (Figure 8.8B). However, there was no significant difference in spheroid diameters between dispersed HUVECs and the combination of HUVECs and MSCs. Generally, cryopreserved spheroids were smaller than spheroids formed from dispersed cells; but this difference was only significant with HUVECs alone. The addition of MSCs had a clear impact on metabolic activity (Figure 8.8C), resulting in an increase in activity with dispersed cells and a decrease with cryopreserved spheroids. Consequently, the conditions that result in more metabolically active cells depend on the inclusion of MSCs. However, the addition of MSCs did not guarantee an increase in metabolic activity. Unlike the change in trends between cryopreservation conditions, caspase activity decreased with cryopreserved spheroids (Figure 8.8D). Notably, the addition of MSCs further decreased caspase activity.

Therefore, although the addition of MSCs potentially reduced apoptosis, the addition could have consequences for proliferation and metabolic activity.

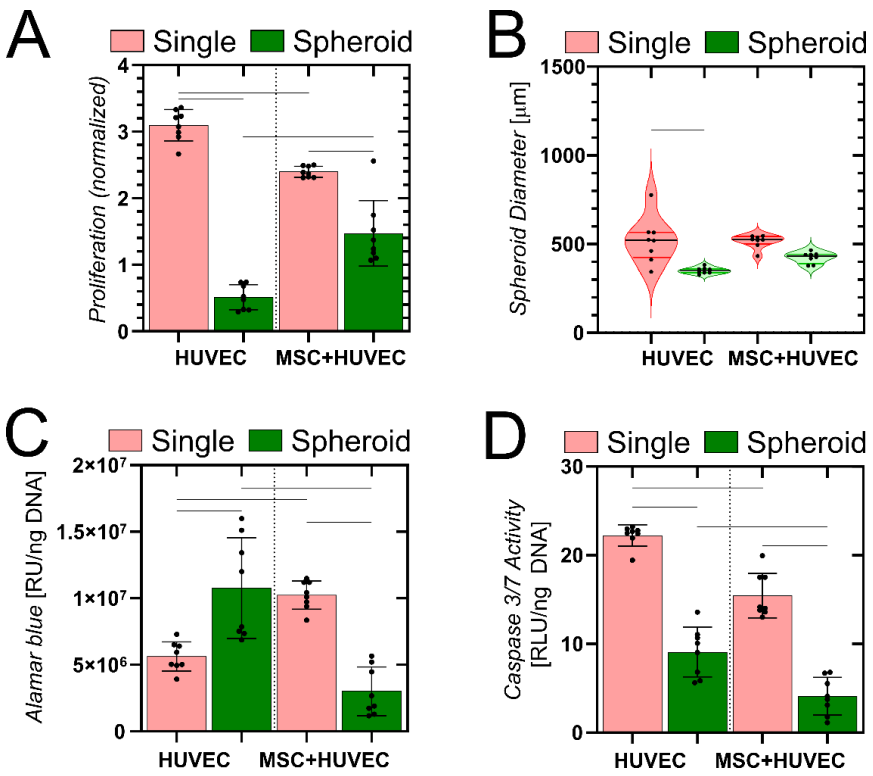

Figure 8.8 A combination of HUVECs and MSCs might improve the spheroid formation of HUVECs post-cryopreservation. For this assessment of the combination of MSCs and HUVECs, both cells were cryopreserved together, either dispersed in solution or as a preformed spheroid. These cells were then cultured in EMB-2 without the supplemental growth factors. While cryopreserved spheroids typically had less proliferation and smaller spheroids (A & B), the addition of MSC improved the proliferation with the preformed spheroids. The addition of MSCs significantly reduced the metabolic activity of preformed spheroids but increased this activity for dispersed cells (C). Overall, preformed spheroids had less caspase activity than dispersed cells, with MSCs further reducing this activity (D). Bar graphs present the mean ± SD with individual data points. The violin plot displays the mean, quartiles, and individual points. Lines between groups represent all statistically significant differences ($P < 0.05$) assessed by performing a one-way ANOVA and a Tukey's multiple comparison test.

8.4 Discussion

8.4.1 Preliminary work for performing TIG with primary HUVECs

The initial work in this chapter mirrors experiments in chapter 6, determining the effect of the modified freezing solutions for HUVECs to perform TIG. Overall, the work in this chapter aimed to address the feasibility of TIG to encapsulate cells and determine what conditions enable decidedly improved metabolic recovery of cryopreserved cells. We focus on HUVECs as they are a valuable model system for studying vascular biology [37]. Their availability has been improved through cryopreservation techniques [38-40]; however, cryopreservation optimization often depends on the context in which cells are utilized. Here, we add calcium chloride to the cellular freezing solution, making an already hypertonic solution more hypertonic. However, we saw no change in initial viability or spheroid formation from cryopreserved cells seeded into microwells. Following established cryopreservation practices, we used a hypertonic solution to dehydrate cells when freezing [41, 42]. It is well understood that dehydration enabled by a hypertonic solution containing either intracellular or extracellular cryopreservation agents reduced the formation of intracellular ice by removing water from inside the cell [27, 43, 44]. This outcome is the fundamental process for vitrification, which uses exceedingly hypertonic solutions and rapid freezing rates to ideally prevent ice formation altogether [45, 46].

Nevertheless, the dehydration of cells can also slow the recovery of cells after cryopreservation, leading to apoptosis [47]. The tolerance to this dehydration has been suggested to depend on the cell type [47, 48], likely a consequence of how hypertonic solutions can induce remodeling of actin [49]. Furthermore, the transition from this

hypertonic solution to an isotonic one is known to cause swelling, leading to osmotic shock and possibly lysis [24, 41, 50]. While we do not observe an increase in necrosis after thawing cells, indicating cells did not lyse due to ice or osmotic shifts, the actin remodeling could have influenced HUVEC spheroid formation.

The difference between the experiments where calcium was added to the freezing solution and the following experiment where TIG was performed was how the calcium was diluted. When seeded into microwells, cryovial-frozen cells were thawed and immersed in new media to dilute the calcium concentration closer to physiologic levels. However, samples undergoing TIG likely had further calcium dilution due to uptake into the hydrogel and dilution into the alginate and washing solutions. We suspected that dilution of freezing solution components by submersion into media would be a marked improvement from traditional practices of waiting for the solutions to thaw within the cryovial, a process we suspected to be in agreement with previous cryopreservation studies whose results encourage the practice of serial dilution [51]. While this result is promising on its own, the role of calcium suggests a potential benefit to supplementing freezing solutions with calcium.

Most notably, we had significantly more proliferation when the amount of calcium chloride in the freezing solution was increased from 75 to 100 mM. Calcium is a ubiquitous secondary messenger that regulates a wide variety of cellular functions [52]. Previous studies would suggest that the addition of calcium would be harmful to cryopreserved cells. Notably, many studies involving cryopreservation and the effects of calcium were with spermatozoa [53-55]. In these studies, spermatozoa had elevated intracellular calcium post-cryopreservation, which affected hyperactivation and

capacitation functions. Therefore, cryopreservation influenced calcium homeostasis by decreasing calcium entry through the membrane and increasing release from internal stores [54, 56]. This release of calcium from internal stores while cooling was also observed in platelets, with damage being reduced by adding calcium chelators [57]. For endothelial cells, there is evidence that cryopreservation activates protein kinase C, increasing intracellular calcium, but not likely from extracellular calcium influx through voltage-operated calcium channels [58]. The loss of calcium would impact metabolic activity, an outcome that could be cytoprotective immediately after thawing cryopreserved cells. Cytosolic calcium leads to cell death via apoptosis [59]. The process leads to cas-3 activation, as calcium activation of calcineurin dephosphorylated Bad [60]. However, the reduction in metabolic processes post-cryopreservation could further inhibit plasma membrane Ca2+ ATPases [61], potentially providing resistance to tumor necrosis factor [62]. While extracellular calcium in the freezing solution has not been previously explored, the results presented here suggest calcium's role could be more than an osmotic one. More generally, this work in the context of previous literature highlights the current gap in knowledge for understanding how ion channels influence post-cryopreservation viability and function. Nevertheless, these perspectives extend beyond the objectives presented in this chapter. Consequently, we transition to studying how the aggregation of cells and preformed spheroids are impacted by cryopreservation.

8.4.2 Obtaining HUVEC spheroids post-cryopreservation

A better understanding of how spheroids form or respond after cryopreservation could be immediately applicable to its implementation with TIG techniques. Moreover, this knowledge can also reveal what processes of cryopreservation are most damaging towards cell function. Here, we examined cryopreserved spheroids formed over three days and quantified post-cryopreservation spheroids three days after seeing onto microwells. These timelines align with previous work in which this time was sufficient to ensure complete spheroid formation [63] and capturing apoptotic events due to freeze/thawing of cells [64, 65]. We found HUVECs had more difficulty forming aggregates from dispersed cells while the cryopreserved spheroids had more metabolic activity and less apoptosis after seeding. While this result has not been previously described in the literature, one study from 1999 suggests how cryopreservation alters the HUVEC cytoskeleton [66], potentially causing similar negative consequences as observed in MSC, embryonic stem cells, and hepatocytes [27, 67-69].

There was only slight improvement for HUVECs with the addition of the ROCK inhibitor, Y-27632. According to previous reports, Y-27632 has shown beneficial outcomes for cryopreserved cells and endothelial cell spheroids formation alone [31-33, 70], but not together. Under both conditions, apoptosis due to inhibition of cell binding capacity or dissociation can be altered by this inhibitor. Nevertheless, the improved proliferation with only dissociated cells suggests a potential benefit of adding the inhibitor compared to cryopreserved spheroids. Because spheroids improve the relevance of *in vitro* results and act as building blocks for larger tissues [63; 71], understanding how cryopreservation affects cell-cell contacts might be crucial for endothelial-based cell therapies' vasculogenic potential.

8.4.3 Obtaining MSC spheroids post-cryopreservation contrasts trends with HUVECs

We performed similar experiments as the HUVEC cells with MSCs, which resulted in a contrasting conclusion. Most pertinent was the apparent damage caused by cryopreserving MSC spheroids. Not only did the spheroid lose its defined boundary two days post-thawing, but the metabolic activity was significantly lower than the dispersed cells despite the similar spheroid size. Notably, cell debris could only be removed from the microwells with media replacement or autophagy from surrounding cells. Media replacement was not performed because it removed cells or disrupted spheroid formation. While the alginate hydrogel capsules could potentially bypass this issue, here, cells would need to adapt through autophagy or continue down an apoptosis cascade [71-73]. Regardless, this does not explain the inverse trends in spheroid formation and metabolic activity. One explanation is that dispersed cells can better regulate their dehydration during cryopreservation than aggregated or adherent cells. In accordance with previous reports, MSCs have a high ineffective cell volume, 59% compared to the 30-40% found in other cells, making them sensitized to osmotic shock [74]. This ineffective cell volume represents an insoluble volume fraction that is not liquid, and therefore not osmotically active. With this ineffective volume and 3D structure, the semipermeable membranes become more prone to cryodamage [75]. Furthermore, diffusion of the CPA may be slowed by the semipermeable membranes of cells, resulting in a further opportunity for osmotic shock or CPA cytotoxicity [76, 77]. Notably, MSCs have been shown to have imperfect osmotic sensing post-thawing [76], suggesting the cause of the differences between dispersed cells and cryopreserved

spheroids to be from osmotic damages in addition to cryodamage from ice formation. Overall, spheroids formed from MSCs exhibited enhanced therapeutic potential and greater resistance to apoptosis compared to individual cells [36, 78, 79]. Our work suggests that the optimal pathway for obtaining MSC spheroids is from dispersed cells placed in aggregation-enabling materials post-thawing.

8.4.4 Comparative analysis of post-cryopreservation outcomes of MSCs and HUVECs

HUVECs had greater activity post-thawing from cryopreserved spheroids, despite MSCs being generally more metabolically active. Alternatively, the difficulty of HUVECs to aggregate likely influenced the reduced metabolic activity and more apoptosis activity in microwells seeded with previously cryopreserved dispersed cells. Anoikis is the term describing anchorage-dependent cell death. This process is integrin dependent, such that integrin clustering promotes cell survival in downstream pathways [80]. While MSCs were more capable of forming spheroids from dispersed cells, HUVECs likely needed components of an extracellular matrix to promote aggregation and cell survival. The deposited ECM of preformed HUVEC spheroids could be the source of integrin clustering, supporting the improved outcomes from cryopreserved HUVEC spheroids. Cryopreservation has been shown to disrupt the cytoskeleton in MSCs, potentially making them distinct from non-cryopreserved MSCs [22], and HUVECs [66]. Notably, cell-cell adhesion in endothelial cells is primarily performed by VE-cadherins [81]. However, there is currently no direct evidence of how cryopreservation affects VE-cadherin expression or performance. Nevertheless, alterations to the actin cytoskeleton are expected to influence VE-cadherin localization [82, 83]. Moreover, processes

important for cell-cell and cell-ECM interactions are impacted more with endothelial cells than MSCs. One study found that while cryoinjury led to a reduced integrin and cadherin binding capacity, MSCs had a 40% reduction in fibronectin deposition, and human endothelial cells had an 80% reduction [22]. Consistent with this previous report, the inability of HUVECs to deposit ECM could be a partial explanation for the outcomes we observed. Together, the differences in the efficacy of spheroid formation could be partially explained by different capacities to produce ECM and form cell-cell interactions.

8.4.5 The order-of-operations influence how MSCs and HUVECs perform together

Given the different responses to cryopreservation between MSC and HUVECs, we then combined both cells post-thawing using the same conditions explored with each cell independently. Compellingly, single spheroids formed dispersed cells, but the cryopreserved spheroids remain distinct. The combination of both cells in dispersion resulted in more effective aggregation compared to HUVECs alone, but these spheroids were not as smooth at the boundary as only MSCs. This result suggests a difference in spheroid packing, which could influence nutrient transport within the spheroid [84]. However, it is unclear how the supporting matrix alters these properties and alters osmotic transients involved with cryopreservation. The supporting matrix seems especially relevant for the cryopreserved spheroids that did not aggregate together despite remaining attached at the same point. Unexpectedly, these spheroids did not aggregate together, remodeling their ECM and partitioning themselves based on the differential adhesion hypothesis (DAH) [85, 86], suggesting a potential detrimental outcome of cryopreservation of spheroids. As previously described, one of the primary

shortcomings of cryopreservation of spheroids is the inability of the cryoprotectant to diffuse through thicker samples, resulting in more osmotic stress than in dispersed cells [87]. While cell-adhesion might reduce anoikis, the outcome could still negatively impact metabolic activity, EMC remodeling, and cell migration.

When MSCs and HUVECs were cryopreserved together, the detrimental trends from cryopreserving MSC spheroids dispersed cells or spheroids were also observed. While this primarily negatively affects metabolic activity, proliferation was enhanced, and apoptosis was reduced compared to utilizing HUVECs alone. Combining both MSCs and HUVECs as spheroids is interesting as it has been shown to accelerate vascularization in ischemic tissue *in vivo* [88]. While it is still unclear from this work which process remains optimal for vascularization, these data could indicate that the optimal combination is one that we have not tried. Specifically, cryopreserving HUVEC spheroids with dispersed MSCs. Regardless of the order of operations, immediate exposure of the cell types to each other did reduce apoptosis activity post-thawing, suggesting a potential enhancement of therapeutic cells. To facilitate post-thawing interactions of these cell types, future work could incorporate TIG to encapsulate HUVEC spheroids and dispersed MSCs. While explored in our concluding chapter, the permeable alginate capsule could not only promote dilution of cell debris and the CPA, but the capsule can act as a mini-bioreactor, and transwell inserts to study the paracrine signaling between cells post-cryopreservation.

8.5 Conclusion

This chapter described the condition of spheroids either cryopreserved whole or formed from previously cryopreserved dispersed cells. To our knowledge, this work is the first to systematically compare the order of cryopreservation to obtain spheroids, which we performed with both HUVEC and MSCs. Our results described how each technique could likely dramatically improve post-cryopreservation recovery dependent on the cell type. Combining both cell types enabled beneficial outcomes observed with each cell type individually. For example, dispersed MSCs and HUVECs together enabled more rapid spheroid formation than with HUVECs alone. Although we focus on cell survival, metabolism, spheroid formation, and apoptosis, this work does not address the function of these cells. The work also does not determine the cause of the different outcomes for MSCs and HUVECs. Therefore, future work should address what is the sources of this cryopreservation; how is integrin and cadherin clustering impacted by cryopreservation; and if the optimal outcomes for metabolic recovery confer similar improvements to cell functions. These will be further addressed in the following concluding chapter.

8.6 References

[1] Y.-C. Lu *et al.*, "Scalable Production and Cryostorage of Organoids Using Core–Shell Decoupled Hydrogel Capsules," *Advanced Biosystems,* vol. 1, no. 12, p. 1700165, 2017/12/01 2017, doi: https://doi.org/10.1002/adbi.201700165.

[2] H. Gurruchaga *et al.*, "Advances in the slow freezing cryopreservation of microencapsulated cells," *Journal of Controlled Release,* vol. 281, pp. 119-138, 2018/07/10/ 2018, doi: https://doi.org/10.1016/j.jconrel.2018.05.016.

[3] R. Malpique *et al.*, "Alginate Encapsulation as a Novel Strategy for the Cryopreservation of Neurospheres," *Tissue Engineering Part C: Methods,* vol. 16, no. 5, pp. 965-977, 2010/10/01 2009, doi: 10.1089/ten.tec.2009.0660.

[4] K. Arai, D. Murata, S. Takao, A. R. Verissiomo, and K. Nakayama, "Cryopreservation method for spheroids and fabrication of scaffold-free tubular constructs," (in eng), *PLoS One,* vol. 15, no. 4, p. e0230428, 2020.

[5] X. Guo, S. Li, Q. Ji, R. Lian, and J. Chen, "Enhanced viability and neural differential potential in poor post-thaw hADSCs by agarose multi-well dishes and spheroid culture," in *Hum Cell*, vol. 28, no. 4). Japan, 2015, pp. 175-89.

[6] F. C. Tan *et al.*, "Optimization of cryopreservation of stem cells cultured as neurospheres: comparison between vitrification, slow-cooling and rapid cooling freezing protocols," (in eng), *Cryo Letters,* vol. 28, no. 6, pp. 445-60, Nov-Dec 2007.

[7] H.-J. Kim *et al.*, "Three-Dimensional Spheroid Formation of Cryopreserved Human Dental Follicle-Derived Stem Cells Enhances Pluripotency and

Osteogenic Induction Properties," (in eng), *Tissue engineering and regenerative medicine,* vol. 16, no. 5, pp. 513-523, 2019, doi: 10.1007/s13770-019-00203-0.

[8] B. Desoize and J. Jardillier, "Multicellular resistance: a paradigm for clinical resistance?," in *Crit Rev Oncol Hematol*, vol. 36, no. 2-3). Netherlands, 2000, pp. 193-207.

[9] J. Friedrich, C. Seidel, R. Ebner, and L. A. Kunz-Schughart, "Spheroid-based drug screen: considerations and practical approach," *Nature Protocols,* vol. 4, no. 3, pp. 309-324, 2009/03/01 2009, doi: 10.1038/nprot.2008.226.

[10] A. M. Laib, A. Bartol, A. Alajati, T. Korff, H. Weber, and H. G. Augustin, "Spheroid-based human endothelial cell microvessel formation in vivo," in *Nat Protoc*, vol. 4, no. 8). England, 2009, pp. 1202-15.

[11] R. Foty, "A simple hanging drop cell culture protocol for generation of 3D spheroids," (in eng), *J Vis Exp,* no. 51, May 6 2011.

[12] M. Chatzinikolaidou, "Cell spheroids: the new frontiers in in vitro models for cancer drug validation," *Drug Discovery Today,* vol. 21, no. 9, pp. 1553-1560, 2016/09/01/ 2016, doi: https://doi.org/10.1016/j.drudis.2016.06.024.

[13] M. W. Laschke and M. D. Menger, "Life is 3D: Boosting Spheroid Function for Tissue Engineering," *Trends in Biotechnology,* vol. 35, no. 2, pp. 133-144, 2017/02/01/ 2017, doi: https://doi.org/10.1016/j.tibtech.2016.08.004.

[14] M. A. Gionet-Gonzales and J. K. Leach, "Engineering principles for guiding spheroid function in the regeneration of bone, cartilage, and skin," *Biomedical Materials,* vol. 13, no. 3, p. 034109, 2018/03/21 2018, doi: 10.1088/1748-605x/aab0b3.

[15] H. Byun, Y. Bin Lee, E. M. Kim, and H. Shin, "Fabrication of size-controllable human mesenchymal stromal cell spheroids from micro-scaled cell sheets," (in eng), *Biofabrication,* vol. 11, no. 3, p. 035025, Jun 7 2019, doi: 10.1088/1758-5090/ab21f6.

[16] E. J. Woods, S. Thirumala, S. S. Badhe-Buchanan, D. Clarke, and A. J. Mathew, "Off the shelf cellular therapeutics: Factors to consider during cryopreservation and storage of human cells for clinical use," *Cytotherapy,* vol. 18, no. 6, pp. 697-711, 2016/06/01/ 2016, doi: https://doi.org/10.1016/j.jcyt.2016.03.295.

[17] C. M. Madl, S. C. Heilshorn, and H. M. Blau, "Bioengineering strategies to accelerate stem cell therapeutics," *Nature,* vol. 557, no. 7705, pp. 335-342, 2018/05/01 2018, doi: 10.1038/s41586-018-0089-z.

[18] C. J. Hunt, "Technical Considerations in the Freezing, Low-Temperature Storage and Thawing of Stem Cells for Cellular Therapies," *Transfusion Medicine and Hemotherapy,* vol. 46, no. 3, pp. 134-150, 2019, doi: 10.1159/000497289.

[19] A. Bissoyi, B. Nayak, K. Pramanik, and S. K. Sarangi, "Targeting cryopreservation-induced cell death: a review," (in eng), *Biopreserv Biobank,* vol. 12, no. 1, pp. 23-34, Feb 2014, doi: 10.1089/bio.2013.0032.

[20] M. V. Puzanov, L. B. Vasilyeva, P. V. Popova, E. N. Grineva, and R. I. Dmitrieva, "New Approach to Cryopreservation of Primary Noncultivated Human Umbilical Vein Endothelium in Biobanking," *Biopreservation and Biobanking,* vol. 16, no. 2, pp. 114-119, 2018/04/01 2018, doi: 10.1089/bio.2017.0086.

[21] S. M. Zeisberger, B. Weber, and S. P. Hoerstrup, "Biobanking and Cryopreservation of Obstetrical Cell Sources for Cardiovascular Tissue

Engineering: Implications for Future Therapies," in *Human Fetal Tissue Transplantation*, N. Bhattacharya and P. Stubblefield Eds. London: Springer London, 2013, pp. 423-436.

[22] R. Chinnadurai *et al.*, "Actin cytoskeletal disruption following cryopreservation alters the biodistribution of human mesenchymal stromal cells in vivo," (in eng), *Stem Cell Reports,* vol. 3, no. 1, pp. 60-72, Jul 8 2014.

[23] C. S. Chen, M. Mrksich, S. Huang, G. M. Whitesides, and D. E. Ingber, "Geometric Control of Cell Life and Death," *Science,* vol. 276, no. 5317, p. 1425, 1997, doi: 10.1126/science.276.5317.1425.

[24] D. Gao and J. K. Critser, "Mechanisms of Cryoinjury in Living Cells," *ILAR Journal,* vol. 41, no. 4, pp. 187-196, 2000, doi: 10.1093/ilar.41.4.187.

[25] K. Liu, Y. Yang, and J. Mansbridge, "Comparison of the stress response to cryopreservation in monolayer and three-dimensional human fibroblast cultures: stress proteins, MAP kinases, and growth factor gene expression," (in eng), *Tissue Eng,* vol. 6, no. 5, pp. 539-54, Oct 2000, doi: 10.1089/107632700750022189.

[26] X. Xu, Y. Liu, Z. Cui, Y. Wei, and L. Zhang, "Effects of osmotic and cold shock on adherent human mesenchymal stem cells during cryopreservation," in *J Biotechnol*, vol. 162, no. 2-3). Netherlands: © 2012 Elsevier B.V, 2012, pp. 224-31.

[27] D. Freimark *et al.*, "Systematic parameter optimization of a Me(2)SO- and serum-free cryopreservation protocol for human mesenchymal stem cells," in *Cryobiology*, vol. 63, no. 2). Netherlands: © 2011 Elsevier Inc, 2011, pp. 67-75.

[28] R. Malpique, F. Ehrhart, A. Katsen-Globa, H. Zimmermann, and P. M. Alves, "Cryopreservation of Adherent Cells: Strategies to Improve Cell Viability and Function After Thawing," *Tissue Engineering Part C: Methods,* vol. 15, no. 3, pp. 373-386, 2009/09/01 2009, doi: 10.1089/ten.tec.2008.0410.

[29] K. T. Campbell, R. S. Stilhano, and E. A. Silva, "Enzymatically degradable alginate hydrogel systems to deliver endothelial progenitor cells for potential revasculature applications," (in eng), *Biomaterials,* vol. 179, pp. 109-121, 2018, doi: 10.1016/j.biomaterials.2018.06.038.

[30] K. T. Campbell, K. Wysoczynski, D. J. Hadley, and E. A. Silva, "Computational-Based Design of Hydrogels with Predictable Mesh Properties," *ACS Biomaterials Science & Engineering,* vol. 6, no. 1, pp. 308-319, 2020/01/13 2020, doi: 10.1021/acsbiomaterials.9b01520.

[31] X. Li, G. Meng, R. Krawetz, S. Liu, and D. E. Rancourt, "The ROCK inhibitor Y-27632 enhances the survival rate of human embryonic stem cells following cryopreservation," (in eng), *Stem Cells Dev,* vol. 17, no. 6, pp. 1079-85, Dec 2008, doi: 10.1089/scd.2007.0247.

[32] R. Martin-Ibañez, C. Unger, A. Strömberg, D. Baker, J. M. Canals, and O. Hovatta, "Novel cryopreservation method for dissociated human embryonic stem cells in the presence of a ROCK inhibitor," in *Hum Reprod*, vol. 23, no. 12). England, 2008, pp. 2744-54.

[33] Y. Guo *et al.*, "The effects of ROCK inhibitor Y-27632 on injectable spheroids of bovine corneal endothelial cells," (in eng), *Cellular reprogramming,* vol. 17, no. 1, pp. 77-87, 2015/02// 2015, doi: 10.1089/cell.2014.0070.

[34] S. So *et al.*, "The Rho-associated kinase inhibitor fasudil can replace Y-27632 for use in human pluripotent stem cell research," (in eng), *PloS one,* vol. 15, no. 5, pp. e0233057-e0233057, 2020, doi: 10.1371/journal.pone.0233057.

[35] in *Assay Guidance Manual*, S. Markossian *et al.* Eds. Bethesda MD, 2004.

[36] K. C. Murphy, S. Y. Fang, and J. K. Leach, "Human mesenchymal stem cell spheroids in fibrin hydrogels exhibit improved cell survival and potential for bone healing," (in eng), *Cell Tissue Res,* vol. 357, no. 1, pp. 91-9, Jul 2014.

[37] A. B. Sultani, L. A. Marquez-Curtis, J. A. Elliott, and L. E. McGann, "Improved Cryopreservation of Human Umbilical Vein Endothelial Cells: A Systematic Approach," (in eng), *Sci Rep,* vol. 6, p. 34393, Oct 6 2016.

[38] D. E. Pegg, "Cryopreservation of vascular endothelial cells as isolated cells and as monolayers," in *Cryobiology*, vol. 44, no. 1). Netherlands: 2002 Elsevier Science (USA). 2002, pp. 46-53.

[39] K. Lehle, M. Hoenicka, V. R. Jacobs, F. X. Schmid, and D. E. Birnbaum, "Cryopreservation of human endothelial cells for vascular tissue engineering," in *Cryobiology*, vol. 50, no. 2). Netherlands, 2005, pp. 154-61.

[40] K. Lehle, M. Hoenicka, V. R. Jacobs, F. X. Schmid, and D. E. Birnbaum, "Identification and reduction of cryoinjury in endothelial cells: a first step toward establishing a cell bank for vascular tissue engineering," (in eng), *Tissue Eng,* vol. 12, no. 12, pp. 3439-47, Dec 2006, doi: 10.1089/ten.2006.12.3439.

[41] D. E. Pegg and M. P. Diaper, "The effect of initial tonicity on freeze/thaw injury to human red cells suspended in solutions of sodium chloride," *Cryobiology,* vol. 28,

no. 1, pp. 18-35, 1991/02/01/ 1991, doi: https://doi.org/10.1016/0011-2240(91)90004-8.

[42] D. E. Pegg, "Principles of Cryopreservation," in *Cryopreservation and Freeze-Drying Protocols*, J. G. Day and G. N. Stacey Eds. Totowa, NJ: Humana Press, 2007, pp. 39-57.

[43] P. Mazur, S. P. Leibo, and E. H. Y. Chu, "A two-factor hypothesis of freezing injury: Evidence from Chinese hamster tissue-culture cells," *Experimental Cell Research,* vol. 71, no. 2, pp. 345-355, 1972/04/01/ 1972, doi: https://doi.org/10.1016/0014-4827(72)90303-5.

[44] J. P. Acker, A. Larese, H. Yang, A. Petrenko, and L. E. McGann, "Intracellular ice formation is affected by cell interactions," in *Cryobiology*, vol. 38, no. 4). Netherlands: 1999 Academic Press., 1999, pp. 363-71.

[45] L. L. Kuleshova, S. S. Gouk, and D. W. Hutmacher, "Vitrification as a prospect for cryopreservation of tissue-engineered constructs," *Biomaterials,* vol. 28, no. 9, pp. 1585-1596, 2007/03/01/ 2007, doi: https://doi.org/10.1016/j.biomaterials.2006.11.047.

[46] B. Wowk, "Thermodynamic aspects of vitrification," *Cryobiology,* vol. 60, no. 1, pp. 11-22, 2010/02/01/ 2010, doi: https://doi.org/10.1016/j.cryobiol.2009.05.007.

[47] R. Raju, S. J. Bryant, B. L. Wilkinson, and G. Bryant, "The need for novel cryoprotectants and cryopreservation protocols: Insights into the importance of biophysical investigation and cell permeability," in *Biochim Biophys Acta Gen Subj*, vol. 1865, no. 1). Netherlands: © 2020 Elsevier B.V, 2021, p. 129749.

[48] J. E. Lovelock, "The haemolysis of human red blood-cells by freezing and thawing," *Biochimica et Biophysica Acta,* vol. 10, pp. 414-426, 1953/01/01/ 1953, doi: https://doi.org/10.1016/0006-3002(53)90273-X.

[49] S. B. Rizoli, O. D. Rotstein, J. Parodo, M. J. Phillips, and A. Kapus, "Hypertonic inhibition of exocytosis in neutrophils: central role for osmotic actin skeleton remodeling," (in eng), *Am J Physiol Cell Physiol,* vol. 279, no. 3, pp. C619-33, Sep 2000, doi: 10.1152/ajpcell.2000.279.3.C619.

[50] J. O. M. Karlsson and M. Toner, "Long-term storage of tissues by cryopreservation: critical issues," *Biomaterials,* vol. 17, no. 3, pp. 243-256, 1996/01/01/ 1996, doi: https://doi.org/10.1016/0142-9612(96)85562-1.

[51] R. L. Levin and T. W. Miller, "An optimum method for the introduction or removal of permeable cryoprotectants: Isolated cells," *Cryobiology,* vol. 18, no. 1, pp. 32-48, 1981/02/01/ 1981, doi: https://doi.org/10.1016/0011-2240(81)90004-3.

[52] H. W. Snoeck, "Calcium regulation of stem cells," (in eng), *EMBO Rep,* vol. 21, no. 6, p. e50028, Jun 4 2020.

[53] A. Herrler, S. Eisner, V. Bach, U. Weissenborn, and H. M. Beier, "Cryopreservation of spermatozoa in alginic acid capsules," *Fertility and Sterility,* vol. 85, no. 1, pp. 208-213, 2006/01/01/ 2006, doi: https://doi.org/10.1016/j.fertnstert.2005.06.049.

[54] J. C. Kim, Y. Li, S. Lee, Y. J. Yi, C. S. Park, and S. H. Woo, "Effects of cryopreservation on Ca2+ signals induced by membrane depolarization, caffeine, thapsigargin and progesterone in boar spermatozoa," in *Mol Cells*, vol. 26, no. 6). Korea South, 2008, pp. 558-65.

[55] J. L. Bailey, J.-F. Blodeau, and N. Cormier, "Semen Cryopreservation in Domestic Animals: A Damaging and Capacitating Phenomenon Minireview," *Journal of Andrology,* vol. 21, no. 1, pp. 1-7, 2000/01/02 2000, doi: https://doi.org/10.1002/j.1939-4640.2000.tb03268.x.

[56] J. L. Bailey and M. M. Buhr, "Regulation of Internal Ca2+ by Chilled Bull and Boar Spermatozoa," *Cryobiology,* vol. 32, no. 3, pp. 259-269, 1995/06/01/ 1995, doi: https://doi.org/10.1006/cryo.1995.1025.

[57] L. Waters, M. P. Padula, D. C. Marks, and L. Johnson, "Calcium chelation: a novel approach to reduce cryopreservation-induced damage to frozen platelets," (in eng), *Transfusion,* vol. 60, no. 7, pp. 1552-1563, Jul 2020, doi: 10.1111/trf.15799.

[58] E. Müller-Schweinitzer, D. C. Reineke, E. Glusa, A. B. Ebeigbe, M. T. R. Grapow, and T. P. Carrel, "Activated Rho/Rho kinase and modified calcium sensitivity in cryopreserved human saphenous veins," *Cryobiology,* vol. 57, no. 1, pp. 37-45, 2008/08/01/ 2008, doi: https://doi.org/10.1016/j.cryobiol.2008.05.003.

[59] J. I. E. Bruce, "Metabolic regulation of the PMCA: Role in cell death and survival," (in eng), *Cell Calcium,* vol. 69, pp. 28-36, Jan 2018, doi: 10.1016/j.ceca.2017.06.001.

[60] H. G. Wang *et al.*, "Ca2+-induced apoptosis through calcineurin dephosphorylation of BAD," (in eng), *Science,* vol. 284, no. 5412, pp. 339-43, Apr 9 1999, doi: 10.1126/science.284.5412.339.

[61] P. K. Janicki, P. E. Wise, A. E. Belous, and C. W. Pinson, "Interspecies differences in hepatic Ca(2+)-ATPase activity and the effect of cold preservation

on porcine liver Ca(2+)-ATPase function," in *Liver Transpl*, vol. 7, no. 2). United States, 2001, pp. 132-9.

[62] K. Ono, X. Wang, and J. Han, "Resistance to tumor necrosis factor-induced cell death mediated by PMCA4 deficiency," (in eng), *Mol Cell Biol,* vol. 21, no. 24, pp. 8276-88, Dec 2001.

[63] C. E. Vorwald, K. C. Murphy, and J. K. Leach, "Restoring vasculogenic potential of endothelial cells from diabetic patients through spheroid formation," (in eng), *Cell Mol Bioeng,* vol. 11, no. 4, pp. 267-278, Aug 2018.

[64] X. Xu, S. Cowley, C. J. Flaim, W. James, L. Seymour, and Z. Cui, "The roles of apoptotic pathways in the low recovery rate after cryopreservation of dissociated human embryonic stem cells," (in eng), *Biotechnology progress,* vol. 26, no. 3, pp. 827-837, May-Jun 2010, doi: 10.1002/btpr.368.

[65] M. A. Savitskaya and G. E. Onishchenko, "Apoptosis in cryopreserved eukaryotic cells," *Biochemistry (Moscow),* vol. 81, no. 5, pp. 445-452, 2016/05/01 2016, doi: 10.1134/S0006297916050023.

[66] T. Eberl *et al.*, "Ultrastructural analysis of human endothelial cells after hypothermic storage in organ preservation solutions," in *J Surg Res*, vol. 82, no. 2). United States: 1999 Academic Press., 1999, pp. 253-60.

[67] S. Renzi, T. Lombardo, S. Dotti, S. S. Dessì, P. De Blasio, and M. Ferrari, "Mesenchymal stromal cell cryopreservation," (in eng), *Biopreserv Biobank,* vol. 10, no. 3, pp. 276-81, Jun 2012, doi: 10.1089/bio.2012.0005.

[68] V. Wagh *et al.*, "Effects of cryopreservation on the transcriptome of human embryonic stem cells after thawing and culturing," (in eng), *Stem Cell Rev Rep,* vol. 7, no. 3, pp. 506-17, Sep 2011, doi: 10.1007/s12015-011-9230-1.

[69] X. Stéphenne, M. Najimi, and E. M. Sokal, "Hepatocyte cryopreservation: is it time to change the strategy?," (in eng), *World J Gastroenterol,* vol. 16, no. 1, pp. 1-14, Jan 7 2010.

[70] K. Watanabe *et al.*, "A ROCK inhibitor permits survival of dissociated human embryonic stem cells," in *Nat Biotechnol*, vol. 25, no. 6). United States, 2007, pp. 681-6.

[71] W. Chaabane *et al.*, "Autophagy, Apoptosis, Mitoptosis and Necrosis: Interdependence Between Those Pathways and Effects on Cancer," *Archivum Immunologiae et Therapiae Experimentalis,* vol. 61, no. 1, pp. 43-58, 2013/02/01 2013, doi: 10.1007/s00005-012-0205-y.

[72] Q. Chen, J. Kang, and C. Fu, "The independence of and associations among apoptosis, autophagy, and necrosis," *Signal Transduction and Targeted Therapy,* vol. 3, no. 1, p. 18, 2018/07/01 2018, doi: 10.1038/s41392-018-0018-5.

[73] M. Noguchi, N. Hirata, T. Tanaka, F. Suizu, H. Nakajima, and J. A. Chiorini, "Autophagy as a modulator of cell death machinery," *Cell Death & Disease,* vol. 11, no. 7, p. 517, 2020/07/08 2020, doi: 10.1038/s41419-020-2724-5.

[74] B. Parekkadan, P. Sethu, D. van Poll, M. L. Yarmush, and M. Toner, "Osmotic Selection of Human Mesenchymal Stem/Progenitor Cells from Umbilical Cord Blood," *Tissue Engineering,* vol. 13, no. 10, pp. 2465-2473, 2007/10/01 2007, doi: 10.1089/ten.2007.0054.

[75] B. C. Heng, H. Yu, and S. C. Ng, "Strategies for the cryopreservation of microencapsulated cells," *Biotechnology and Bioengineering,* vol. 85, no. 2, pp. 202-213, 2004/01/20 2004, doi: https://doi.org/10.1002/bit.10837.

[76] E. Casula, G. P. Asuni, V. Sogos, S. Fadda, F. Delogu, and A. Cincotti, "Osmotic behaviour of human mesenchymal stem cells: Implications for cryopreservation," *PLOS ONE,* vol. 12, no. 9, p. e0184180, 2017, doi: 10.1371/journal.pone.0184180.

[77] E. Casula, G. Traversari, S. Fadda, O. V. Klymenko, C. Kontoravdi, and A. Cincotti, "Modelling the osmotic behaviour of human mesenchymal stem cells," *Biochemical Engineering Journal,* vol. 151, p. 107296, 2019/11/15/ 2019, doi: https://doi.org/10.1016/j.bej.2019.107296.

[78] S. S. Ho, K. C. Murphy, B. Y. Binder, C. B. Vissers, and J. K. Leach, "Increased Survival and Function of Mesenchymal Stem Cell Spheroids Entrapped in Instructive Alginate Hydrogels," (in eng), *Stem Cells Transl Med,* vol. 5, no. 6, pp. 773-81, Jun 2016.

[79] K. C. Murphy, J. Whitehead, P. C. Falahee, D. Zhou, S. I. Simon, and J. K. Leach, "Multifactorial Experimental Design to Optimize the Anti-Inflammatory and Proangiogenic Potential of Mesenchymal Stem Cell Spheroids," (in eng), *Stem Cells,* vol. 35, no. 6, pp. 1493-1504, Jun 2017.

[80] N. Mitrousis, A. Fokina, and M. S. Shoichet, "Biomaterials for cell transplantation," *Nature Reviews Materials,* vol. 3, no. 11, pp. 441-456, 2018/11/01 2018, doi: 10.1038/s41578-018-0057-0.

[81] P. Carmeliet *et al.*, "Targeted deficiency or cytosolic truncation of the VE-cadherin gene in mice impairs VEGF-mediated endothelial survival and angiogenesis," in *Cell*, vol. 98, no. 2). United States, 1999, pp. 147-57.

[82] V. Vouret-Craviari, D. Grall, G. Flatau, J. Pouysségur, P. Boquet, and E. Van Obberghen-Schilling, "Effects of cytotoxic necrotizing factor 1 and lethal toxin on actin cytoskeleton and VE-cadherin localization in human endothelial cell monolayers," (in eng), *Infect Immun,* vol. 67, no. 6, pp. 3002-8, Jun 1999.

[83] V. Golubkov, D. Hawes, and F. S. Markland, "Anti-angiogenic activity of contortrostatin, a disintegrin from Agkistrodon contortrix contortrix snake venom," in *Angiogenesis*, vol. 6, no. 3). Germany, 2003, pp. 213-24.

[84] K. C. Murphy *et al.*, "Measurement of oxygen tension within mesenchymal stem cell spheroids," (in eng), *J R Soc Interface,* vol. 14, no. 127, Feb 2017.

[85] R. A. Foty and M. S. Steinberg, "Cadherin-mediated cell-cell adhesion and tissue segregation in relation to malignancy," in *Int J Dev Biol*, vol. 48, no. 5-6). Spain, 2004, pp. 397-409.

[86] R. A. Foty and M. S. Steinberg, "The differential adhesion hypothesis: a direct evaluation," in *Dev Biol*, vol. 278, no. 1). United States, 2005, pp. 255-63.

[87] H. Zimmermann, S. G. Shirley, and U. Zimmermann, "Alginate-based encapsulation of cells: Past, present, and future," *Current Diabetes Reports,* vol. 7, no. 4, pp. 314-320, 2007/08/01 2007, doi: 10.1007/s11892-007-0051-1.

[88] D. Y. Chen *et al.*, "Three-dimensional cell aggregates composed of HUVECs and cbMSCs for therapeutic neovascularization in a mouse model of hindlimb

ischemia," in *Biomaterials*, vol. 34, no. 8). Netherlands: © 2012 Elsevier Ltd, 2013, pp. 1995-2004.

CHAPTER 9

Conclusions, challenges, and future directions

9.1 Results and implications

The key themes of the experimental findings in this thesis are the establishment of alginate gelation protocols that align with the cryopreservation of cells. Several different hydrogels were developed and characterized for application with cryopreserved cells and potential therapeutic cargo, such as growth factors. Not only were these hydrogels being applied within the perspective of cold storage, but these outcomes appear to be the first of their kind in the field of biomedical engineering. While it will not be apparent which system works best for any specific application, we hope that the variety described in this thesis will enable further creativity to flourish in this area.

These studies establish a potential benefit towards developing hydrogels with tunable release profiles based on the expected electrostatic interactions between polymers comprising the scaffold and the cargo. Because the process would likely incorporate at least one polymer to electrostatically interact, there is also a potential cryoprotective outcome with frozen storage. Specifically, we observed this protection by the improved efficacy of refrozen VEGF in alginate. Moreover, we could reduce the diffusive release rate of various test cargos smaller than our hydrogels' calculated mesh size when the polymer and cargo with opposing net charges were frozen together. Hydrogels are generally appreciated for their capacity to protect the efficacy of the loaded cargo [1, 2]. More recently, the logistic cold chain for delivering mRNA vaccines

for COVID-19 has renewed motivations to improve the stability of therapies. The stability of these vaccines in a non-frozen state can be as short as five days, whereas frozen storage can be up to six months [3]. Therefore, the new hydrogel systems presented in this thesis addresses two aspects of protecting the efficacy of cargo, frozen storage and encapsulation, while also suggesting additional control over mechanical properties and release profiles.

Our results also indicate a capacity to encapsulate cells in hydrogels formed while thawing. These permeable hydrogels had controllable shapes and mechanical properties that resulted in an instructive material that promoted the formation of cell aggregates. In the context of cryopreservation, the formation of hydrogels while thawing could enable better control over the post-cryopreservation viability of cells that previous methods could only accomplish with serial dilutions [4]. Surprisingly, the addition of additional salts, specifically $CaCl_2$, did not detrimentally harm cell viability post-cryopreservation. Abstractly, the formation of an alginate hydrogel acts as a dynamic osmotic buffer, which could prevent damaging osmotic transients [5, 6]. Moreover, the ability to instruct aggregation in a permeable capsule post-cryopreservation could significantly reduce the time to prepare functional units for regenerative medicine. The effective long-term cryopreservation of therapeutic cells is an essential prerequisite for their sustained supply in basic research and off-the-shelf availability to clinics [7]. The formation of these permeable capsules is the development of small isolated bioreactors with many avenues for degradation [8, 9]. Therefore, these capsules provide new opportunities for cell culture without culturing in 2D tissue culture plastic [10-13], new

methods for spheroid culture without diffusion-limiting well structures [14], and with implications for priming cells for hypoxia conditions [15].

Lastly, our results indicate the optimal methods to develop spheroids from cells that will undergo cryopreservation. While we hoped that the HUVECs would aggregate together post-cryopreservation in a similar efficiency as the HEK-293 and HEK-293T cells, this was not our observed outcome. Whether TIG was used to encapsulate the cells in a capsule or after seeding into microwells, the post-cryopreserved state of HUVECs suggested it was better to preform spheroids prior to cryopreservation. However, we observed an opposite trend with the MSCs, which appeared to be structurally damaged and less viable when spheroids were cryopreserved. These results could be a crucial foundation for future research trends that seek to incorporate cryopreservation into their potential regenerative medicine strategies using spheroids. Significantly, it is well understood in cryobiology that each cell type requires an optimized cryopreservation strategy due to unique intrinsic intracellular water content, metabolic activity, and susceptibility to osmotic stress [4, 16-22]. Nevertheless, most cell providers and the researchers who use those cells follow standardized concentrations and protocols for cryopreservation. At a minimum, this work indicates that these cell types are different, and the influences from these differences can be amplified if the cells are aggregated into a larger construct.

9.2 Challenges

Several significant obstacles remain before the strategies presented here can be translated to clinical applications. Many of these obstacles are based on the need to better understand biological interactions involved with freezing and thawing cells and hydrogel formation. However, addressing these hurdles will be engineering challenges due to the inevitable trade-off between biological outcomes and the desired therapeutic outcomes.

The work in chapters 3 – 5 revealed the formation of an alginate hydrogel that was astonishingly stable, imparting a controllable change in the release profiles of cargo and was potential cryoprotective for VEGF, or at lease potentiating. However, the exact nature of these hydrogels remains a mystery. This difficulty is partly due to the complexity in modeling the movement of thermal energy in the context of liquids and phase transitions. For example, the change in temperature due to conduction-based heat transfer creates a fluid flow that impacts heat transfer and the diffusion of molecules. These aspects of heat, combined with the changes in polymer solubility and diffusion in an environment that changes its temperature, result in confounding interactions that influence thawing rate and hydrogel formation. While we abstracted these interactions to understand better what might be occurring, these outcomes will likely change based on the size scale of the hydrogels. Specifically, we suspect both micrometer and centimeter-scale hydrogels to be different from the millimeter scale hydrogels presented in this thesis. As we expanded the frozen alginate solution to 5 cm, the time to fully cross-link a hydrogel appeared to increase exponentially, coinciding with size limitations of diffusion. Nevertheless, the formation of the alginate cryogels

presented in chapter 5 did not require TIG and could bypass the challenges presented with that technique. Moving forward, firmly identifying the objectives of the proposed technology will be essential for selecting the best technique that incorporates cold storage.

Further challenges exist with the utilization of the alginate hydrogel capsules. The cryopreservation of cells inevitably leads to some level of cell death. While shifting this death to apoptosis would be advantageous to avoid inflammatory consequences of necrosis [23-28], it is unclear what happens to cell debris within the capsule. Our data suggest that large proteins, like albumin, can pass through the hydrogel shell, but what happens to organelles and apoptotic vesicles is unclear. Therefore, a permeable membrane is conceptually an improvement for post-cryopreserved cells over microwell systems without permeable walls.

Nevertheless, to improve post-cryopreservation outcomes regardless of culture condition, how cells respond to thawing remains a challenge to be addressed. Another challenge with these capsules is how the additional calcium will influence post-cryopreservation cell viability. The role of calcium is an engineering challenge due to the confounding benefit and harm this ion can have. The benefits could include hydrogel formation, further prevention of intracellular ice formation, and potentially altering transcellular calcium voltages to promote reestablishing cytosolic homeostasis [29-34]. However, the supplemental calcium could trigger calcium-sensitive apoptotic pathways, over dehydration during freezing, osmotic shock, and deviations from pre-determined cooling rates [4, 35-38]. Despite the success observed with the techniques presented in this thesis, many factors need to be accounted for in the future. The cells' resilience to

these processes is not a justification to progress without accounting for these challenges.

On a technical note, crucial timing and order-of-operation considerations are required to perform the TIG technique adequately. Although the technique is accessible to perform and was developed on a shoe-string budget, the process requires a proficient understanding of cryopreservation and alginate hydrogel cross-linking to be successful. Specifically, the alginate polymer source significantly alters the polymer's capacity to form cross-linked hydrogels due to the number of G-blocks on each polymer [2, 39]. Furthermore, the source of the divalent cation is essential. In contrast to our success with $CaCl_2$, $CaCO_3$ and $CaSO_4$ cross-link alginate too slowly in relation to the thawing of the frozen solution [40-42]. If the calcium source is frozen to form an alginate hydrogel capsule, $CaCO_3$ and $CaSO_4$ will not work as described in this thesis. Even though they could potentially still form a capsule by carefully controlling the thawing rate, cryopreserved cells must be rapid and decisive thawed to prevent ice from reforming [4, 43, 44]. Consequently, the aspects of cryopreservation are just as important. For example, the cryopreserved cells must remain frozen prior to thawing. We accomplish this with dry ice directly outside the biosafety cabinet, but we still need to move these cells aseptically. While we succeeded in this preliminary work, reducing the risk of contamination presents a significant obstacle with the products available in the marketplace. For example, commercially available cryopreservation vessels that enable the cryopreservation of samples in molds might not currently exist but could feasibly be developed.

9.3 Future directions

The work described within this thesis illustrates the utility of engineered alginate systems that coincide with cold storage techniques. This work provides a foundation of several techniques that contrast the more prominent trend in biomedical engineering of cryopreserving the cells in the encapsulated material scaffold. Expectedly, this groundwork requires additional research to develop and further motivate cold storage applications in regenerative medicine techniques.

Most apparent is the application of these techniques to a pre-existing application of tissue engineering. Specifically, the application of HUVEC spheroids as a model for angiogenesis could be performed from post-cryopreserved cells using techniques described in this thesis to determine the influences of freezing cells and the potential implications it would have on the delivery of endothelial cells for cell therapy applications. Additionally, given the apparent consequences of cryopreserving MSC spheroids, future studies should further inquire about the mechanism for this damage and why it is different for the endothelial cells in our studies. The purpose of cryopreservation research is not only to keep cells viable; cells need to retain their desired function.

Furthermore, future work should be dedicated to investigating the influence of calcium ions on cryopreserved cells. Although cryopreservation negatively impacts the responsiveness of progenitor endothelial cells to hypoxia conditions, impaired plasma membrane Ca^{2+} ATPase (PMCA) and dysregulation of cytosolic calcium is paradoxically cytoprotective by reducing responsiveness to apoptotic signals directly post-cryopreservation [34]. Unlike conditions where extended calcium ion exposure leads to

cell death [10], the influence of calcium ions with post-cryopreserved cells might have a different outcome. Our work and previous studies suggest that the influences of the calcium ion are osmotic; however, future work investigating the influences of calcium signaling post-cryopreservation could discover novel cryoprotective methods or at least determine how intracellular calcium and metabolic disruption differs with cryopreservation. Notably, this work could establish for the first time how calcium ion channels in endothelial cells are influenced by cryopreservation and how this can impact their efficacy as therapies. Therefore, these future studies would elucidate best practices for incorporating hydrogels into cryopreservation applications.

On a similar theme, future work could also be directed towards modeling cryopreservation and encapsulation to enhance our understanding of the phase transition of polymer, calcium ions, and cryoprotectants in solution. The movement of thermal energy is dependent on the temperature gradient, consequential convective flow due to density changes in solution, and the conductivity of the material. Likewise, the solute diffusion in solution depends on temperature, the concentration gradient, the permeability of the solution and can be impacted by any osmotic pressure. With the addition of a phase transition, changes in solubility due to changes in ionic strength with dilution and temperature changes, and binding kinetics of calcium to alginate also changing due to changes in concentration and temperature, many complex processes are interacting within the process of TIG. Adding cells increases the intricacy, as cells need to be dehydrated and rehydrated throughout the freezing and thawing steps. The outcomes from altering these parameters are addressed within this thesis, but the complex interactions remain a significant challenge that should be addressed in future

research. Understanding this would assuredly also apply to understanding the effects of cryopreserving spheroids or hydrogel-encapsulated cells, providing the insight required to determine optimal standard operation procedures for future cell therapies.

Moreover, some chapters motivate future research into specific areas. In chapter 3, we explored how TIG could enhance the electrostatic-based release of various cargo. Specifically, improving the electrostatic interactions between alginate and chitosan could improve the oral delivery of hydrogels by enhancing their stability through the gastric system to deliver cargo to the small intestines. In chapter 4, we described the formation of what we describe as a homo-IPN. To confirm the potential interpenetrating polymeric networks, techniques that use confocal microscopy could determine any localized differences in the hydrated network [45, 46]. In chapter 5, we discovered that the freezing of alginate with dimethyl sulfoxide led to the formation of an alginate cryogel. Combining these components to form a hydrogel has been previously described [47]. However, our results from freezing indicate that a reduced concentration of dimethyl sulfoxide is required. Additional work should address what happens to the cryopreserving agent since it stabilizes hydrogen bonding between the alginate polymers. While we already discussed some potential future directions with chapters 6 – 8, further research into possible two independent gelation events, as described in Appendix B with alginate and fibrin, could expand the potential application of the techniques described in this thesis.

Additionally, new internal geometries of the capsules could promote different outcomes, as is observed with microwell systems [14, 48-51]. We also explored the use of cell cycle indicators in chapter 7. Given the challenges with assessing spheroids

without destructive techniques, such as fixing and staining or digesting the spheroid, this technique shows promise for spheroidal analysis. We could not develop a protocol for using the FUCCI system with spheroids with the resources at our disposal and time constraints. Nevertheless, the system is likely to have a higher chance of success as an informative assay with confocal imaging.

Overall, this thesis generated a foundation for future cryobiology research, bridging cryopreservation and tissue engineering perspectives to potentially improve the therapeutic potency and efficacy of future research in regenerative medicine.

9.4 References

[1] C. M. Silva, A. J. Ribeiro, I. V. Figueiredo, A. R. Gonçalves, and F. Veiga, "Alginate microspheres prepared by internal gelation: Development and effect on insulin stability," *International Journal of Pharmaceutics,* vol. 311, no. 1, pp. 1-10, 2006/03/27/ 2006, doi: https://doi.org/10.1016/j.ijpharm.2005.10.050.

[2] K. Y. Lee and D. J. Mooney, "Alginate: properties and biomedical applications," (in eng), *Progress in polymer science,* vol. 37, no. 1, pp. 106-126, 2012, doi: 10.1016/j.progpolymsci.2011.06.003.

[3] D. J. A. Crommelin, T. J. Anchordoquy, D. B. Volkin, W. Jiskoot, and E. Mastrobattista, "Addressing the Cold Reality of mRNA Vaccine Stability," (in eng), *J Pharm Sci,* vol. 110, no. 3, pp. 997-1001, Mar 2021.

[4] C. J. Hunt, "Technical Considerations in the Freezing, Low-Temperature Storage and Thawing of Stem Cells for Cellular Therapies," *Transfusion Medicine and Hemotherapy,* vol. 46, no. 3, pp. 134-150, 2019, doi: 10.1159/000497289.

[5] B. J. Fuller, "Cryoprotectants: the essential antifreezes to protect life in the frozen state," *Cryoletters,* vol. 25, no. 6, pp. 375-388, // 2004.

[6] G. D. Elliott, S. Wang, and B. J. Fuller, "Cryoprotectants: A review of the actions and applications of cryoprotective solutes that modulate cell recovery from ultra-low temperatures," *Cryobiology,* vol. 76, pp. 74-91, 2017/06/01/ 2017, doi: https://doi.org/10.1016/j.cryobiol.2017.04.004.

[7] Y. Xu *et al.*, "Optimization of UC-MSCs cold-chain storage by minimizing temperature fluctuations using an automatic cryopreservation system,"

Cryobiology, vol. 99, pp. 131-139, 2021/04/01/ 2021, doi: https://doi.org/10.1016/j.cryobiol.2020.11.010.

[8] K. T. Campbell, R. S. Stilhano, and E. A. Silva, "Enzymatically degradable alginate hydrogel systems to deliver endothelial progenitor cells for potential revasculature applications," (in eng), *Biomaterials,* vol. 179, pp. 109-121, 2018, doi: 10.1016/j.biomaterials.2018.06.038.

[9] K. T. Campbell, K. Wysoczynski, D. J. Hadley, and E. A. Silva, "Computational-Based Design of Hydrogels with Predictable Mesh Properties," *ACS Biomaterials Science & Engineering,* vol. 6, no. 1, pp. 308-319, 2020/01/13 2020, doi: 10.1021/acsbiomaterials.9b01520.

[10] S. S. Ho, K. C. Murphy, B. Y. Binder, C. B. Vissers, and J. K. Leach, "Increased Survival and Function of Mesenchymal Stem Cell Spheroids Entrapped in Instructive Alginate Hydrogels," (in eng), *Stem Cells Transl Med,* vol. 5, no. 6, pp. 773-81, Jun 2016.

[11] K. C. Murphy, J. Whitehead, P. C. Falahee, D. Zhou, S. I. Simon, and J. K. Leach, "Multifactorial Experimental Design to Optimize the Anti-Inflammatory and Proangiogenic Potential of Mesenchymal Stem Cell Spheroids," (in eng), *Stem Cells,* vol. 35, no. 6, pp. 1493-1504, Jun 2017.

[12] K. C. Murphy, S. Y. Fang, and J. K. Leach, "Human mesenchymal stem cell spheroids in fibrin hydrogels exhibit improved cell survival and potential for bone healing," (in eng), *Cell Tissue Res,* vol. 357, no. 1, pp. 91-9, Jul 2014.

[13] E. Fennema, N. Rivron, J. Rouwkema, C. van Blitterswijk, and J. de Boer, "Spheroid culture as a tool for creating 3D complex tissues," *Trends in*

Biotechnology, vol. 31, no. 2, pp. 108-115, 2013/02/01/ 2013, doi: https://doi.org/10.1016/j.tibtech.2012.12.003.

[14] R. J. McMurtrey, "Roles of Diffusion Dynamics in Stem Cell Signaling and Three-Dimensional Tissue Development," *Stem Cells and Development,* vol. 26, no. 18, pp. 1293-1303, 2017/09/15 2017, doi: 10.1089/scd.2017.0066.

[15] E. Shearier, Q. Xing, Z. Qian, and F. Zhao, "Physiologically Low Oxygen Enhances Biomolecule Production and Stemness of Mesenchymal Stem Cell Spheroids," *Tissue Engineering Part C: Methods,* vol. 22, no. 4, pp. 360-369, 2016/04/01 2016, doi: 10.1089/ten.tec.2015.0465.

[16] C. J. Hunt, "Cryopreservation: Vitrification and Controlled Rate Cooling," (in eng), *Methods Mol Biol,* vol. 1590, pp. 41-77, 2017, doi: 10.1007/978-1-4939-6921-0_5.

[17] G. N. Stacey *et al.*, "Preservation and stability of cell therapy products: recommendations from an expert workshop," *Regenerative Medicine,* vol. 12, no. 5, pp. 553-564, 2017/07/01 2017, doi: 10.2217/rme-2017-0073.

[18] A. Bissoyi, B. Nayak, K. Pramanik, and S. K. Sarangi, "Targeting cryopreservation-induced cell death: a review," (in eng), *Biopreserv Biobank,* vol. 12, no. 1, pp. 23-34, Feb 2014, doi: 10.1089/bio.2013.0032.

[19] E. J. Woods, S. Thirumala, S. S. Badhe-Buchanan, D. Clarke, and A. J. Mathew, "Off the shelf cellular therapeutics: Factors to consider during cryopreservation and storage of human cells for clinical use," *Cytotherapy,* vol. 18, no. 6, pp. 697-711, 2016/06/01/ 2016, doi: https://doi.org/10.1016/j.jcyt.2016.03.295.

[20] E. Casula, G. P. Asuni, V. Sogos, S. Fadda, F. Delogu, and A. Cincotti, "Osmotic behaviour of human mesenchymal stem cells: Implications for cryopreservation," *PLOS ONE,* vol. 12, no. 9, p. e0184180, 2017, doi: 10.1371/journal.pone.0184180.

[21] H. Gurruchaga *et al.*, "Advances in the slow freezing cryopreservation of microencapsulated cells," *Journal of Controlled Release,* vol. 281, pp. 119-138, 2018/07/10/ 2018, doi: https://doi.org/10.1016/j.jconrel.2018.05.016.

[22] R. Raju, S. J. Bryant, B. L. Wilkinson, and G. Bryant, "The need for novel cryoprotectants and cryopreservation protocols: Insights into the importance of biophysical investigation and cell permeability," *Biochimica et Biophysica Acta (BBA) - General Subjects,* vol. 1865, no. 1, p. 129749, 2021/01/01/ 2021, doi: https://doi.org/10.1016/j.bbagen.2020.129749.

[23] W. Chaabane *et al.*, "Autophagy, Apoptosis, Mitoptosis and Necrosis: Interdependence Between Those Pathways and Effects on Cancer," *Archivum Immunologiae et Therapiae Experimentalis,* vol. 61, no. 1, pp. 43-58, 2013/02/01 2013, doi: 10.1007/s00005-012-0205-y.

[24] Q. Chen, J. Kang, and C. Fu, "The independence of and associations among apoptosis, autophagy, and necrosis," *Signal Transduction and Targeted Therapy,* vol. 3, no. 1, p. 18, 2018/07/01 2018, doi: 10.1038/s41392-018-0018-5.

[25] M. Noguchi, N. Hirata, T. Tanaka, F. Suizu, H. Nakajima, and J. A. Chiorini, "Autophagy as a modulator of cell death machinery," *Cell Death & Disease,* vol. 11, no. 7, p. 517, 2020/07/08 2020, doi: 10.1038/s41419-020-2724-5.

[26] R. Martin-Ibañez, C. Unger, A. Strömberg, D. Baker, J. M. Canals, and O. Hovatta, "Novel cryopreservation method for dissociated human embryonic stem cells in the presence of a ROCK inhibitor," in *Hum Reprod*, vol. 23, no. 12). England, 2008, pp. 2744-54.

[27] X. Xu, S. Cowley, C. J. Flaim, W. James, L. Seymour, and Z. Cui, "The roles of apoptotic pathways in the low recovery rate after cryopreservation of dissociated human embryonic stem cells," (in eng), *Biotechnology progress,* vol. 26, no. 3, pp. 827-837, May-Jun 2010, doi: 10.1002/btpr.368.

[28] M. A. Savitskaya and G. E. Onishchenko, "Apoptosis in cryopreserved eukaryotic cells," *Biochemistry (Moscow),* vol. 81, no. 5, pp. 445-452, 2016/05/01 2016, doi: 10.1134/S0006297916050023.

[29] M. J. Berridge, M. D. Bootman, and P. Lipp, "Calcium - a life and death signal," *Nature,* vol. 395, no. 6703, pp. 645-648, 1998/10/01 1998, doi: 10.1038/27094.

[30] P. K. Janicki, P. E. Wise, A. E. Belous, and C. W. Pinson, "Interspecies differences in hepatic Ca(2+)-ATPase activity and the effect of cold preservation on porcine liver Ca(2+)-ATPase function," in *Liver Transpl*, vol. 7, no. 2). United States, 2001, pp. 132-9.

[31] Y. C. Song *et al.*, "Vitrification of tissue engineered pancreatic substitute," in *Transplant Proc*, vol. 37, no. 1). United States, 2005, pp. 253-5.

[32] J. I. E. Bruce, "Metabolic regulation of the PMCA: Role in cell death and survival," (in eng), *Cell Calcium,* vol. 69, pp. 28-36, Jan 2018, doi: 10.1016/j.ceca.2017.06.001.

[33] L. Waters, M. P. Padula, D. C. Marks, and L. Johnson, "Calcium chelation: a novel approach to reduce cryopreservation-induced damage to frozen platelets," (in eng), *Transfusion,* vol. 60, no. 7, pp. 1552-1563, Jul 2020, doi: 10.1111/trf.15799.

[34] K. Ono, X. Wang, and J. Han, "Resistance to tumor necrosis factor-induced cell death mediated by PMCA4 deficiency," (in eng), *Mol Cell Biol,* vol. 21, no. 24, pp. 8276-88, Dec 2001.

[35] H. G. Wang *et al.*, "Ca2+-induced apoptosis through calcineurin dephosphorylation of BAD," (in eng), *Science,* vol. 284, no. 5412, pp. 339-43, Apr 9 1999, doi: 10.1126/science.284.5412.339.

[36] A. J. Caride, A. R. Penheiter, A. G. Filoteo, Z. Bajzer, A. Enyedi, and J. T. Penniston, "The plasma membrane calcium pump displays memory of past calcium spikes. Differences between isoforms 2b and 4b," in *J Biol Chem*, vol. 276, no. 43). United States, 2001, pp. 39797-804.

[37] D. Gao and J. K. Critser, "Mechanisms of Cryoinjury in Living Cells," *ILAR Journal,* vol. 41, no. 4, pp. 187-196, 2000, doi: 10.1093/ilar.41.4.187.

[38] X. Xu, Y. Liu, Z. Cui, Y. Wei, and L. Zhang, "Effects of osmotic and cold shock on adherent human mesenchymal stem cells during cryopreservation," in *J Biotechnol*, vol. 162, no. 2-3). Netherlands: © 2012 Elsevier B.V, 2012, pp. 224-31.

[39] K. Y. Lee, J. A. Rowley, P. Eiselt, E. M. Moy, K. H. Bouhadir, and D. J. Mooney, "Controlling Mechanical and Swelling Properties of Alginate Hydrogels Independently by Cross-Linker Type and Cross-Linking Density,"

Macromolecules, vol. 33, no. 11, pp. 4291-4294, 2000/05/01 2000, doi: 10.1021/ma9921347.

[40] K. T. Campbell, D. J. Hadley, D. L. Kukis, and E. A. Silva, "Alginate hydrogels allow for bioactive and sustained release of VEGF-C and VEGF-D for lymphangiogenic therapeutic applications," (in eng), *PloS one,* vol. 12, no. 7, pp. e0181484-e0181484, 2017, doi: 10.1371/journal.pone.0181484.

[41] P. A. Williams, K. T. Campbell, H. Gharaviram, J. L. Madrigal, and E. A. Silva, "Alginate-Chitosan Hydrogels Provide a Sustained Gradient of Sphingosine-1-Phosphate for Therapeutic Angiogenesis," *Annals of Biomedical Engineering,* vol. 45, no. 4, pp. 1003-1014, 2017/04/01 2017, doi: 10.1007/s10439-016-1768-2.

[42] J. L. Madrigal, S. N. Sharma, K. T. Campbell, R. S. Stilhano, R. Gijsbers, and E. A. Silva, "Microgels produced using microfluidic on-chip polymer blending for controlled released of VEGF encoding lentivectors," (in eng), *Acta biomaterialia,* vol. 69, pp. 265-276, 2018/03// 2018, doi: 10.1016/j.actbio.2018.01.013.

[43] R. Malpique, F. Ehrhart, A. Katsen-Globa, H. Zimmermann, and P. M. Alves, "Cryopreservation of Adherent Cells: Strategies to Improve Cell Viability and Function After Thawing," *Tissue Engineering Part C: Methods,* vol. 15, no. 3, pp. 373-386, 2009/09/01 2009, doi: 10.1089/ten.tec.2008.0410.

[44] C. Terry, A. Dhawan, R. R. Mitry, S. C. Lehec, and R. D. Hughes, "Optimization of the cryopreservation and thawing protocol for human hepatocytes for use in cell transplantation," *Liver Transplantation,* vol. 16, no. 2, pp. 229-237, 2010/02/01 2010, doi: https://doi.org/10.1002/lt.21983.

[45] O. Chaudhuri *et al.*, "Substrate stress relaxation regulates cell spreading," *Nature Communications,* vol. 6, no. 1, p. 6365, 2015/02/19 2015, doi: 10.1038/ncomms7365.

[46] O. Chaudhuri *et al.*, "Hydrogels with tunable stress relaxation regulate stem cell fate and activity," *Nature Materials,* vol. 15, no. 3, pp. 326-334, 2016/03/01 2016, doi: 10.1038/nmat4489.

[47] M. M. Pérez-Madrigal, J. Torras, J. Casanovas, M. Häring, C. Alemán, and D. D. Díaz, "Paradigm Shift for Preparing Versatile M2+-Free Gels from Unmodified Sodium Alginate," *Biomacromolecules,* vol. 18, no. 9, pp. 2967-2979, 2017/09/11 2017, doi: 10.1021/acs.biomac.7b00934.

[48] Z. Zhao, J. Gu, Y. Zhao, Y. Guan, X. X. Zhu, and Y. Zhang, "Hydrogel Thin Film with Swelling-Induced Wrinkling Patterns for High-Throughput Generation of Multicellular Spheroids," *Biomacromolecules,* vol. 15, no. 9, pp. 3306-3312, 2014/09/08 2014, doi: 10.1021/bm500722g.

[49] D. M. Dean, A. P. Napolitano, J. Youssef, and J. R. Morgan, "Rods, tori, and honeycombs: the directed self-assembly of microtissues with prescribed microscale geometries," *The FASEB Journal,* vol. 21, no. 14, pp. 4005-4012, 2007/12/01 2007, doi: https://doi.org/10.1096/fj.07-8710com.

[50] J. A. Brassard and M. P. Lutolf, "Engineering Stem Cell Self-organization to Build Better Organoids," *Cell Stem Cell,* vol. 24, no. 6, pp. 860-876, 2019/06/06/ 2019, doi: https://doi.org/10.1016/j.stem.2019.05.005.

[51] R. Mori, Y. Sakai, and K. Nakazawa, "Micropatterned organoid culture of rat hepatocytes and HepG2 cells," in *J Biosci Bioeng*, vol. 106, no. 3). Japan, 2008, pp. 237-42.

Appendix A

Open-source 3D printed air-jet for generating monodispersed alginate microhydrogels

The 3D model is available at https://3dprint.nih.gov/discover/3dpx-012141

Introduction

Researchers, funding agencies, and publishers recognize the importance of reproducibility in scientific publications [1-3]. Several tools, including a growing number of online repositories: Github, Figshare, and Protocols.io, are being developed to encourage replicable science [4-6]. Specifically, FOSH encourages participation in science by reducing supply limitations, fostering new research opportunities, and facilitating translation of these tools for educational purposes [7]. For example, open-source tools are currently available on the National Institutes of Health (NIH) website for cell cultures, microfluidics, drug delivery systems, and clinical safety [8]. The open-source license benefits researchers and clinicians because building equipment yields a deeper understanding and allows modifications of designs [9]. One appealing strategy for creating FOSH is designing for 3D printing because of its potential for rapid prototyping and customization. The accessibility of 3D printing has translated into increasing inventiveness within different communities: from amateur hobbyists to aerospace engineers [9-14]. Furthermore, the reduced cost of 3D printers in the past

couple of years results in their increasing availability to the public at Makerspaces, public libraries, and universities [15].

An air-based system to generate microbeads would benefit from a FOSH design due to the diverse application of these hydrogels for drug and cell delivery, cryopreservation, and as scaffolds for tissue engineering strategies [16-18]. These microbead generators commonly employ polymer and crosslinker solutions to form microscale hydrogel [18-21]. Alginate is a desirable polymer for microbeads in biomedical science, as it is biocompatible, undergoes rapid gelation under cell-friendly conditions, and has controllable mesh size [22]. Alginate, a copolymer comprised of (1,4)-linked β-D-mannuronate (M) and α-L-guluronate (G) residues, crosslinks in the presence of divalent cations, such as Ca^{2+}, resulting in the formation of a 3D polymeric network characteristic of hydrogels [23-25]. Alginate microbeads are commonly generated using droplet microfluidics, coaxial airflow units, two-channel air-jackets, and electrostatic forces [17, 26-28]. Specifically, our group has previously used alginate microhydrogels generated by microfluidics to deliver lentivectors, encapsulate stem cells, and guide the morphogenesis of endothelial progenitor cells [26, 27, 29]. It is common to use alginate microhydrogels to encapsulate probiotics [30-32]. The wide range of applications further motivates the benefit of an available air-jet system to ensure the reproducibility of the work in different lab environments.

To generate alginate microbeads, we designed a 3D printable air-jet system that generates microdroplets by focusing an airflow that shears the solution from the needle. This axisymmetric air-jet is similar to commonly employed air bifurcation or electrostatic bead generators [17, 28, 33]. The polymer solution is extruded via a needle attached to

a syringe, forming droplets that fall into a calcium bath and generate hydrogel beads. Our design objective was to create a device that could be entirely 3D printed and reliably generate microdroplets. The proposed design permitted modularity and sterility while having low complexity and manufacturing cost. We hypothesized that controlling airflow, pump speed, and needle size for the 3D printed air-jet can control alginate microbeads characteristics similar to other extrusion systems that use airflow. Specifically, the design needed to generate monodispersed beads, which we defined as beads with a coefficient of variation of less than 10%. The device was characterized via a design of experiments (DOE) methodology using a definitive screening design. We expect this system to be reasonably reproducible between experiments and laboratories due to well-defined setup parameters in this report than other publications using air-based droplet generating methods [33-35].

Materials and Methods

Device design and manufacture

The air-jet was designed using Fusion 360® software (Autodesk, Inc) and prepared for 3D printing using the open-source slicer program, Cura software (Ultimaker). The device was split into three components: the air-jet, the air intake, and supports. The intake component of the device was printed with the air inlet parallel to the plane of the printing bed to prevent the nozzle from fracturing along the printed layers due to the air tubing. The air-jet was oriented for printing with the exit orifice normal to the plane of the printing bed, such that the designed geometry does not require support material and no bridging at the area where the air is compressed around

the needle. Components were printed on an MP Select Mini V2 (Monoprice, Inc) with poly (lactic acid) (Hatchbox®) at a layer thickness of 0.0875 mm and a printing speed of 50 mm/s. The extrusion temperature was 190 °C, and the heat bed temperature was 60 °C.

Generation of alginate microbeads

LF 10/60 alginate polymer (~120-150 kDa) with higher G-block content (>60% as specified by the manufacturer) obtained from Novamatrix (FMC) was used to generate the microbeads. Alginate solutions were prepared by dissolving alginate polymer in either deionized water (diH_2O) or phosphate buffer solution with added magnesium and calcium (PBS^{++}; Life Technologies), as previously described [36]. The open-source air-jet and a syringe pump (Braintree Scientific) were run in parallel in a vertical position above a calcium bath. Syringes (Becton Dickinson) with varying needle sizes (PrecisionGlide™; Becton Dickinson) were positioned within the syringe pump and air-jet. The distance from the needle to the calcium bath was constant at 15 cm [37]. The air-jet was then centered over the needle to generate a uniform airflow across the needle. The tip of the needle was placed slightly protruding from the outlet of air-jet. Nitrogen gas was then run through the air-jet before starting the syringe pump to prevent alginate from getting stuck in the air-jet chamber. After activating the syringe pump, the direction of droplets was checked using a flat surface. Adjustments were made in response to poor alignment of the needle through the center of the air-jet to ensure alginate droplets fell directly downwards. Finally, 5 mL of 100 mM calcium chloride ($CaCl_2$) (Sigma) was used as the calcium bath for all experiments and placed

underneath the air-jet, in line with the flow of alginate droplets after performing needle alignment. Alginate microbeads were generated for one minute with this setup before being analyzed directly from the wells using ImageJ software (NIH). Microbead diameters, coefficient of variation of diameters, and circularity were analyzed. The coefficient of variation is the standard deviation normalized to the mean and was used to quantitatively examine bead uniformity [37, 38]. The circularity was defined below in the following equation:

$$Bead\ Circularity = 4 * \pi * (\frac{Area}{Perimeter^2}),$$

where the value of bead circularity varies between 0 to 1, with 1 being a perfect circle.

Design of Experiments: Definitive Screening Design

A definitive screening design (JMP software) was performed to identify the factors influential on the microbead characteristics of bead size, coefficient of variation (CV), and circularity. This screening design permitted the factors of buffer type, needle diameter, air pressure, alginate concentration, and pump speed to be studied from a relatively small experiment. Eighteen groups were used for the screening design, with n=10 per group, representing different combinations of the potential factors influencing microbead. In contrast, a full factorial design would involve examining 162 groups to encompass all the values used for this initial analysis.

The effect of polymer solution viscosity was investigated using alginate dissolved at different concentrations (1, 2, and 3% (w/v)) and in different solvents (PBS^{++} and diH_2O). The various needle gauges of 27, 21, and 18 were tested, which have an internal opening diameter of approximately 0.210, 0.524, and 0.840 mm, respectively.

Nitrogen gas pressure was adjusted between 200 to 800 kPa using a pressure gauge attached to a compressed nitrogen gas tank as a method to alter the flow rate of air. Syringe pump speeds were also varied between 100, 250, and 400 µL/min.

The analysis includes a fit-definitive screening to determine the main effect estimates effects on the bead diameter, coefficient of variation for bead diameters, and circularity [39]. The fit-definitive screening report incorporates the following estimates: main effect, even order, and combined model parameter using the average of n = 10 for each of the 18 groups determined by the definitive screening design. Briefly, the main effect estimates list factors that are considered active via a p-value less than the threshold ($p < 0.05$); even order effect estimates list second-order effects that are considered active, and combined model parameter estimates list the factors considered active in the final model. The Prob>|t| represents the computed p-value using the t Ratio and the degrees of freedom for error.

Characterization of Microbeads resulting from tunable factors: Nitrogen Gas Pressure and Pump Speed

Additional experiments were performed to determine how the influence of airflow rate and pump speed on microbead formation. Nitrogen gas pressures were used from 0 to 800 kPa in 100 kPa increments to vary the rate of airflow, with higher pressures resulting in more airflow. For 0 kPa, the air-jet was removed to prevent alginate solution from getting stuck within the device, and droplets were formed by gravity. The pump speeds of 10, 50, 100, 150, and 200 µL/min were used with a calcium bath. Both experimental setups utilized a 27G needle with 2% (w/v) alginate and 100 mM $CaCl_2$

baths. Bead diameter, diameter coefficient of variation, and circularity were determined using ImageJ (NIH).

Encapsulation of Bacteria and alginate lyase in alginate microbeads

Green fluorescent protein (GFP) expressing *Escherichia coli (E. coli)* were loaded into 2% (w/v) alginate solution and dropping into 100 mM $CaCl_2$ solution containing 0.25% (w/v) chitosan (Sigma). Chitosan was initially dissolved at 4% within 0.066 M glacial acetic acid (Sigma) before being diluted to the final concentration. Microbeads were made by passing alginate solution through a 25G needle at 100 µL/min with the air-jet fed by nitrogen gas at 600kPa. *E. coli* loaded microbeads were cultures in Lysogeny broth (LB; VWR). For the generation of Alginate lyase, an enzyme that cleaves glycosidic bonds in alginate polymers was added at the concentrations of 0, 5, and 50 mU/mL to the alginate polymer solution to make degradable microcapsules [40]. The alginate solution containing alginate lyase was loaded into a syringe with a 27G needle, and microbeads were generated with the air-jet as described above. These alginate microbeads were left to crosslink for 15 minutes, washed in DI water, and approximately 100 microliters of beads were transferred to 12 well plates, topped in 4 mL of EGM-2MV media (Lonza), and incubated at 37 °C. Microbeads were imaged at 1 hour and 1, 3, 5, 7, 14, and 21 days. The size of the beads was analyzed with ImageJ. The initial distribution of microbead sizes at 1 hour is reported as a histogram, and the change in microbead size was reported over 21 days (n = 50).

Statistical analysis

Comparisons were assessed by Student's unpaired t-tests. Differences between conditions were considered significant if $P < 0.05$. All analyses were performed using GraphPad Prism software (GraphPad Software) and JMP software.

Results

Design of a 3D printed air-jet

The open-source air-jet system was designed from known systems that utilize the flow of gases to induce shear forces on a liquid for microdroplet generation (Figure 1A). Specifically, we used a flow-focusing design to isolate the airflow chamber from our polymer solutions. Additionally, this method increases the air pressure due to the air jacket. The design of the air-jet was optimized for use with a Fused Deposition Modeling (FDM) 3D printer, including an objective to be printed as one piece without internal support material (Figure 1B). First, the distance between the internal cylinder that orients the needle, and the outer wall (teal) was set to 1 mm to increase the air pressure and prevent fusion between features while printing. The air around this ring (teal) has a cross-sectional area of approximately 33 mm^2. Second, the airflow chamber expands outwards to a maximum of 103.9 mm^2 before being focused to an area of 7.1 mm^2 at the air jacket (green). Initial iterations did not have this focusing outlet, being more similar to a coaxial-flow design and resulted in larger droplets. Third, the needle inlet (orange) has a cross-sectional area of approximately 1.77 mm^2, which is further reduced with the needle inserted. The small area reduces the backflow of gas and helps orient the needle to the center of the airflow. Furthermore, including a chamfer needle inlet (red) permitted smaller needles to be used without decreasing the length of the air-

jet. The air-jet was directly aligned with the syringe pump in the setup we employed, using an inverted syringe pump such that the needle pointed downwards (Figure 1C). Next, the air-jet was raised until the needle was through the air jacket by adjusting the supports. The air source was attached via tubing that was in-line with the syringe pump. Alternative setups should include compressed gas and a method to have the polymer solution reach the edge of the air jacket.

Design of Experiments: Definitive Screening Design

A definitive screening design was performed to identify the factors altering the microbead characteristics of bead size, coefficient of variation (CV), and circularity. This screening design included the factors of buffer type, needle diameter, air pressure, alginate concentration, and pump speed to be studied from a relatively small experiment. Microbead size, CV, or circularity values were used to calculate potential first-order or second-order relationships using the JMP software. Representative images of the beads under similar conditions are shown as well (Figure 2A-E). Analysis from the DOE software suggests alginate has a non-linear trend with microbead diameter (Prob > |t|, 0.0107). There was no effect on bead characteristics due to the buffers used to dissolve the alginate polymer; however, beads formed with alginate dissolved in diH_2O appear more uniformly round compared to alginate dissolved in a phosphate buffer (Figure 2C). Additionally, needle diameter had no significant effect on bead diameter; however, images show smaller needle diameters creating smaller beads (Figure 2C). A faster pump speed of 400 µL/min led to more uniformly round beads that appear slightly larger than those formed with a pump speed of 250 µL/min (Figure 2D).

Indeed, pump speed had a significant effect on bead circularity (Prob > |t|, 0.0401). Although similar trends as increasing alginate concentration were observed with a decrease in nitrogen gas pressure (Figure 2E), there was only a significant difference found from with circularity in combination with alginate concentration (Prob > |t|, 0.0071) and pump speed (Prob > |t|, 0.0455). In summary, alginate concentration and pressure of nitrogen gas had the largest impact on microbead properties.

Characterization of Microbeads resulting from tunable factors: Nitrogen Gas Pressure and Pump Speed

Next, airflow and syringe pump speed were investigated as possible methods for controlling bead size. A 27G (0.21mm) needle made hydrogel beads from 2% (w/v) alginate. The nitrogen gas flow was adjusted by altering the pressure on the tank regulator. The resulting change in airflow through the air-jet had a drastic effect on the bead size (Figure 3A). From the initial addition of airflow using nitrogen gas, the bead diameter decreased from 789 µm to 188 µm, suggesting a wide dynamic range of bead sizes through pressure changes with a statistically significant negative correlation ($r = -0.9060$). However, increasing nitrogen gas pressure increased the coefficient of variation to be above 5% as the gas pressure went above 400kPa (Figure 3B). Regardless, no nitrogen gas flow creates hydrogel beads with the largest coefficient of variation, highlighting the difference due to gravity and airflow. The coefficient of variation in bead diameters has a statistically significant positive correlation ($r = 0.8249$), increasing nitrogen gas pressure above 500 kPa, having a CV above 5% (Figure 3B). An increase in nitrogen gas pressure beyond 500 kPa also led to a decrease in bead

circularity, with a statistically significant negative correlation (r = -0.7581) (Figure 3C). Representative images of these beads show these drastic changes in bead diameters with the addition of nitrogen gas flow through the air-jet and loss of circularity of hydrogel beads at higher nitrogen gas pressures (Figure 3D).

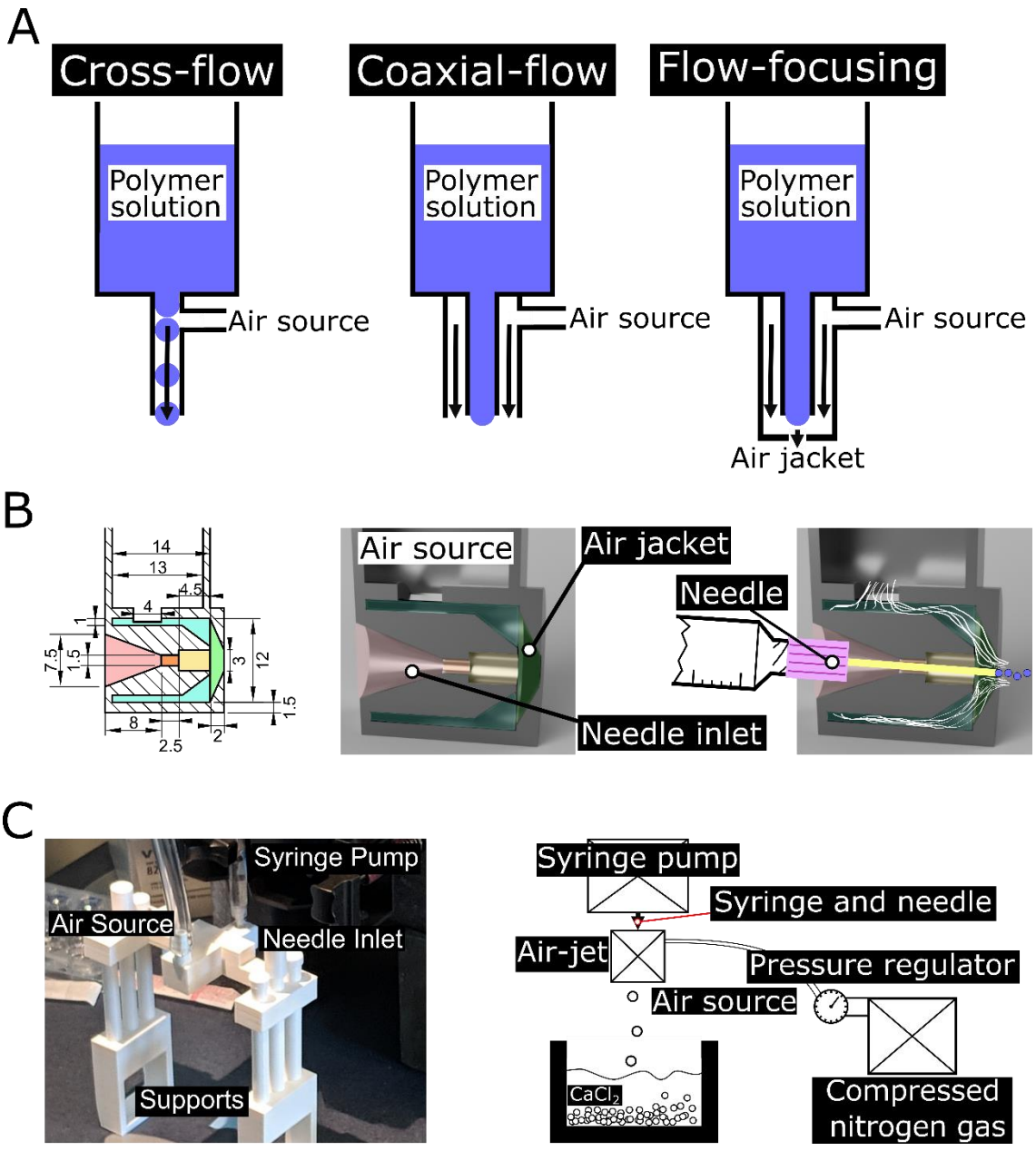

Figure 1. 3D Printed Air-jet design and setup. Air-assisted generation of microdroplets typically falls under three categories: cross-flow, coaxial-flow, and coaxial chambers with flow-focusing (A). The present design shifted to flow-focusing, shown in an engineering drawing of the internal dimensions (A, left). Cross-sectional model renderings show how the needle is inserted into the air-jet and how air focuses over the needle tip due to the air jacket, shearing off microdroplets (A, right). The 3D printed air-jet can be manipulated into different positions via the adjustable leg supports (C, left) or through other custom arrangements; however, at minimum in addition to the air-jet, a beaker of crosslinker, a compressed gas source, a needle, a syringe, and a syringe pump are required (C, right).

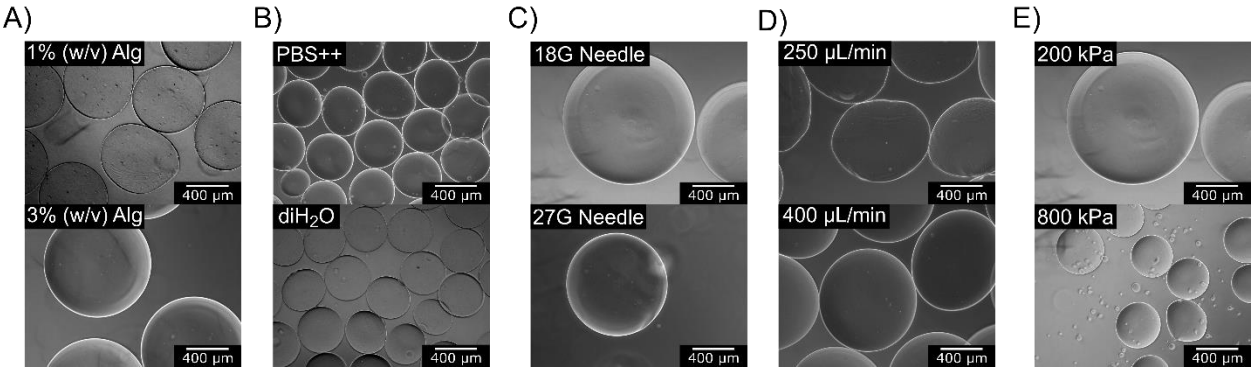

Figure 2. Representative images of microbeads formed during the Definitive Screening Design of Experiments. Comparable groups of microbeads generated from the definitive screening design of experiment groups were imaged and displayed together to highlight differences due to the condition of each factor. A 27G (0.21 mm) needle with 200 kPa of nitrogen gas was used to dispense alginate at a rate of 400 µL/min using concentrations of 1 or 3% (w/v) (A). Different buffers were tested with a

21G (0.534 mm) needle supplied with 2% (w/v) alginate at 250 µL/min with 500 kPa of nitrogen gas (B). Next, 18G (0.838 mm) and 27G (0.21 mm) needles were tested with 100 µL/min of 3% (w/v) alginate with 200 kPa nitrogen gas pressure (C). Additinally, an 18G (0.838 mm) needle with 200 kPa of nitrogen gas was used to dispense 1% (w/v) alginate at 250 or 400 µL/min (D). Lastly, an 18G (0.838 mm) needle was used to dispense 3% (w/v) alginate at 200 and 100 µL/min using 100 kPa or 800kPa of nitrogen gas pressure, respectively.

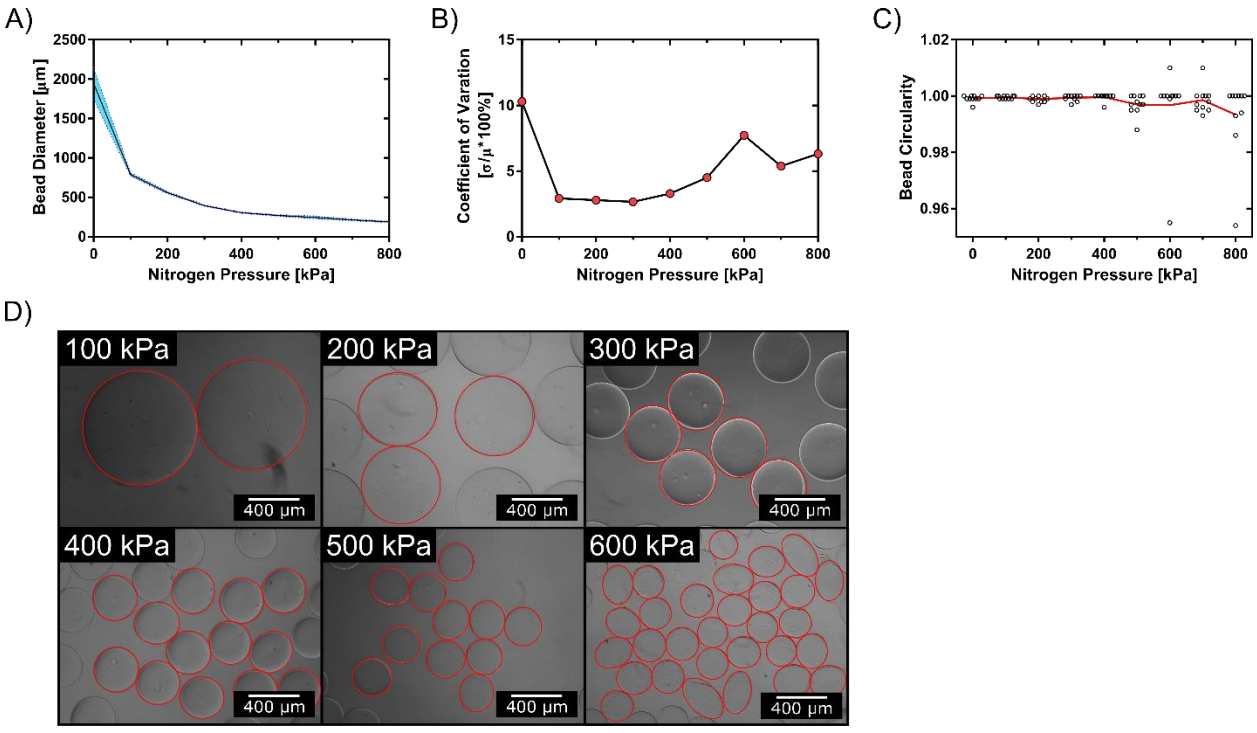

Figure 3. Characterization of air pressure effect on alginate microbeads. Beads were generated using a 27G needle (0.21 mm) with 2 % (w/v) alginate 10 cm from the calcium bath. The microbeads were generated with changing nitrogen gas pressure with a constant syringe pump speed (100 µL/min). Generally, an increase in nitrogen gas

pressure led to a decrease in the microbead diameters (A) and circularity (C). The coefficient of variation was calculated from bead diameters (B). The mean is represented by the central line with the shaded areas denoting the error envelope of the standard deviation (n = 11) (A). The coefficient of variation of microbead diameters is the standard deviation normalized to the mean from the samples in panel A. In figure panel C, each data point represents the circularity of an individual microbead (n=11), with the mean of each condition represented by the central connecting line. Representative images of microbeads from air pressures 100-600 kPa are displayed with red outlined to highlight the resulting change in diameter and uniformity (D).

The speed in which polymer solution is fed through the air-jet using a syringe pump was also examined to tune the size of hydrogel beads. Alginate microbeads were created with various pump speeds using a 2% (w/v) alginate polymer solution and 400 kPa nitrogen gas pressure. There was a correlation for bead diameters to increase with pump speed, r = 0.9814 (Figure 4A). The bead diameter increased by approximately 40 µm per 100 µL/min change in pump speed in the range tested and with the specific alginate concentration, alginate source, and solvent. Pump speed has no statistically significant correlation with a coefficient of variation nor circularity (r = -0.3208 and -0.7689, respectively) (Figure 4B-C). Together, these data demonstrate how the bead formation is dependent on controllable factors that occur at the air-jet rather than the composition of the polymer solution.

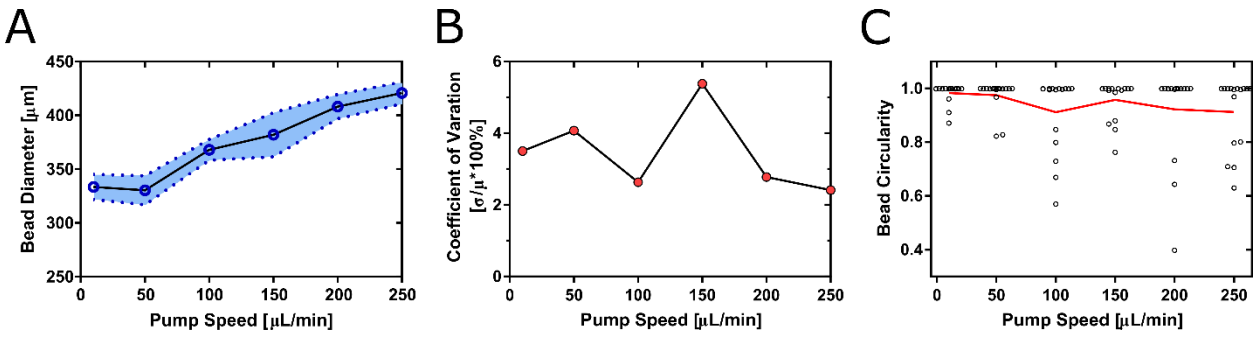

Figure 4. Formation of consistently monodispersed microhydrogels under varying syringe pump speeds. The diameter of microbeads increased with faster syringe pump speed at a constant nitrogen gas pressure (A). The coefficient of variation (B) and circularity (C) remains relatively constant, with circularity decreasing with faster syringe pump speeds. In figure panel A, the mean is represented by the central line with the shaded areas denoting the error envelope of the standard deviation (n = 16). Figure panel B represents the coefficient of variation of microbead diameters, calculated with the standard deviation normalized to the mean. In figure panel C, each data point represents the circularity of an individual microbead (n = 16), with the mean of each condition represented by the connecting line.

Validation of the Open-Source Air-jet System for Encapsulation Strategies

Alginate microbeads generated from the air-jet could be utilized for potential biomedical applications. Bacteria were successfully encapsulated in alginate microbeads of varying diameters by changing the nitrogen gas pressure (Figure 5A). Furthermore, these bacteria were viable and proliferated within the alginate microbeads (Figure 5B). The air-jet could also generate degradable alginate microbeads. Alginate microbeads containing various alginate lyase concentrations were initially found to have similar distributions of bead diameters, with CV < 6% (Figure 5C). Initial differences in bead diameters for each condition of enzyme concentrations are statistically significant from each other. However, this difference does not follow a trend with increasing enzyme concentration. Regardless, the alginate microbeads containing more alginate lyase were observed to decrease in size over 21 days, with the largest change occurring within the first few days (Figure 5D). An approximate 27.3% reduction in microbead diameter was observed with 50 mU/mL of the enzyme.

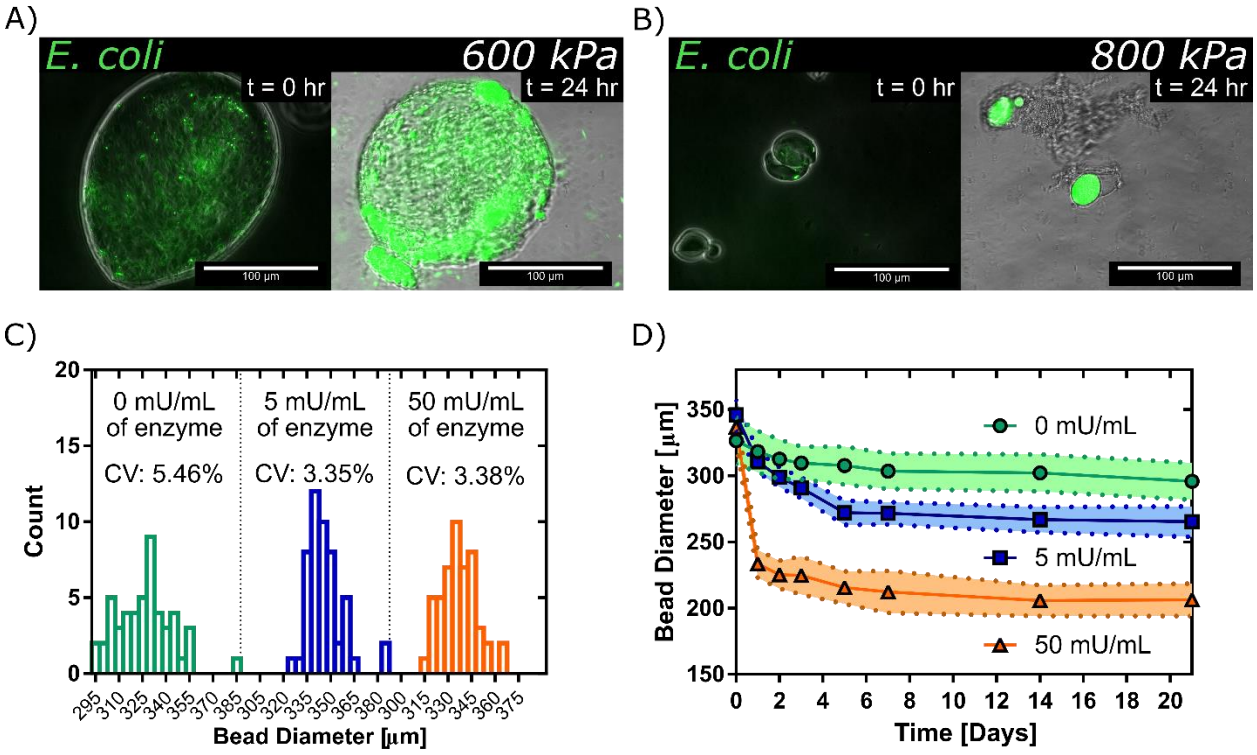

Figure 5. Encapsulation of bacteria and alginate degrading enzyme. GFP expressing *E. coli* were encapsulated in alginate microbeads through the air-jet with varying air pressures, 600kPa (A) and 800 kPa (B), and imaged for the change in fluorescence between 24 hours. In both cases, enhanced distribution of the bacteria is observed over this timespan. In addition, varying concentrations of alginate lyase were encapsulated in alginate microbeads utilizing the air-jet system. The diameters of 50 microbeads per alginate lyase concentration suggest these hydrogels are monodispersed (C). As expected, there was more reduction in microbead diameter due to enzymatic degradation with larger enzyme concentrations (D). In figure panel D, the mean is represented by the central line with the shaded areas denoting the error envelope of the standard deviation (n = 50)

Discussion

The designed air-jet reliably generated monodispersed microbeads. To our knowledge, this is the first fully 3D printable air-jet system. This device provides a distinct improvement to setup reproducibility compared to previously described alternatives, including focusing air over a syringe at a 90-degree angle or aligning a needle into the airflow tubing [20, 34, 41, 42]. Notably, the presented device's design is outlined by its 3D file, resulting in an easier to decipher setup and controls for needle placement and airflow, permitting reproducibility not available with other custom air-jet systems [20, 41]. Furthermore, the geometries of internal features take advantage of FDM 3D printers to generate the air-jet as one piece, benefiting the accessibility and affordability of the design. In comparison, specific geometries of microfluidics are not often provided. Without the soft lithography mask design, details of the device can be lost, creating additional practical challenges to replicating microfluidic devices and specialized fabrication equipment [43]. Overall, the described air-jet system controls microbeads characteristics due to defined setup parameters while ensuring reproducibility.

The DOE allowed us to dramatically reduce the total number of groups to test, from 162 to 18, where a group represents a specific combination of different conditions. Specifically, the definitive screening design determined the influences of polymer concentration, air pressure, needle diameter, and buffer type on microbead formation. The results suggest that a higher alginate concentration, larger needle diameter, or lower air pressure leads to larger circular beads. This is consistent with alginate microbeads formed via other extrusion dripping and air-jet systems [19, 20, 44, 45].

However, this approach did not accurately describe the dynamic range of bead diameters and their monodispersity. Regardless, alginate microbead properties can be controlled through known methods employed by other described extrusion dripping methods.

Pump speed and air pressure were further interrogated as methods to control microbead characteristics due to the accessibility to tune these factors with a syringe pump and pressure regulator. While air pressure could control the size of beads from 2 mm to 200 µm, adjusting pump speed changed bead sizes from 350 to 425 µm, suggesting air pressure provides a greater dynamic range of bead sizes. However, both methods generate beads in the range of 200-800 microns in diameter. Furthermore, these beads had a coefficient of variation of less than 10%, which is often desired for encapsulation of cell applications [37]. Although microbeads smaller than 200 microns can be made with higher air pressures, tear-shaped droplets could form without sufficient time for the droplet to become round [46]. Other factors that could be adjusted to improve circularity include the addition of a surfactant to the calcium solution [45]. Overall, the designed open-source system generates microbeads with desirable characteristics. To further reduce bead size, customization will be required by the user to reduce the backflow of air.

The encapsulation of bacteria is promising for numerous biomedical applications, including probiotic delivery, where the bacteria must safely pass-through gastric acid [16, 30-32, 47]. Furthermore, using the air-jet system with nitrogen gas in a nitrogen-enriched chamber could generate microbeads for anaerobic bacteria that cannot tolerate atmospheric oxygen concentrations. The growth of bacteria over 24 hours in the

hydrogels results in pockets of bacteria. Additionally, the use of enzymes to degrade alginate has been previously used by our group to control the delivery of endothelial progenitor cells and adeno-associated vectors [48, 49]. Similarly, degradation of alginate in probiotic delivery applications could be beneficial to free the bacteria from the hydrogel. The rapid degradation of microbeads observed here suggests the microbeads can undergo enzymatic degradation similar to microbeads generated with microfluidic methods [26]. The air-jet would be less prone to clogging than microfluidics and does not require washing to remove oil. Washing steps could lead to a loss of enzyme or expose anaerobic bacteria to oxygen. Furthermore, the air-jet can generate monodispersed alginate microbeads from a highly viscous polymer solution faster than oil-emulsion microfluidics [26, 45]. Herein, we demonstrate the utility of this open-source air-jet system to generate monodispersed microbeads for encapsulation applications.

The open-source air-jet described here provides an advantage in ensuring reproducibility and reliability by defining and controlling setup parameters. Specifically, the separation from the needle and the airflow is comparable to other air-jets that shear droplets off a needle tip [18, 35, 44]; however, the needle is positioned by the chamfered needle inlet, ensuring central alignment with the airflow. Consequently, the 3D printed air-jet requires consideration of needle size to prevent the backflow of solution or air. Appropriately, by nature of being 3D printable, a CAD program can be used to adjust the geometries of the design. We encourage the modification of the air-jet design presented here to improve the microbeads' reproducibility or make it more applicable to each lab's specific needs.

In conclusion, we present an open-source air-jet with simple features printed on a low-budget 3D printer. The system's modular design allows easy cleaning, interchangeability to customized setups, and rapid replacement. We have demonstrated that alginate microbeads can be generated using this open-source air jet system with reasonable microbead diameters and dispersity. We expect that this device will enable other research labs and other fields to generate polymer microbeads.

References

[1] L. J. Hofseth, "Getting rigorous with scientific rigor," (in eng), *Carcinogenesis,* vol. 39, no. 1, pp. 21-25, Jan 12 2018, doi: 10.1093/carcin/bgx085.

[2] F. S. Collins and L. A. Tabak, "Policy: NIH plans to enhance reproducibility," (in eng), *Nature,* vol. 505, no. 7485, pp. 612-3, Jan 30 2014, doi: 10.1038/505612a.

[3] B. Brembs, "Prestigious Science Journals Struggle to Reach Even Average Reliability," (in eng), *Frontiers in human neuroscience,* vol. 12, p. 37, 2018, doi: 10.3389/fnhum.2018.00037.

[4] S. N. Goodman, D. Fanelli, and J. P. Ioannidis, "What does research reproducibility mean?," (in eng), *Science translational medicine,* vol. 8, no. 341, p. 341ps12, Jun 1 2016, doi: 10.1126/scitranslmed.aaf5027.

[5] J. T. Leek and R. D. Peng, "Opinion: Reproducible research can still be wrong: adopting a prevention approach," (in eng), *Proceedings of the National Academy of Sciences of the United States of America,* vol. 112, no. 6, pp. 1645-6, Feb 10 2015, doi: 10.1073/pnas.1421412111.

[6] W. P. Anderson, "Reproducibility: Stamp out shabby research conduct," (in eng), *Nature,* vol. 519, no. 7542, p. 158, Mar 12 2015, doi: 10.1038/519158a.

[7] A. Maia Chagas, "Haves and have nots must find a better way: The case for open scientific hardware," (in eng), *PLoS biology,* vol. 16, no. 9, pp. e3000014-e3000014, 2018, doi: 10.1371/journal.pbio.3000014.

[8] N. I. o. Health. "NIH 3D Print Exchange." https://3dprint.nih.gov/ (accessed 2018).

[9] T. Baden, A. M. Chagas, G. Gage, T. Marzullo, L. L. Prieto-Godino, and T. Euler, "Open Labware: 3-D Printing Your Own Lab Equipment," *PLOS Biology,* vol. 13, no. 3, p. e1002086, 2015, doi: 10.1371/journal.pbio.1002086.

[10] T. C. Marzullo and G. J. Gage, "The SpikerBox: A Low Cost, Open-Source BioAmplifier for Increasing Public Participation in Neuroscience Inquiry," *PloS one,* vol. 7, no. 3, p. e30837, 2012, doi: 10.1371/journal.pone.0030837.

[11] J. M. Pearce, "Building Research Equipment with Free, Open-Source Hardware," *Science,* 10.1126/science.1228183 vol. 337, no. 6100, p. 1303, 2012.

[12] M. S. Sulkin *et al.*, "Three-dimensional printing physiology laboratory technology," *American Journal of Physiology-Heart and Circulatory Physiology,* vol. 305, no. 11, pp. H1569-H1573, 2013/12/01 2013, doi: 10.1152/ajpheart.00599.2013.

[13] J. S. Cybulski, J. Clements, and M. Prakash, "Foldscope: Origami-Based Paper Microscope," *PloS one,* vol. 9, no. 6, p. e98781, 2014, doi: 10.1371/journal.pone.0098781.

[14] C. Zhang, N. C. Anzalone, R. P. Faria, and J. M. Pearce, "Open-Source 3D-Printable Optics Equipment," *PloS one,* vol. 8, no. 3, p. e59840, 03/27, doi: 10.1371/journal.pone.0059840.

[15] S. Pryor, "Implementing a 3D Printing Service in an Academic Library," *Journal of Library Administration,* vol. 54, no. 1, pp. 1-10, 2014/01/01 2014, doi: 10.1080/01930826.2014.893110.

[16] K. Kailasapathy, "Microencapsulation of probiotic bacteria: technology and potential applications," (in eng), *Current issues in intestinal microbiology,* vol. 3, no. 2, pp. 39-48, Sep 2002.

[17] O. Khanna, J. C. Larson, M. L. Moya, E. C. Opara, and E. M. Brey, "Generation of alginate microspheres for biomedical applications," (in eng), *Journal of visualized experiments : JoVE,* no. 66, p. 3388, 2012, doi: 10.3791/3388.

[18] M. Serra *et al.*, "Microencapsulation Technology: A Powerful Tool for Integrating Expansion and Cryopreservation of Human Embryonic Stem Cells," *PloS one,* vol. 6, no. 8, p. e23212, 2011, doi: 10.1371/journal.pone.0023212.

[19] S. Ahn and G. Kim, "Cell-encapsulating alginate microsized beads using an air-assisted atomization process to obtain a cell-laden hybrid scaffold," *Journal of Materials Chemistry B,* 10.1039/C5TB01629K vol. 3, no. 47, pp. 9132-9139, 2015, doi: 10.1039/C5TB01629K.

[20] J. M. Chan, I. K. Zervantonakis, T. Rimchala, W. J. Polacheck, J. Whisler, and R. D. Kamm, "Engineering of In Vitro 3D Capillary Beds by Self-Directed Angiogenic Sprouting," *PloS one,* vol. 7, no. 12, p. e50582, 2012, doi: 10.1371/journal.pone.0050582.

[21] S. Jitraruch *et al.*, "Alginate Microencapsulated Hepatocytes Optimised for Transplantation in Acute Liver Failure," *PloS one,* vol. 9, no. 12, p. e113609, 2014, doi: 10.1371/journal.pone.0113609.

[22] K. Y. Lee and D. J. Mooney, "Alginate: properties and biomedical applications," *Progress in polymer science,* vol. 37, no. 1, pp. 106-126, 2012, doi: 10.1016/j.progpolymsci.2011.06.003.

[23] O. Smidsrod and G. Skjak-Braek, "Alginate as immobilization matrix for cells," (in eng), *Trends Biotechnol,* vol. 8, no. 3, pp. 71-8, Mar 1990.

[24] U. Remminghorst and B. H. Rehm, "Bacterial alginates: from biosynthesis to applications," (in eng), *Biotechnology letters,* vol. 28, no. 21, pp. 1701-12, Nov 2006, doi: 10.1007/s10529-006-9156-x.

[25] H. H. Tonnesen and J. Karlsen, "Alginate in drug delivery systems," (in eng), *Drug development and industrial pharmacy,* vol. 28, no. 6, pp. 621-30, Jul 2002, doi: 10.1081/ddc-120003853.

[26] J. L. Madrigal *et al.*, "Microfluidic generation of alginate microgels for the controlled delivery of lentivectors," *Journal of Materials Chemistry B,* 10.1039/C6TB02150F vol. 4, no. 43, pp. 6989-6999, 2016, doi: 10.1039/C6TB02150F.

[27] A. L. Torres, S. J. Bidarra, M. T. Pinto, P. C. Aguiar, E. A. Silva, and C. C. Barrias, "Guiding morphogenesis in cell-instructive microgels for therapeutic

angiogenesis," *Biomaterials,* vol. 154, pp. 34-47, 2018/02/01/ 2018, doi: https://doi.org/10.1016/j.biomaterials.2017.10.051.

[28] O. Gryshkov, D. Pogozhykh, N. Hofmann, O. Pogozhykh, T. Mueller, and B. Glasmacher, "Encapsulating Non-Human Primate Multipotent Stromal Cells in Alginate via High Voltage for Cell-Based Therapies and Cryopreservation," *PloS one,* vol. 9, no. 9, p. e107911, 2014, doi: 10.1371/journal.pone.0107911.

[29] S. K. Leslie, D. J. Cohen, J. Sedlaczek, E. J. Pinsker, B. D. Boyan, and Z. Schwartz, "Controlled release of rat adipose-derived stem cells from alginate microbeads," *Biomaterials,* vol. 34, no. 33, pp. 8172-8184, 2013/11/01/ 2013, doi: https://doi.org/10.1016/j.biomaterials.2013.07.017.

[30] A. Sohail, M. S. Turner, A. Coombes, T. Bostrom, and B. Bhandari, "Survivability of probiotics encapsulated in alginate gel microbeads using a novel impinging aerosols method," *International Journal of Food Microbiology,* vol. 145, no. 1, pp. 162-168, 2011/01/31/ 2011, doi: https://doi.org/10.1016/j.ijfoodmicro.2010.12.007.

[31] K. Sultana, G. Godward, N. Reynolds, R. Arumugaswamy, P. Peiris, and K. Kailasapathy, "Encapsulation of probiotic bacteria with alginate–starch and evaluation of survival in simulated gastrointestinal conditions and in yoghurt," *International Journal of Food Microbiology,* vol. 62, no. 1, pp. 47-55, 2000/12/05/ 2000, doi: https://doi.org/10.1016/S0168-1605(00)00380-9.

[32] T. W. Yeung, E. F. Üçok, K. A. Tiani, D. J. McClements, and D. A. Sela, "Microencapsulation in Alginate and Chitosan Microgels to Enhance Viability of Bifidobacterium longum for Oral Delivery," (in eng), *Frontiers in microbiology,* vol. 7, pp. 494-494, 2016, doi: 10.3389/fmicb.2016.00494.

[33] M. L. Moya, M. Morley, O. Khanna, E. C. Opara, and E. M. Brey, "Stability of alginate microbead properties in vitro," (in eng), *Journal of materials science. Materials in medicine,* vol. 23, no. 4, pp. 903-912, 2012, doi: 10.1007/s10856-012-4575-9.

[34] G. H. Wolters, W. M. Fritschy, D. Gerrits, and R. van Schilfgaarde, "A versatile alginate droplet generator applicable for microencapsulation of pancreatic islets,"

(in eng), *Journal of applied biomaterials : an official journal of the Society for Biomaterials,* vol. 3, no. 4, pp. 281-6, Winter 1991, doi: 10.1002/jab.770030407.

[35] W. F. Kendall, M. D. Darrabie, H. M. El-Shewy, and E. C. Opara, "Effect of alginate composition and purity on alginate microspheres," *Journal of Microencapsulation,* vol. 21, no. 8, pp. 821-828, 2004/12/01 2004, doi: 10.1080/02652040400015452.

[36] K. T. Campbell, D. J. Hadley, D. L. Kukis, and E. A. Silva, "Alginate hydrogels allow for bioactive and sustained release of VEGF-C and VEGF-D for lymphangiogenic therapeutic applications," (in eng), *PloS one,* vol. 12, no. 7, p. e0181484, 2017, doi: 10.1371/journal.pone.0181484.

[37] B. B. Lee, P. Ravindra, and E. S. Chan, "Size and Shape of Calcium Alginate Beads Produced by Extrusion Dripping," *Chemical Engineering & Technology,* vol. 36, no. 10, pp. 1627-1642, 2013/10/01 2013, doi: 10.1002/ceat.201300230.

[38] K. Liu, H.-J. Ding, J. Liu, Y. Chen, and X.-Z. Zhao, "Shape-Controlled Production of Biodegradable Calcium Alginate Gel Microparticles Using a Novel Microfluidic Device," *Langmuir,* vol. 22, no. 22, pp. 9453-9457, 2006/10/01 2006, doi: 10.1021/la061729+.

[39] B. Jones and C. J. Nachtsheim, "Effective Design-Based Model Selection for Definitive Screening Designs," *Technometrics,* vol. 59, no. 3, pp. 319-329, 2017/07/03 2017, doi: 10.1080/00401706.2016.1234979.

[40] T. Y. Wong, L. A. Preston, and N. L. Schiller, "ALGINATE LYASE: review of major sources and enzyme characteristics, structure-function analysis, biological roles, and applications," (in eng), *Annual review of microbiology,* vol. 54, pp. 289-340, 2000, doi: 10.1146/annurev.micro.54.1.289.

[41] J. W. Andrejecsk, J. Cui, W. G. Chang, J. Devalliere, J. S. Pober, and W. M. Saltzman, "Paracrine exchanges of molecular signals between alginate-encapsulated pericytes and freely suspended endothelial cells within a 3D protein gel," *Biomaterials,* vol. 34, no. 35, pp. 8899-8908, 2013/11/01/ 2013, doi: https://doi.org/10.1016/j.biomaterials.2013.08.008.

[42] S. Boninsegna, R. Dal Toso, R. Dal Monte, and G. Carturan, "Alginate Microspheres Loaded with Animal Cells and Coated by a Siliceous Layer,"

Journal of Sol-Gel Science and Technology, vol. 26, no. 1, pp. 1151-1157, 2003/01/01 2003, doi: 10.1023/A:1020731429533.

[43] D. T. Chiu *et al.*, "Small but Perfectly Formed? Successes, Challenges, and Opportunities for Microfluidics in the Chemical and Biological Sciences," *Chem,* vol. 2, no. 2, pp. 201-223, 2017/02/09/ 2017, doi: https://doi.org/10.1016/j.chempr.2017.01.009.

[44] H. Zimmermann, S. G. Shirley, and U. Zimmermann, "Alginate-based encapsulation of cells: Past, present, and future," *Current Diabetes Reports,* vol. 7, no. 4, pp. 314-320, 2007/08/01 2007, doi: 10.1007/s11892-007-0051-1.

[45] S. Koch, C. Schwinger, J. Kressler, C. Heinzen, and N. G. Rainov, "Alginate encapsulation of genetically engineered mammalian cells: comparison of production devices, methods and microcapsule characteristics," (in eng), *J Microencapsul,* vol. 20, no. 3, pp. 303-16, May-Jun 2003, doi: 10.1080/0265204021000058438.

[46] F. Davarcı, D. Turan, B. Ozcelik, and D. Poncelet, "The influence of solution viscosities and surface tension on calcium-alginate microbead formation using dripping technique," *Food Hydrocolloids,* vol. 62, pp. 119-127, 2017/01/01/ 2017, doi: https://doi.org/10.1016/j.foodhyd.2016.06.029.

[47] S. Shimamura *et al.*, "Relationship Between Oxygen Sensitivity and Oxygen Metabolism of Bifidobacterium Species," *Journal of Dairy Science,* vol. 75, no. 12, pp. 3296-3306, 1992/12/01/ 1992, doi: https://doi.org/10.3168/jds.S0022-0302(92)78105-3.

[48] K. T. Campbell, R. S. Stilhano, and E. A. Silva, "Enzymatically degradable alginate hydrogel systems to deliver endothelial progenitor cells for potential revasculature applications," (in eng), *Biomaterials,* vol. 179, pp. 109-121, 2018/10// 2018, doi: 10.1016/j.biomaterials.2018.06.038.

[49] J. L. Madrigal, S. Shams, R. S. Stilhano, and E. A. Silva, "Characterizing the encapsulation and release of lentivectors and adeno-associated vectors from degradable alginate hydrogels," *Biomaterials Science,* 10.1039/C8BM01218K vol. 7, no. 2, pp. 645-656, 2019, doi: 10.1039/C8BM01218K.

[50] T. R. Henderson, R. F. Henderson, and J. L. York, "Effects of dimethyl sulfoxide on subunit proteins," (in eng), *Ann N Y Acad Sci,* vol. 243, pp. 38-53, Jan 27 1975, doi: 10.1111/j.1749-6632.1975.tb25342.x.

[51] G. Bhakta *et al.*, "Cryopreservation of alginate-fibrin beads involving bone marrow derived mesenchymal stromal cells by vitrification," in *Biomaterials*, vol. 30, no. 3). Netherlands, 2009, pp. 336-43.

[52] M. N. Egorikhina, Y. P. Rubtsova, and D. Y. Aleynik, "Long-Term Cryostorage of Mesenchymal Stem Cell-Containing Hybrid Hydrogel Scaffolds Based on Fibrin and Collagen," (in eng), *Gels,* vol. 6, no. 4, Nov 25 2020.

[53] R. Malpique *et al.*, "Alginate Encapsulation as a Novel Strategy for the Cryopreservation of Neurospheres," *Tissue Engineering Part C: Methods,* vol. 16, no. 5, pp. 965-977, 2010/10/01 2009, doi: 10.1089/ten.tec.2009.0660.

[54] L. Canaple, N. Nurdin, N. Angelova, D. Saugy, D. Hunkeler, and B. Desvergne, "Maintenance of primary murine hepatocyte functions in multicomponent polymer capsules--in vitro cryopreservation studies," in *J Hepatol*, vol. 34, no. 1). Netherlands, 2001, pp. 11-8.

[55] Y. C. Song *et al.*, "Vitrification of tissue engineered pancreatic substitute," in *Transplant Proc*, vol. 37, no. 1). United States, 2005, pp. 253-5.

[56] M. L. Ormiston *et al.*, "Generation and Culture of Blood Outgrowth Endothelial Cells from Human Peripheral Blood," (in eng), *J Vis Exp,* no. 106, p. e53384, Dec 23 2015.

[57] K. C. Murphy, J. Whitehead, D. Zhou, S. S. Ho, and J. K. Leach, "Engineering fibrin hydrogels to promote the wound healing potential of mesenchymal stem cell spheroids," (in eng), *Acta biomaterialia,* vol. 64, pp. 176-186, 2017, doi: 10.1016/j.actbio.2017.10.007.

[58] E. Regañón, V. Vila, and J. Aznar, "Effect of calcium ions on fibrin gel formation in normal plasma," in *Thromb Res*, vol. 35, no. 3). United States, 1984, pp. 365-9.

[59] M. Okada and B. Blombäck, "Calcium and fibrin gel structure," in *Thromb Res*, vol. 29, no. 3). United States, 1983, pp. 269-80.

[60] C. V. Dang, R. F. Ebert, and W. R. Bell, "Localization of a fibrinogen calcium binding site between gamma-subunit positions 311 and 336 by terbium fluorescence," *Journal of Biological Chemistry,* vol. 260, no. 17, pp. 9713-9719, 1985/08/15/ 1985, doi: https://doi.org/10.1016/S0021-9258(17)39297-9.

[61] C. H. Scudamore *et al.*, "Aprotinin reduces the need for blood products during liver transplantation," in *Am J Surg*, vol. 169, no. 5). United States, 1995, pp. 546-9.

[62] R. F. Roberts *et al.*, "Addition of aprotinin to organ preservation solutions decreases lung reperfusion injury," in *Ann Thorac Surg*, vol. 66, no. 1). Netherlands, 1998, pp. 225-30.

Appendix B

Dual thaw-induced gelation of fibrin and alginate hydrogels as a core-shell hydrogel capsule

Introduction

In this brief appendix, we will discuss our preliminary work with applying TIG to create alginate hydrogel capsules that surround a fibrin gel's precursors while the frozen solution is thawing from a frozen state. We then specifically use a cellular freezing solution with these components to encapsulate outgrowth endothelial cells. Three says post-cryopreservation, we observe cells sprouting within the capsules, suggesting the fibrin gel was formed and that the previously cryopreserved cells remain viable and functional.

The application of cryopreserved cells with fibrin is commonly studied in platelet-rich plasma and cell encapsulation. However, dimethyl sulfoxide (Me_2SO) has been known to hinder fibrin gel formation since the 1970s [1]. With one search on pubmed.gov, we found only 27 results relating to fibrin and Me_2SO, but over 150 results for fibrin and cryopreservation. Of these studies, those using cryopreservation often still incorporate dimethyl sulfoxide (Me_2SO), also abbreviated as DMSO, but cells are encapsulated in the fibrin gels prior to cryopreservation [2, 3]. While this bypasses the cryopreservation agent's potential hindrance, the cryopreservation of encapsulated cells is known to damage the polymeric structure and potentially reduce cell viability if the sample size is not adequately accounted for [3-6]. As an alternative, we hypothesized

that the formation of hydrogel material during the phase transition of frozen-cryopreserved cells to a liquid solution would encapsulate viable endothelial cells and promote their sprouting. Mainly, this will be using TIG as previously described to form alginate hydrogel capsules. However, in addition to a freezing solution containing calcium chloride to form the alginate capsule, the solution will also contain precursors for a fibrin gel, fibrinogen and thrombin. Given the relative size of these molecules with respect to the gelation time and release profiles described in chapter 3, we hypothesized that a fibrin gel should form within the first half-hour post-thawing, creating an alginate hydrogel shell encapsulating a fibrin core. To determine the sprouting behavior of post-cryopreserved endothelial cells, we used outgrowth endothelial cells that expressed green fluorescence protein. If the cells were viable to produce that protein, we suspected this choice to enable facile observation of sprouting behavior.

Select materials and methods

Outgrowth endothelial cell (OEC) culture

- EGM-2MV medium (Lonza) supplemented 5% FBS, ascorbic acid, hydrocortisone, GA-1000 antibiotic, hEGF, VEGF, hFGF-beta, and IGF-1 as supplied by the vendor
- Detach cells with 0.05% trypsin
- P8 cells were used for this experiment

Alginate solution for TIG thawing bath

- A 1% sterile charcoal filtered alginate solution prepared in phosphate buffer solution (PBS) was created as previously described in chapter 6.
- A PBS washing bath was also prepared to rinse hydrogels after alginate gelation via TIG.

OEC freezing solution for alginate and fibrin gelation

- 10% (v/v) Me_2SO, 80% (v/v) FBS, 100 mM $CaCl_2$, and EMB-2 media were used as a control freezing solution without a fibrin gel. FBS and Me_2SO concentrations were selected based on previous lab members' protocols (Pricilla Williams and Kevin Campbell). The use of 10% (v/v) Me2SO is a common concentration for slow freezing techniques with these cells [7].
- 10% (v/v) Me_2SO, 100 mM $CaCl_2$, fibrin gel precursors, and EMB-2 media were used as the fibrin-forming freezing solution. The fibrin-forming reagents were fibrinogen and thrombin. Fibrinogen solution was prepared in a saline solution by first adding 0.9 g of NaCl to 100 mL of diH_2O. This solution was used to make a final concentration in the freezing solution of 1.5 mg/mL. Before adding to the freezing solution, the concentrated stock solution was sterile filtered with a 0.22 µm syringe filter. These solutions were prepared fresh and stored at 4 °C until ready to use. Thrombin solutions were prepared at 25 U/mL in PBS. These were added to the freezing solution to obtain a final concentration of 2.5 U/mL. For mechanical and physical measurements, samples did not contain cells or thrombin to determine how those components affected hydrogel formation.

Cryopreservation

- The cryopreservation vessel was precooled in a 4 °C refrigerator along with the cryopreservation solution.
- 100k cells were cryopreserved per 100 µL frozen volumes in rubber molds described in chapter 6.

- For thawing, cells solutions were submerged in the alginate thawing bath for 2 minutes. Next, the samples were scooped into the washing bath for 5 minutes before moving to tissue culture wells filled with EMB-2. All solutions were pre-warmed to 37 °C.

Results and discussion

Here, we present the next step to the TIG process: forming a fibrin core within alginate hydrogel capsules. The alginate hydrogels form rapidly during thawing; the fibrin hydrogels take significantly longer, about 30 minutes. Consequently, we believed that the alginate hydrogel could sufficiently encapsulate the fibrin precursors long enough to form a fibrin gel. While the fibrin gel formation was not visible, mechanical testing compared to a capsule without fibrin precursors suggested the capsules became stiffer with fibrinogen and thrombin (Figure 1). Because fibrinogen is the polymeric component of the fibrin gel, this data indicates that the additional strength is likely due to the formation of a fibrin gel. An interesting interaction that is possible with this process is the three calcium-binding sites on fibrinogen and can improve the stiffness of fibrin gels [8-11]. Specifically, it has been suggested that calcium ions alter gelation kinetics by affecting the fibrinopeptide release rate from thrombin. However, Me_2SO has been shown to inhibit fibrin gel formation: a linear dependence between fibrin coating rate and DMSO percentage was found, where 10% Me_2SO led to a 50% reduction in gelling [1]. This study concluded that DMSO influenced thrombin's ability to break fibrinogen to fibrin. It is possible that immediate dilution of Me_2SO to the surrounding medium can allow for further gelling of fibrin despite this known influence of Me_2SO and could even have protective effects on the individual components during cryopreservation. Notably,

thrombin was not inhibited itself, but the binding of Me_2SO to fibrinogen was suggested to be inhibiting. Although there has been no characterization of the combined effects of Me_2SO and calcium ions on fibrin formation, both additives' role on fibrinogen binding sites suggests the divalent cation might prevent the hindering effects of Me_2SO.

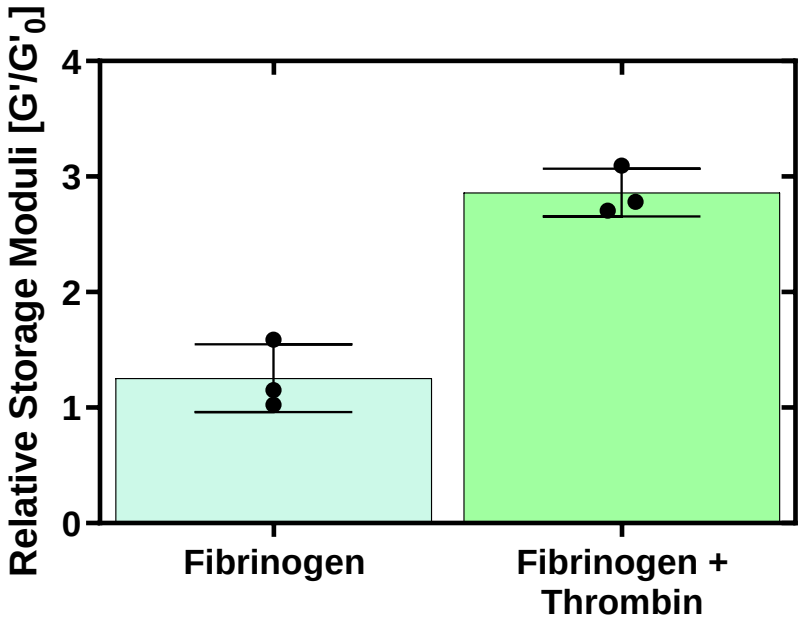

Figure 1. Storage moduli results support the formation of a fibrin hydrogel within the alginate capsules. The addition of fibrinogen alone does appear to increase the storage moduli slightly from the freezing solutions without any precursors; however, the addition of thrombin also led to a significant increase in the capsule stiffness. Bar graphs represent the mean and SD from n = 3 samples. Measurements were normalized to the average measurement from an alginate hydrogel capsule without any precursors (n = 3).

We next wanted to determine if the formation of the fibrin gel and the addition of cryopreserved cells had a significant impact on the formation of alginate hydrogel

capsules. Overall, it appears that the addition of additional components did reduce the shell thickness. While there does appear to be a downward trend with capsules containing fibrin gels, the decrease was not statistically significant after a one-way ANOVA followed by a Tukey's multiple comparison test ($p > 0.05$) (Figure 2). This is a similar observation we had in chapter 6, where an increasing concentration of FBS to the freezing solution resulted in a reduction in the capsule's shell thickness.

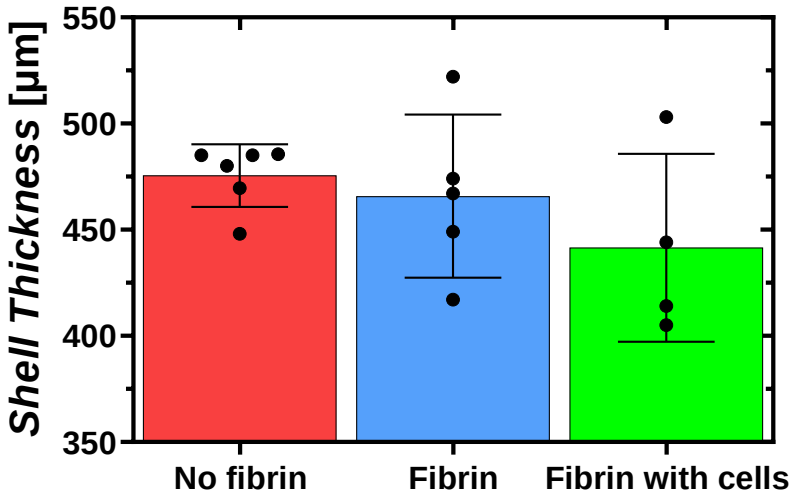

Figure 2. There was no significant change in alginate hydrogel shell thickness due to fibrin precursors and fibrin formation or cells. Phase-contrast images measured shell thickness. There is potentially a decreasing trend in alginate hydrogel gelation with more additives to the freezing solution. Bar graphs represent the mean and SD of each condition. Individual sample measurements are also shown as symbols (n = 4 – 6).

One day after thawing the cryopreserved OECs via TIG, sprouting behavior was observed. While the majority of cells appear to retain their rounded shape, small clusters of cells exhibited sprouts, branching out multiple times within the capsules (Figure 3). While we believe this to be a positive indicator for fibrin formation, there is also a possibility of fibrinogen molecules becoming interlocked with the alginate hydrogel on the inner surface of the capsules. Indeed, the cells primarily appeared at the bottom of the capsules. While this could have multiple causes, the two more probable causes are that fibrin gelation took significantly more time than OECs to fall to the bottom of the capsule, or the fibrin gel did not form. To further determine the cause, capsules could be placed in a rotator, spins the capsules, preventing OECs from settling. Beneficially, this process would induce shear forces that the OECs are not exposed to because of the alginate capsules.

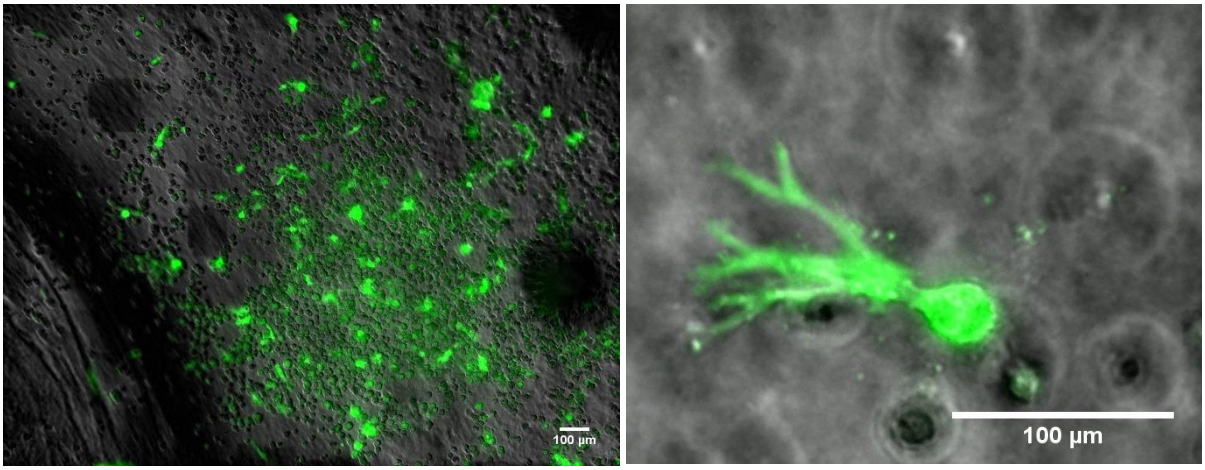

Figure 3. OECs begin sprouting one day post-thawing within the alginate hydrogel capsules formed by TIG. These images suggest the formation of a fibrin gel that enables cell sprouting of recently thawed OEC. This work suggest that the fibrin gel does form, and the post-cryopreserved cells are functional. Representative images were taken on an inverted fluorescence microscope (Zeiss) and composite images of brightfield, and green fluorescence were prepared in ImageJ (NIH).

Conclusion

This work suggests the formation of a fibrin gel after TIG of an alginate hydrogel capsule. This process was able to support the post-thaw encapsulation of OECs that sprouted within the capsules. Notably, because of the dynamic nature of the cytoskeleton and no apparent need to prevent fibrinolysis, aprotinin was not added to the freezing solution. If necessary, we believe this protein could be added to the cell culture post-cryopreservation. Not only could this protein denature or loss efficacy due to being frozen, but there is limited evidence of how aprotinin will impact previously cryopreserved cells. Only two studies have explored the use of this protein with

cryopreservation: one of the studies added aprotinin as a supplement to previously cryopreserved blood products with some potential benefit [12], and the second study was for cold, not frozen, storage of organs in Euro-Collins and University of Wisconsin solutions, where aprotinin decreased organ injury [13]. Future work into this technique should address the interplay between Me_2SO and calcium ions on fibrin gel formation, the role of aprotinin, and any cryoprotective potential the fibrinogen polymer in the freezing solution might have on cryopreserved cells.

References

[1] T. R. Henderson, R. F. Henderson, and J. L. York, "Effects of dimethyl sulfoxide on subunit proteins," (in eng), *Ann N Y Acad Sci,* vol. 243, pp. 38-53, Jan 27 1975, doi: 10.1111/j.1749-6632.1975.tb25342.x.

[2] G. Bhakta *et al.*, "Cryopreservation of alginate-fibrin beads involving bone marrow derived mesenchymal stromal cells by vitrification," in *Biomaterials*, vol. 30, no. 3). Netherlands, 2009, pp. 336-43.

[3] M. N. Egorikhina, Y. P. Rubtsova, and D. Y. Aleynik, "Long-Term Cryostorage of Mesenchymal Stem Cell-Containing Hybrid Hydrogel Scaffolds Based on Fibrin and Collagen," (in eng), *Gels,* vol. 6, no. 4, Nov 25 2020.

[4] R. Malpique *et al.*, "Alginate Encapsulation as a Novel Strategy for the Cryopreservation of Neurospheres," *Tissue Engineering Part C: Methods,* vol. 16, no. 5, pp. 965-977, 2010/10/01 2009, doi: 10.1089/ten.tec.2009.0660.

[5] L. Canaple, N. Nurdin, N. Angelova, D. Saugy, D. Hunkeler, and B. Desvergne, "Maintenance of primary murine hepatocyte functions in multicomponent polymer capsules--in vitro cryopreservation studies," in *J Hepatol*, vol. 34, no. 1). Netherlands, 2001, pp. 11-8.

[6] Y. C. Song *et al.*, "Vitrification of tissue engineered pancreatic substitute," in *Transplant Proc*, vol. 37, no. 1). United States, 2005, pp. 253-5.

[7] M. L. Ormiston *et al.*, "Generation and Culture of Blood Outgrowth Endothelial Cells from Human Peripheral Blood," (in eng), *J Vis Exp,* no. 106, p. e53384, Dec 23 2015.

[8] K. C. Murphy, J. Whitehead, D. Zhou, S. S. Ho, and J. K. Leach, "Engineering fibrin hydrogels to promote the wound healing potential of mesenchymal stem cell spheroids," (in eng), *Acta biomaterialia,* vol. 64, pp. 176-186, 2017, doi: 10.1016/j.actbio.2017.10.007.

[9] E. Regañón, V. Vila, and J. Aznar, "Effect of calcium ions on fibrin gel formation in normal plasma," in *Thromb Res*, vol. 35, no. 3). United States, 1984, pp. 365-9.

[10] M. Okada and B. Blombäck, "Calcium and fibrin gel structure," in *Thromb Res*, vol. 29, no. 3). United States, 1983, pp. 269-80.

[11] C. V. Dang, R. F. Ebert, and W. R. Bell, "Localization of a fibrinogen calcium binding site between gamma-subunit positions 311 and 336 by terbium fluorescence," *Journal of Biological Chemistry,* vol. 260, no. 17, pp. 9713-9719, 1985/08/15/ 1985, doi: https://doi.org/10.1016/S0021-9258(17)39297-9.

[12] C. H. Scudamore *et al.*, "Aprotinin reduces the need for blood products during liver transplantation," in *Am J Surg*, vol. 169, no. 5). United States, 1995, pp. 546-9.

[13] R. F. Roberts *et al.*, "Addition of aprotinin to organ preservation solutions decreases lung reperfusion injury," in *Ann Thorac Surg*, vol. 66, no. 1). Netherlands, 1998, pp. 225-30.